5-15-2009

Mineralogy of Eudialyte Group Minerals From the East Hill Suite Of the Mont Saint-Hilaire Alkaline Plutonic Complex, Including an Alternative Site-Assignment Algorithm & A Proposed Classification System

Peter Tice
University of New Orleans

Mineralogy of Eudialyte Group Minerals From the East Hill Suite Of the Mont Saint-Hilaire Alkaline Plutonic Complex, Including an Alternative Site-Assignment Algorithm & A Proposed Classification System

A Thesis

Submitted to the Graduate Faculty of the
University of New Orleans
in partial fulfillment of the
requirements for the degree of

Master of Science
in
The Department of Earth and Environmental Sciences

by

Peter E. Tice

B.Sc. McGill University, 1995

May, 2009

ACKNOWLEDGEMENTS

This work greatly benefited from the guidance and assistance of a number of people; to them should be conveyed deep gratitude.

Dr. Wm. B. Simmons, Jr. is to be thanked first and foremost for his thoughtful commentary on research methodology, analytical procedures, and petrological and mineralogical interpretations. He deserves a great deal of further appreciation for his dedication and patience. Dr. Simmons was gracious and accommodating in allowing the author to choose and direct the subject of his research; he was tolerant of changes in the direction of research, while still providing guidance and leadership; and he was unwavering in his support of the completion of this study.

Dr. Simmons and Mr. Alexander U. Falster, as joint operators of the analytical facilities in the Department of Geology and Geophysics at the University of New Orleans, deserve many collective thanks for providing a laboratory at which students are able, instrumentally and financially, to carry out analyses of both a broad scope and a deep extent. This work required a variety of instruments and a number of instrument-hours that would have made its proper development and completion financially unattainable at virtually any other institution.

Dr. Matthew W. Totten lent a valuable alternative perspective to this work and gave constant encouragement to the author in all his endeavours. He helped to develop the author's breadth of expertise by giving the author the opportunity to collaborate on mineralogical projects in the realm of sedimentary petrology. He was an inspiration and role model throughout their relationship at the University of New Orleans.

Dr. Karen L. Webber helped to develop the author's understanding of mineralogical research in a petrological context, assisted the author in preliminary literature searches, gave

insightful editorial commentary, and served as an example by whom to measure the standards that characterize research of high quality.

Dr. Christopher D. Parkinson provided constructive criticism on the organization of this paper.

Dr. Robert F. Martin, of McGill University, first inspired the interest of the author in pegmatites, alkaline igneous rocks, and Mont Saint-Hilaire. As advisor for the author's undergraduate thesis on the mineralogy and crystallization dynamics of a pegmatite dike at Mont Saint-Hilaire, he accompanied the author on several excursions to the locality, provided expert instruction in scientific writing, and participated in numerous discussions on alkaline melts and mineralogy that shaped that thesis and led to this current work.

Monsieur J.G. Poudrette of the Poudrette quarry graciously allows limited access to his property for the collection of aesthetic and research specimens. This beneficence is instrumental in the continuing efforts by all researchers to understand Mont Saint-Hilaire and is deeply appreciated.

The author's Mother and Father nurtured the author's education and interest in the sciences in school and museums and through talks, both formal and informal. They provided the financial means for the author's undergraduate education and were unconditionally loving and supportive through challenging and trying times. They were always there; they were true parents.

The author's wife, Sherri, was wonderfully understanding of the author's needs for private, quiet writing time, spending many hours watching their children and looking after the author's usual chores so that this work could be completed; although, the children did sometimes get to have a look at what daddy was doing—"Look at all the numbers!" In addition to taking

care of this practical issue, she was unfaltering in her encouragement to bring this research to its written conclusion.

Mr. Alexander U. Falster, although a major contributor to this work, is saved until the end to make more conspicuous his inclusion in this section. Through the entire course of his relationship with the author, he has been as a brother, always ready to offer advice, assistance, laughter, or consolation. Mr. Falster operated the electron microprobe for a total of approximately 150 hours to generate the chemical analyses for this work. He, along with Dr. Simmons, instructed the author on the theoretical and practical aspects of operating the electron microprobe, scanning electron microscope, X-ray diffractometer, and direct-coupled plasma spectrometer. Mr. Falster further assisted, when needed, in the author's operation of the latter three instruments. Also, Mr. Falster is responsible for maintenance, repairs, and upkeep of all of the instruments used by the author at the University of New Orleans. Without his tremendous efforts, a work of this scope would have been impossible.

To any family and friends who gave of themselves but who were not mentioned by name, many thanks.

This thesis is dedicated to my chemistry teacher from Wyomissing Area High School,

Mr. William C. Dowling,

who first showed me the magic of chemistry.

TABLE OF CONTENTS

LIST OF TABLES ..... **IX**

LIST OF FIGURES ..... **X**

ABSTRACT ..... **XII**

INTRODUCTION **1**

PREVIOUS WORK **3**

HISTORICAL PERSPECTIVE 3
EUDIALYTE GROUP MINERALS AT MONT SAINT-HILAIRE 4

GEOLOGIC SETTING **5**

REGIONAL GEOLOGY 5
GEOLOGY OF MONT SAINT-HILAIRE 7
OCCURRENCE OF EUDIALYTE GROUP MINERALS AT MONT SAINT-HILAIRE 9
Introduction *9*
Eudialyte Syenite *9*
Descriptive Mineralogy of Eudialyte Group Minerals *10*

ANALYTICAL METHODS **11**

SCANNING ELECTRON MICROSCOPY 11
Background *11*
Sample Preparation *11*
Operating Conditions *11*
X-RAY DIFFRACTOMETRY 12
Background *12*
Operating Conditions *12*
ELECTRON MICROPROBE ANALYSIS 13
Background *13*
Operating Conditions & Standards *13*
OPTICAL MICROSCOPY 14
Background *14*
Photomicroscopy *14*

A EUDIALYTE GROUP PRIMER **14**

PHYSICAL PROPERTIES 14
OPTICAL PROPERTIES 15
CRYSTALLOGRAPHY 16
CRYSTAL CHEMISTRY 18
NOMENCLATURE 21

RECALCULATION OF ANALYSES **23**

INTRODUCTION 23
A COMPARISON OF PUBLISHED SCHEMES 23

A Novel Site-Assignment Algorithm 24
Introduction & Purpose *24*
General Description *25*
The Algorithm *26*

COMPARATIVE PERFORMANCE OF THE SCHEMES 29

Introduction 29
Results 30
Statistical Significance *30*
Statistical Analysis of the Recalculation Schemes *31*
N(4) *32*
M(1) *38*
M(2) *42*
Z *45*
M(3) *48*

PROPOSED EUDIALYTE GROUP CLASSIFICATION SYSTEM 51

Introduction 51
Classification on Site-Occupancy of *M*(3) 51
Graphical Representation 53

EUDIALYTE GROUP MINERALS OF THE EAST HILL SUITE, MONT SAINT-HILAIRE 54

Introduction 54
Survey of Speciation 55
Proposed Eudialyte Subgroup 57
Proposed Kentbrooksite Subgroup 66
Proposed Khomyakovite Subgroup 76
Proposed "Zr-eudialyte" Subgroup 80
Proposed "Hf-eudialyte" Subgroup 89
Major Element Crystal Chemistry 91
Introduction *91*
Main Group Elements *91*
High Field Strength Elements (HFSE) *91*
Other Transition Elements *94*
Alkali & Alkaline Earth Elements *94*
Trace Element Crystal Chemistry 96
Proposed Eudialyte Subgroup *96*
Proposed Kentbrooksite Subgroup *98*
Proposed "Zr-eudialyte" Subgroup *98*
Proposed Khomyakovite and "Hf-eudialyte" Subgroups *98*
High Field Strength Elements (HFSE) *99*
Main Group Elements *107*
Rare-Earth Elements (REE) *107*
Other Transition Elements *115*
Alkali & Alkaline Earth Elements *116*
Volatiles *120*
Site-Occupancy Totals 127

DISCUSSION 128
RATIONALE FOR THE ALTERNATIVE ALGORITHM 128
Site Assignment of Y 128
Sodium Site Splitting 128
Further Musings on Sodium 129
COMPARATIVE PERFORMANCE OF THE SCHEMES 130
Goals of the Alternative Algorithm Revisited 130
Site-Occupancy in N(ϕ) & N(4) 130
Vacancies in M(2) 133
Partitioning of Mn 133
Partitioning of Nb & Hf 135
Summary 135
Suggestions for Future Work 136
PROPOSED EUDIALYTE GROUP CLASSIFICATION SYSTEM 138
Introduction 138
Rationale for M(3) 138
Site-Occupancy of X 139
Graphical Representation of Data 141
EUDIALYTE GROUP SPECIATION IN THE EAST HILL SUITE 143
CRYSTAL CHEMISTRY OF EUDIALYTE GROUP MINERALS FROM MONT SAINT-HILAIRE 144
Overview 144
Possible Implications for Parental Magma Chemistry 148
Control on Potassium Content 149
Paragenesis of Eudialyte Group Minerals 147
CONCLUSIONS 154
REFERENCES 156
VITA 161

LIST OF TABLES

TABLE 1 – MEMBERS OF THE EUDIALYTE GROUP. 22
TABLE 2 – SITE-ASSIGNMENT PRIORITY MATRIX FOR THE ALTERNATIVE ALGORITHM. 25
TABLE 3 – PROPOSED SUBGROUPS OF THE EUDIALYTE GROUP. 52
TABLE 4 – ALLOCATION OF APPROVED EUDIALYTE GROUP MINERALS TO THE PROPOSED SUBGROUPS. 52
TABLE 5 – APPROVED EUDIALYTE GROUP MINERALS AT MONT SAINT-HILAIRE. 54
TABLE 6 – PROPOSED SUBGROUPS REPRESENTED IN THE EAST HILL SUITE ANALYSES. 55
TABLE 7 – SPECIATION OF THE EUDIALYTE GROUP IN THE EAST HILL SUITE ANALYSES..... 56
TABLE 8 – REPRESENTATIVE EMP ANALYSES OF THE PROPOSED EUDIALYTE SUBGROUP. 58
TABLE 9 – SITE-OCCUPANCY OF PROPOSED EUDIALYTE SUBGROUP ANALYSES I. 59
TABLE 10 – SITE-OCCUPANCY OF PROPOSED EUDIALYTE SUBGROUP ANALYSES II. 60
TABLE 11 – REPRESENTATIVE EMP ANALYSES OF THE PROPOSED KENTBROOKSITE SUBGROUP. 67
TABLE 12 – SITE-OCCUPANCY OF PROPOSED KENTBROOKSITE SUBGROUP ANALYSES I. 68
TABLE 13 – SITE-OCCUPANCY OF PROPOSED KENTBROOKSITE SUBGROUP ANALYSES II. 69
TABLE 14 – REPRESENTATIVE EMP ANALYSES OF THE PROPOSED KHOMYAKOVITE & "HF-EUDIALYTE" SUBGROUPS. 77
TABLE 15 – SITE-OCCUPANCY OF PROPOSED KHOMYAKOVITE & "HF-EUDIALYTE" SUBGROUP ANALYSES. 78
TABLE 16 – REPRESENTATIVE EMP ANALYSES OF THE PROPOSED "ZR-EUDIALYTE" SUBGROUP. 81
TABLE 17 – SITE-OCCUPANCY OF PROPOSED "ZR-EUDIALYTE" SUBGROUP ANALYSES I. 82
TABLE 18 – SITE-OCCUPANCY OF PROPOSED "ZR-EUDIALYTE" SUBGROUP ANALYSES II. 83
TABLE 19 – VACANCIES IN MONT SAINT-HILAIRE EUDIALYTE GROUP EMP ANALYSES. 127
TABLE 20 – SURPLUSES IN MONT SAINT-HILAIRE EUDIALYTE GROUP EMP ANALYSES. 127
TABLE 21 – COMPARATIVE PERFORMANCE OF RECALCULATION SCHEMES AND CORRECTIONS *VERSUS* STRUCTURAL DATA GIVEN IN JOHNSEN & GRICE (1999) FOR SITE-OCCUPANCY IN $N(\phi)$ & $N(4)$. 132
TABLE 22 – SUMMARY OF THE PERFORMANCE OF THE TWO RECALCULATION SCHEMES, THE CATIONIC SCHEME OF JOHNSEN & GRICE (1999) (SUBSCRIPT J&G) AND THE ALTERNATIVE ALGORITHM (SUBSCRIPT AA). 135

LIST OF FIGURES

FIGURE 1 – MAP OF THE MONTEREGIAN HILLS AND THE EASTERN TOWNSHIPS OF QUÉBEC. (AFTER PHILPOTTS 1970) 5
FIGURE 2 – THE SAINT LAWRENCE RIFT SYSTEM. (CURRIE 1970) 6
FIGURE 3 – GEOLOGIC MAP OF MONT SAINT-HILAIRE. (AFTER CURRIE 1983)..... 8
FIGURE 4 – THE *R*3M STRUCTURE OF THE EUDIALYTE GROUP, VIEWED ALONG [001], SHOWING THE RING STRUCTURE. *N* SITES ARE OMITTED FOR CLARITY. (JOHNSEN *ET AL*. 2003A) 17
FIGURE 5 – THE *R*3M STRUCTURE OF THE EUDIALYTE GROUP, VIEWED ALONG [100], SHOWING THE SLAB ARRANGEMENT. *N* SITES ARE OMITTED FOR CLARITY. (JOHNSEN *ET AL*. 2003A)..... 18
FIGURE 6 – THE *R*3M STRUCTURE OF THE EUDIALYTE GROUP, VIEWED APPROXIMATELY ALONG [210], SHOWING THE REPEATING LAYER STRUCTURE. (JOHNSEN *ET AL*. 2003A) 19
FIGURE 7 – PERFORMANCE COMPARISON BETWEEN THE RECALCULATION SCHEMES FOR NA IN THE *N*(4) SITE..... 33
FIGURE 8 – PERFORMANCE COMPARISON BETWEEN THE RECALCULATION SCHEMES FOR SR IN THE *N*(4) SITE..... 34
FIGURE 9 – PERFORMANCE COMPARISON BETWEEN THE RECALCULATION SCHEMES FOR K IN THE *N*(4) SITE..... 35
FIGURE 10 – PERFORMANCE COMPARISON BETWEEN THE RECALCULATION SCHEMES FOR CA IN THE *N*(4) SITE..... 36
FIGURE 11 – PERFORMANCE COMPARISON BETWEEN THE RECALCULATION SCHEMES FOR *REE* IN THE *N*(4) SITE. 37
FIGURE 12 – PERFORMANCE COMPARISON BETWEEN THE RECALCULATION SCHEMES FOR CA IN THE *M*(1) SITE..... 39
FIGURE 13 – PERFORMANCE COMPARISON BETWEEN THE RECALCULATION SCHEMES FOR MN IN THE *M*(1) SITE..... 40
FIGURE 14 – PERFORMANCE COMPARISON BETWEEN THE RECALCULATION SCHEMES FOR *REE* IN THE *M*(1) SITE..... 41
FIGURE 15 – PERFORMANCE COMPARISON BETWEEN THE RECALCULATION SCHEMES FOR FE IN THE *M*(2) SITE..... 43
FIGURE 16 – PERFORMANCE COMPARISON BETWEEN THE RECALCULATION SCHEMES FOR MN IN THE *M*(2) SITE..... 44
FIGURE 17 – PERFORMANCE COMPARISON BETWEEN THE RECALCULATION SCHEMES FOR ZR IN THE *Z* SITE..... 46
FIGURE 18 – PERFORMANCE COMPARISON BETWEEN THE RECALCULATION SCHEMES FOR TI IN THE *Z* SITE..... 47
FIGURE 19 – PERFORMANCE COMPARISON BETWEEN THE RECALCULATION SCHEMES FOR SI IN THE *M*(3) SITE..... 49
FIGURE 20 – PERFORMANCE COMPARISON BETWEEN THE RECALCULATION SCHEMES FOR NB IN THE *M*(3) SITE..... 50
FIGURE 21 – $^{[M(3)]}$(SI-NB-ZR)-DOMINANT PROPOSED EUDIALYTE SUBGROUP ANALYSES. 61
FIGURE 22 – $^{[M(3)]}$(SI-NB-TA)-DOMINANT PROPOSED EUDIALYTE SUBGROUP ANALYSES. 62
FIGURE 23 – $^{[M(3)]}$(SI-NB-TI)-DOMINANT PROPOSED EUDIALYTE SUBGROUP ANALYSIS. 63
FIGURE 24 – $^{[M(3)]}$(SI-TA-TI)-DOMINANT PROPOSED EUDIALYTE SUBGROUP ANALYSIS. 64
FIGURE 25 – $^{[M(3)]}$(SI-TA-ZR)-DOMINANT PROPOSED EUDIALYTE SUBGROUP ANALYSIS. 65
FIGURE 26 – $^{[M(3)]}$(SI-NB-HF)-DOMINANT PROPOSED KENTBROOKSITE SUBGROUP ANALYSIS. 70
FIGURE 27 – $^{[M(3)]}$(TA-NB-HF)-DOMINANT PROPOSED KENTBROOKSITE SUBGROUP ANALYSIS. 71

FIGURE 28 – $^{[M(3)]}$(TA-NB-ZR)-DOMINANT PROPOSED KENTBROOKSITE SUBGROUP ANALYSIS. 72
FIGURE 29 – $^{[M(3)]}$(SI-NB-TI)-DOMINANT PROPOSED KENTBROOKSITE SUBGROUP ANALYSIS..... 73
FIGURE 30 – $^{[M(3)]}$(HF-NB-ZR)-DOMINANT PROPOSED KENTBROOKSITE SUBGROUP ANALYSIS. 74
FIGURE 31 – $^{[M(3)]}$(SI-NB-ZR)-DOMINANT PROPOSED KENTBROOKSITE SUBGROUP ANALYSIS..... 75
FIGURE 32 – $^{[M(3)]}$(W-NB-TA)-DOMINANT PROPOSED KHOMYAKOVITE SUBGROUP ANALYSIS. 79
FIGURE 33 – $^{[M(3)]}$(SI-NB-ZR)-DOMINANT PROPOSED "ZR-EUDIALYTE" SUBGROUP ANALYSES. 84
FIGURE 34 – $^{[M(3)]}$(TI-NB-ZR)-DOMINANT PROPOSED "ZR-EUDIALYTE" SUBGROUP ANALYSES. 85
FIGURE 35 – $^{[M(3)]}$(SI-TA-ZR)-DOMINANT PROPOSED "ZR-EUDIALYTE" SUBGROUP ANALYSES..... 86
FIGURE 36 – $^{[M(3)]}$(TA-NB-ZR)-DOMINANT PROPOSED "ZR-EUDIALYTE" SUBGROUP ANALYSIS..... 87
FIGURE 37 – $^{[M(3)]}$(SI-HF-ZR)-DOMINANT PROPOSED "ZR-EUDIALYTE" SUBGROUP ANALYSIS..... 88
FIGURE 38 – $^{[M(3)]}$(W-NB-HF)-DOMINANT PROPOSED "HF-EUDIALYTE" SUBGROUP ANALYSIS. 90
FIGURE 39 – TOTAL SiO_2 *VERSUS* MOLE FRACTION $^{[M(2)]}$[MN/(MN + FE)]. 92
FIGURE 40 – TOTAL ZrO_2 *VERSUS* MOLE FRACTION $^{[M(2)]}$[MN/(MN + FE)]. 93
FIGURE 41 – TOTAL CAO *VERSUS* MOLE FRACTION $^{[M(2)]}$[MN/(MN + FE)]..... 95
FIGURE 42 – TOTAL Na_2O *VERSUS* MOLE FRACTION $^{[M(2)]}$[MN/(MN + FE)]. 97
FIGURE 43 – TOTAL TiO_2 *VERSUS* MOLE FRACTION $^{[M(2)]}$[MN/(MN + FE)] 100
FIGURE 44 – TOTAL HfO_2 *VERSUS* MOLE FRACTION $^{[M(2)]}$[MN/(MN + FE)]..... 101
FIGURE 45 – TOTAL Nb_2O_5 *VERSUS* MOLE FRACTION $^{[M(2)]}$[MN/(MN + FE)]. 103
FIGURE 46 – TOTAL Ta_2O_5 *VERSUS* MOLE FRACTION $^{[M(2)]}$[MN/(MN + FE)]..... 104
FIGURE 47 – TOTAL MoO_3 *VERSUS* MOLE FRACTION $^{[M(2)]}$[MN/(MN + FE)]..... 105
FIGURE 48 – TOTAL WO_3 *VERSUS* MOLE FRACTION $^{[M(2)]}$[MN/(MN + FE)]..... 106
FIGURE 49 – TOTAL AL_2O_3 *VERSUS* MOLE FRACTION $^{[M(2)]}$[MN/(MN + FE)]. 108
FIGURE 50 – TOTAL Ce_2O_3 *VERSUS* MOLE FRACTION $^{[M(2)]}$[MN/(MN + FE)]..... 109
FIGURE 51 – TOTAL La_2O_3 *VERSUS* MOLE FRACTION $^{[M(2)]}$[MN/(MN + FE)]..... 110
FIGURE 52 – TOTAL Gd_2O_3 *VERSUS* MOLE FRACTION $^{[M(2)]}$[MN/(MN + FE)]. 111
FIGURE 53 – TOTAL Nd_2O_3 *VERSUS* MOLE FRACTION $^{[M(2)]}$[MN/(MN + FE)]. 112
FIGURE 54 – CHONDRITE-NORMALIZED *REE* CONTENT IN THE PROPOSED EUDIALYTE SUBGROUP. 113
FIGURE 55 – CHONDRITE-NORMALIZED *REE* CONTENT IN THE PROPOSED KENTBROOKSITE SUBGROUP. 113
FIGURE 56 – CHONDRITE-NORMALIZED *REE* CONTENT IN THE PROPOSED KHOMYAKOVITE SUBGROUP. 114
FIGURE 57 – CHONDRITE-NORMALIZED *REE* CONTENT IN THE PROPOSED "ZR-EUDIALYTE" SUBGROUP. 114
FIGURE 58 – CHONDRITE-NORMALIZED *REE* CONTENT IN THE PROPOSED "HF-EUDIALYTE" SUBGROUP. 115
FIGURE 59 – TOTAL Y_2O_3 *VERSUS* MOLE FRACTION $^{[M(2)]}$[MN/(MN + FE)]. 117
FIGURE 60 – TOTAL Sc_2O_3 *VERSUS* MOLE FRACTION $^{[M(2)]}$[MN/(MN + FE)]. 118
FIGURE 61 – TOTAL BAO *VERSUS* MOLE FRACTION $^{[M(2)]}$[MN/(MN + FE)]..... 119
FIGURE 62 – TOTAL MGO *VERSUS* MOLE FRACTION $^{[M(2)]}$[MN/(MN + FE)]..... 121
FIGURE 63 – TOTAL K_2O *VERSUS* MOLE FRACTION $^{[M(2)]}$[MN/(MN + FE)]. 122
FIGURE 64 – TOTAL CL *VERSUS* MOLE FRACTION $^{[M(2)]}$[MN/(MN + FE)]. 124
FIGURE 65 – TOTAL F *VERSUS* MOLE FRACTION $^{[M(2)]}$[MN/(MN + FE)]. 125
FIGURE 66 – TOTAL SO_3 *VERSUS* MOLE FRACTION $^{[M(2)]}$[MN/(MN + FE)]. 126
FIGURE 67 – THE SEVEN POSSIBLE OCCUPANTS OF *M*(3) AND THEIR ABUNDANCES IN THE EAST HILL SUITE ANALYSES. 142

ABSTRACT

The twenty approved members of the eudialyte group are complex zirconosilicates, primarily with general formula $N_{15}M(1)_6M(2)_3M(3)M(4)Z_3[Si_{24}O_{72}]O_4X_2$. An algorithm was created to address the inherent recalculation difficulties in the absence of single-crystal X-ray data and was an overall improvement over previous schemes. Eudialyte group minerals were analyzed from the East Hill Suite of the Mont Saint-Hilaire alkaline complex. Recalculations revealed previously undocumented eudialyte-group compositions and degrees of chemical zonation. These data suggest that late-stage melt heterogeneity in alkaline systems is far more pronounced than previously thought. All analyses exhibited a negative neodymium anomaly in chondrite-normalized data. This supports data from other investigators that point to a pre-intrusion fractionation event in the underlying mantle. Potassium content of the eudialyte group minerals from the East Hill Suite was restricted to a narrow range, as was that of analyses from numerous other localities, suggesting some internal control on potassium content in eudialyte group minerals.

Keywords: eudialyte, Mont Saint-Hilaire, recalculation, melt heterogeneity, neodymium anomaly

INTRODUCTION

This study came into being without deliberate intention. Mineralogical research by the author at the Mont Saint-Hilaire alkaline intrusive complex led innocently enough to a suite of electron microprobe analyses of eudialyte group minerals. Microbeam analysis of these minerals is about as straightforward[1] as for any silicate mineral; recalculation proved to be a different story. At the time that the analyses were done, 1997-1998, the perception was that eudialyte group mineral crystal chemistry was comparable to that of the amphibole group; that there were, indeed, a relatively large number of sites available and also a relatively large number of possible occupants, but that recalculation on total oxygen and charge balance was sufficient to establish a good formula. Acting on this perception, however, revealed two serious problems.

As will be discussed in more detail later, the first obstacle to be encountered was a lack of agreement on the formula into which site-assignments were to be worked. Several sources (*e.g.* Mandarino & Anderson 1989; Khomyakov 1995; Coulson & Chambers 1996) proposed different general formulæ for the eudialyte group. Given a particular chemical analysis, a reasonable structural formula could be fitted to the template of a general formula. No one general formula, however, worked for all analyses, and given the available evidence, there was no way to tell which formula best represented reality.

The second obstacle was, ironically, put forth in the solution to the first. JOHNSEN & GRICE (1999) resolved the issue of the formula for the eudialyte group in an article discussing the results of rigorous structural and chemical analysis of a variety of eudialyte group minerals. In

---

[1] Eudialyte group minerals are, in fact, somewhat beam-sensitive, owing to their high sodium content and an easily damaged structure. The latter property is alluded to in the group name, which comes from the Greek, ευδιαλυτος, meaning *easily decomposed*, referring to the ease of dissolving the mineral even in hydrochloric acid, in spite of it being a silicate. (Gaines *et al.* 1997)

their work, they proposed a recalculation scheme and compared structural formulæ derived using this scheme with those generated from single-crystal X-ray structural analyses of the same specimens. The formulæ from the recalculation scheme were, for the most part, good approximations of the X-ray-derived structural formulæ, but there were some systematic mismatches, a few rather serious, that needed resolution.

Site-occupancy is not random, at least not on the scale of a macroscopic crystal. There must be a mechanism that determines the destination of a particular element in a crystal structure. If the mechanism itself is not revealed, the effects it has can be and they can be systematically described. This was the unintended consequence of this examination of eudialyte group minerals: the creation of an alternative site-assignment algorithm that could address these mismatches and that could subsequently be applied to the analyses from the author's original study.

This, then, brings the story full circle to the eudialyte group minerals at Mont Saint-Hilaire. As analysis progressed on the eudialyte group specimens, it became clear that there was a far greater range of compositional variation than had previously been seen at Mont Saint-Hilaire. (*q.v.* Mandarino & Anderson 1989; Johnsen *et al*. 1999a; Johnsen *et al*. 1999b; Johnsen *et al*. 2003b; Grice & Gault 2006) By obtaining reasonable structural formulæ for eudialyte group minerals from Mont Saint-Hilaire from the alternative algorithm, several potential new members of the eudialyte group have been discovered, and the knowledge of the compositional variation of eudialyte at Mont Saint-Hilaire has been extended.

PREVIOUS WORK

HISTORICAL PERSPECTIVE

Work on the eudialyte group began with STROMEYER (1819), in a report that catalogued the discovery of the mineral (eudialyte *sensu stricto*) at the Ilímaussaq complex in Greenland. Until the late 1990s, there existed several formulæ for "eudialyte," then considered a single mineral, rather than a mineral group. Consider the following selected examples:

(Mandarino & Anderson 1989)	$Na_4(Ca,Ce,Fe)_2ZrSi_6O_{17}(OH,Cl)_2$
(Khomyakov 1995)	$Na_4Ca_2FeZrSi_{8+x}(O,OH,Cl)_{24+y}$
(Coulson & Chambers 1996)	$Na_3(Ca,REE)_2(Fe,Mn)Zr(Si_3O_9)_2(OH,Cl,F)$

These variations on a theme were not so much the result of professional disagreement as of the erstwhile inscrutable complexity of the structure of eudialyte group minerals, as well as of the numerous possible chemical substitutions. The elusiveness of a solution is perhaps best demonstrated by the frequency of studies intended to solve the problem: GIUSEPPETTI *ET AL.* (1971), GOLYSHEV *ET AL.* (1971), HARRIS & RICKARD (1987), RASTSVETAEVA & ANDRIANOV (1987), RASTSVETAEVA & BORUTSKII (1988), RASTSVETAEVA *ET AL.* (1988 & 1990).

The most recent, comprehensive, and successful effort at addressing this issue was put forth by JOHNSEN & GRICE (1999), who coupled single-crystal structure-refinement data with electron microprobe analyses, infrared spectroscopy, optical absorption spectroscopy, and Mössbauer spectroscopy. The simultaneous application of multiple, complimentary analytical techniques to individual eudialyte group specimens of a variety of compositions proved to be crucial to unlocking the secrets of eudialyte group crystal chemistry. The practical drawback to the conclusions of JOHNSEN & GRICE (1999) is that a complete eudialyte group analysis requires both electron microprobe and single-crystal X-ray diffraction data, as the complexity of

substitutions and site-occupancy cannot be completely logically resolved from chemical data alone.

The Eudialyte Nomenclature Subcommittee of the IMA CNMMN revisited the nomenclature of the eudialyte group in an effort to standardize the description and naming of new eudialyte group minerals. (Johnsen *et al.* 2003a)

EUDIALYTE GROUP MINERALS AT MONT SAINT-HILAIRE

Although O'NEILL (1914) catalogued the gross mineralogy of Mont Saint-Hilaire as part of a survey of Mont Saint-Hilaire and Rougemont, robust study of the alkaline minerals of Mont Saint-Hilaire really commenced with the opening of the DeMix quarry (now the western part of the Poudrette quarry) in the 1960s. Studies of the eudialyte group, in particular, can be traced to BOISSONAULT & PERRAULT (1965) who described "eucolite" (eudialyte) from the site. This was followed by more general mineralogical surveys by BOISSONAULT (1966) and CHAO *ET AL.* (1967). These surveys were revisited and updated in MANDARINO & ANDERSON (1989) and HORVÁTH & GAULT (1990), but it was not until the very recent works by JOHNSEN *ET AL.* (1999a; 1999b; and 2003b) and GRICE & GAULT (2006) that new eudialyte group minerals were discovered or described at Mont Saint-Hilaire.

GEOLOGIC SETTING

REGIONAL GEOLOGY

Mont Saint-Hilaire rises above the plain of the Saint Lawrence river valley, near the towns of Beloeil and Saint Jean-sur-Richelieu, about 30 km east of Montréal (Figure 1). It is one

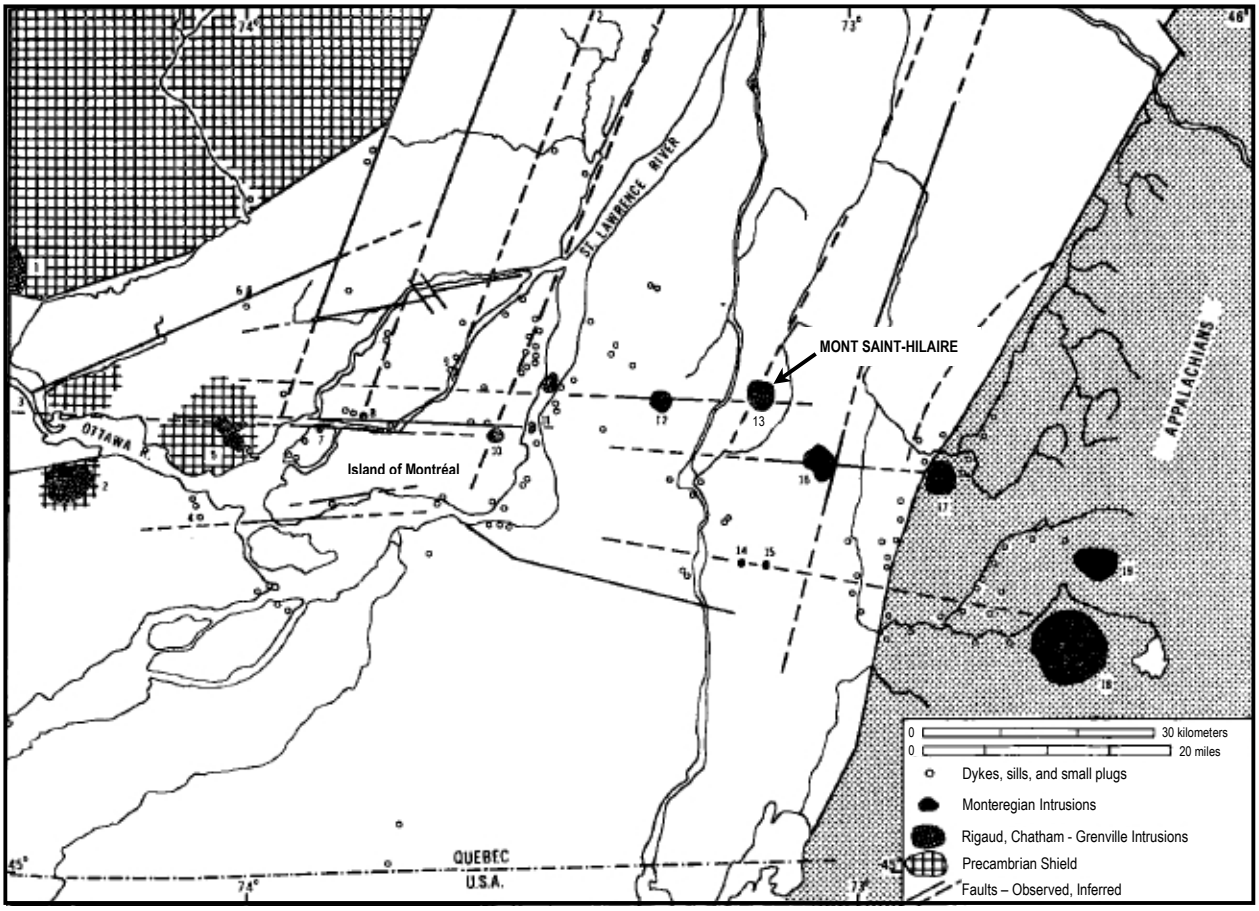

FIGURE 1 – Map of the Monteregian Hills and the Eastern Townships of Québec. Mont Saint-Hilaire is the intrusion labeled "13". (after Philpotts 1970)

of the Monteregian Hills, a series of a dozen-odd fault-controlled Cretaceous age intrusions in the Saint Lawrence lowlands. Mont Saint-Hilaire is the surface expression of a stock that was revealed and made prominent owing to the faster erosion of surrounding sedimentary units. (Philpotts 1970)

Mont Saint-Hilaire and the several intrusions of the Monteregian Hills are associated with the Saint Lawrence rift system (Figure 2), a branched network of failed rift arms that extends for over 2,400 km. The intrusions of the Saint Lawrence rift system are interpreted to share broad genetic characteristics, forming through some combination of partial melting and alkali concentration or desilication, driven by the heat of upwelling mantle material and associated circulation of aqueous fluids. (Currie 1970)

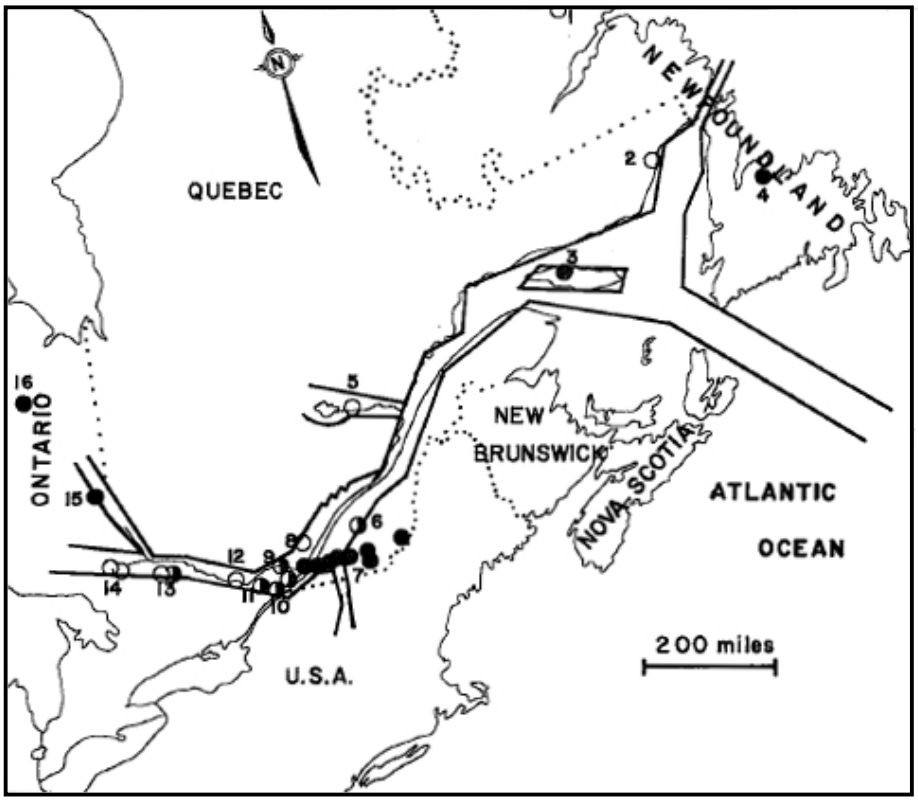

FIGURE 2 – The Saint Lawrence rift system. The Monteregian Hills are the linear trace of filled circles labeled "7". (Currie 1970)

In spite of substantial genetic similarities, the intrusions are neither coeval nor are their lithologies uniform. Alkaline magmatism has intermittently, and semi-regularly, generated intrusions along the rift system over the past 600 Ma. (Kumarapeli & Saull 1966; Doig &

Barton 1968; Currie 1970) Compositions and rock types (with relevant intrusions) are diverse—including carbonatite (Oka), pyroxenite (Rougemont), gabbro (Rougemont, Saint-Hilaire, Saint-Bruno, *et al.*), peridotite (Rougemont, Saint-Bruno, *et al.*), and nepheline syenite (Saint-Hilaire)—to name just a few. (Clark 1955; Philpotts 1976; Currie *et al.* 1986; Gold *et al.* 1986)

Bedrock in the region is Precambrian quartzite and marble with associated masses of granite and gneiss. Overlying strata are composed of Ordovician shales, interbedded with sandstone at depth with limestone and dolostone through the entire succession. Younger strata are not locally present due to erosion and are supplanted by Quaternary overburden (river deposits, varved clay, and glacial sediments). (Wilson 1964)

The igneous rock of Mont Saint-Hilaire contacts grey and red shales, interbedded with dolostone. These sedimentary units are members of the Upper Ordovician Richmond and Lorraine Groups. During magma emplacement, heat transfer from the stock metamorphosed the sedimentary rock forming a biotite-grade hornfels contact zone. Metamorphism is present to about 150 m distance from the contact. (Wilson 1964; Currie *et al.* 1986)

GEOLOGY OF MONT SAINT-HILAIRE

Seen in plan view (Figure 3), Mont Saint-Hilaire has a roughly-equant elliptical outline. Its mean diameter is approximately 2.25 km, and it rises to about 375 m elevation above the surrounding plain. (O'Neill 1914)

Mont Saint-Hilaire is the product of three coaxial intrusions. Although the timing and sequence of these events is not entirely clear, a synthesis of fission-track analyses of apatite and titanite with $^{40}Ar/^{39}Ar$ dates from biotite (Currie *et al.* 1986; Gilbert & Foland 1986) yields an intrusion window of 120-131 ± 9 Ma.

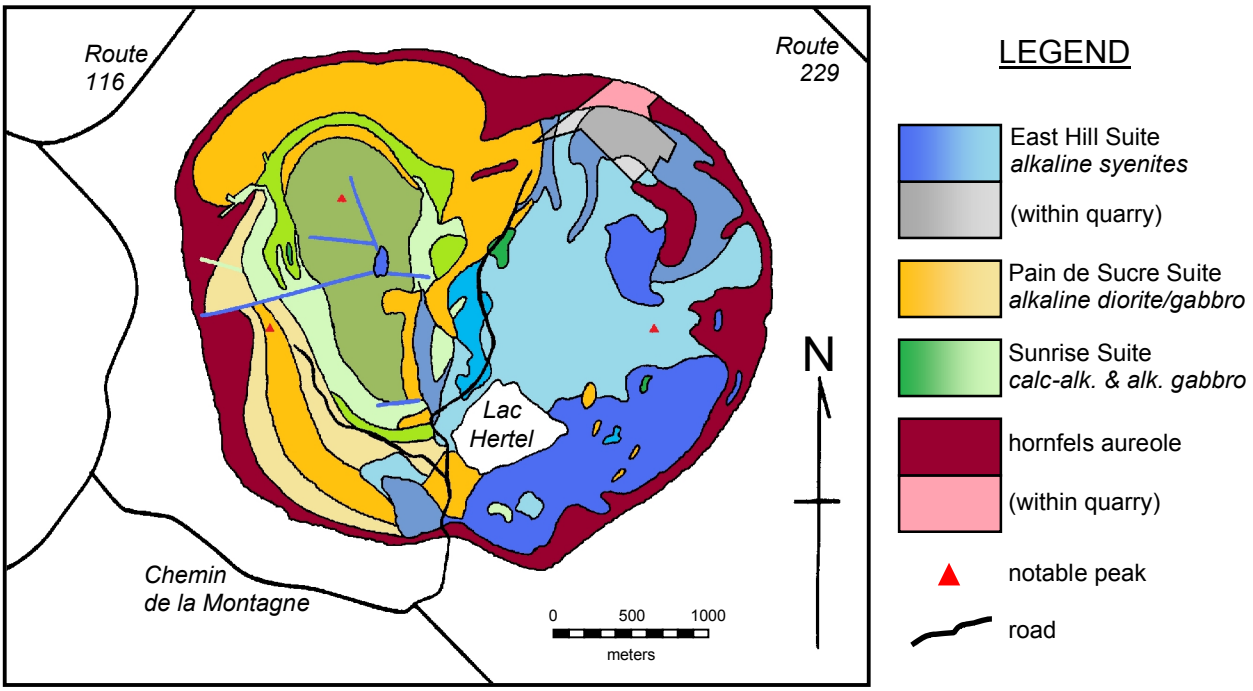

FIGURE 3 – Geologic map of Mont Saint-Hilaire. The light-shaded polygonal area on the north-northeast side of the mountain is the excavation of the Poudrette quarry as of March, 2009. (after Currie 1983)

Each of the three magmas was chemically distinct and yielded its own unique suite of lithologies. The East Hill suite is the most alkaline and is the product of one of the last batches of magma introduced during the formation of the pluton. It is comprised of two series of rock types: older, coarse-grained nepheline- and sodalite-syenites and younger igneous units exhibiting brecciation and flow-banding. (Currie *et al*. 1986)

The East Hill suite may also be the best-exposed group, as well, for it is sectioned to a depth of about 100 m along a several-hundred meter-long drift that defines the working boundaries of the Poudrette quarry. All eudialyte group mineral samples were collected within the Poudrette quarry.

Occurrence of Eudialyte Group Minerals at Mont Saint-Hilaire

Introduction

The occurrence of eudialyte group minerals at Mont Saint-Hilaire is restricted to rocks of the East Hill suite. Previous investigators [whose pre-1990 work is surveyed in Mandarino & Anderson (1989)] have observed East Hill suite eudialyte group minerals in sodalite-bearing syenite, pegmatites, miarolitic cavities, igneous breccia cavities, and, interestingly, marble xenoliths. Several visits by the author to Mont Saint-Hilaire in 1995 and 1997 revealed the prominent occurrence of eudialyte in a previously-undescribed eudialyte-nepheline syenite (hereafter referred to as eudialyte syenite), which is petrologically analogous to the rock type formerly, and currently unfashionably, named *khibinite*. All of the specimens of eudialyte group minerals examined in this study were sampled from eudialyte syenite.

Neither Mandarino & Anderson (1989), nor any other source, mention this rock type or the occurrence therein of eudialyte. Although this is facially surprising, owing to the locally substantial volume observed in the quarry, it truly is not, as frequent blasting and earthmoving may expose, conceal, or destroy smaller outcrops over the course of a few days.

Eudialyte Syenite

The eudialyte syenite is a member of the coarse grained syenites that form the bulk of the volume of the East Hill suite. Although these are interpreted to be, as a group, the older units of the suite (Currie *et al.* 1986), field observations and mineral chemistries (Tice, in prep.) suggest that the eudialyte syenite is a late-stage differentiate of the parental East Hill magma and is one of the last of the coarse-grained lithologies to crystallize. As such, its occurrence is restricted to smaller outcrops and lenses near the center of the suite.

Fundamentally, the eudialyte syenite is a one-feldspar nepheline syenite with major accessory primary zeolites and clinopyroxene. The rock is leucocratic and has an idiomorphic texture. Major phases include microcline, natrolite, aegirine, and sodalite pseudomorphs after nepheline. Minor minerals are members of the pectolite-sérandite series, eudialyte group minerals, albite (almost entirely secondary), and kupletskite.

Descriptive Mineralogy of Eudialyte Group Minerals

The several species are essentially indistinguishable from one another based solely on visual observation, so they are treated collectively in terms of their physical properties. The eudialyte group minerals are found as yellow to reddish brown, anhedral to subhedral (rare euhedral) grains from 0.5 to 5 mm in diameter and as clusters to 3 cm in maximum dimension. They may also occur in vugs, in which a greater proportion of the crystals are euhedral, though otherwise of the same general description. Some such crystals display striations on some faces; this is probably an exhibition of growth hillocks, rather than an expression of a structural feature in the sense of kink-banding in orthopyroxene.

Crystals of eudialyte group minerals have a resinous to splendent vitreous luster, and almost all individuals are gemmy. Crystals that have been altered by late-stage hydrothermal action have a higher degree of opacity and a silky to dull luster. In some such crystals, the color of the crystal changes to a lighter shade of the color of unaltered material or fades away entirely. Catapleiite is the most abundant alteration product.

ANALYTICAL METHODS

SCANNING ELECTRON MICROSCOPY

Background

The scanning electron microscope (SEM) was used for physical examination of microscopic crystals, preliminary phase identification (*via* energy-dispersive X-ray spectroscopy) prior to use of the microprobe, examination of microscopic phase relations, qualitative chemical analyses, and energy-dispersive X-ray mapping of polished sections. SEM analyses were carried out at the University of New Orleans using an AMRAY 1820 Scanning Electron Microscope.

Sample Preparation

Samples for cursory or preliminary mineral identification were examined without substantial preparation. The material was chipped off of the master specimen using either needlepoint tweezers or a small screwdriver and hammer. The sample was then fixed to an aluminum SEM mount using graphite adhesive and coated with an aerosol mist of 2-butoxyethanol. This has proven to be a highly effective alternative to carbon and gold coating for short-term SEM work (Alexander U. Falster, pers. comm.).

Samples for X-ray map generation, for examination prior to electron microprobe analysis, or for imaging of zonation or similar features were prepared as polished mounts.

Operating Conditions

For general specimen examination and imaging, acceleration potential was set at 15 kV, saturation voltage was 5.9 V, and a 300 or 400 μm final aperture was in place. Mineral identification was aided by the use of a Kevex Quantum EDS array. For such work, acceleration

potential was set at 15 kV (25 kV to generate X-rays for Nb, Mo, Pb, Sr, Th, U, Y & Zr; 10 kV for Na), saturation voltage was 6.0 V, and a 400 μm final aperture was in place. To maximize detector efficiency, samples were tilted at an angle of 30º. Patterns were resolved and peaks labeled using an enhanced, PC-resident software package.

X-RAY DIFFRACTOMETRY

Background

X-ray diffractometry (XRD) was employed to confirm or determine the identity of various mineral phases; this technique was used on fragments and single crystals of individual minerals, as well as on fine-grained, polymineralic masses for which physical separation of phases was impractical. XRD analyses were carried out at the University of New Orleans using a Scintag XDS 2000 automated X-ray diffractometer.

Operating Conditions

An X-ray tube emitting CuKα radiation was used at a potential of 40 kV and a current of 20 mA. The scan range was from 2 to 70 degrees-2θ, with a scan increment of 0.02 or 0.04 degrees-2θ and with a dwell time of 1 or 3 to 6 seconds, respectively. Diffraction patterns were processed through the resident software package, which includes a DMS algorithm for smoothing (three to five point smoothing being employed). Patterns were analyzed using the system-resident library and identification program for preliminary identification and were checked *versus* JCPDS standard reference manuals and cards for verification of results.

ELECTRON MICROPROBE ANALYSIS

Background

The electron microprobe (EMP) was used for obtaining quantitative chemical analyses of individual mineral phases. Analyses were done at the University of New Orleans using an ARL SEMQ automated electron microprobe. The microprobe is outfitted with nine wavelength-dispersive X-ray detectors, consisting of six fixed and three tunable detectors. An integral SEM permitted enhanced examination of specimens prior to analysis.

Operating Conditions & Standards

Acceleration potential was set to 20 kV (25 kV for Ba, Hf, Mo, Nb, Sr, Ta, Th, W, Y, Zr & *REE*), with a sample current of 30 nA (measured on brass) and a 2 μm spot size. The following materials [accompanied by the symbol(s) and X-ray line(s) for the relevant element(s)] were used as standards: sodalite ($NaK\alpha_{1,2}$), albite ($NaK\alpha_{1,2}$; $AlK\alpha_{1,2}$), adularia ($KK\alpha_{1,2}$), clinopyroxene ($CaK\alpha_{1,2}$; $FeK\alpha_1$; $SiK\alpha_{1,2}$), synthetic $SrSO_4$ ($SrL\alpha_1$), synthetic $BaSO_4$ ($BaL\alpha_1$), synthetic YPO_4 ($YL\alpha_1$), synthetic TiO_2 ($TiK\alpha_{1,2}$), synthetic ZrO_2 ($ZrL\alpha_1$), synthetic HfO_2 ($HfL\alpha_1$), synthetic $YNbO_4$ ($NbL\alpha_1$), microlite ($TaL\alpha_1$), synthetic $CaMoO_4$ ($MoL\alpha_1$), synthetic $CaWO_4$ ($WM\alpha_1$), rhodonite ($MnK\alpha_1$), fayalite ($FeK\alpha_1$), synthetic ZnO ($ZnK\alpha_1$), fluorite ($FK\alpha_{1,2}$), apatite ($PK\alpha_{1,2}$), labradorite (An_{50}) ($CaK\alpha_{1,2}$; $AlK\alpha_{1,2}$), sillimanite ($AlK\alpha_{1,2}$), synthetic MgO ($MgK\alpha_{1,2}$), synthetic V_2O_5 ($VK\alpha_1$), synthetic ThO_2 ($ThM\alpha_1$), wollastonite ($CaK\alpha_{1,2}$), hematite ($FeK\alpha_1$), synthetic Cr_2O_3 ($CrK\alpha_1$), dolomite ($MgK\alpha_{1,2}$), calcite ($CaK\alpha_{1,2}$), rhodochrosite ($MnK\alpha_1$), synthetic $LaPO_4$ ($LaL\alpha_1$), synthetic $CePO_4$ ($CeL\alpha_1$), synthetic $PrPO_4$ ($PrL\beta_1$), synthetic $NdPO_4$ ($NdL\beta_1$), synthetic $SmPO_4$ ($SmL\beta_1$), synthetic $GdPO_4$ ($GdL\alpha_1$),

synthetic $DyPO_4$ ($DyL\beta_1$), synthetic $ErPO_4$ ($ErL\beta_1$), synthetic $YbPO_4$ ($YbL\alpha_1$), synthetic Gd-Sc-Y oxide ($ScK\alpha_1$), quartz ($SiK\alpha_{1,2}$), and willemite ($ZnK\alpha_1$). Output was processed using an integral enhanced software package to effect ZAF corrections.

Optical Microscopy

Background

Optical microscopes were used for detailed specimen examination and to confirm preliminary mineral identifications made in the SEM. All optical microscopy was done at the University of New Orleans. For hand specimen investigation, an Olympus SZ 60 binocular microscope was used. Examination of thin sections was done on an Olympus BX 60 petrographic microscope, outfitted with a reflected light module.

Photomicroscopy

Photomicrographs were taken as documentary evidence, as well as to illustrate mineralogical features in samples. An Olympus SZ 60 binocular microscope was used for hand specimens. Traditional photomicrographs were taken with an Olympus PM 20 automatic photomicrographic system, using Kodak Gold 100 35 mm film.

A Eudialyte Group Primer

Physical Properties

Members of the eudialyte group range in color from various shades of red through those of brown, orange, and yellow. (Mandarino & Anderson 1989; Gaines *et al.* 1997; Johnsen *et al.* 1999a; Johnsen *et al.* 1999b; Chukanov *et al.* 2003; Johnsen *et al.* 2003b; Khomyakov *et al.*

2003; Petersen *et al.* 2004) They are translucent and have a vitreous, sometimes splendent luster; many individuals exhibit fracturing. This combination of properties allows members of the eudialyte group to be mistaken for a member of the garnet group, especially when abundant. Eudialyte group minerals have a weakly developed conchoidal fracture and exhibit poor cleavage along {0001}. (Mandarino & Anderson 1989)

Optical Properties

Recent work by Johnsen *et al*. (1997) has overturned some long-held conventional thinking about the optical properties of eudialyte group minerals. Whereas eudialyte group minerals were once held to be uniaxial, either positive or negative (*e.g.* Deer *et al*. 1986; Mandarino & Anderson 1989), Johnsen *et al*. (1997) point out that most eudialyte is, at best, pseudouniaxial and, typically, biaxial negative with axial angles up to about 25°. Some samples examined were optically positive, and these consistently exhibited markedly low refractive indices that clustered in a narrow range.

Johnsen *et al*. (1997) find that the measured range of refractive indices of 1.60 to 1.64 is consistent with previously reported values; however, they report that suggestions by Deer *et al*. (1986) relating optical properties to mutual variations in Na and Ca content are without basis. They contend, rather, that the refractive indices in eudialyte are related to substitution of Nb & W for Si and of Sr & *REE* for Na & Ca, these substitutions effecting an increase in mean refractive index. Similarly, substitution of Nb & W for Si is credited with dominating systematic variations in birefringence, but they caution that since this substitution is integral to a change in speciation from eudialyte to kentbrooksite (or to the khomyakovite series, for that matter) there may be other factors, such as subtle structural changes, involved.

CRYSTALLOGRAPHY

Minerals of the eudialyte group are trigonal and are members of space group $R\bar{3}m$, $R3m$, or $R3$. (Johnsen *et al.* 2003a) Crystals in matrix are typically anhedral, but those in vugs or miaroles likely have well-defined faces. Subhedral to euhedral crystals commonly occur as modified rhombohedra, although some specimens may exhibit pseudo-octahedral crystals. (Johnsen *et al.* 2003b) The pinacoid {0001} and the ditrigonal prism $\{10\bar{1}0\}$ or $\{11\bar{2}0\}$ may be present in eudialyte group minerals that crystallize in $R\bar{3}m$ or $R3m$. Other common forms are (for $R\bar{3}m$) the rhombohedron $\{10\bar{1}1\}$ or $\{01\bar{1}1\}$ and the ditrigonal scalenohedron $\{11\bar{2}1\}$; (for $R3m$) the ditrigonal pyramid $\{11\bar{2}1\}$; and (for $R3$) the trigonal pyramid $\{11\bar{2}1\}$. In addition, there are numerous other forms, as yet undetermined numerically. (Mandarino & Anderson 1989; Gaines *et al.* 1997) Axial measurements are generally near 14 Å for *a* and 30 (or 60) Å for *c*; *Z*=3. (Johnsen *et al.* 2003a)

Members of the eudialyte group are cyclosilicates. Viewed along [001], the general structure of eudialyte group minerals (Figure 2) is framed by three- and nine-membered rings of $[SiO_4]^{4-}$ tetrahedra, yielding $[Si_3O_9]^{6-}$ and $[Si_9O_{27}]^{18-}$ groups, respectively. (Giuseppetti *et al.* 1971; Golyshev *et al.* 1971) The $[Si_3O_9]^{6-}$ and $[Si_9O_{27}]^{18-}$ groups are disposed in layers normal to [001]. Two silicate layers are connected across a layer of six-membered *M*(1) rings, themselves interconnected by *M*(2) sites, to form a 2:1 slab (Figure 3). Z sites interconnect these slabs. (Johnsen *et al.* 2003a) The slabs and *Z*-site layers alternate in a fixed pattern that yields a repeating 12-layer sequence (Figure 4). Long channels, whose ends are bounded by $[Si_3O_9]^{6-}$ rings, form up between the second and twelfth layers in the sequence. (Johnsen *et al.* 2003a)

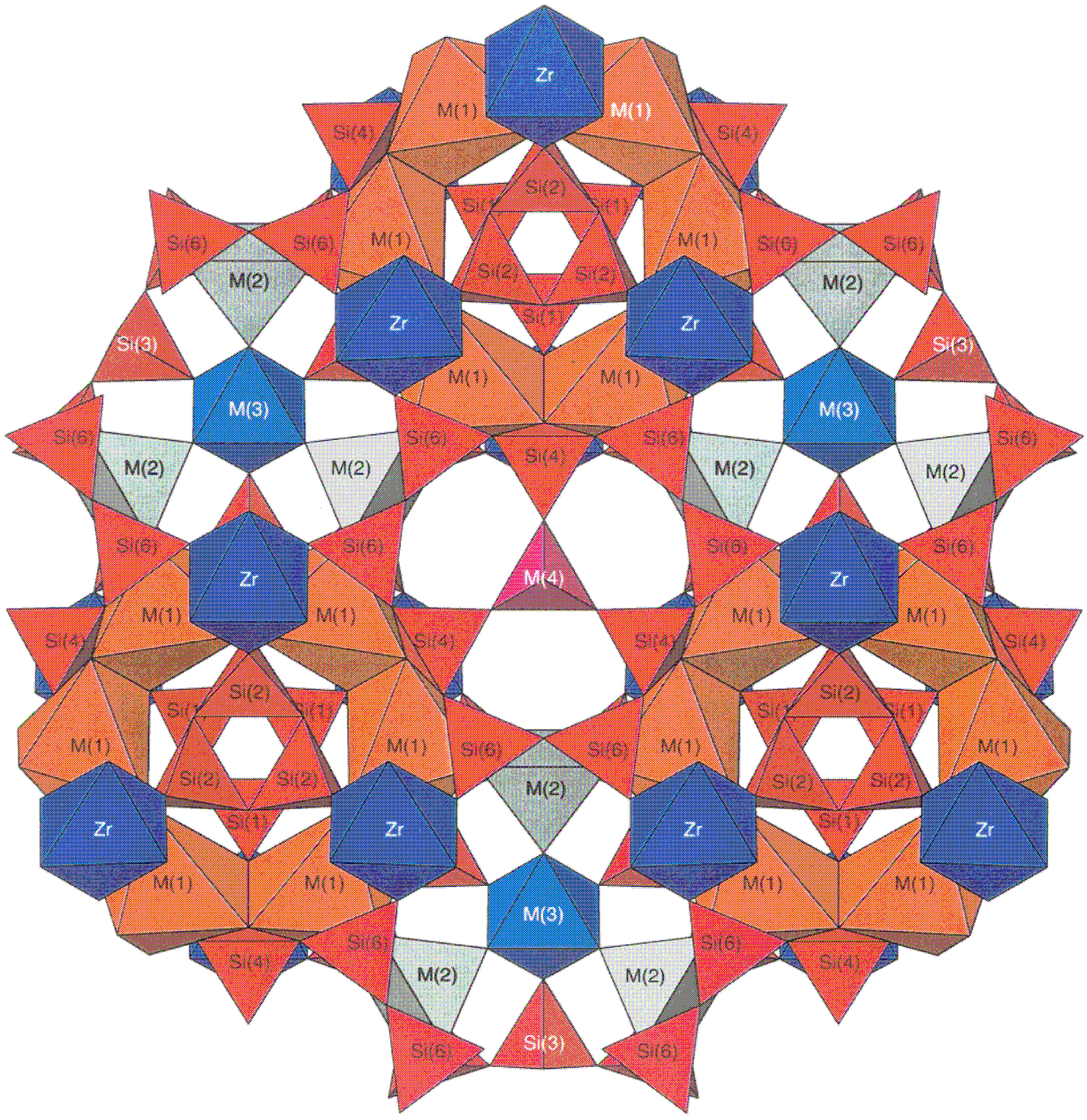

FIGURE 4 – The *R*3m structure of the eudialyte group, viewed along [001], showing the ring structure. *N* sites are omitted for clarity. (Johnsen *et al*. 2003a)

N sites, which align with channels along [110] (Rastsvetaeva *et al*. 1990), are concentrated near *Z*-site layers. Anions in *X* sites concentrate between the 2:1 slabs, and both the *M*(3) and the *M*(4) site are situated at the centers of $[Si_9O_{27}]^{18-}$ rings (Figures 2 & 4). (Johnsen *et al.* 2003a)

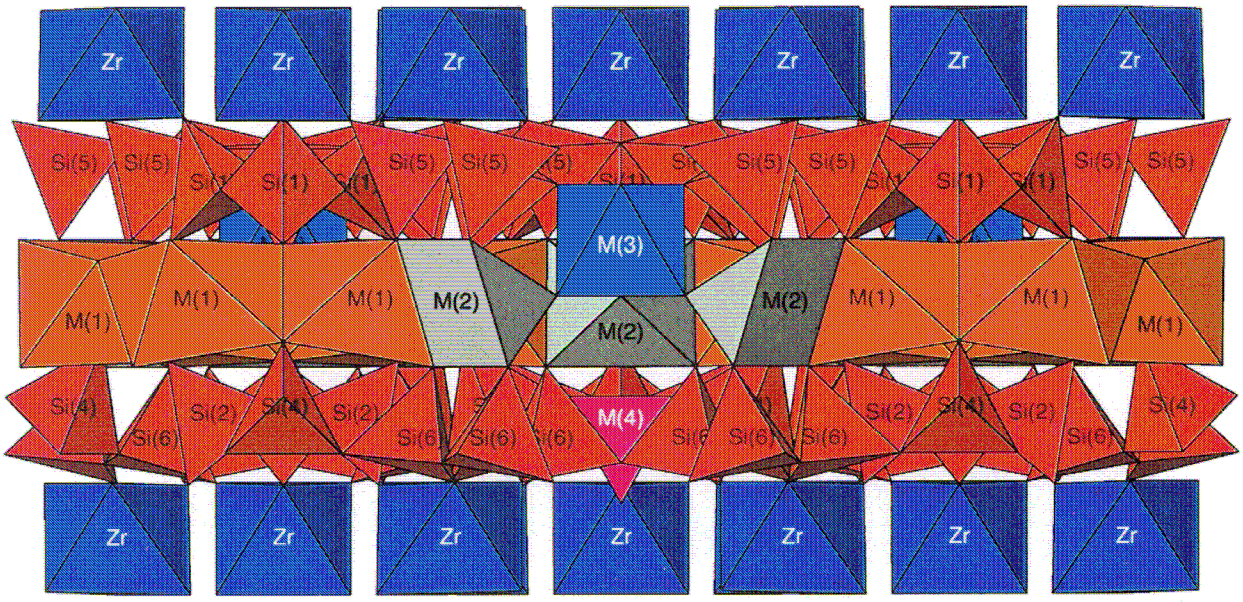

FIGURE 5 – The *R*3m structure of the eudialyte group, viewed along [100], showing the slab arrangement. *N* sites are omitted for clarity. (Johnsen *et al*. 2003a)

CRYSTAL CHEMISTRY

The *N* position (formerly *Na*) is comprised of five sites, *N*(*n*), where *n* = 1 to 5. Sodium is generally the only cation in *N*(1), *N*(2), and *N*(5); these sites are grouped together as *N*(ϕ). Sites *N*(3) and *N*(4) are chemically-equivalent, are notated collectively as *N*(4), and besides Na, incorporate *REE*, Ca, Ba, Sr, and K. (Johnsen & Grice 1999; Johnsen *et al*. 2003a)

The *M*(1) position consists of six sites that are exactly equivalent in eudialyte group minerals with space group *R*3*m*. In eudialyte group minerals belonging to space group *R*3, there are two chemically equivalent, but geometrically distinct, groups of *M*(1) sites. The *M*(1) sites are mainly occupied by Ca, but they will also take up Y, *REE*, Mn^{2+}, and Fe^{2+}. (Johnsen & Grice 1999; Johnsen *et al*. 2003a)

The *M*(2) position includes three sites, two 4-coordinated sites and one 5-coordinated site. Although there are subtle site-preferences for Fe^{2+}, for purposes of determining a formula the

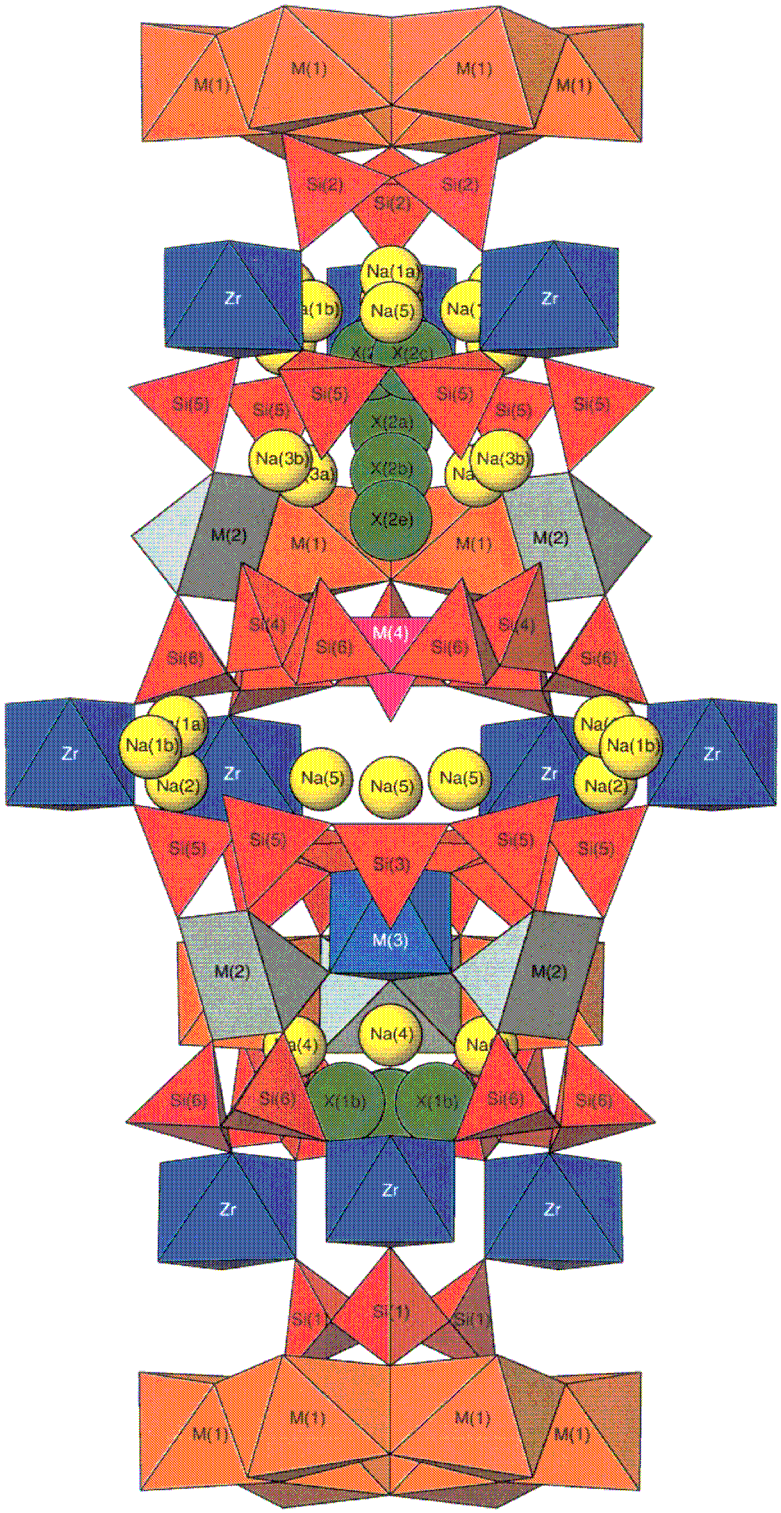

FIGURE 6 – The *R*3m structure of the eudialyte group, viewed approximately along [210], showing the repeating layer structure. (Johnsen *et al*. 2003a)

three sites may be considered chemically equivalent. The *M*(2) sites are the primary hosts of Fe^{2+} and Mn^{2+}, and they are the sole hosts of Mg. Residual Zr, Hf, and Ti that do not fit in other, more-favored sites may be taken up by *M*(2) sites. (Johnsen & Grice 1999; Johnsen *et al*. 2003a)

The *Z* site (formerly *Zr*) is the preferred position for Zr in eudialyte group minerals. It will also host Hf and Ti, and it will incorporate residual Nb, Ta, and W. (Johnsen & Grice 1999; Johnsen *et al*. 2003a)

The existence of the *M*(3) site is dependent on the symmetry of the particular eudialyte group mineral in question. In eudialyte group minerals with space groups *R*3*m* and *R*3 (noncentrosymmetric), *M*(3) is present as an octahedrally coordinated site. As the overall chemistry shifts such that disorder in *M*(3) and *M*(4) (formerly *Si*(7), *q.v.*) is dominant, the symmetry shifts to the centrosymmetric space group $R\bar{3}m$, and the *M*(3) site degenerates to a second tetrahedrally-coordinated *M*(4) site. (Johnsen & Grice 1999) Although this is noted for the sake of completeness, this distinction will be impossible to make in analyses lacking single-crystal structure refinements. *M*(3) is the primary host of Nb and W. Substituent Si, Zr, Hf, Ti, and Ta may also be found. (Johnsen & Grice 1999; Johnsen *et al*. 2003a)

The *Si* position is comprised of 25 sites, 24 of which are equivalent (Si_{24}) and which exclusively contain Si. The other site, once named *Si*(7), now referred to as *M*(4), will also incorporate Al. (Johnsen & Grice 1999; Johnsen *et al*. 2003a)

The *O* position is comprised of 4 sites that contain O, OH, and H_2O. Comparison of the eudialyte group formulæ from JOHNSEN & GRICE (1999) and JOHNSEN *ET AL*. (2003a) reveals that one of these sites is likely filled by an O from the silicate portion of the structure.

The *X* position is an anionic site group and consists of two sites. They host Cl, F, and OH, but they may also take up H_2O. (Johnsen & Grice 1999; Johnsen *et al.* 2003a)

JOHNSEN & GRICE (1999) proposed the following general formula for the eudialyte group:

$$Na_{15}[M1]_6[M2]_3Zr_3[M3](Si_{25}O_{73})(O,OH,H_2O)_3X_2$$

The chemical symbols for sodium, zirconium, and silicon are shown in italics for the purposes of this discussion to distinguish them as representing structural sites, rather than chemical elements. As of 1999, there existed five members in the eudialyte group. By 2003, there were seventeen, and these new compositions introduced chemical substitutions that necessitated a revised general formula (Johnsen *et al*. 2003a):

$$[N(1)N(2)N(3)N(4)N(5)]_3[M(1a)M(1b)]_3M(2)_3M(3)M(4)Z_3[Si_{24}O_{72}]O_4X_2$$

This formula accounts for chemical and structural preferences at different sites within a site group. It may be written in a simplified fashion thussly:

$$N_{15}M(1)_6M(2)_3M(3)M(4)Z_3[Si_{24}O_{72}]O_4X_2$$

This truly is a general formula, as each atomic position may be comprised of up to five discrete sites, each of which may exhibit individual stereochemical and bond-valence preferences.

NOMENCLATURE

The eudialyte group is currently comprised of twenty members (Table 1). There does not, as yet, exist a formal system of subdivision nor of diagrammatic compositional presentation. Unless referenced otherwise to reflect subsequent updates, the tabulated names and formulæ of eudialyte group members are those defined in the final report of the IMA CNMMN Eudialyte Nomenclature Subcommittee. (Johnsen *et al.* 2003a)

It should be noted that there are several instances of "new" eudialyte group minerals (*e.g.* Rastsvetaeva *et al*. 2006) that attain the status of peer-reviewed description prior to being

TABLE 1 – Members of the eudialyte group.

alluaivite	$Na_{19}(Ca,Mn)_6(Ti,Nb)_3Si_{26}O_{74}Cl \cdot 2\ H_2O$
aqualite	$(H_3O)_8(Na,K,Sr)_5Ca_6Zr_3Si_{26}O_{66}(OH)_9Cl$
carbokentbrooksite (Khomyakov *et al.*, 2003)	$(Na,\square)_{12}(Na,Ce)_3Ca_6Mn_3Zr_3Nb(Si_{25}O_{73})(OH)_3(CO_3) \cdot H_2O$
eudialyte	$Na_{15}Ca_6Fe_3Zr_3Si(Si_{25}O_{73})(O,OH,H_2O)_3(Cl,OH)_2$
feklichevite (Pekov *et al.* 2001)	$Na_{11}Ca_9(Fe^{3+},Fe^{2+})_2Zr_3Nb[Si_{25}O_{73}](OH,H_2O,Cl,O)_5$
ferrokentbrooksite	$Na_{15}Ca_6Fe_3Zr_3Nb(Si_{25}O_{73})(O,OH,H_2O)_3(F,Cl)_2$
georgbarsanovite (Khomyakov *et al.* 2005)	$Na_{12}(Mn,Sr,REE)_3Ca_6Fe_3^{2+}Zr_3NbSi_{25}O_{76}Cl_2 \cdot H_2O$
golyshevite (Chukanov *et al*. 2005)	$(Na,Ca)_{10}Ca_9(Fe^{3+},Fe^{2+})_2Zr_3NbSi_{25}O_{72}(CO_3)(OH)_3 \cdot H_2O$
ikranite (Chukanov *et al.* 2003; Rastsvetaeva & Chukanov 2003)	$(Na,H_3O)_{15}(Ca,Mn,REE)_6Fe_2^{3+}Zr_3(\square,Zr)(\square,Si)Si_{24}O_{66}(O,OH)_6Cl \cdot n\,H_2O,\ 2 < n < 3$
johnsenite-(Ce) (Grice & Gault 2006)	$Na_{12}(Ce,La,Sr,Ca,\square)_3Ca_6Mn_3Zr_3W(Si_{25}O_{73})(CO_3)(OH,Cl)_2$
kentbrooksite	$Na_{15}Ca_6Mn_3Zr_3Nb(Si_{25}O_{73})(O,OH,H_2O)_3(F,Cl)_2$
khomyakovite	$Na_{12}Sr_3Ca_6Fe_3Zr_3W(Si_{25}O_{73})(O,OH,H_2O)_3(Cl,OH)_2$
labyrinthite (Khomyakov *et al.* 2006b)	$(Na,K,Sr)_{35}Ca_{12}Fe_3Zr_6TiSi_{51}O_{144}(O,OH,H_2O)_9Cl_3$
manganokhomyakovite	$Na_{12}Sr_3Ca_6Mn_3Zr_3W(Si_{25}O_{73})(O,OH,H_2O)_3(Cl,OH)_2$
mogovidite (Chukanov *et al*. 2005)	$Na_9(Ca,Na)_6Ca_6(Fe^{3+},Fe^{2+})_2Zr_3\square Si_{25}O_{72}(CO_3)(OH,H_2O)_4$
oneillite	$Na_{15}Ca_3Mn_3Fe_3Zr_3Nb(Si_{25}O_{73})(O,OH,H_2O)_3(OH,Cl)_2$
raslakite (Chukanov *et al.* 2003)	$Na_{15}(Ca_3Fe_3)(Na,Zr)_3(Si,Nb)(Si_{25}O_{73})(OH,H_2O)_3(Cl,OH)_2$
rastsvetaevite (Khomyakov *et al.* 2006a)	$Na_{27}K_8Ca_{12}Fe_3Zr_6Si_{52}O_{144}(O,OH,H_2O)_6Cl_2$
taseqite (Petersen *et al.* 2004)	$Na_{12}Sr_3Ca_6Fe_3Zr_3NbSi_{25}O_{73}(O,OH,H_2O)_3Cl_2$
zirsilite-(Ce) (Khomyakov *et al.* 2003)	$(Na,\square)_{12}(Ce,Na)_3Ca_6Mn_3Zr_3Nb(Si_{25}O_{73})(OH)_3(CO_3) \cdot H_2O$

officially named. With no suggestion of disparaging the quality or validity of these investigations, such minerals are excluded from this tabulation; only eudialyte group minerals that have attained full named status are included.

RECALCULATION OF ANALYSES

INTRODUCTION

Recalculating microprobe analyses for members of the eudialyte group proved to be a project in and of itself. Although the number of analyzed elements is no greater than that in a typical amphibole group analysis, the issue of site assignment is not nearly so straightforward. This is, in fact, a subject of some historical debate that has only been recently clarified, though at the expense of simplicity.

A COMPARISON OF PUBLISHED SCHEMES

In recognition of the frequency with which chemical data will be the sole basis for developing a formula, JOHNSEN & GRICE (1999) propose two recalculation schemes for eudialyte group minerals. The first is an anionic scheme in which the formula is recalculated to 78 anions ($Z = 3$) per formula unit. This system, however, has the limitation that it relies on an analysis of H_2O to yield reliable results.

The second scheme is based on recalculating to 29 cations ($Z = 3$) per formula unit, strictly considering site-occupancy in the three Z sites, $M(3)$, the 24 equivalent Si sites, and $M(4)$. This system produces results that are quite reliable, and it can be used with electron microprobe data alone, but it falters in two respects: 1) it does not account for unusual substitutions of elements (in particular, Al, Ti & Zr) outside of their normal sites and 2) it does not account for vacancies in $M(3)$. (Johnsen & Grice 1999)

During the course of this work, the 17 analyses discussed in JOHNSEN & GRICE (1999), which were recalculated by the anionic scheme and which were supplemented with single-crystal structure refinement data, were crosschecked using the cationic scheme, as the latter scheme is

more amenable to the data of this study. In doing so, shortcomings in the cationic recalculation scheme appeared, in addition to the two aforementioned that were addressed by JOHNSEN & GRICE (1999):

1) a ubiquitous positive difference in Na *apfu* in recalculated microprobe data relative to structural data
2) frequent, substantial vacancies (*ca.* 0.5-1.0 out of 3.0 *apfu*) in *M*(2)
3) concomitant inaccuracy in the partitioning of Mn between *M*(1) & *M*(2)
4) further variability in site-occupancy by Nb & Hf

A NOVEL SITE-ASSIGNMENT ALGORITHM

Introduction & Purpose

The original impetus to create an alternative recalculation scheme was based on the fact that most mineralogical and petrological studies do not rely extensively on single-crystal X-ray analyses of mineral phases, even for the purposes of phase identification, let alone chemical analyses. For reasons of expediency, budgetary constraints, or instrumental limitations, most such studies rely largely on electron microprobe data for chemical analysis of mineral phases.

With this practical consideration in mind, and in order to attempt to mitigate the recalculation problems of the cationic scheme that were noted by JOHNSEN & GRICE (1999) and by this study, an alternative recalculation and site-assignment scheme was developed. Based on the cationic scheme of JOHNSEN & GRICE (1999), it yields formulæ that, compared to that cationic scheme, are much more comparable to those obtained using site-scattering, bond-valence sum, and valence sum data. An X-ray-based structural analysis is still required for a truly precise formula for a eudialyte group mineral; however, this modified system provides a highly accurate

analysis that can stand as-is for more general studies or can winnow out analyses that straddle compositional boundaries for further X-ray examination, thus streamlining that process, as well.

General Description

The system was reverse-engineered by comparatively examining the structural formulæ and corresponding chemical analyses given in JOHNSEN & GRICE (1999) and setting up a logic tree that filtered elements in such a way that recalculated analyses made a better fit to structural data.

This logic tree can be visualized in its entirety as a priority matrix (Table 2). The vertical position of elements in the matrix denotes logical priority within a site. Superscript Roman numerals denote the actual chemical preference of a site to that element; bold-face type and the lack of a Roman numeral indicate that that is the sole site for that element.

TABLE 2 – Site-assignment priority matrix for the alternative algorithm.

Si$_{24}$	*M*(4)	*M*(3)	*Z*	*M*(2)$_3$	*M*(1)$_6$	*N*$_{15}$
Si^{I}	**Al**	Si^{III}	Zr^{I}	Fe^{I}	**Y**	**Sr**
	Si^{II}	Nb^{I}	Nb^{II}	Mn^{II}	Ca^{I}	**Ba**
		Ta^{I}	Ta^{II}	**Mg**	REE^{II}	**K**
		W^{I}	W^{II}	Zr^{III}	Mn^{I}	**Na**
		Hf^{II}	Hf^{I}	Hf^{III}	Fe^{II}	REE^{I}
		Ti^{II}	Ti^{I}	Ti^{III}		Ca^{II}
		Zr^{II}				

As noted above, the scheme is based on the concept that each element holds a certain logical priority within a given site. This priority does not have so much to do with actual bonding or steric preferences as it does with improving the approximation of microprobe data to observed X-ray structural data and satisfying the realities of structural formulæ.

For example, Na is low in line in terms of logic-priority in its own site, but this is because the elements that are higher in priority in the *N* site (Sr, Ba & K) do not have another home in the structure. As another example, Al must enter the *M*(4) site first so that there is room for it, and so that excess Si may then be partitioned to the remaining 24 *Si* sites (and to *M*(3) if necessary).

Similarly, a given site has priority with respect to a particular element. For example, *M*(1) is a higher logic-priority site for Mn than is *M*(2)—that is, Mn tries to enter *M*(1) first. This is in marked contrast to the scheme of JOHNSEN & GRICE (1999), in which the reverse is the case, being based on actual chemical preferences [Mn is partitioned preferentially to *M*(2)], rather than preferences based on a reverse-engineered logic table.

The Algorithm

The priority matrix translates into a step-wise system of site assignment. Obviously, recalculations may be accomplished by hand using this system, but for ease of repetitive use, it was programmed into an automated Excel spreadsheet:

1) Use the empirical formula $N_{15}M(1)_6M(2)_3Z_3M(3)M(4)(Si_{24}O_{72})O_4X_2$
2) Calculate the *apfu* based on 29 cations (Σ Si + Al + Zr + Ti + Hf + Nb + W + Ta) with $Z = 3$. Make all Fe and Mn divalent.
3) Add Si to Al to sum to 1 *apfu* in *M*(4). Add excess Si first to Si_{24}, then to *M*(3).

4) Assign Zr to *Z* up to 3 *apfu*. Assign excess Zr according to the priority matrix. That is, excess Zr may enter *M*(3) first, but some to all of it may then be bumped to *M*(2) to make room for Si, Nb, Ta, or W, all of which have higher logical priorities within *M*(3).
5) If there is room, assign Hf to *Z* up to 3 *apfu* total (Zr + Hf). As with Zr, assign excess to *M*(3) first, then *M*(2). Hf may be bumped, just as may Zr.
6) If there is room, assign Ti to *Z* up to 3 *apfu* total (Zr + Hf + Ti). As with Zr and Hf, assign excess to *M*(3) first, then *M*(2). Ti may be bumped, just as may Zr and Hf.
7) Assign Nb to *M*(3) up to 1 *apfu* total (Si + Nb). Bump Zr, Hf, and Ti to *M*(2) to make room. Assign excess Nb to *Z*; again, bump Hf, Ti, and Zr (in that order) to make room.
8) Assign Ta to *M*(3) up to 1 *apfu* total (Si + Nb + Ta). Bump Zr, Hf, and Ti to *M*(2) to make room. Assign excess Ta to *Z*; again, bump Hf, Ti, and Zr (in that order) to make room.
9) Assign W to *M*(3) up to 1 *apfu* total (Si + Nb + Ta + W). Bump Zr, Hf, and Ti to *M*(2) to make room. Assign excess W to *Z*; again, bump Hf, Ti, and Zr (in that order) to make room.
10) Assign Fe to *M*(2) up to 3 *apfu*. Assign excess to *M*(1).
11) Assign Mn to *M*(1) up to 6 *apfu*. Assign excess to *M*(2). Note that Mn is second-to-last in the priority matrix for *M*(1), meaning that some of it will be bumped to *M*(2) by Y, Ca, and *REE*.
12) Assign Mg to *M*(2).
13) Let *N*(4) represent the combined sites *N*(3) and *N*(4), as in the case of the structural formulæ for disordered structures. Similarly, let *N*(ϕ) represent the combined sites *N*(1),

N(2), and *N*(5). Excess *REE* may be bumped to *M*(1) upon the addition of Na; this may then result in Mn being bumped to *M*(2).

14) Assign Y to *M*(1). In nature, Y sometimes appears in *N*(4), but in this scheme, Y is forced to remain in *M*(1)—see the discussion for further elaboration.

15) Assign Ca to *M*(1) up to 6 *apfu* total (Ca + Y + *REE* + Mn). Bump Mn to *M*(2) to make room for Ca. If after all the Mn is bumped, there is excess Ca, assign it to *N*(4).

16) Assign (in this order) Sr, Ba, and K to *N*(4).

17) Correct Na to correspond more accurately with formulæ that incorporate structural data (see below for discussion). Let Na* ≡ first corrected Na. Then,

$$Na^* = Na - (K + Ba + Sr + Y + REE + {}^{[N(4)]}Ca)$$

18) Calculate average Na site-occupancy, represented as $\overline{Na}$. Then,

$$\overline{Na} = \frac{Na^*}{5}$$

19) Correct Na to correspond more accurately with the distribution of sodium between *N* sites (see below for discussion). Let $\hat{Na}$ ≡ second corrected Na. Then,

$$\hat{Na} = \left(\frac{K + Ba + Sr + Y + REE + {}^{[N(4)]}Ca}{3}\right)$$

20) Assign Na to *N*(4) according to the following expression,

$${}^{[N(4)]}Na = (2 \times \overline{Na}) - \hat{Na}$$

21) Bump *REE* from *N*(4) to *M*(1) to make room for Na. Bump Mn from *M*(1) to *M*(2) to make room for bumped *REE*.

22) Assign remaining Na to *N*(ϕ).

The remainder of the scheme follows the oxygen, anion, and hydrogen assignment system of JOHNSEN & GRICE (1999).

COMPARATIVE PERFORMANCE OF THE SCHEMES

INTRODUCTION

JOHNSEN & GRICE (1999) present 17 eudialyte group analyses, representing several different eudialyte group members from a variety of locations. They analyzed each sample using an electron microprobe and a single-crystal X-ray diffractometer. The electron microprobe data were recalculated using their cationic site-assignment scheme, and the X-ray data were used to create structural formulæ for each sample.

Since these analyses have both microprobe and structural data from single-crystal study, they form an excellent basis for comparing the performance of the cationic scheme of JOHNSEN & GRICE (1999) and the alternative algorithm described above. Firstly, by using precisely the same raw microprobe data, an exact comparison may be made between the results of the two systems. Secondly, having single-crystal structural analyses of precisely the same samples yields a strong benchmark against which *both* schemes may be measured.

Raw microprobe data from the analyses of JOHNSEN & GRICE (1999) were fed into the alternative algorithm, and the results were both tabulated and plotted to examine difference between the schemes. The schemes were compared on both a site-by-site and an element-by-element basis; so, for example, iron residing in *M*(1) was examined separately from iron residing

in *M*(2). This resulted in 33 plots of site assignments of the major common eudialyte-group cations discussed in the site-assignment algorithm.[2]

RESULTS

Statistical Significance

Each of the 33 plots of site assignments contained three recalculation results (from the cationic scheme of JOHNSEN & GRICE (1999), the alternative algorithm, and the X-ray data) for each of the 17 samples. Statistical examination of these 1,683 data points revealed, unsurprisingly, that not all of the data are significant.

The significance of the data for each element in each site was established by using the t-test to determine the significance of the correlation coefficient of each recalculation scheme, as measured against the X-ray data. The t-test was used because of the small ($n < 30$) sample sizes. The form of the t-test that is best suited to determining the significance of a correlation coefficient is:

$$t = r\sqrt{\frac{n-2}{1-r^2}}$$

where t is the t-test discriminant, r is the Pearson correlation coefficient, n is the number of samples, and r^2 is the coefficient of determination. The discriminants were compared against the table for the one-tailed t-test at the 95% confidence level. In order to make the most meaningful comparison between the schemes, only data for which the correlation coefficients for both

---

[2] This excludes Si in Si_{24}, as it shows no meaningful variability in occupancy, and Al in *M*(4), as it has but one destination in all three schemes, but it includes *total* Na distributed between *N*(ϕ) and *N*(4).

schemes were significant at the 95% confidence level were deemed useful for further examination.

Correlation coefficients for both site assignment schemes achieved significance at the 95% confidence level for 14 out of the 33 site assignments: Na, Sr, K, Ca, and *REE* in *N*(4); Ca, Mn, and *REE* in *M*(1); Fe and Mn in *M*(2); Zr and Ti in *Z*; and Si and Nb in *M*(3).

Statistical Analysis of the Recalculation Schemes

The cationic scheme of JOHNSEN & GRICE (1999) and the alternative algorithm were both measured on two bases: 1) their coefficient of determination, which established their degree of correlation to the X-ray data (their precision), and 2) their relative deviation, which gauged how closely each site assignment matched that of the X-ray data (their accuracy).

The coefficient of determination was calculated as the square of the Pearson correlation coefficient, *r*, which is given by:

$$r = \frac{n\sum_{i=1}^{n} x_i y_i - \sum_{i=1}^{n} x_i y_i}{\sqrt{n\sum_{i=1}^{n} x_i^2 - \left(\sum_{i=1}^{n} x_i\right)^2}\sqrt{n\sum_{i=1}^{n} y_i^2 - \left(\sum_{i=1}^{n} y_i\right)^2}}$$

where *n* is the number of samples, and *x* and *y* are the individual measurements in the two sample sets.

The relative deviation (which expresses deviations as a percentage of the total possible occupancy of a site) was calculated as:

$$RD = \frac{\bar{d}}{N} \times 100$$

where N equals the maximum *apfu* of a site, and $\bar{d}$, the average absolute deviation is given by:

$$\bar{d} = \frac{\sum_{i=1}^{n} |x_i - y_i|}{n}$$

where n is the number of samples, and x and y are the individual measurements in the two sample sets. Finding the relative deviation gives a more meaningful assessment of accuracy, as a deviation of 0.5 *apfu* is more significant in a site that can only hold 1.0 *apfu* total *versus* a site with a capacity of 6.0 *apfu*.

A perfect recalculation scheme has $r^2 = 1.00$ and $RD = 0.00\%$; the practical goal is to maximize r^2 while minimizing RD.

N(4)

Five plots of site-occupancy for $N(4)$ satisfied the standards of significance: Na, Sr, K, Ca, and *REE* (Figures 5-9).

The alternative algorithm performed dramatically better ($r^2_{J\&G} = 0.41$ *versus* $r^2_{AA} = 0.80$, and $RD_{J\&G} = 24.78\%$ *versus* $RD_{AA} = 5.19\%$) than the cationic scheme at assigning Na to $N(4)$. Site-occupancies, as determined by the cationic scheme, were uniformly too high and were inconsistent with those of the X-ray data.

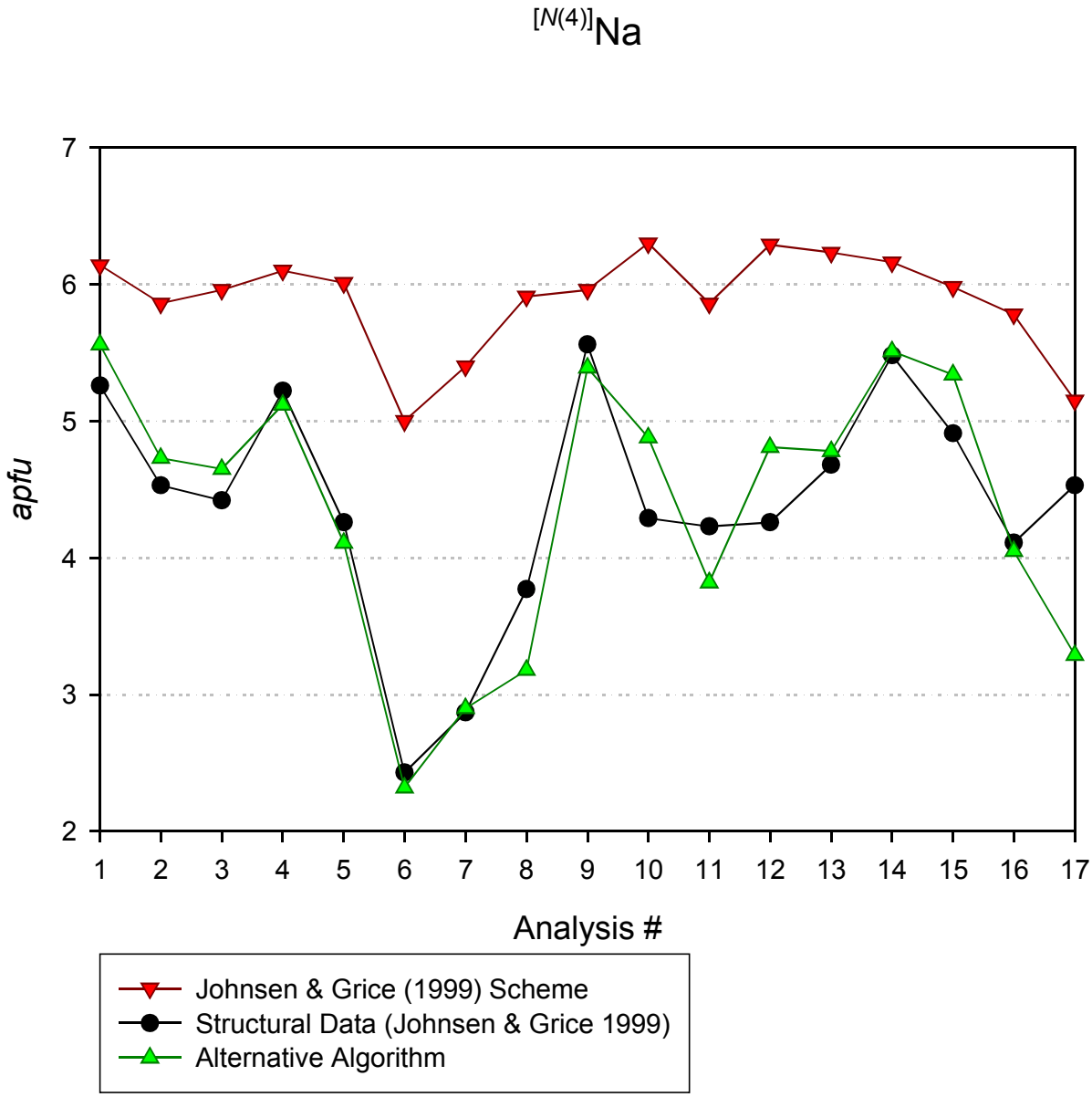

FIGURE 7 – Performance comparison between the recalculation schemes for Na in the *N*(4) site.

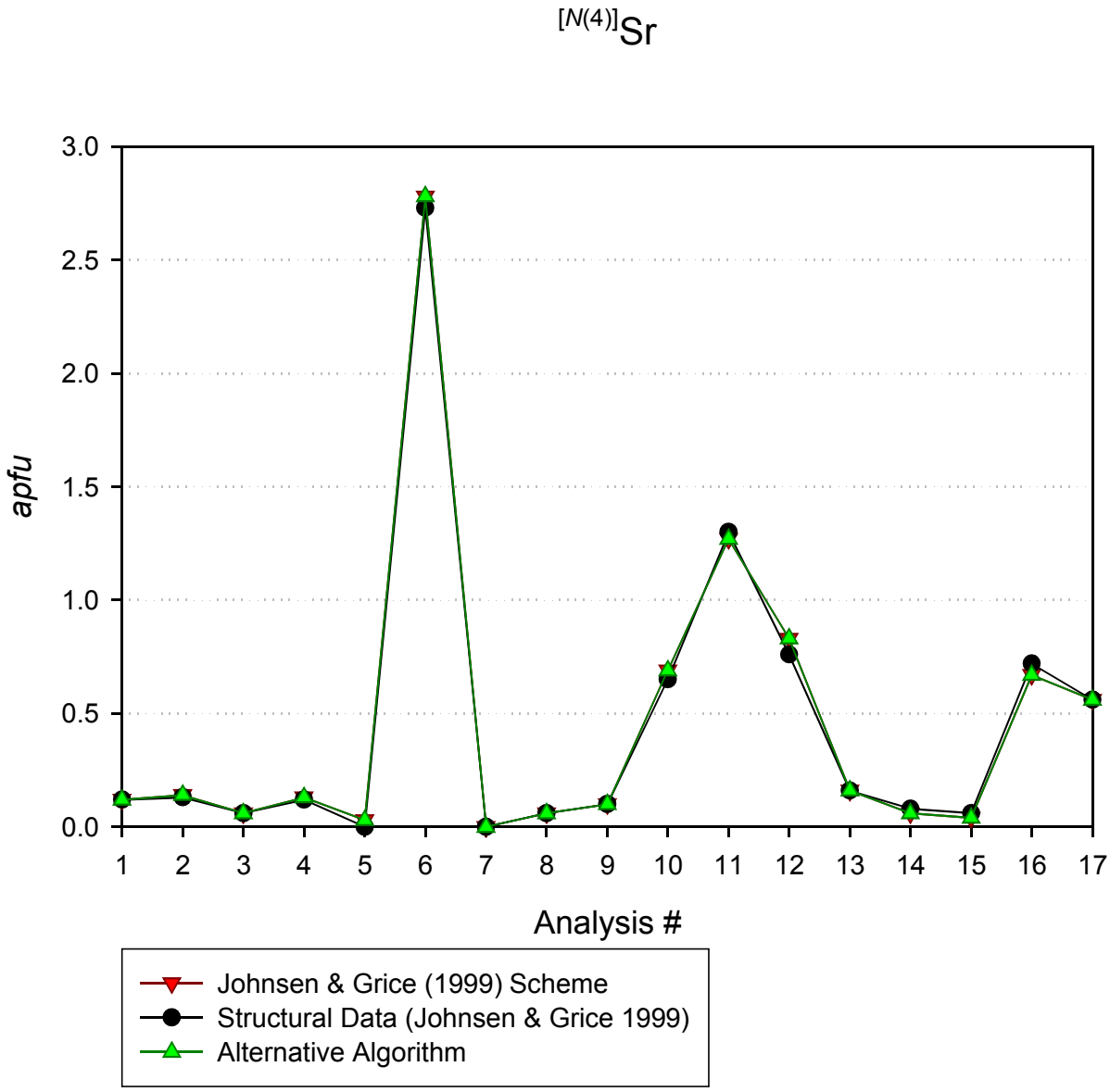

FIGURE 8 – Performance comparison between the recalculation schemes for Sr in the *N*(4) site.

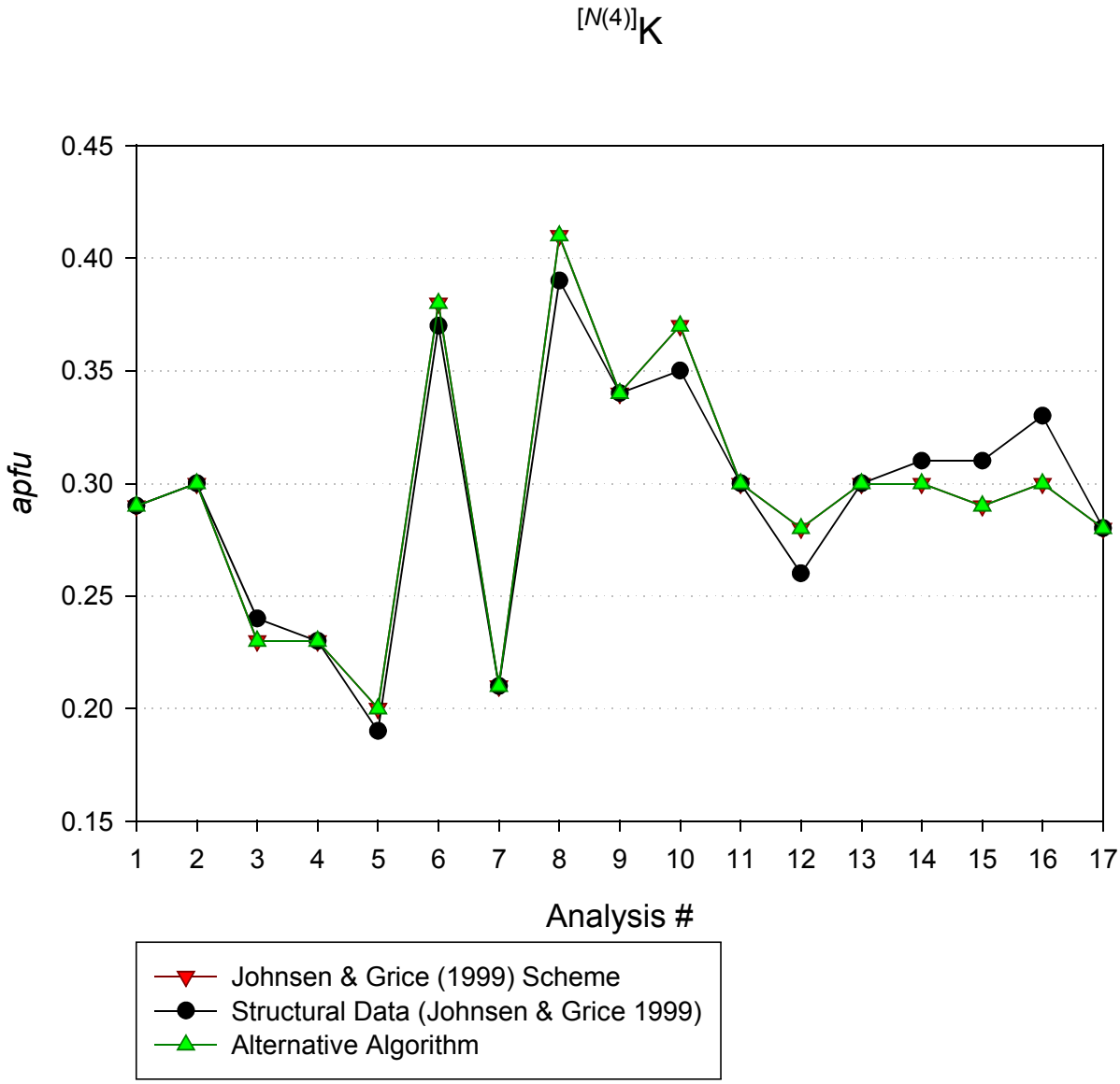

FIGURE 9 – Performance comparison between the recalculation schemes for K in the *N*(4) site.

Both schemes performed equally well in assigning Sr ($r^2_{J\&G} = 1.00$ *versus* $r^2_{AA} = 1.00$, and $RD_{J\&G} = 0.32\%$ *versus* $RD_{AA} = 0.32\%$) and K ($r^2_{J\&G} = 0.95$ *versus* $r^2_{AA} = 0.95$, and $RD_{J\&G} = 0.15\%$ *versus* $RD_{AA} = 0.15\%$) to *N*(4).

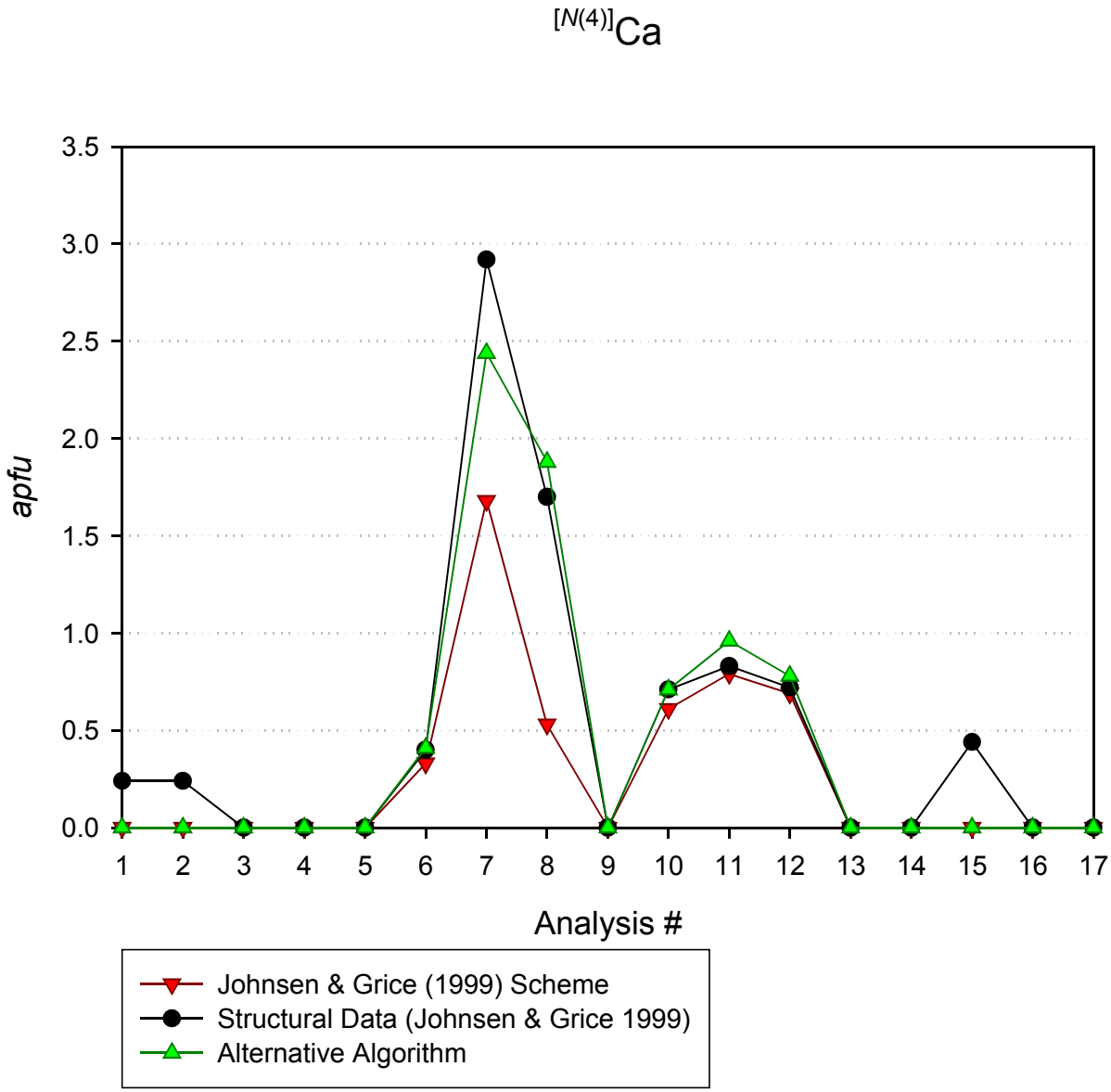

FIGURE 10 – Performance comparison between the recalculation schemes for Ca in the *N*(4) site.

The alternative algorithm was slightly more precise ($r^2_{J\&G} = 0.85$ *versus* $r^2_{AA} = 0.95$) and accurate ($RD_{J\&G} = 3.50\%$ *versus* $RD_{AA} = 1.75\%$) than the cationic scheme in assigning Ca to *N*(4).

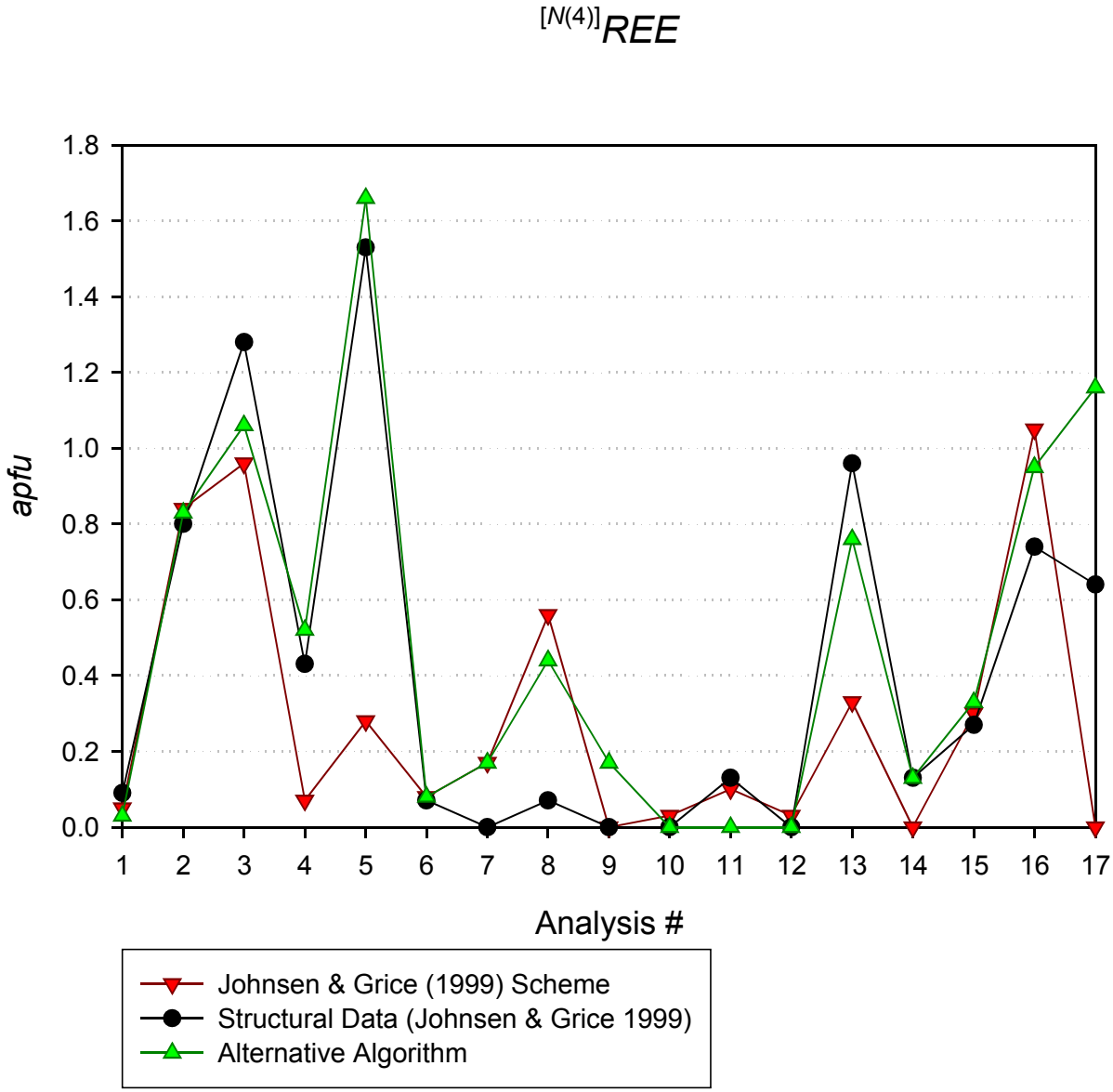

FIGURE 11 – Performance comparison between the recalculation schemes for *REE* in the *N*(4) site.

The alternative algorithm was markedly more precise ($r^2_{J\&G} = 0.32$ *versus* $r^2_{AA} = 0.86$) and slightly more accurate ($RD_{J\&G} = 4.42\%$ *versus* $RD_{AA} = 2.32\%$) than the cationic scheme in assigning *REE* to *N*(4).

M(1)

Three plots of site-occupancy in the *M*(1) site were deemed significant: Ca, Mn, and *REE* (Figures 10-12).

The alternative algorithm was marginally more precise ($r^2_{J\&G} = 0.92$ *versus* $r^2_{AA} = 0.98$) and slightly more accurate ($RD_{J\&G} = 3.80\%$ *versus* $RD_{AA} = 1.83\%$) than the cationic scheme in assigning Ca to *M*(1). The cationic scheme exhibits an interesting excursion from an otherwise good fit to the X-ray data at analysis #6, #7, and #8, in which it assigns the maximum site-occupancy of 6 *apfu* to Ca. The same exclusive assignment of Ca to *M*(1) occurs again for analysis #10, #11, and #12, although in those cases it aligns with the X-ray data.

Both assignment schemes performed essentially equally well ($r^2_{J\&G} = 0.92$ *versus* $r^2_{AA} = 0.94$, and $RD_{J\&G} = 3.69\%$ *versus* $RD_{AA} = 3.37\%$) in assigning Mn to *M*(1). Allocation of Mn in *M*(1) tended to be skewed high against X-ray data for the alternative algorithm and low for the cationic scheme. The cationic scheme and the X-ray data matched particularly well for analysis #6, #7, and #8, both assigning zero Mn to *M*(1), with all three assigning zero Mn for analysis #10, #11, and #12.

The cationic scheme of JOHNSEN & GRICE (1999) was more precise ($r^2_{J\&G} = 0.46$ *versus* $r^2_{AA} = 0.23$) than the alternative algorithm in partitioning *REE* in *M*(1), but the alternative algorithm was slightly more accurate ($RD_{J\&G} = 4.35\%$ *versus* $RD_{AA} = 3.37\%$). Overall, however, neither scheme was particularly good at matching the X-ray data.

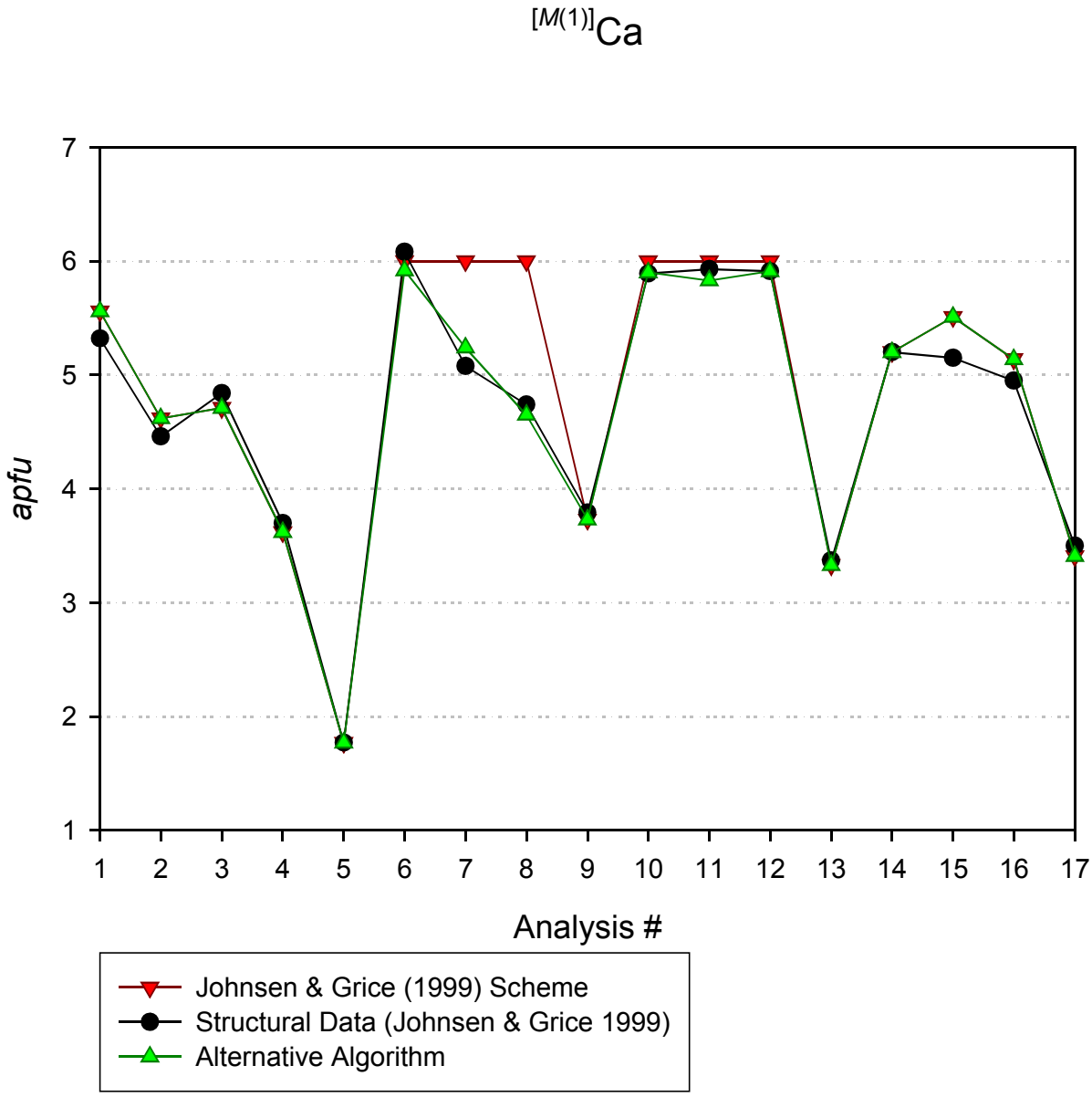

FIGURE 12 – Performance comparison between the recalculation schemes for Ca in the *M*(1) site.

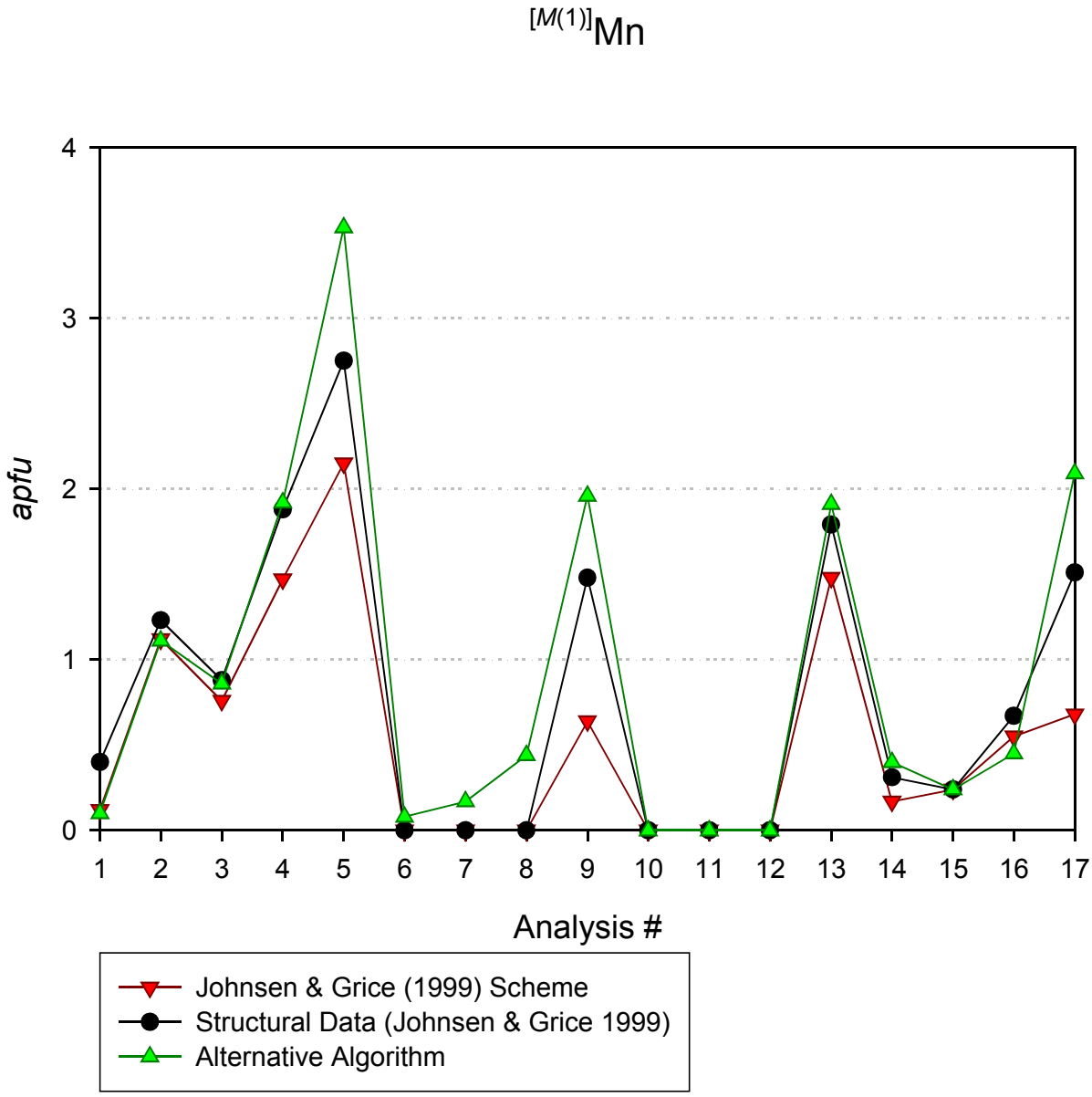

FIGURE 13 – Performance comparison between the recalculation schemes for Mn in the *M*(1) site.

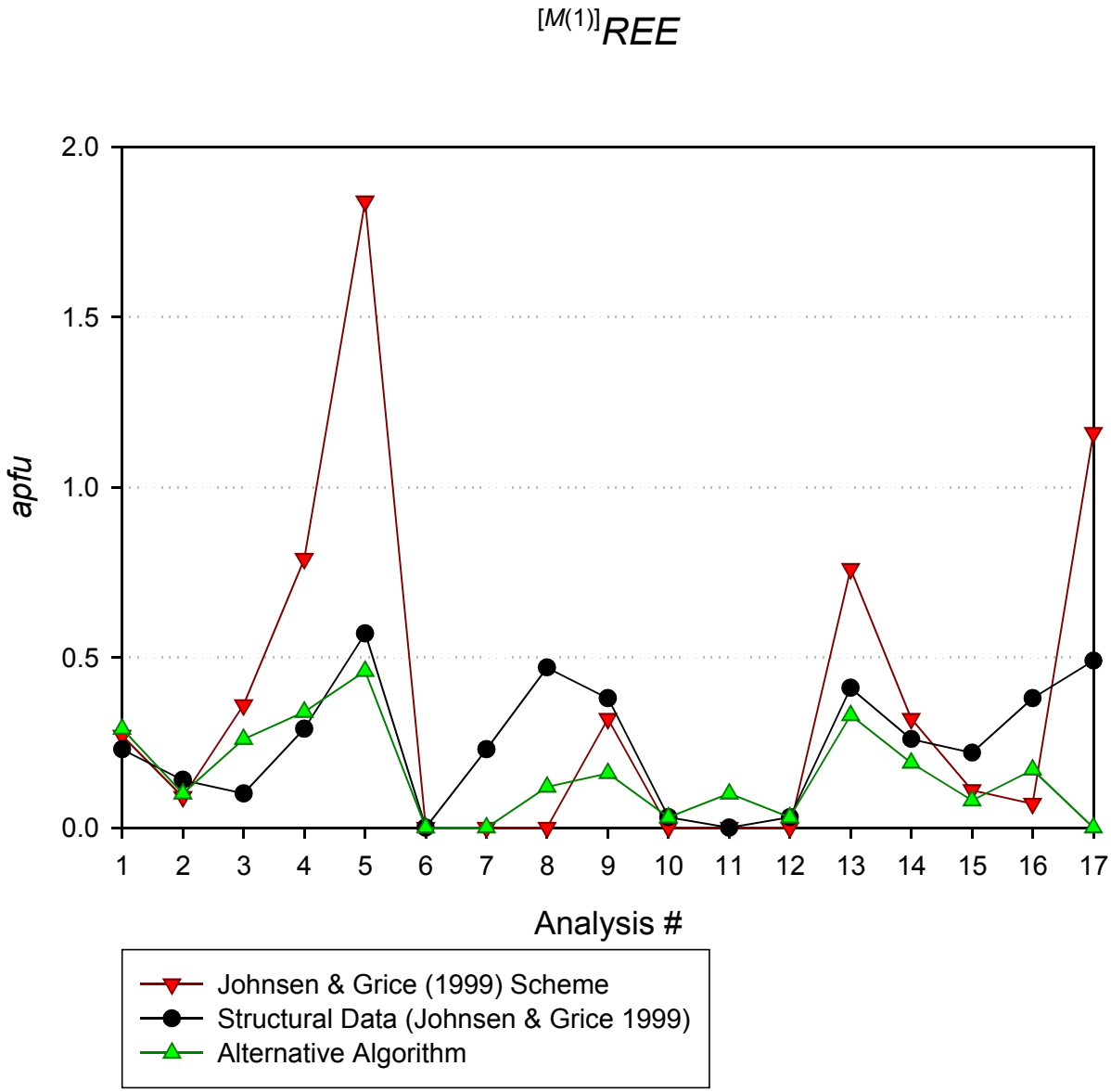

FIGURE 14 – Performance comparison between the recalculation schemes for *REE* in the *M*(1) site.

M(2)

Two plots of site-occupancy for *M*(2) satisfied the standards of significance: Fe and Mn (Figures 13 & 14).

Both site-assignment schemes performed with strikingly equal capability ($r^2_{J\&G} = 0.85$ *versus* $r^2_{AA} = 0.85$, and $RD_{J\&G} = 3.96\%$ *versus* $RD_{AA} = 3.86\%$) in assigning Fe to *M*(2), not only in terms of their coefficient of determination but also in terms of coincidence of assignments. Both schemes showed the same erroneous variance from the X-ray data for analysis #7 and #8.

Both assignment schemes performed essentially equally well ($r^2_{J\&G} = 0.78$ *versus* $r^2_{AA} = 0.83$, and $RD_{J\&G} = 7.98\%$ *versus* $RD_{AA} = 7.75\%$) in assigning Mn to *M*(2). Allocation of Mn in *M*(2) tended to be skewed low against X-ray data for the alternative algorithm and high for the cationic scheme.

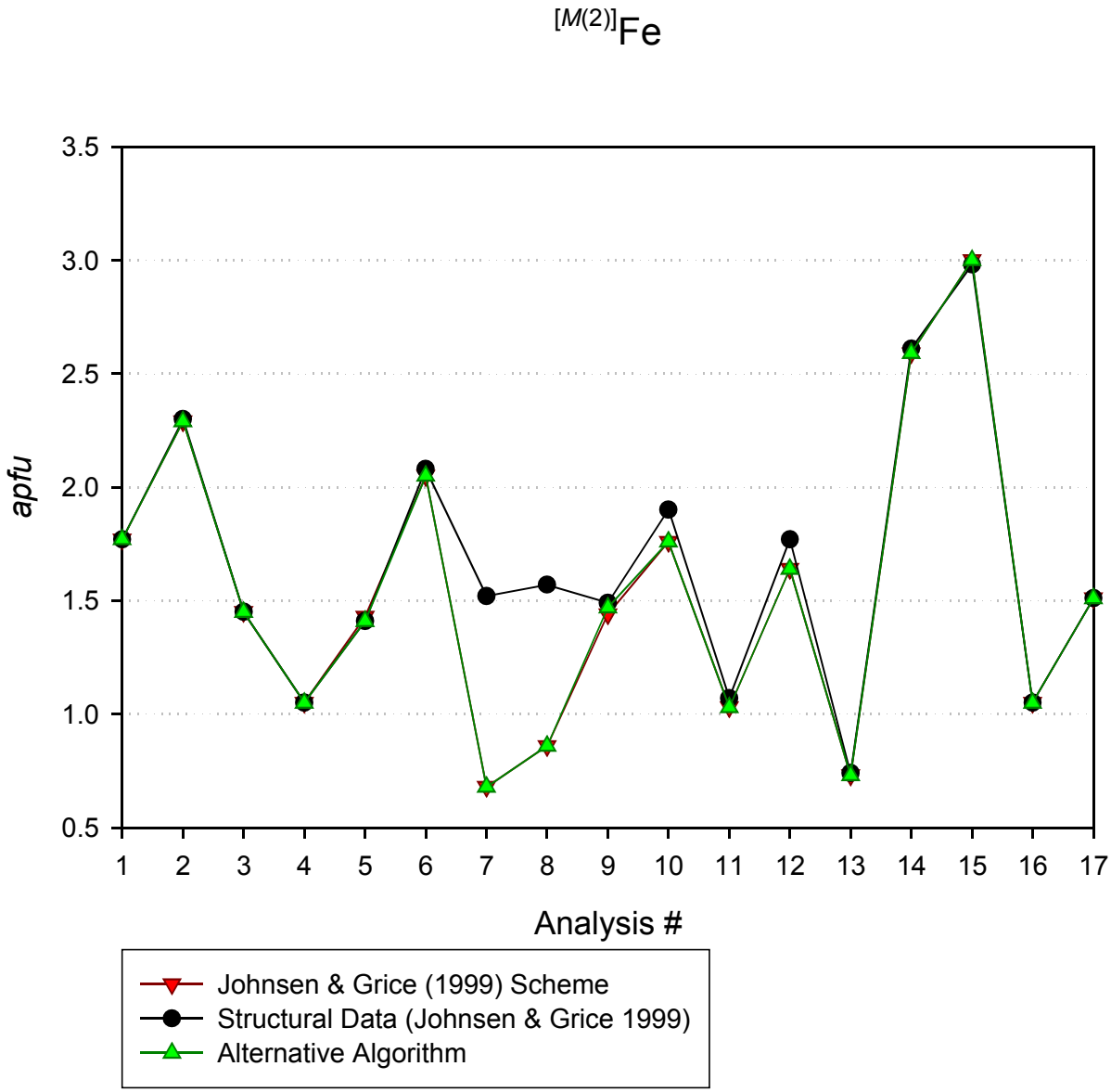

FIGURE 15 – Performance comparison between the recalculation schemes for Fe in the *M*(2) site.

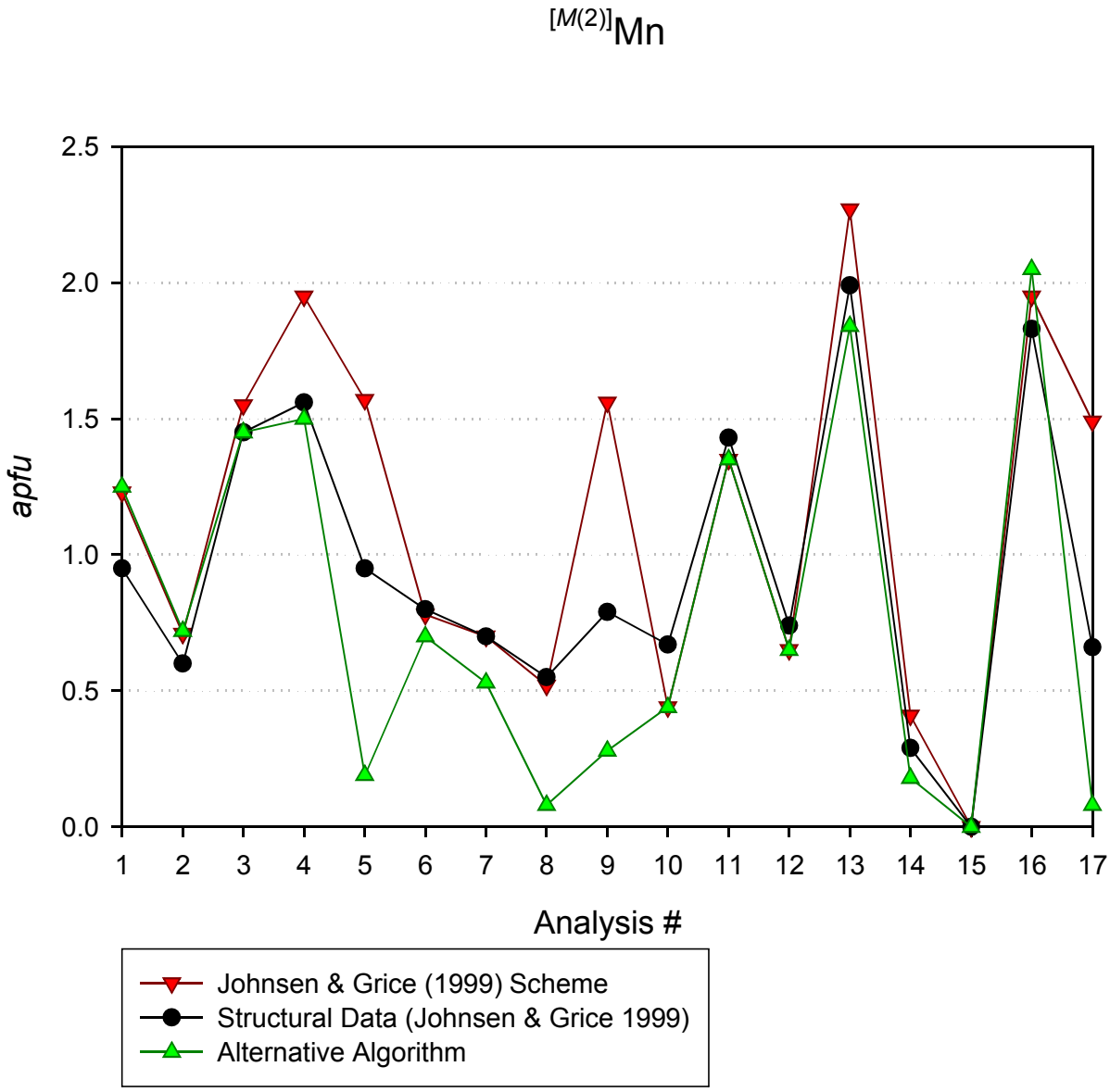

FIGURE 16 – Performance comparison between the recalculation schemes for Mn in the *M*(2) site.

Z

Two plots of site-occupancy for *Z* satisfied the standards of significance: Zr and Ti (Figures 15 & 16).

Both assignment schemes performed essentially equally well ($r^2_{J\&G} = 0.65$ *versus* $r^2_{AA} = 0.70$, and $RD_{J\&G} = 1.94\%$ *versus* $RD_{AA} = 1.69\%$) in assigning Zr to *Z*.

The cationic scheme of Johnsen & Grice did a better job ($r^2_{J\&G} = 0.85$ *versus* $r^2_{AA} = 0.75$, and $RD_{J\&G} = 1.20\%$ *versus* $RD_{AA} = 1.76\%$) than the alternative algorithm at allocating Ti to *Z*.

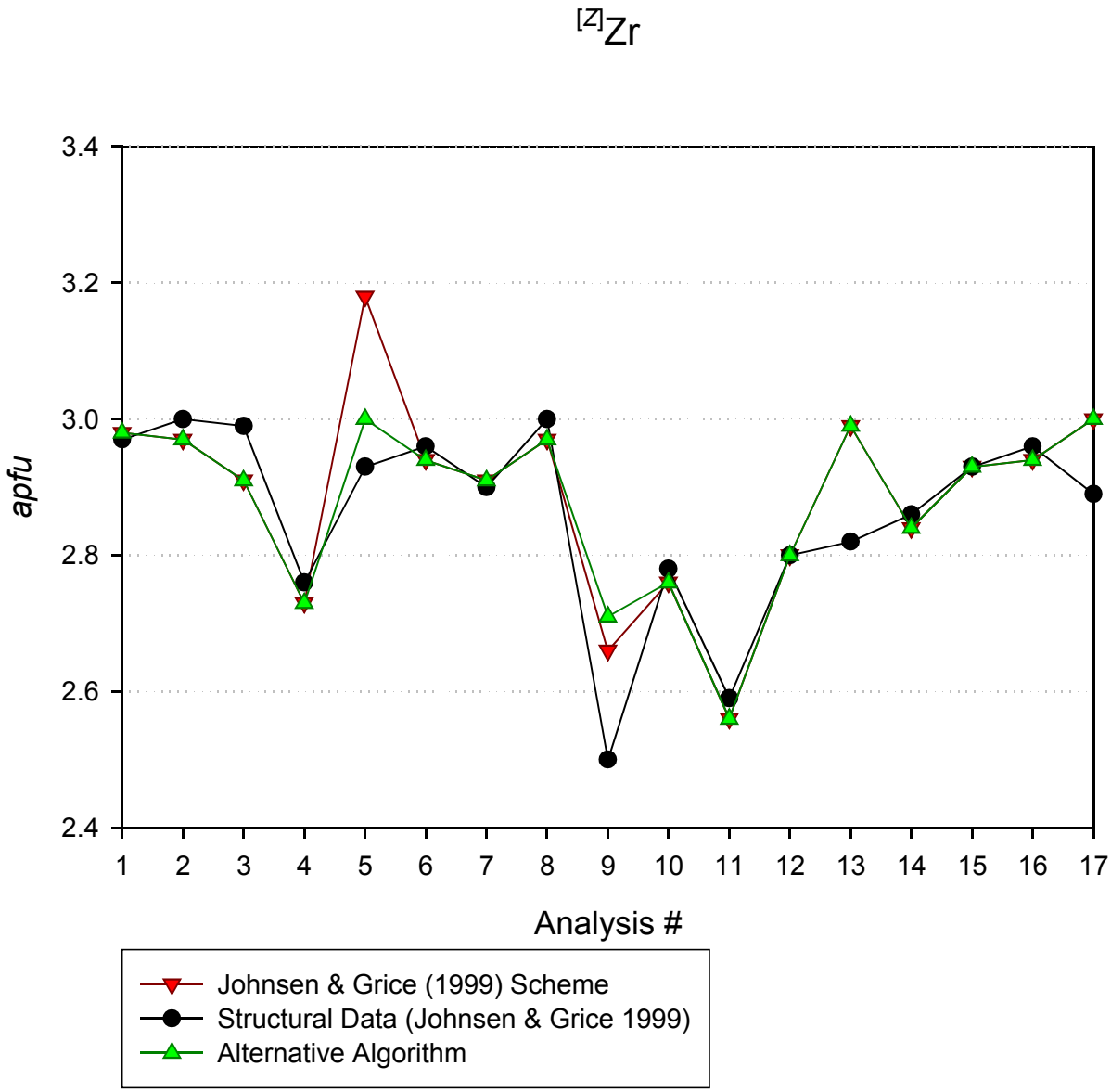

FIGURE 17 – Performance comparison between the recalculation schemes for Zr in the *Z* site.

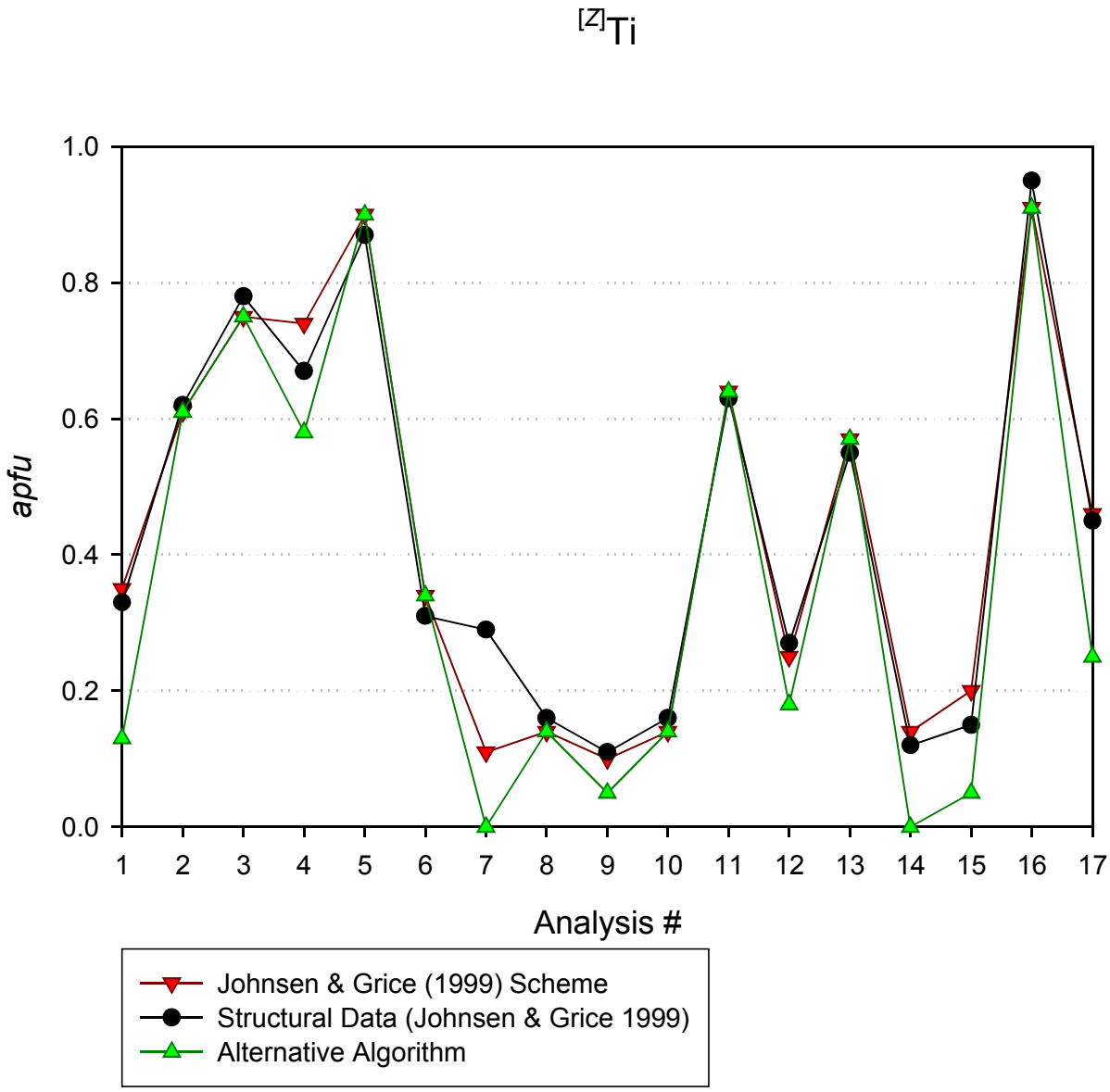

FIGURE 18 – Performance comparison between the recalculation schemes for Ti in the *Z* site.

M(3)

Two plots of site-occupancy for *M*(3) satisfied the standards of significance: Si and Nb (Figures 17 & 18).

The alternative algorithm was marginally more precise ($r^2_{J\&G} = 0.63$ *versus* $r^2_{AA} = 0.73$) than the cationic scheme in assigning Si to *M*(3), but neither scheme was especially accurate ($RD_{J\&G} = 17.82\%$ *versus* $RD_{AA} = 15.94\%$). The plot for Si in *M*(3) is mostly unremarkable, but both assignment schemes made the same erroneous high-allocation for analysis #7 and #17.

Both assignment schemes were essentially equally precise ($r^2_{J\&G} = 0.96$ *versus* $r^2_{AA} = 0.93$) in assigning Nb to *M*(3), but the cationic scheme of JOHNSEN & GRICE (1999) was markedly more accurate ($RD_{J\&G} = 3.47\%$ *versus* $RD_{AA} = 8.00\%$).

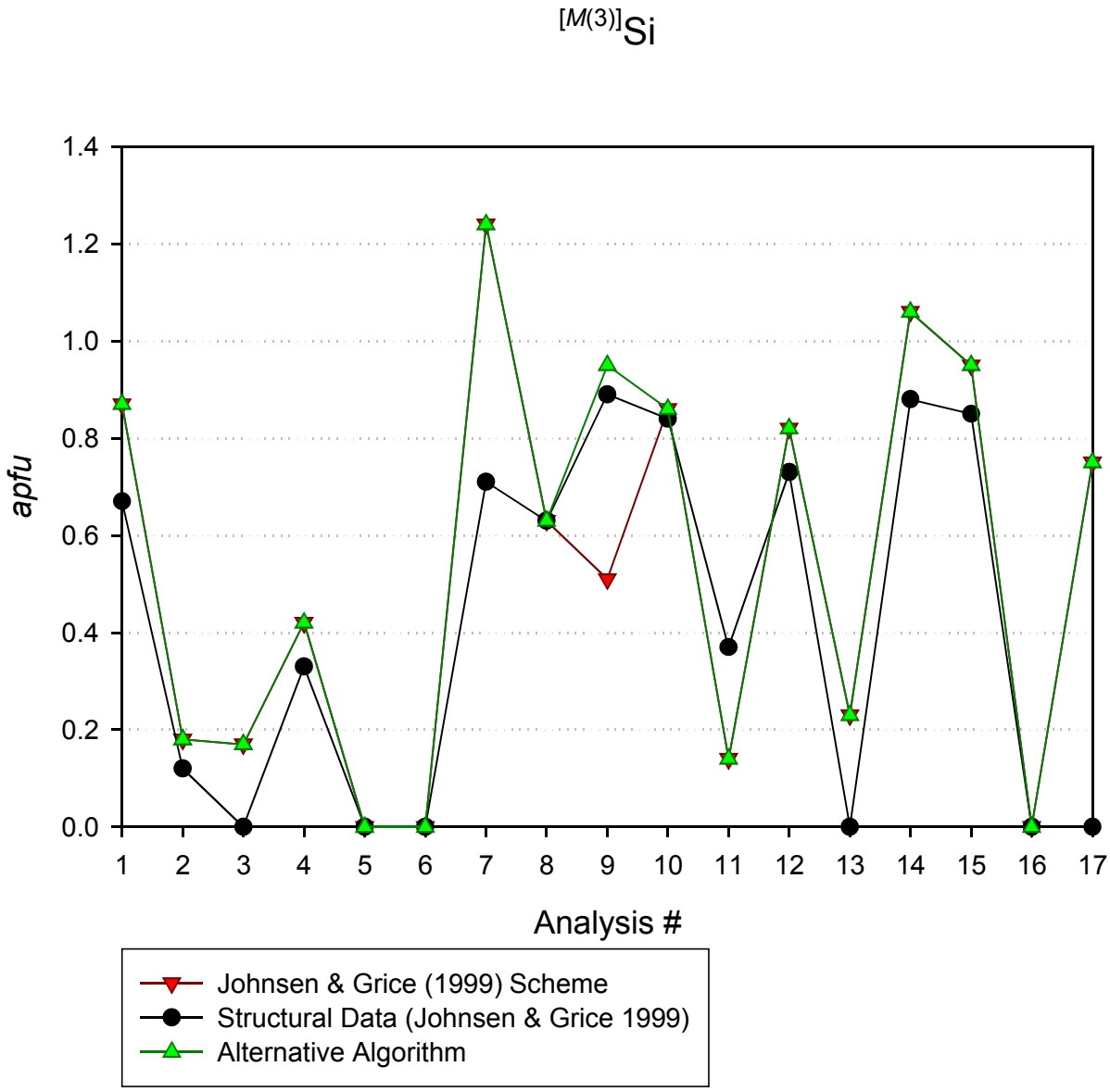

FIGURE 19 – Performance comparison between the recalculation schemes for Si in the *M*(3) site.

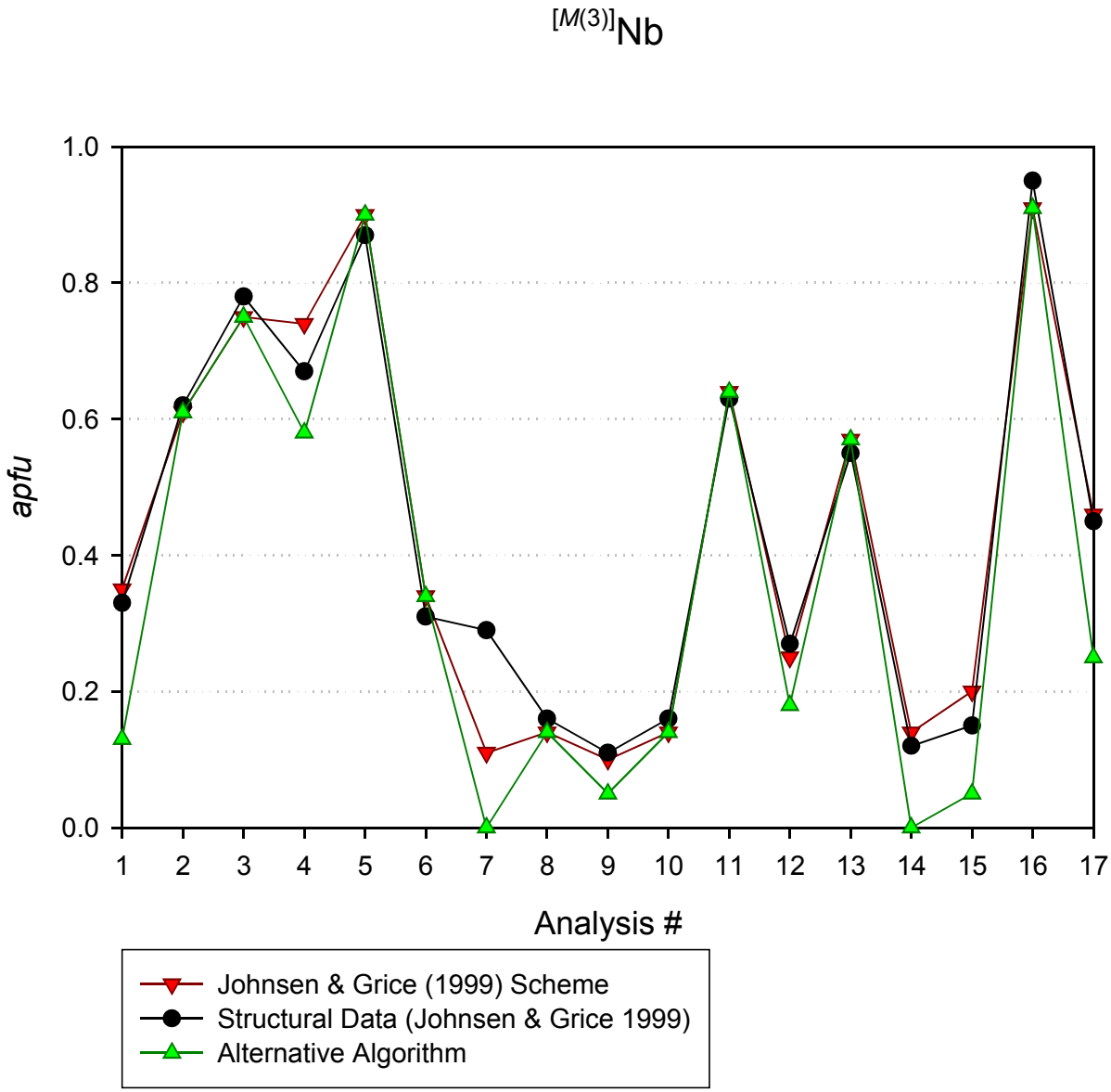

FIGURE 20 – Performance comparison between the recalculation schemes for Nb in the *M*(3) site.

PROPOSED EUDIALYTE GROUP CLASSIFICATION SYSTEM

INTRODUCTION

Two of the ultimate goals of a descriptive investigation of a burgeoning mineral group are the classification of its members and the graphical representation of analytical data. JOHNSEN *ET AL*. (2003a) evaluated several possible systems of nomenclature and concluded that a conventional scheme of unique species names with up to one single-cation prefix—based on occupancy of *M*(2) [*e.g. ferro*kentbrooksite, from Fe^{2+} dominance in *M*(2)]—was, at the time, most useful and versatile for dealing with the intricacies of the eudialyte group. Their conclusions are fundamentally sensible and valid, and there is no compelling reason to substantially alter the guidelines that they laid out.

Nevertheless, in the eudialyte group, there is no firmly established classification scheme, only good suggestions. Furthermore, there does not exist a systematic method of plotting chemical analyses into compositional fields. Considering the focus on crystal chemistry, partitioning, and speciation in eudialyte group minerals, it seemed natural that developing and proposing a diagrammatic classification system be part of this work.

CLASSIFICATION ON SITE-OCCUPANCY OF *M*(3)

In the proposed system, the eudialyte group would be divided into subgroups based on the dominant cation in *M*(3) (Table 3). TABLE 4 indicates how the four proposed subgroups would be populated by 19 of the 20 members of the eudialyte group—excepting labyrinthite, as indicated in TABLE 3.

TABLE 3 – Proposed subgroups of the eudialyte group.

Dominant M(3) Cation	*Proposed Subgroup*
Si	eudialyte
Nb	kentbrooksite
Ta	*no approved species*
W	khomyakovite
Zr	*no approved species*
Hf	*no approved species*
Ti	*no approved species*
Si / Ti	*labyrinthite**
□	ikranite

* only one species, labyrinthite, has this *M*(3) occupancy situation, so it is not recommended for subgroup status (modified after Nickel 2001)

TABLE 4 – Allocation of approved eudialyte group minerals to the proposed subgroups.

Proposed Subgroup	*Members*		
eudialyte	alluaivite aqualite eudialyte	raslakite rastsvetaevite	
kentbrooksite	carbokentbrooksite feklichevite ferrokentbrooksite	georgbarsanovite golyshevite kentbrooksite	oneillite taseqite zirsilite-(Ce)
khomyakovite	johnsenite-(Ce) khomyakovite manganokhomyakovite		
ikranite	ikranite mogovidite		

Once a eudialyte group analysis has been placed in a subgroup by its occupancy in *M*(3), nomenclature next follows the recommendation of JOHNSEN *ET AL.* (2003a) of using a base species name with, if necessary, a prefix that denotes deviant, dominant occupancy of *M*(2). For example, as Fe^{2+} supersedes Mn as the dominant cation in *M*(2), kentbrooksite transitions to ferrokentbrooksite.

Similarly—although it is, in fact, discouraged by JOHNSEN *ET AL.* (2003a)—the next step is to consider occupancy of the *X* site as compared to the occupancy for the base species; a prefix is used to denote variation. For example, as $(CO_3)^{2-}$ supersedes F^-, kentbrooksite transitions to carbokentbrooksite.

GRAPHICAL REPRESENTATION

Eudialyte group compositions would be plotted on a ternary diagram whose vertices represent the three most abundant occupants of *M*(3) for that analysis.

Since there are only two elements to consider in *M*(2) for purposes of speciation, occupancy of *M*(2) can be displayed in combination with occupancy of *M*(3) as ternary space diagrams or quadrilaterals. Ternary diagrams that include *M*(2) may be based on any previously described ternary that displays occupancy in *M*(3). The ternary is projected along its face-normal to form a triangular prism, with the height above the base corresponding to an increasing mole fraction of the substituent element in *M*(2).

Occupancy in *M*(2) can also be displayed between two end-member species or series by using the edge of a ternary diagram as the base of a quadrilateral and making the vertical component the mole fraction of substituent element in *M*(2).

When it is not as critical to express absolute numeric data about occupancy in *M*(2), *M*(2)-based end-members may be differentiated on a ternary diagram by using different symbols.

EUDIALYTE GROUP MINERALS OF THE EAST HILL SUITE, MONT SAINT-HILAIRE

INTRODUCTION

Currently, seven minerals of the eudialyte group (Table 5) are known to occur at Mont Saint-Hilaire. (Mandarino & Anderson 1989; Johnsen *et al*. 1999a; Johnsen *et al*. 1999b; Johnsen *et al*. 2003b; Grice & Gault 2006)

TABLE 5 – Approved eudialyte group minerals at Mont Saint-Hilaire.

eudialyte	$Na_{15}Ca_6Fe^{2+}_3Zr_3Si(Si_{25}O_{73})(O,OH,H_2O)_3(Cl,OH)_2$
ferrokentbrooksite	$Na_{15}Ca_6(Fe^{2+},Mn)_3Zr_3Nb(Si_{25}O_{73})(O,OH,H_2O)_3(F,Cl)_2$
johnsenite-(Ce)	$Na_{12}(Ce,La,Sr,Ca,\square)_3Ca_6Mn_3Zr_3W(Si_{25}O_{73})(CO_3)(OH,Cl)_2$
kentbrooksite	$Na_{15}Ca_6Mn_3Zr_3Nb(Si_{25}O_{73})(O,OH,H_2O)_3(F,Cl)_2$
khomyakovite	$Na_{12}Sr_3Ca_6Fe_3Zr_3W(Si_{25}O_{73})(O,OH,H_2O)_3(Cl,OH)_2$
manganokhomyakovite	$Na_{12}Sr_3Ca_6Mn_3Zr_3W(Si_{25}O_{73})(O,OH,H_2O)_3(Cl,OH)_2$
oneillite	$Na_{15}Ca_3Mn_3Fe^{2+}_3Zr_3Nb(Si_{25}O_{73})(O,OH,H_2O)_3(OH,Cl)_2$

They occur as single phases, but evidence suggests that they may more commonly occur in solid solution with one another or as zoned crystals. They are found as minor minerals in a variety of lithologies.

Twenty-three specimens of eudialyte group minerals were sampled from eudialyte syenite of the East Hill Suite for electron microprobe analysis. Five spots were analyzed on each specimen for a total of 115 analyses. After analyses with bad totals or other analytical issues were excluded, 51 analyses, representing 22 specimens, remained for further examination. Raw

microprobe data was processed through the alternative algorithm for recalculation. Electron microprobe analyses from this study suggest that the range of species of eudialyte group minerals at Mont Saint-Hilaire may be nearly three times as broad as previously thought.

SURVEY OF SPECIATION

The 51 analyses of eudialyte group minerals recalculated to 15 different species representing five proposed subgroups (Table 6). Two of those subgroups are even more tentative, so to speak, as they would be comprised of species that are not currently IMA-approved.

TABLE 6 – Proposed subgroups represented in the East Hill Suite analyses.

Dominant M(3) Cation	*Proposed Subgroup*
Si	eudialyte
Nb	kentbrooksite
W	khomyakovite
Zr	"Zr-eudialyte"
Hf	"Hf-eudialyte"

Only 13 of the analyses corresponded to IMA-approved members of the eudialyte group, and together they represent only two species, eudialyte (12 analyses) and ferrokentbrooksite (1 analysis). The other 38 analyses represented structural formulæ of 13 potentially new members of the eudialyte group. Considering the speciation of the 51 analyses (Table 7), 35 plotted in the proposed eudialyte subgroup, six in the proposed kentbrooksite subgroup, one in

the proposed khomyakovite subgroup, eight in the proposed "Zr-eudialyte" subgroup, and one in the proposed "Hf-eudialyte" subgroup.

TABLE 7 – Speciation of the eudialyte group in the East Hill Suite analyses.

Proposed Subgroup	*Species/Compositions in the East Hill Suite*	
eudialyte	eudialyte (12) "F-eudialyte" (3) "Mn-eudialyte" (9)	"F-Mn-eudialyte" (11)
kentbrooksite	ferrokentbrooksite (1) "Cl-ferrokentbrooksite" (2) "OH-ferrokentbrooksite" (1)	"Cl-kentbrooksite" (2)
khomyakovite	"Cl-Mn" *unidentified* (1)	
"Zr-eudialyte"	"Zr-eudialyte" (1) "F-Zr-eudialyte" (3) "S-Zr-eudialyte" (1)	"Mn-Zr-eudialyte" (1) "F-Mn-Zr-eudialyte" (2)
"Hf-eudialyte"	"Hf-eudialyte" (1)	
The number of analyses recalculating to a particular species or composition is indicated in parentheses after the species or composition name.		

PROPOSED EUDIALYTE SUBGROUP

Representative analyses of the proposed eudialyte subgroup are shown in TABLE 8. Site-occupancies for the same analyses, recalculated using the alternative algorithm, are shown in TABLES 9 & 10.

Composition plots for the proposed eudialyte subgroup, based on the three most-abundant occupants of *M*(3), resulted in five ternary plots (Figures 19-23). Apart from the essential inclusion of Si in all plots, three include Nb and Ta, and two include Ti and Zr. Solid solution in the proposed eudialyte subgroup exists mainly between Si and Nb & Zr in the *M*(3) site; tantalum and titanium appear to be lesser participants.

TABLE 8 – Representative EMP analyses of the proposed eudialyte subgroup.

Analysis #:	*6-5*	*8-3*	*15-4*	*2-5*	*3-5*	*4-3*
SiO_2 (*wt.%*)	45.66	46.17	46.54	44.61	45.99	47.24
TiO_2	0.07	0.11	0.07	0.18	0.13	0.24
ZrO_2	11.97	11.36	10.96	10.31	10.42	11.71
HfO_2	0.33	0.00	0.00	0.00	0.00	0.00
Nb_2O_5	0.96	1.04	0.67	1.43	0.70	0.82
Ta_2O_5	0.09	0.00	0.41	0.00	1.02	1.20
MoO_3	0.00	0.00	0.00	0.00	0.00	0.00
WO_3	0.23	0.00	0.00	0.00	0.00	0.00
Al_2O_3	0.22	0.07	0.16	0.32	0.16	0.08
Sc_2O_3	0.00	0.18	0.06	0.00	0.00	0.05
REE_2O_3	6.17	6.41	3.40	7.31	5.37	2.75
La_2O_3	1.71	1.38	0.96	1.46	0.91	0.61
Ce_2O_3	3.96	4.50	2.11	4.02	1.76	1.84
Pr_2O_3	0.00	0.00	0.00	0.00	0.00	0.00
Nd_2O_3	0.00	0.00	0.19	0.55	1.04	0.09
Sm_2O_3	0.00	0.00	0.00	0.00	0.00	0.00
Gd_2O_3	0.49	0.52	0.14	1.29	1.67	0.21
Dy_2O_3	0.00	0.00	0.00	0.00	0.00	0.00
Er_2O_3	0.00	0.00	0.00	0.00	0.00	0.00
Yb_2O_3	0.00	0.00	0.00	0.00	0.00	0.00
Y_2O_3	0.94	1.43	1.08	1.57	0.98	1.80
FeO	4.78	4.72	5.20	3.60	4.18	3.84
MnO	6.51	4.75	4.79	8.58	7.12	7.70
ZnO	0.00	0.00	0.00	0.00	0.00	0.00
CaO	7.25	8.40	8.58	7.76	7.49	8.44
SrO	na	na	na	na	na	na
BaO	0.00	1.81	0.00	0.49	0.70	0.00
MgO	0.02	0.09	0.06	0.00	0.00	0.00
Na_2O	13.35	12.40	13.91	12.18	13.56	12.83
K_2O	0.51	0.48	0.55	0.40	0.52	0.49
Cl	0.93	0.28	1.00	0.87	0.62	0.50
F	0.01	0.00	0.92	0.17	0.58	0.75
SO_3	0.03	0.00	0.00	0.00	0.59	0.46
H_2O*	0.15	0.02	0.59	0.23	0.33	0.39
O≡Cl	-0.21	-0.06	-0.23	-0.20	-0.14	-0.11
O≡F	-0.01	0.00	-0.39	-0.07	-0.24	-0.31
TOTAL	99.94	99.63	98.32	99.73	100.07	100.84
Species:	*eudialyte*	*eudialyte*	*"F-eudialyte"*	*"Mn-eudialyte"*	*"F-Mn-eudialyte"*	*"F-Mn-eudialyte"*

Normalized to 29 cations (Σ Si + Al + Zr + Ti + Hf + Nb + W + Ta) *apfu*
na = not analyzed
*H_2O calculated based on charge-balance, assuming presence as OH

TABLE 9 – Site-occupancy of proposed eudialyte subgroup analyses I.

	6-5	*8-3*	*15-4*
N(ϕ)			
Na	8.090	7.338	8.560
□	0.910	1.662	0.440
N(4)			
REE	1.242	1.291	0.678
Ca	0.000	0.000	0.000
Sr	na	na	na
Ba	0.000	0.393	0.000
K	0.356	0.338	0.387
Na	4.353	3.533	4.935
□	0.049	0.445	0.000
M(1)			
REE	0.000	0.000	0.007
Y	0.276	0.423	0.317
Fe^{2+}	0.000	0.000	0.000
Mn^{2+}	1.430	0.591	0.604
Ca	4.294	4.986	5.072
□	0.000	0.000	0.000
M(2)			
Zr	0.000	0.001	0.000
Hf	0.000	0.000	0.000
Ti	0.000	0.000	0.000
Fe^{2+}	2.210	2.185	2.398
Mn^{2+}	1.619	1.636	1.633
Mg	0.014	0.072	0.047
□	0.000	0.000	0.000

	6-5	*8-3*	*15-4*
Z			
W	0.000	0.000	0.000
Nb	0.000	0.000	0.000
Ta	0.000	0.000	0.019
Zr	3.000	3.000	2.950
Hf	0.000	0.000	0.000
Ti	0.000	0.000	0.031
□	0.000	0.000	0.000
M(3)			
W	0.033	0.000	0.000
Nb	0.241	0.260	0.167
Ta	0.013	0.000	0.043
Zr	0.228	0.069	0.000
Hf	0.052	0.000	0.000
Ti	0.031	0.045	0.000
Si	0.401	0.626	0.790
□	0.001	0.000	0.000
M(4) + Si			
Si	24.854	24.956	24.897
Al	0.146	0.044	0.103
□	0.000	0.000	0.000
X			
Cl	0.871	0.261	0.934
F	0.021	0.000	1.611
S	0.012	0.000	0.000
OH	0.536	0.077	0.000
□	0.560	1.662	0.000

TABLE 10 – Site-occupancy of proposed eudialyte subgroup analyses II.

	2-5	*3-5*	*4-3*
N(ϕ)			
Na	7.456	8.305	7.656
□	1.544	0.695	1.344
N(4)			
REE	1.502	0.981	0.537
Ca	0.000	0.000	0.000
Sr	na	na	na
Ba	0.109	0.153	0.000
K	0.291	0.373	0.339
Na	3.649	4.493	4.330
□	0.449	0.000	0.794
M(1)			
REE	0.000	0.080	0.000
Y	0.476	0.292	0.516
Fe^{2+}	0.000	0.000	0.000
Mn^{2+}	0.779	1.151	0.623
Ca	4.745	4.477	4.861
□	0.000	0.000	0.000
M(2)			
Zr	0.000	0.000	0.000
Hf	0.000	0.000	0.000
Ti	0.000	0.000	0.000
Fe^{2+}	1.720	1.949	1.729
Mn^{2+}	3.371	2.217	2.884
Mg	0.000	0.000	0.000
□	0.000	0.000	0.000

	2-5	*3-5*	*4-3*
Z			
W	0.000	0.000	0.000
Nb	0.051	0.000	0.000
Ta	0.000	0.110	0.000
Zr	2.870	2.836	3.000
Hf	0.000	0.000	0.000
Ti	0.079	0.053	0.000
□	0.000	0.001	0.000
M(3)			
W	0.000	0.000	0.000
Nb	0.318	0.175	0.200
Ta	0.000	0.045	0.176
Zr	0.000	0.000	0.070
Hf	0.000	0.000	0.000
Ti	0.000	0.000	0.097
Si	0.682	0.780	0.457
□	0.000	0.000	0.000
M(4) + Si			
Si	24.787	24.892	24.951
Al	0.213	0.108	0.049
□	0.000	0.000	0.000
X			
Cl	0.843	0.588	0.453
F	0.307	1.021	1.267
S	0.000	0.249	0.185
OH	0.850	0.143	0.095
□	0.000	0.000	0.000

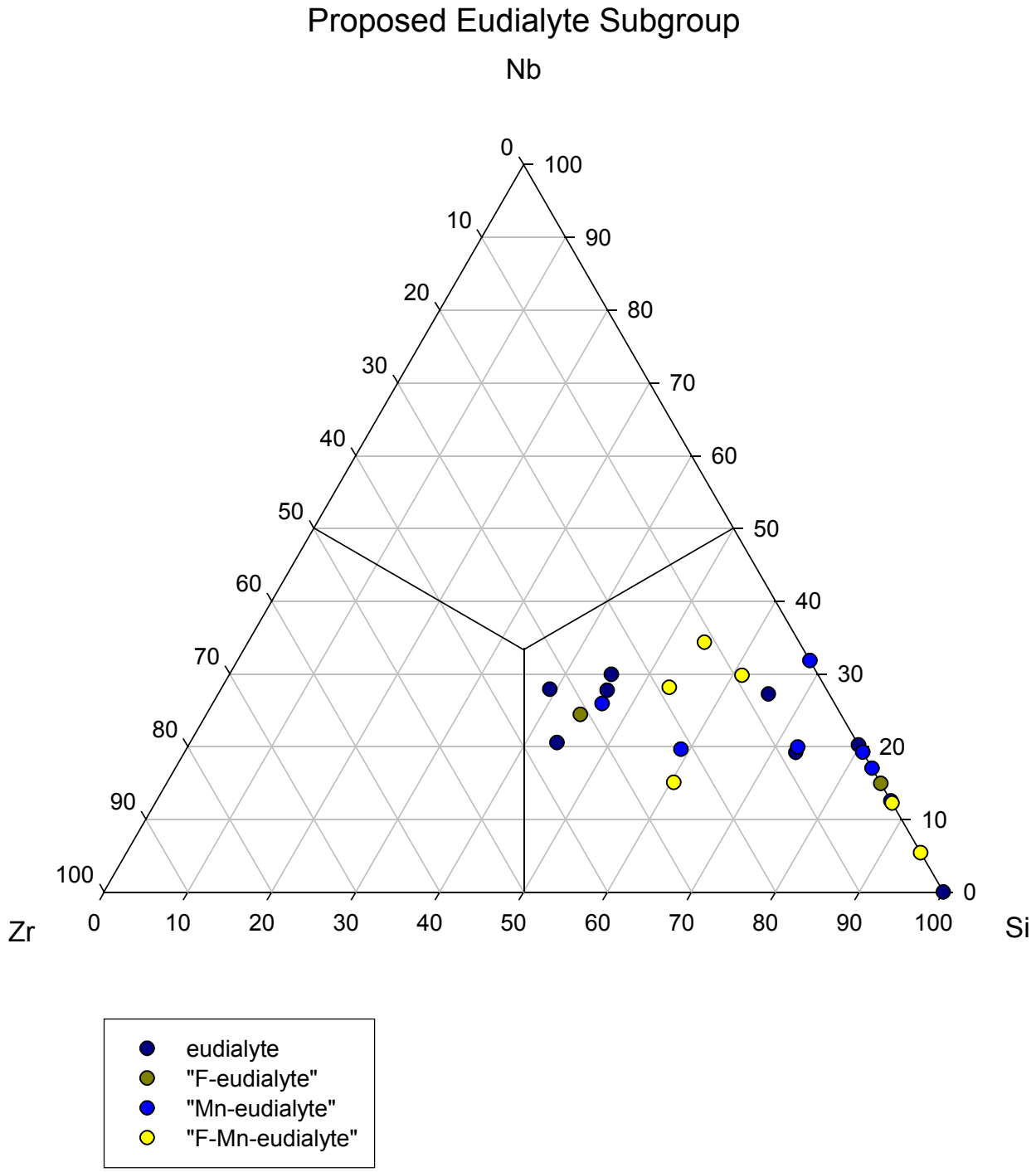

FIGURE 21 – [M(3)](Si-Nb-Zr)-dominant proposed eudialyte subgroup analyses.

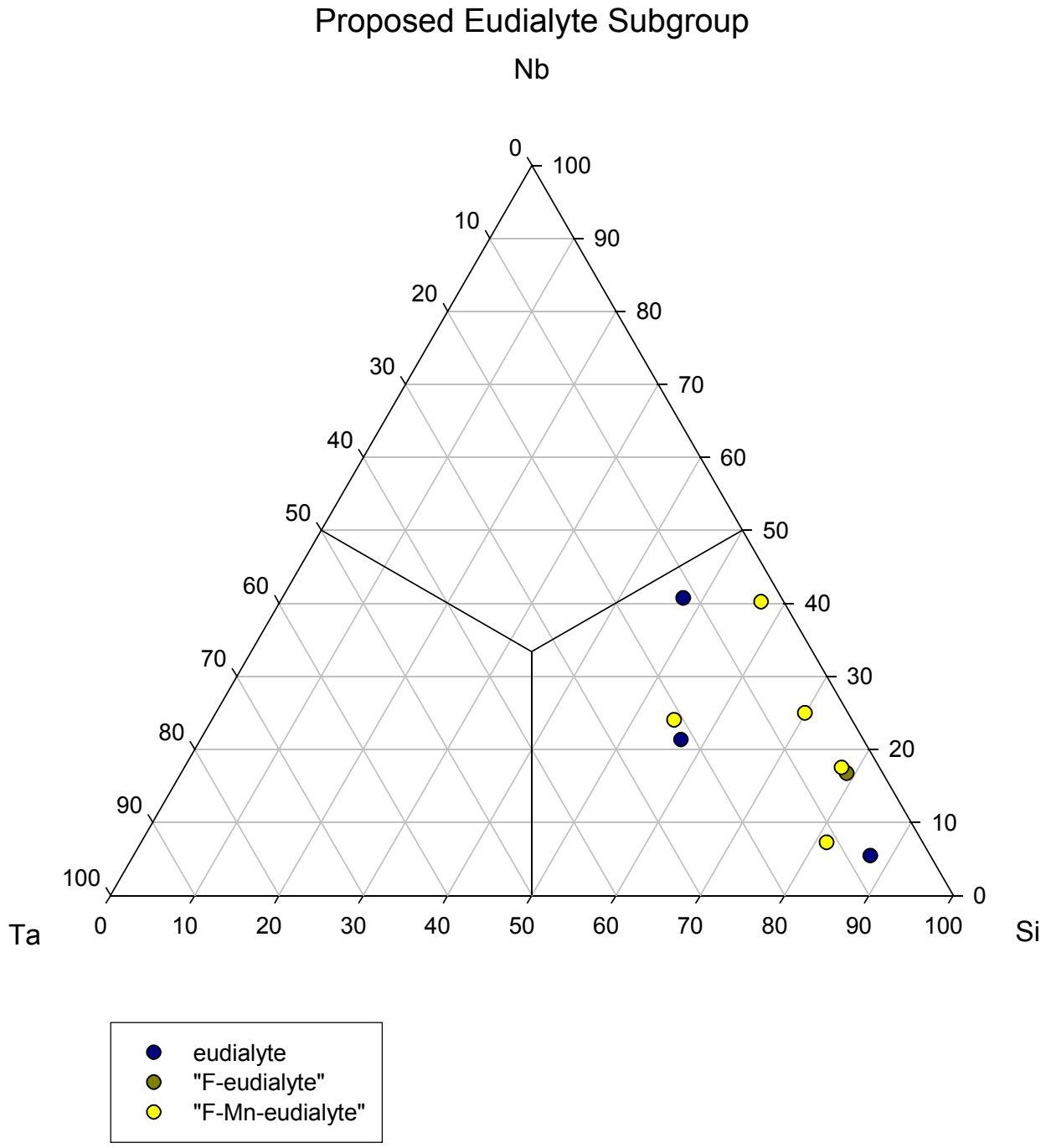

FIGURE 22 – [M(3)](Si-Nb-Ta)-dominant proposed eudialyte subgroup analyses.

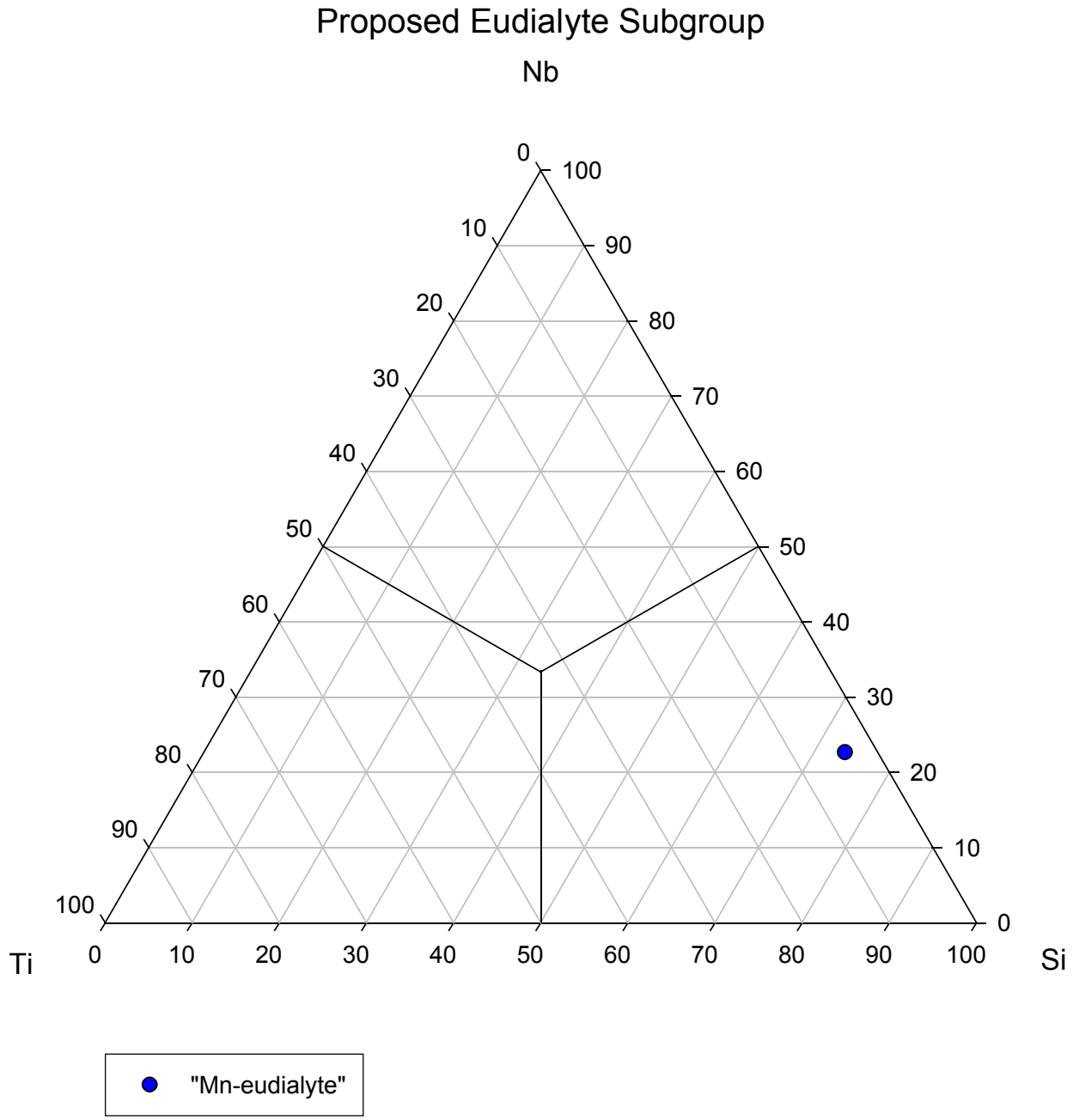

FIGURE 23 – [M(3)](Si-Nb-Ti)-dominant proposed eudialyte subgroup analysis.

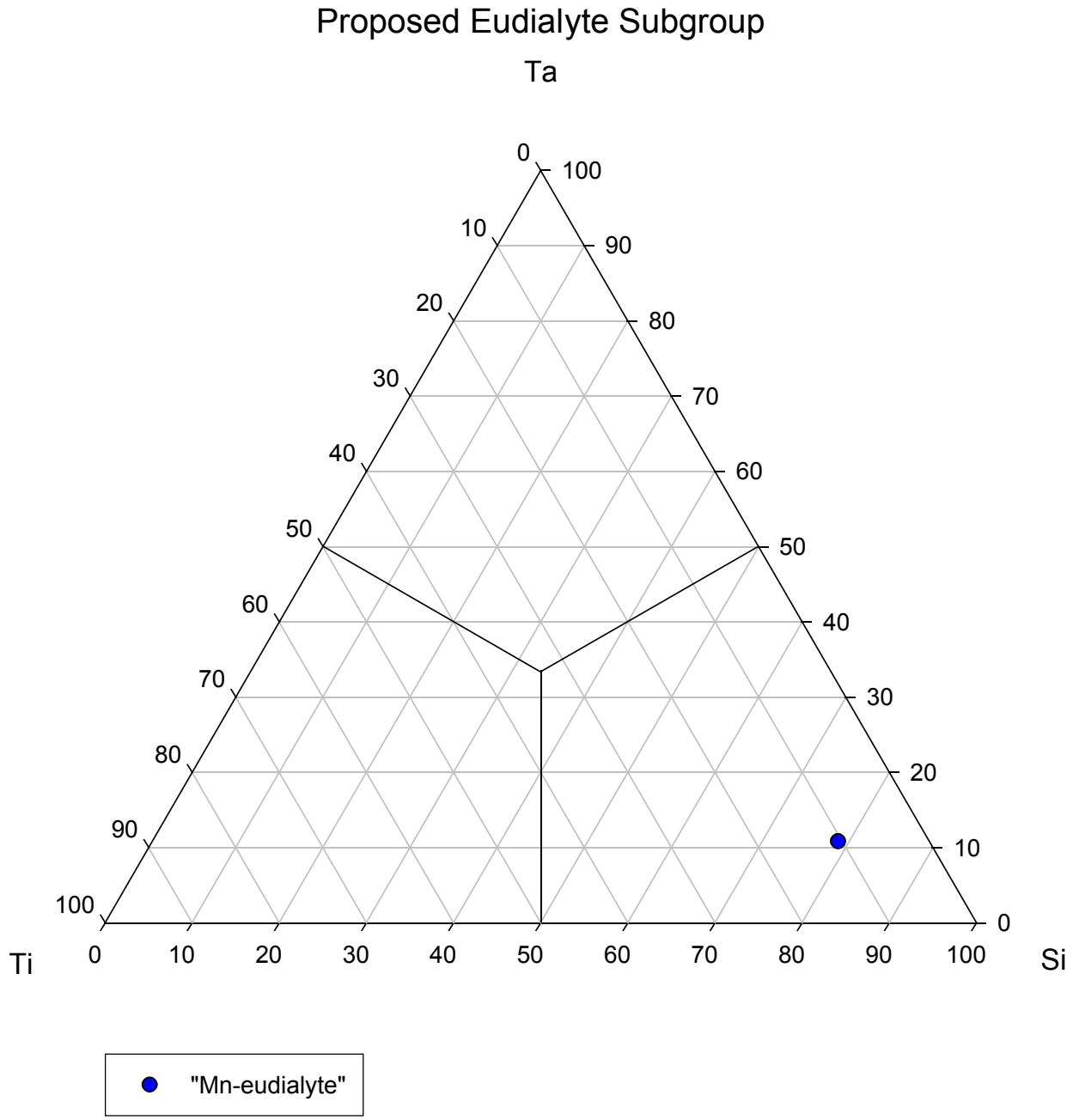

FIGURE 24 – [M(3)](Si-Ta-Ti)-dominant proposed eudialyte subgroup analysis.

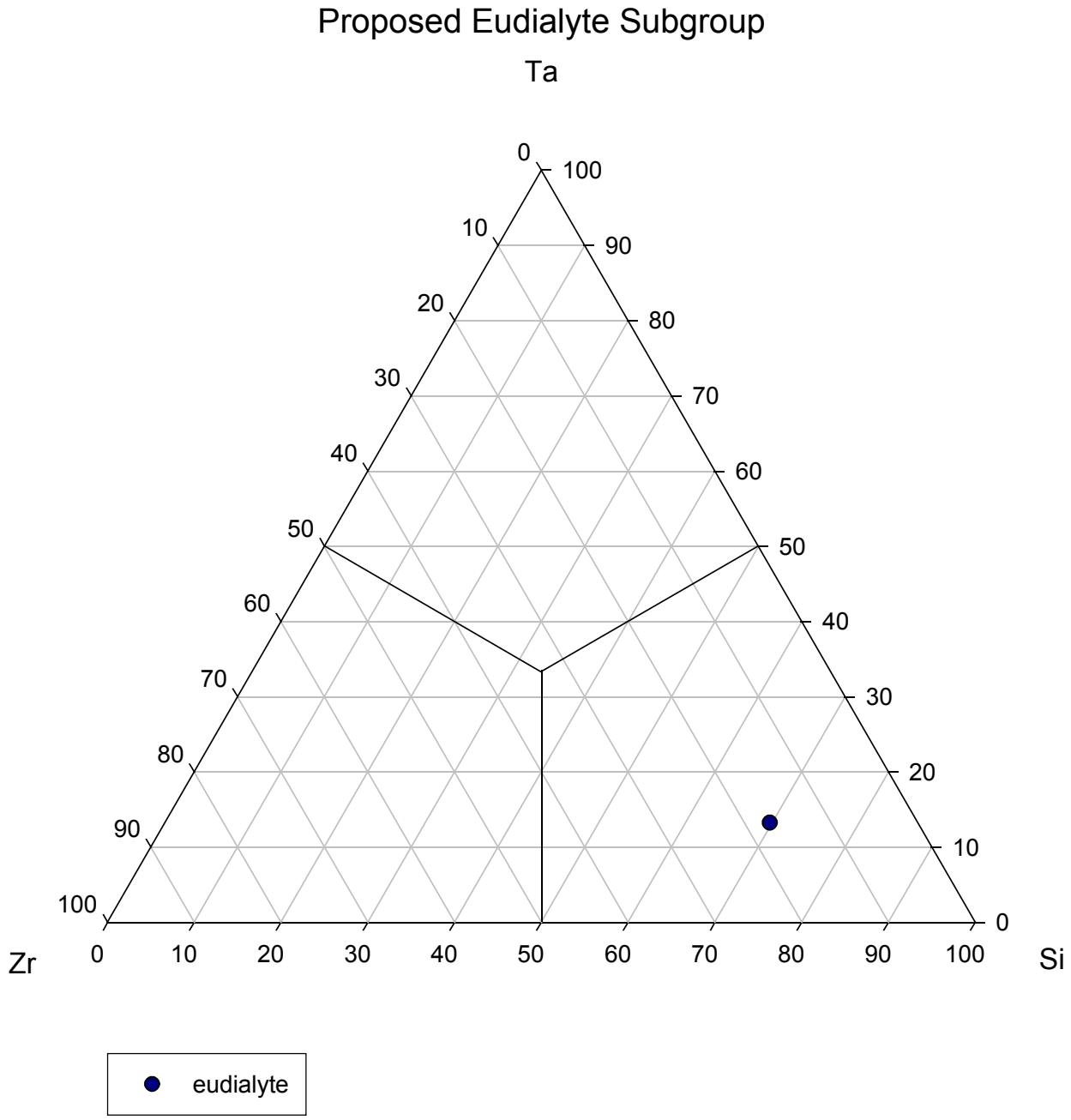

FIGURE 25 – [M(3)](Si-Ta-Zr)-dominant proposed eudialyte subgroup analysis.

PROPOSED KENTBROOKSITE SUBGROUP

Representative analyses of the proposed kentbrooksite subgroup are shown in TABLE 11. Site-occupancies for the same analyses, recalculated using the alternative algorithm, are shown in TABLES 12 & 13.

Composition plots for the proposed kentbrooksite subgroup, based on the three most-abundant occupants of *M*(3), resulted in six ternary plots (Figures 24-29). Apart from the essential inclusion of Nb in all plots, three include Si, Hf, and Zr, two include Ta, and one includes Ti. Solid solution in the proposed kentbrooksite subgroup exists mainly between Nb and Hf, Si & Ta in the *M*(3) site; titanium and zirconium appear to be lesser participants.

TABLE 11 – Representative EMP analyses of the proposed kentbrooksite subgroup.

Analysis #:	*20-5*	*2-4*	*1-5*	*16-4*	*3-4*	*18-1*
SiO_2 (*wt.%*)	44.33	45.75	46.01	44.20	46.84	45.19
TiO_2	0.12	0.10	0.14	0.12	0.21	0.11
ZrO_2	11.69	11.16	10.31	13.67	11.03	10.94
HfO_2	1.29	3.63	0.00	0.00	2.89	0.00
Nb_2O_5	1.11	2.18	3.13	1.87	1.72	2.45
Ta_2O_5	1.13	1.34	0.00	1.95	0.00	0.00
MoO_3	0.00	0.00	0.00	0.00	0.00	0.00
WO_3	0.00	0.00	0.00	0.00	0.00	0.00
Al_2O_3	0.05	0.11	0.12	0.08	0.00	0.09
Sc_2O_3	0.00	0.00	0.00	0.00	0.00	0.01
REE_2O_3	5.02	5.27	3.18	4.64	2.01	5.79
La_2O_3	1.40	0.80	0.51	0.93	0.57	1.79
Ce_2O_3	2.88	3.43	2.17	2.17	1.09	3.33
Pr_2O_3	0.00	0.00	0.00	0.00	0.00	0.00
Nd_2O_3	0.00	0.32	0.32	1.19	0.19	0.28
Sm_2O_3	0.00	0.00	0.00	0.00	0.00	0.00
Gd_2O_3	0.75	0.72	0.18	0.35	0.15	0.39
Dy_2O_3	0.00	0.00	0.00	0.00	0.00	0.00
Er_2O_3	0.00	0.00	0.00	0.00	0.00	0.00
Yb_2O_3	0.00	0.00	0.00	0.00	0.00	0.00
Y_2O_3	0.88	1.67	0.66	0.00	0.46	2.02
FeO	4.71	4.73	3.93	5.17	4.55	5.15
MnO	7.51	5.16	8.87	4.48	7.87	6.86
ZnO	0.00	0.00	0.00	0.00	0.00	0.00
CaO	6.54	7.41	6.95	8.56	7.49	7.52
SrO	na	na	na	na	na	na
BaO	0.00	0.00	0.78	0.00	0.15	0.66
MgO	0.00	0.00	0.00	0.00	0.00	0.05
Na_2O	14.00	12.78	14.37	12.60	14.55	11.89
K_2O	0.46	0.50	0.53	0.42	0.57	0.38
Cl	0.98	0.74	0.66	0.70	0.60	0.00
F	0.00	0.00	0.24	0.74	0.00	0.00
SO_3	0.14	0.21	0.00	0.17	0.00	0.14
H_2O*	0.16	0.09	0.18	0.45	0.04	0.07
O≡Cl	-0.22	-0.17	-0.15	-0.16	-0.14	0.00
O≡F	0.00	0.00	-0.10	-0.31	0.00	0.00
TOTAL	99.88	102.64	99.82	99.34	100.83	99.31
Species:	*"Cl-ferro-kentbrooksite"*	*"Cl-ferro-kentbrooksite"*	*"Cl-kentbrooksite"*	*ferro-kentbrooksite*	*"Cl-kentbrooksite"*	*"OH-ferro-kentbrooksite"*

Normalized to 29 cations (Σ Si + Al + Zr + Ti + Hf + Nb + W + Ta) *apfu*
na = not analyzed
*H_2O calculated based on charge-balance, assuming presence as OH

TABLE 12 – Site-occupancy of proposed kentbrooksite subgroup analyses I.

	20-5	*2-4*	*1-5*
N(ϕ)			
Na	8.763	7.522	8.832
□	0.237	1.478	0.168
N(4)			
REE	0.728	1.027	0.334
Ca	0.000	0.000	0.000
Sr	na	na	na
Ba	0.000	0.000	0.168
K	0.329	0.341	0.373
Na	4.943	3.989	5.125
□	0.000	0.643	0.000
M(1)			
REE	0.298	0.000	0.303
Y	0.263	0.479	0.194
Fe^{2+}	0.000	0.000	0.000
Mn^{2+}	1.484	1.242	1.408
Ca	3.955	4.279	4.095
□	0.000	0.000	0.000
M(2)			
Zr	0.001	0.000	0.000
Hf	0.000	0.221	0.000
Ti	0.000	0.041	0.000
Fe^{2+}	2.223	2.131	1.810
Mn^{2+}	2.109	1.113	2.727
Mg	0.000	0.003	0.000
□	0.000	0.000	0.000

	20-5	*2-4*	*1-5*
Z			
W	0.000	0.000	0.000
Nb	0.000	0.000	0.174
Ta	0.000	0.000	0.000
Zr	3.000	2.935	2.767
Hf	0.000	0.065	0.000
Ti	0.000	0.000	0.058
□	0.000	0.000	0.001
M(3)			
W	0.000	0.000	0.000
Nb	0.283	0.531	0.604
Ta	0.173	0.196	0.000
Zr	0.217	0.000	0.000
Hf	0.208	0.273	0.000
Ti	0.051	0.000	0.000
Si	0.068	0.000	0.396
□	0.000	0.000	0.000
M(4) + Si			
Si	24.967	24.671	24.922
Al	0.033	0.067	0.078
□	0.000	0.262	0.000
X			
Cl	0.934	0.675	0.618
F	0.000	0.000	0.419
S	0.060	0.085	0.000
OH	0.605	0.335	0.665
□	0.401	0.905	0.297

TABLE 13 – Site-occupancy of proposed kentbrooksite subgroup analyses II.

	16-4	*3-4*	*18-1*
N(ϕ)			
Na	7.779	8.839	7.159
□	1.221	0.161	1.841
N(4)			
REE	0.929	0.210	1.179
Ca	0.000	0.000	0.000
Sr	0.000	0.000	0.000
Ba	0.000	0.032	0.144
K	0.299	0.391	0.270
Na	4.503	5.367	3.553
□	0.269	0.000	0.854
M(1)			
REE	0.000	0.182	0.000
Y	0.000	0.130	0.602
Fe^{2+}	0.000	0.000	0.000
Mn^{2+}	0.929	1.380	0.887
Ca	5.071	4.308	4.511
□	0.000	0.000	0.000
M(2)			
Zr	0.499	0.000	0.000
Hf	0.000	0.000	0.000
Ti	0.000	0.000	0.000
Fe^{2+}	2.392	2.042	2.413
Mn^{2+}	1.169	2.202	2.367
Mg	0.000	0.000	0.038
□	0.000	0.000	0.000

	16-4	*3-4*	*18-1*
Z			
W	0.000	0.000	0.000
Nb	0.000	0.000	0.000
Ta	0.000	0.000	0.000
Zr	3.000	2.891	2.987
Hf	0.000	0.109	0.000
Ti	0.000	0.000	0.013
□	0.000	0.000	0.000
M(3)			
W	0.000	0.000	0.000
Nb	0.467	0.417	0.619
Ta	0.293	0.000	0.000
Zr	0.188	0.000	0.000
Hf	0.000	0.334	0.000
Ti	0.052	0.084	0.031
Si	0.000	0.165	0.350
□	0.000	0.000	0.000
M(4) + Si			
Si	24.453	25.000	24.944
Al	0.049	0.000	0.056
□	0.498	0.000	0.000
X			
Cl	0.659	0.549	0.000
F	1.298	0.000	0.000
S	0.070	0.000	0.057
OH	0.000	0.158	0.270
□	0.000	1.293	1.673

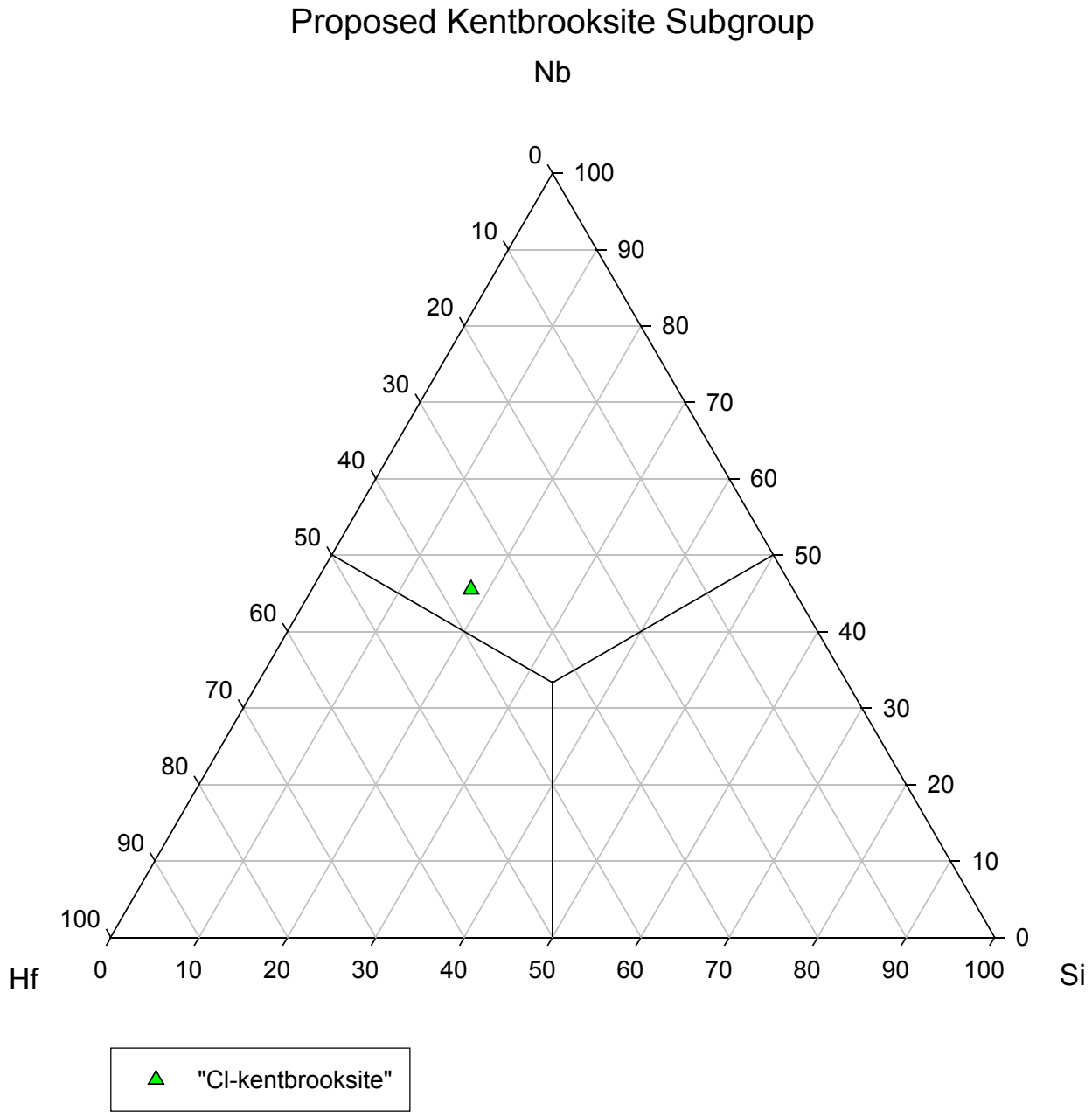

FIGURE 26 – [M(3)](Si-Nb-Hf)-dominant proposed kentbrooksite subgroup analysis.

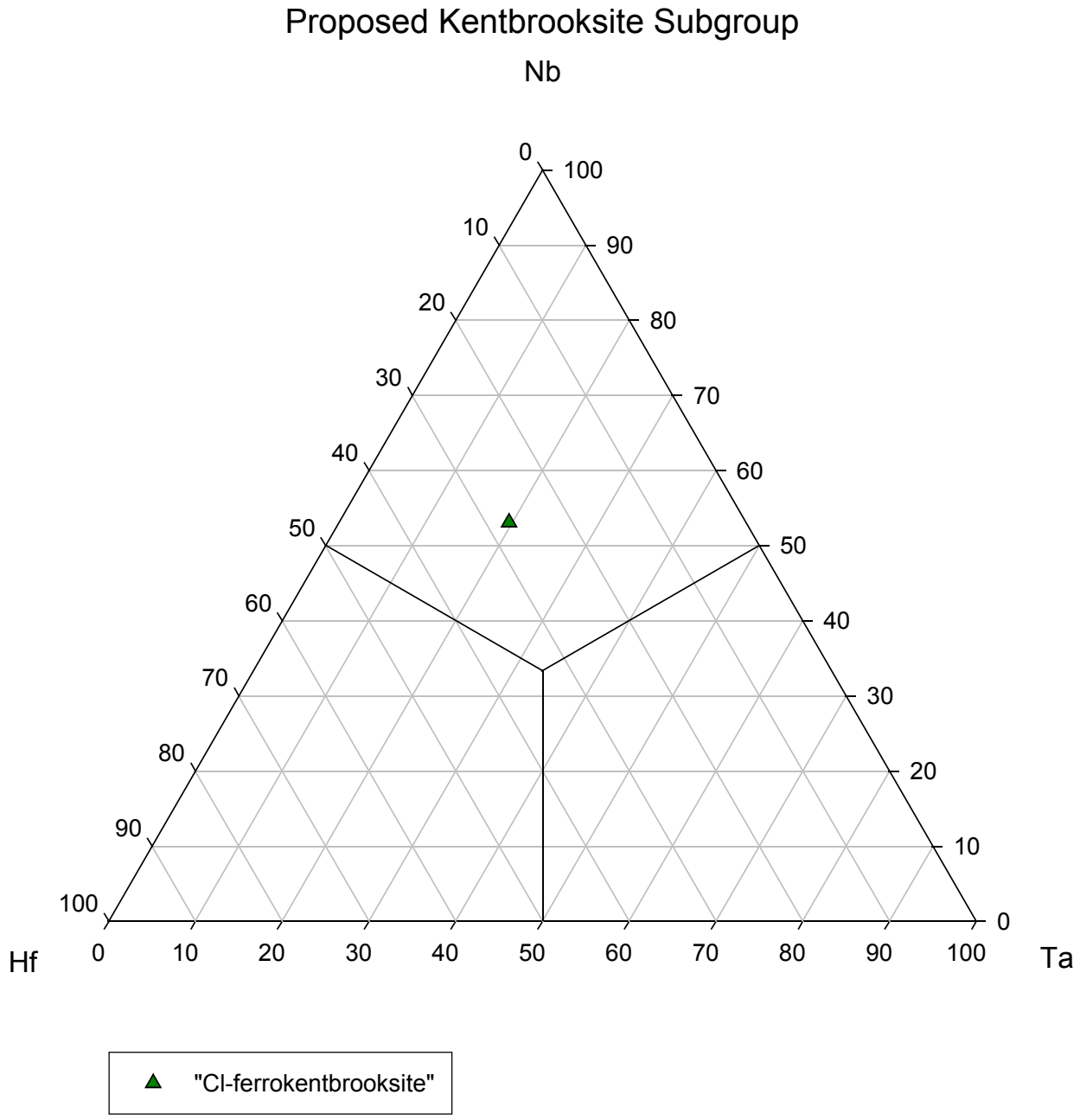

FIGURE 27 – [M(3)](Ta-Nb-Hf)-dominant proposed kentbrooksite subgroup analysis.

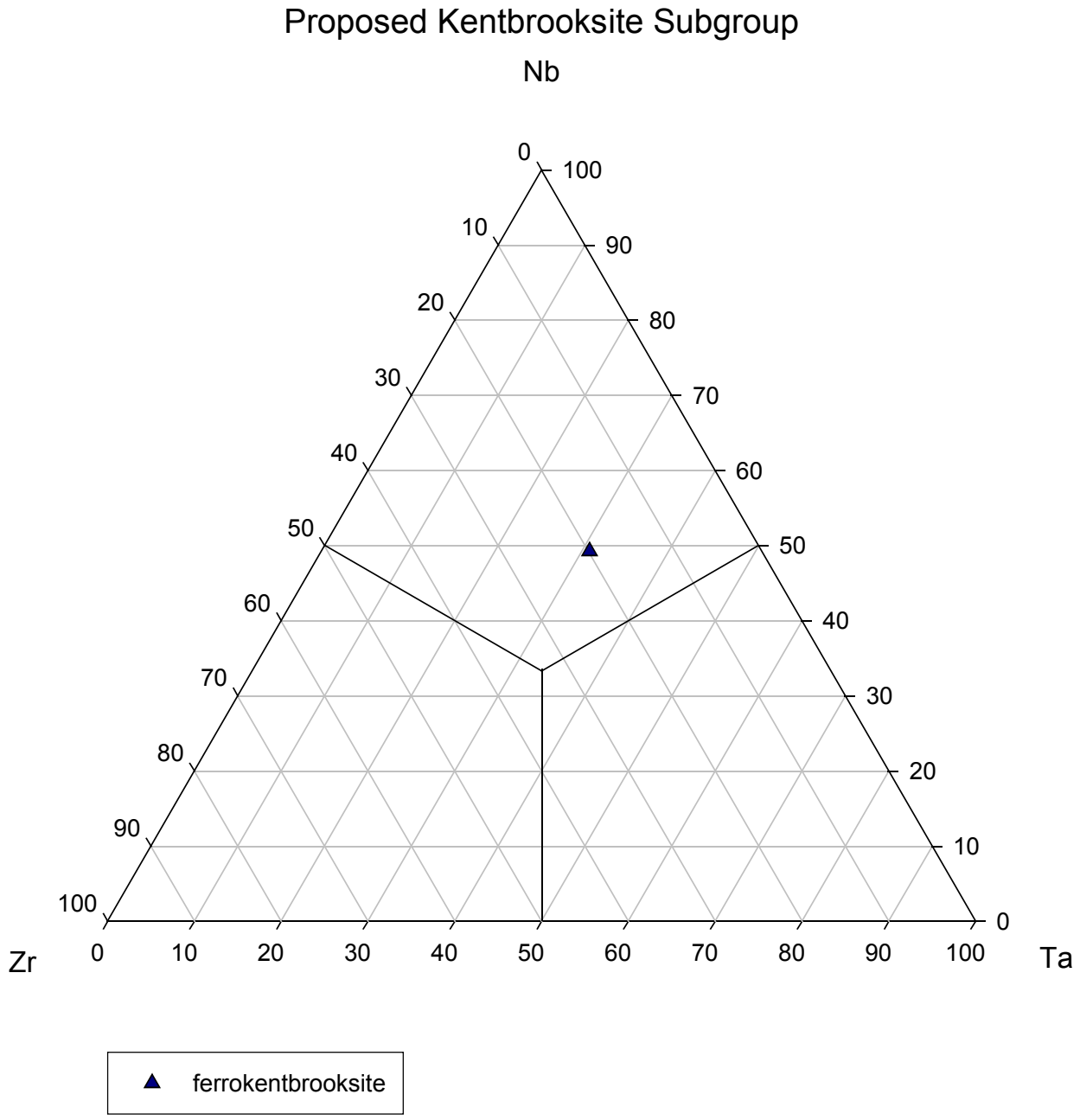

FIGURE 28 – [M(3)](Ta-Nb-Zr)-dominant proposed kentbrooksite subgroup analysis.

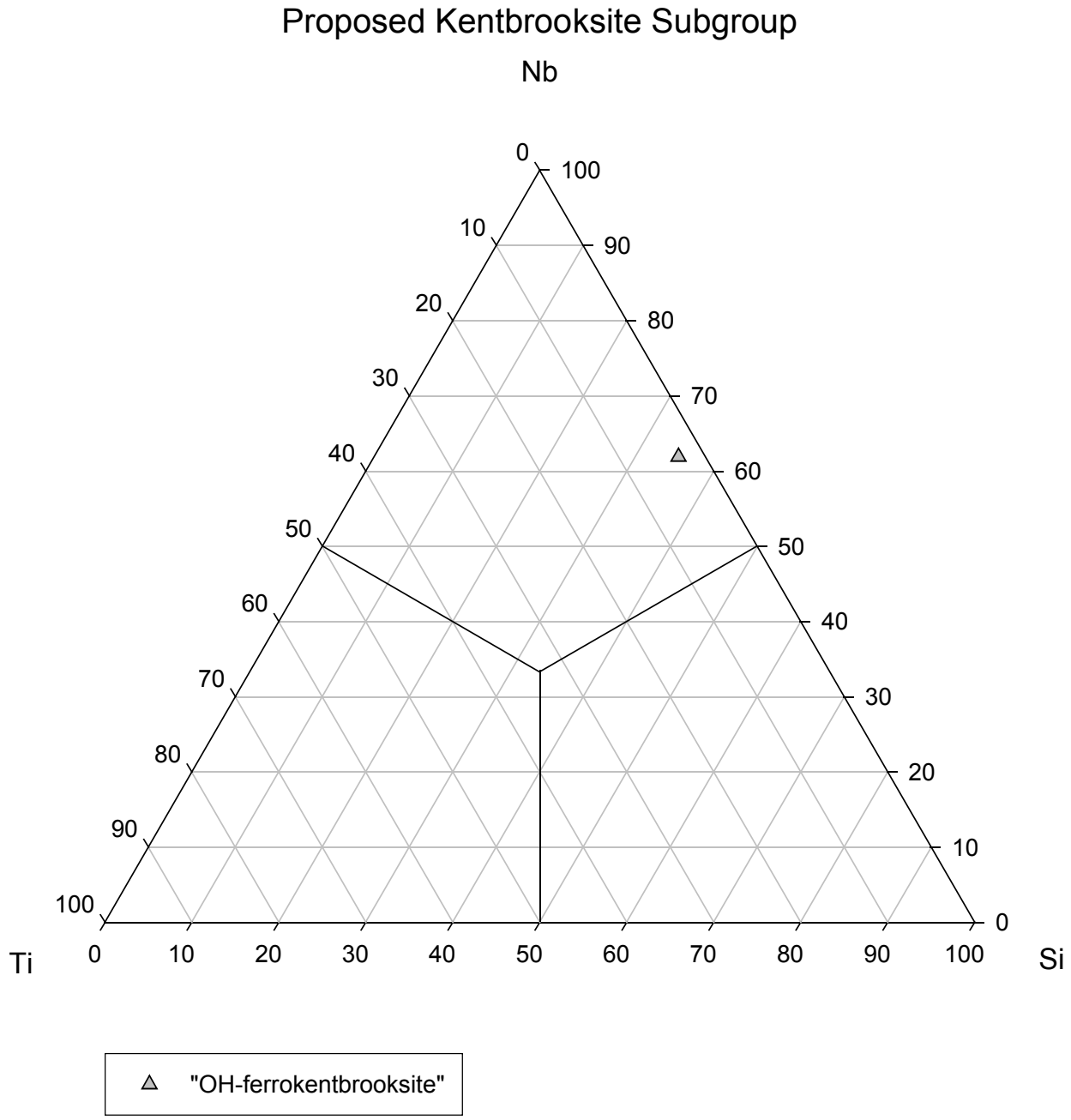

FIGURE 29 – [M(3)](Si-Nb-Ti)-dominant proposed kentbrooksite subgroup analysis.

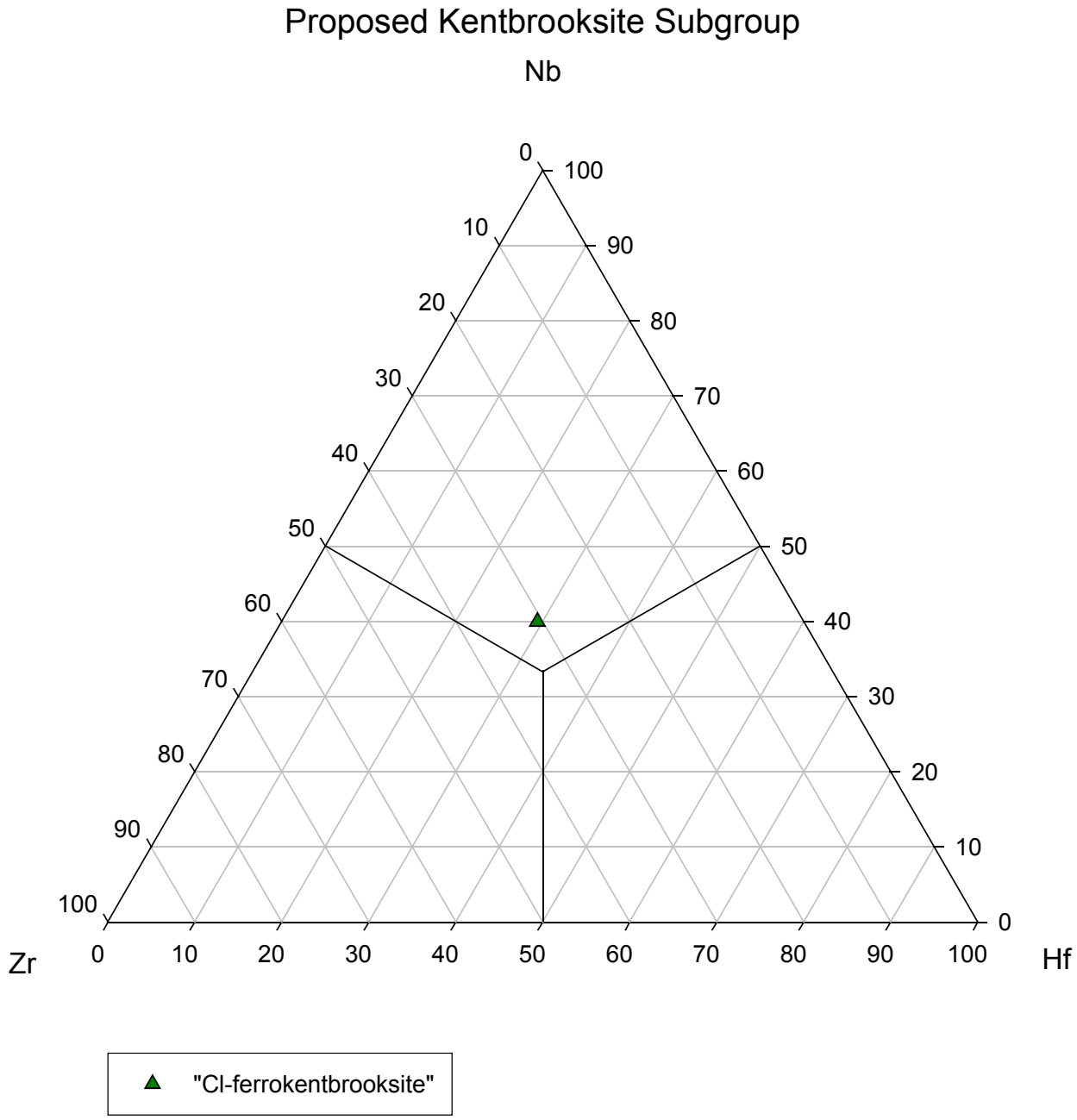

FIGURE 30 – [M(3)](Hf-Nb-Zr)-dominant proposed kentbrooksite subgroup analysis.

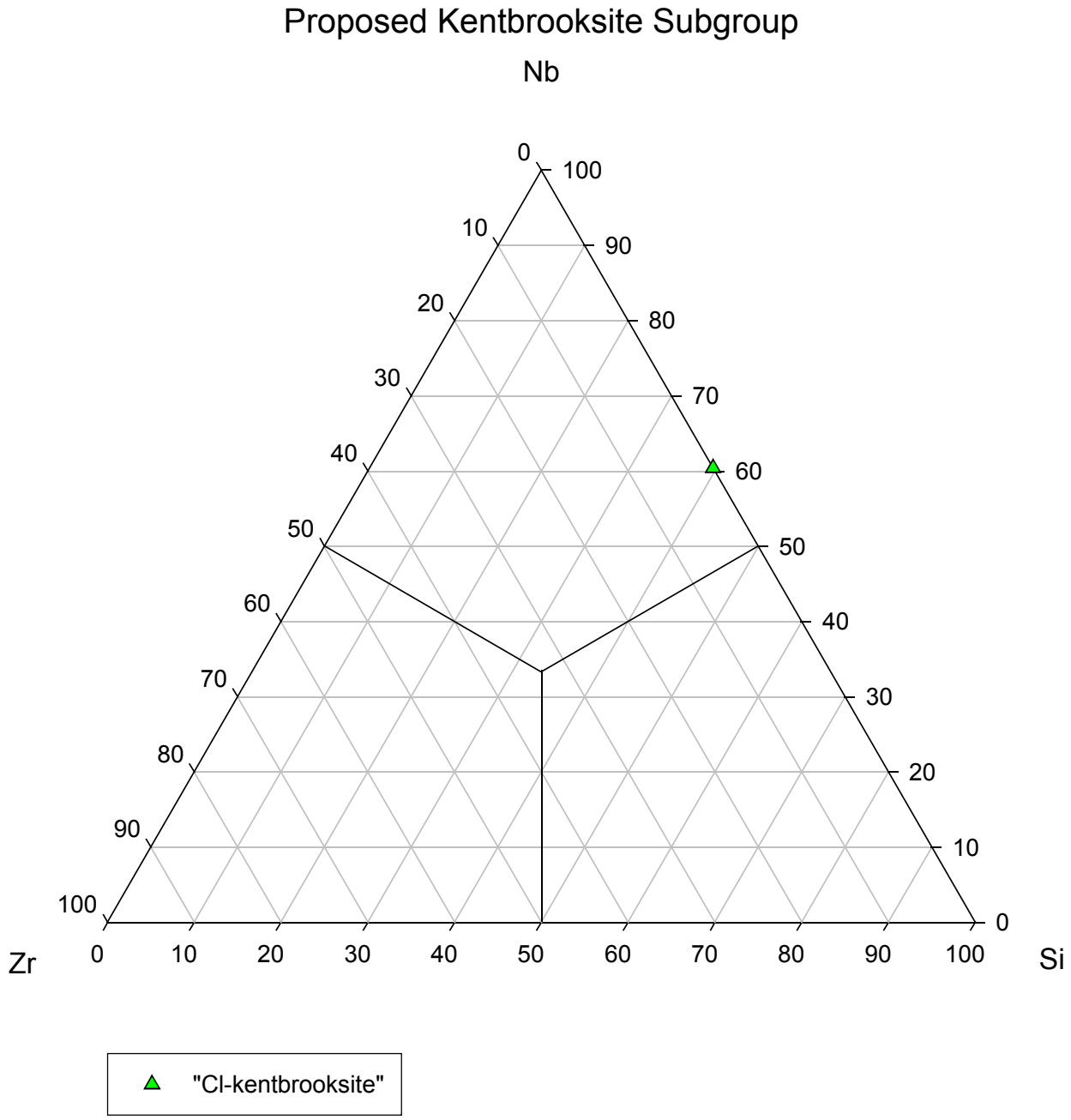

FIGURE 31 – [M(3)](Si-Nb-Zr)-dominant proposed kentbrooksite subgroup analysis.

PROPOSED KHOMYAKOVITE SUBGROUP

The representative analysis of the proposed khomyakovite subgroup is shown in TABLE 14. Site-occupancies for the same analysis, recalculated using the alternative algorithm, are shown in TABLE 15. Because the analysis lacks Sr data, a definitive species cannot be named; the recalculation shares aspects of manganokhomyakovite and oneillite.

Composition plots for the proposed khomyakovite subgroup, based on the three most-abundant occupants of *M*(3), resulted in one ternary plot (Figure 30). Apart from the essential inclusion of W, the plot includes Nb and Ta.

TABLE 14 – Representative EMP analyses of the proposed khomyakovite & "Hf-eudialyte" subgroups.

Analysis #:	*17-5*	*16-3*
SiO_2 (*wt.%*)	39.11	45.14
TiO_2	0.15	0.09
ZrO_2	10.85	10.73
HfO_2	0.00	4.47
Nb_2O_5	0.73	0.64
Ta_2O_5	1.06	0.00
MoO_3	0.00	0.00
WO_3	3.58	0.71
Al_2O_3	0.00	0.00
Sc_2O_3	0.00	0.08
REE_2O_3	6.67	2.40
La_2O_3	1.55	0.96
Ce_2O_3	3.56	0.70
Pr_2O_3	0.00	0.00
Nd_2O_3	1.01	0.45
Sm_2O_3	0.00	0.00
Gd_2O_3	0.55	0.29
Dy_2O_3	0.00	0.00
Er_2O_3	0.00	0.00
Yb_2O_3	0.00	0.00
Y_2O_3	3.19	0.69
FeO	5.15	5.26
MnO	7.45	4.85
ZnO	0.00	0.00
CaO	4.99	8.91
SrO	na	na
BaO	0.49	0.00
MgO	0.02	0.02
Na_2O	14.33	12.96
K_2O	0.38	0.48
Cl	0.87	0.87
F	0.00	0.00
SO_3	0.03	0.56
H_2O*	0.15	0.13
O≡Cl	-0.20	-0.20
O≡F	0.00	0.00
TOTAL	98.99	98.78
Species:	*"Cl-Mn" unidentified*	*"Hf-eudialyte"*

Normalized to 29 cations (Σ Si + Al + Zr + Ti + Hf + Nb + W + Ta) *apfu*
na = not analyzed
*H_2O calculated based on charge-balance, assuming presence as OH

TABLE 15 – Site-occupancy of proposed khomyakovite & "Hf-eudialyte" subgroup analyses.

	17-5	*16-3*
N(ϕ)		
Na	9.687	8.107
□	*0.000*	*0.893*
N(4)		
REE	0.791	0.481
Ca	0.000	0.000
Sr	0.000	0.000
Ba	0.121	0.000
K	0.308	0.338
Na	4.780	4.837
□	*0.000*	*0.344*
M(1)		
REE	0.730	0.000
Y	1.070	0.204
Fe^{2+}	0.000	0.000
Mn^{2+}	0.832	0.489
Ca	3.368	5.307
□	*0.000*	*0.000*
M(2)		
Zr	0.330	0.000
Hf	0.000	0.000
Ti	0.045	0.000
Fe^{2+}	2.710	2.444
Mn^{2+}	3.140	1.791
Mg	0.015	0.019
□	*0.000*	*0.000*

	17-5	*16-3*
Z		
W	0.000	0.000
Nb	0.000	0.000
Ta	0.000	0.000
Zr	3.000	2.907
Hf	0.000	0.093
Ti	0.000	0.000
□	*0.000*	*0.000*
M(3)		
W	0.584	0.102
Nb	0.208	0.160
Ta	0.181	0.000
Zr	0.000	0.000
Hf	0.000	0.616
Ti	0.027	0.037
Si	0.000	0.085
□	*0.000*	*0.000*
M(4) + Si		
Si	24.624	25.000
Al	0.000	0.000
□	*0.376*	*0.000*
X		
Cl	0.928	0.821
F	0.000	0.000
S	0.012	0.231
OH	0.621	0.483
□	*0.439*	*0.464*

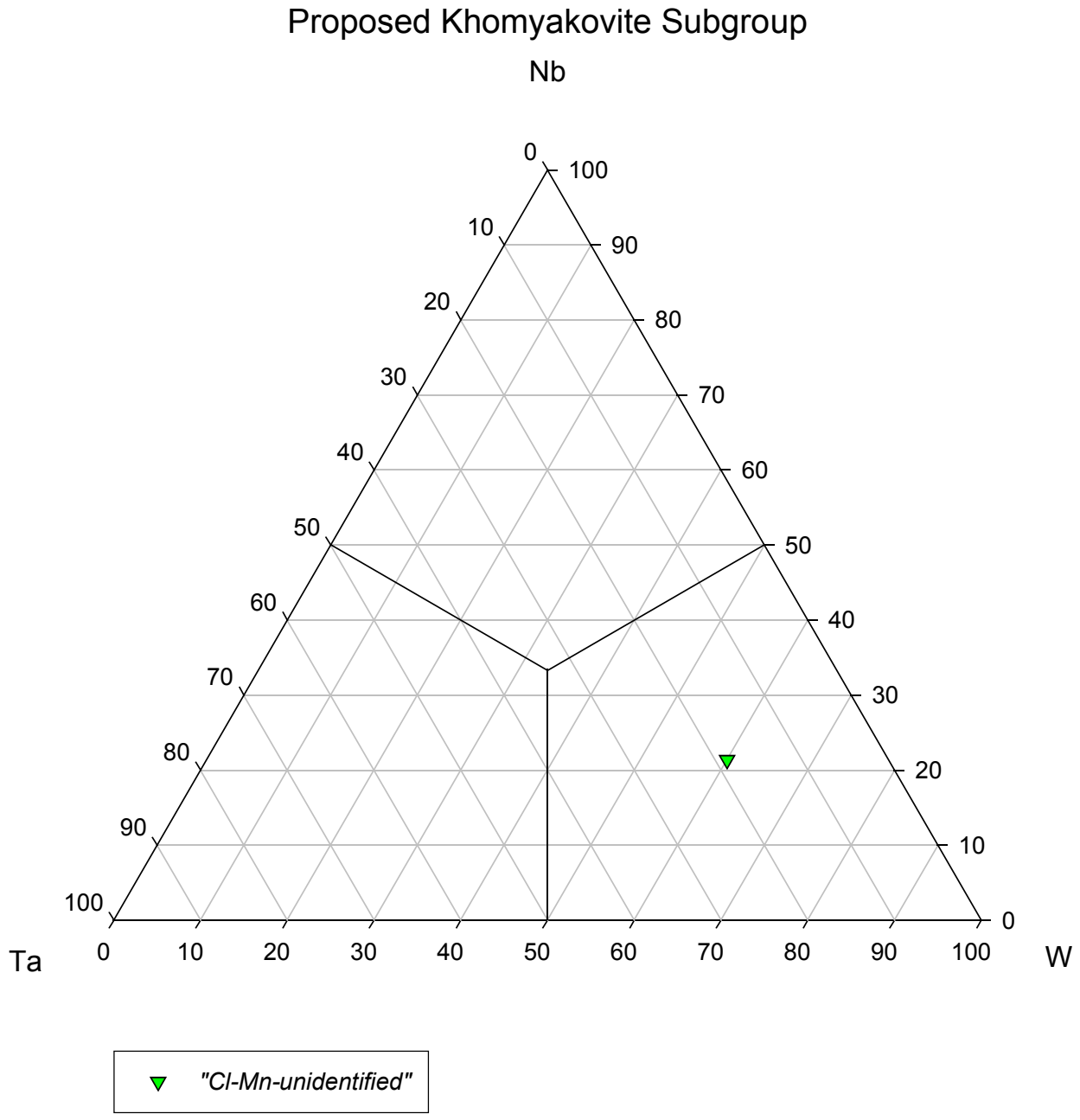

FIGURE 32 – [M(3)](W-Nb-Ta)-dominant proposed khomyakovite subgroup analysis.

PROPOSED "ZR-EUDIALYTE" SUBGROUP

Representative analyses of the proposed "Zr-eudialyte" subgroup are shown in TABLE 16. Site-occupancies for the same analyses, recalculated using the alternative algorithm, are shown in TABLES 17 & 18.

Composition plots for the proposed "Zr-eudialyte" subgroup, based on the three most-abundant occupants of *M*(3), resulted in five ternary plots (Figures 31-35). Apart from the essential inclusion of Zr in all plots, three include Nb and Si, two include Ta, one includes Hf, and one includes Ti. Solid solution in the proposed "Zr-eudialyte" subgroup exists mainly between Zr and Nb & Si in the *M*(3) site; hafnium, tantalum, and titanium appear to be lesser participants.

TABLE 16 – Representative EMP analyses of the proposed "Zr-eudialyte" subgroup.

Analysis #:	*22-2*	*21-5*	*19-3*	*2-1*	*19-2*	*10-2*
SiO_2 (*wt.%*)	45.67	47.92	44.18	45.21	42.52	45.09
TiO_2	0.09	0.05	0.08	0.04	0.07	0.10
ZrO_2	12.71	15.54	12.51	14.37	11.71	13.80
HfO_2	0.00	0.00	0.00	0.00	0.00	0.00
Nb_2O_5	0.76	0.90	1.09	1.30	0.39	0.82
Ta_2O_5	0.06	0.43	0.00	0.00	1.05	0.00
MoO_3	0.00	0.07	0.00	0.00	0.11	0.00
WO_3	0.00	0.00	0.00	0.00	0.00	0.00
Al_2O_3	0.17	0.09	0.26	0.17	0.17	0.13
Sc_2O_3	0.00	0.00	0.00	0.00	0.00	0.06
REE_2O_3	7.07	3.32	6.89	4.66	7.50	4.95
La_2O_3	1.47	0.79	1.42	1.62	1.90	1.06
Ce_2O_3	2.88	1.46	3.21	2.27	3.47	2.48
Pr_2O_3	0.00	0.00	0.00	0.00	0.00	0.00
Nd_2O_3	0.82	0.76	0.91	0.60	1.11	0.71
Sm_2O_3	0.00	0.00	0.00	0.00	0.00	0.00
Gd_2O_3	1.90	0.32	1.35	0.18	1.03	0.70
Dy_2O_3	0.00	0.00	0.00	0.00	0.00	0.00
Er_2O_3	0.00	0.00	0.00	0.00	0.00	0.00
Yb_2O_3	0.00	0.00	0.00	0.00	0.00	0.00
Y_2O_3	0.00	0.00	1.20	0.76	1.42	1.32
FeO	3.97	4.38	4.91	4.56	5.03	4.45
MnO	7.37	6.79	6.21	6.60	7.26	7.19
ZnO	0.00	0.04	0.00	0.00	0.00	0.00
CaO	7.49	8.67	6.91	6.66	6.59	6.62
SrO	na	na	na	na	na	na
BaO	0.34	0.03	0.00	0.17	0.00	0.51
MgO	0.00	0.04	0.00	0.00	0.00	0.00
Na_2O	12.29	11.38	12.79	13.69	13.21	14.50
K_2O	0.49	0.49	0.42	0.44	0.35	0.47
Cl	0.63	1.01	0.81	0.71	0.90	0.33
F	0.74	0.00	0.70	0.56	0.96	0.24
SO_3	0.22	0.00	0.25	0.00	0.00	1.94
H_2O*	0.42	0.16	0.46	0.36	0.62	0.11
O≡Cl	-0.14	-0.23	-0.18	-0.16	-0.20	-0.07
O≡F	-0.31	0.00	-0.29	-0.23	-0.40	-0.10
TOTAL	100.04	101.08	99.21	99.84	99.25	102.46
Species:	*"F-Mn-Zr-eudialyte"*	*"Zr-eudialyte"*	*"F-Zr-eudialyte"*	*"F-Zr-eudialyte"*	*"F-Zr-eudialyte"*	*"S-Zr-eudialyte"*

Normalized to 29 cations (Σ Si + Al + Zr + Ti + Hf + Nb + W + Ta) *apfu*
na = not analyzed
*H_2O calculated based on charge-balance, assuming presence as OH

TABLE 17 – Site-occupancy of proposed "Zr-eudialyte" subgroup analyses I.

	22-2	*21-5*	*19-3*
N(ϕ)			
Na	7.415	6.583	7.888
□	*1.585*	*2.417*	*1.112*
N(4)			
REE	1.392	0.619	1.401
Ca	0.000	0.000	0.000
Sr	0.000	0.000	0.000
Ba	0.074	0.006	0.000
K	0.345	0.322	0.305
Na	3.937	3.863	4.109
□	*0.252*	*1.190*	*0.185*
M(1)			
REE	0.000	0.000	0.000
Y	0.000	0.000	0.363
Fe^{2+}	0.000	0.000	0.000
Mn^{2+}	1.565	1.206	1.438
Ca	4.435	4.794	4.199
□	*0.000*	*0.000*	*0.000*
M(2)			
Zr	0.001	0.200	0.000
Hf	0.000	0.000	0.000
Ti	0.000	0.000	0.000
Fe^{2+}	1.835	1.891	2.329
Mn^{2+}	1.882	1.764	1.545
Mg	0.000	0.031	0.000
□	*0.000*	*0.000*	*0.000*

	22-2	*21-5*	*19-3*
Z			
W	0.000	0.000	0.000
Nb	0.000	0.000	0.000
Ta	0.000	0.000	0.000
Zr	3.000	3.000	3.000
Hf	0.000	0.000	0.000
Ti	0.000	0.000	0.000
□	*0.000*	*0.000*	*0.000*
M(3)			
W	0.000	0.000	0.000
Nb	0.189	0.210	0.280
Ta	0.010	0.060	0.000
Zr	0.423	0.713	0.458
Hf	0.000	0.000	0.000
Ti	0.039	0.017	0.035
Si	0.339	0.000	0.226
□	*0.000*	*0.000*	*0.001*
M(4) + Si			
Si	24.887	24.743	24.828
Al	0.113	0.057	0.172
□	*0.000*	*0.200*	*0.000*
X			
Cl	0.593	0.880	0.779
F	1.295	0.000	1.248
S	0.090	0.000	0.108
OH	0.023	0.558	0.000
□	*0.000*	*0.561*	*0.000*

TABLE 18 – Site-occupancy of proposed "Zr-eudialyte" subgroup analyses II.

	2-1	*19-2*	*10-2*
N(ϕ)			
Na	8.311	8.491	8.849
□	*0.689*	*0.509*	*0.151*
N(4)			
REE	0.930	1.363	0.670
Ca	0.000	0.000	0.000
Sr	0.000	0.000	0.000
Ba	0.036	0.000	0.111
K	0.303	0.262	0.330
Na	4.713	4.375	4.889
□	*0.018*	*0.000*	*0.000*
M(1)			
REE	0.000	0.241	0.318
Y	0.222	0.448	0.390
Fe^{2+}	0.000	0.000	0.000
Mn^{2+}	1.875	1.126	1.369
Ca	3.903	4.185	3.923
□	*0.000*	*0.000*	*0.000*
M(2)			
Zr	0.168	0.000	0.000
Hf	0.000	0.000	0.000
Ti	0.000	0.000	0.000
Fe^{2+}	2.084	2.492	2.059
Mn^{2+}	1.180	2.515	2.003
Mg	0.000	0.002	0.000
□	*0.000*	*0.000*	*0.000*

	2-1	*19-2*	*10-2*
Z			
W	0.000	0.000	0.000
Nb	0.000	0.000	0.000
Ta	0.000	0.000	0.000
Zr	3.000	3.000	3.000
Hf	0.000	0.000	0.000
Ti	0.000	0.000	0.000
□	*0.000*	*0.000*	*0.000*
M(3)			
W	0.000	0.000	0.000
Nb	0.321	0.104	0.205
Ta	0.000	0.169	0.000
Zr	0.665	0.383	0.724
Hf	0.000	0.000	0.000
Ti	0.014	0.032	0.040
Si	0.000	0.311	0.030
□	*0.000*	*0.001*	*0.001*
M(4) + Si			
Si	24.725	24.885	24.917
Al	0.107	0.115	0.083
□	*0.168*	*0.000*	*0.000*
X			
Cl	0.654	0.906	0.311
F	0.965	1.795	0.420
S	0.000	0.000	0.806
OH	0.380	0.000	0.401
□	*0.000*	*0.000*	*0.062*

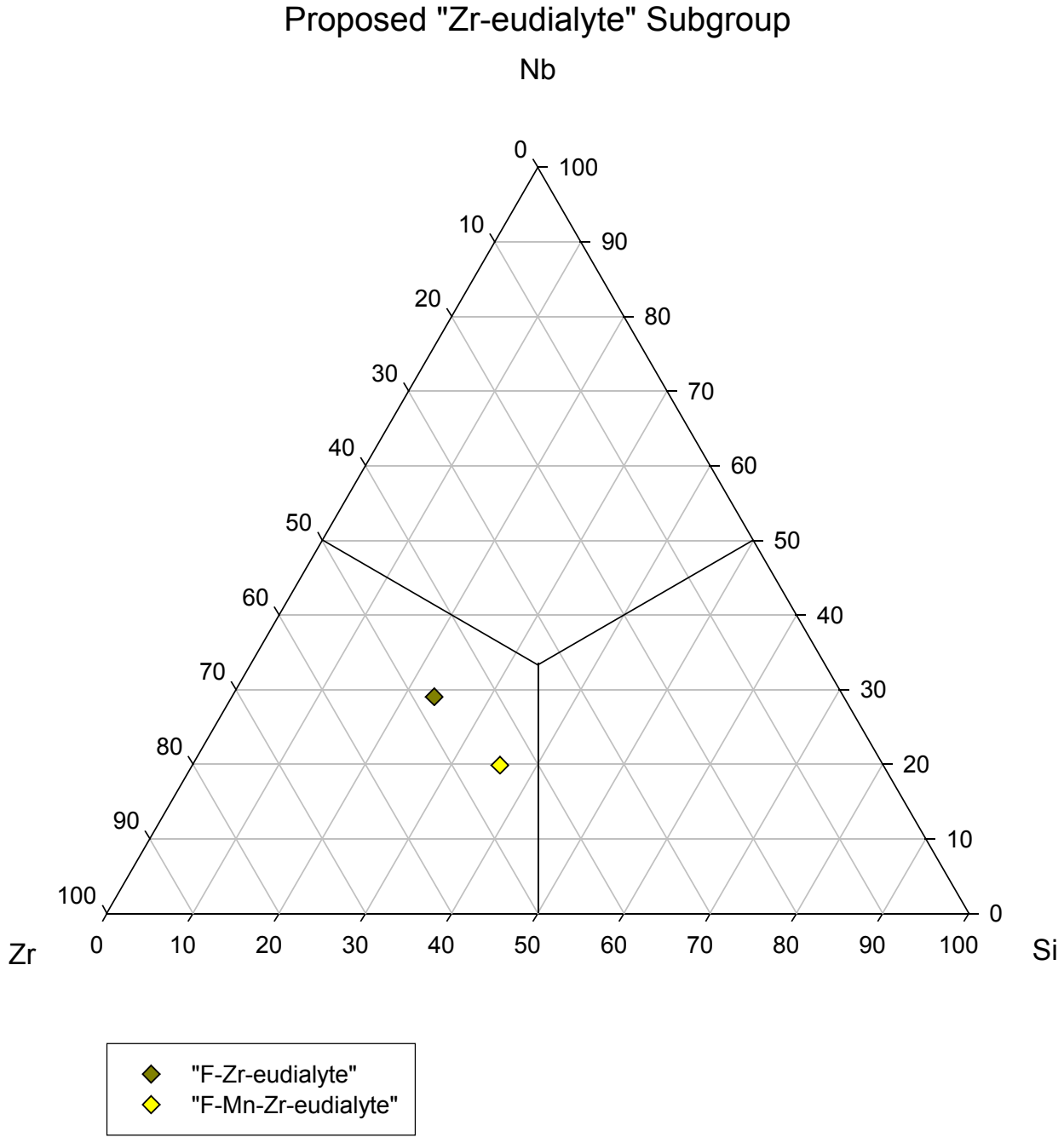

FIGURE 33 – [M(3)](Si-Nb-Zr)-dominant proposed "Zr-eudialyte" subgroup analyses.

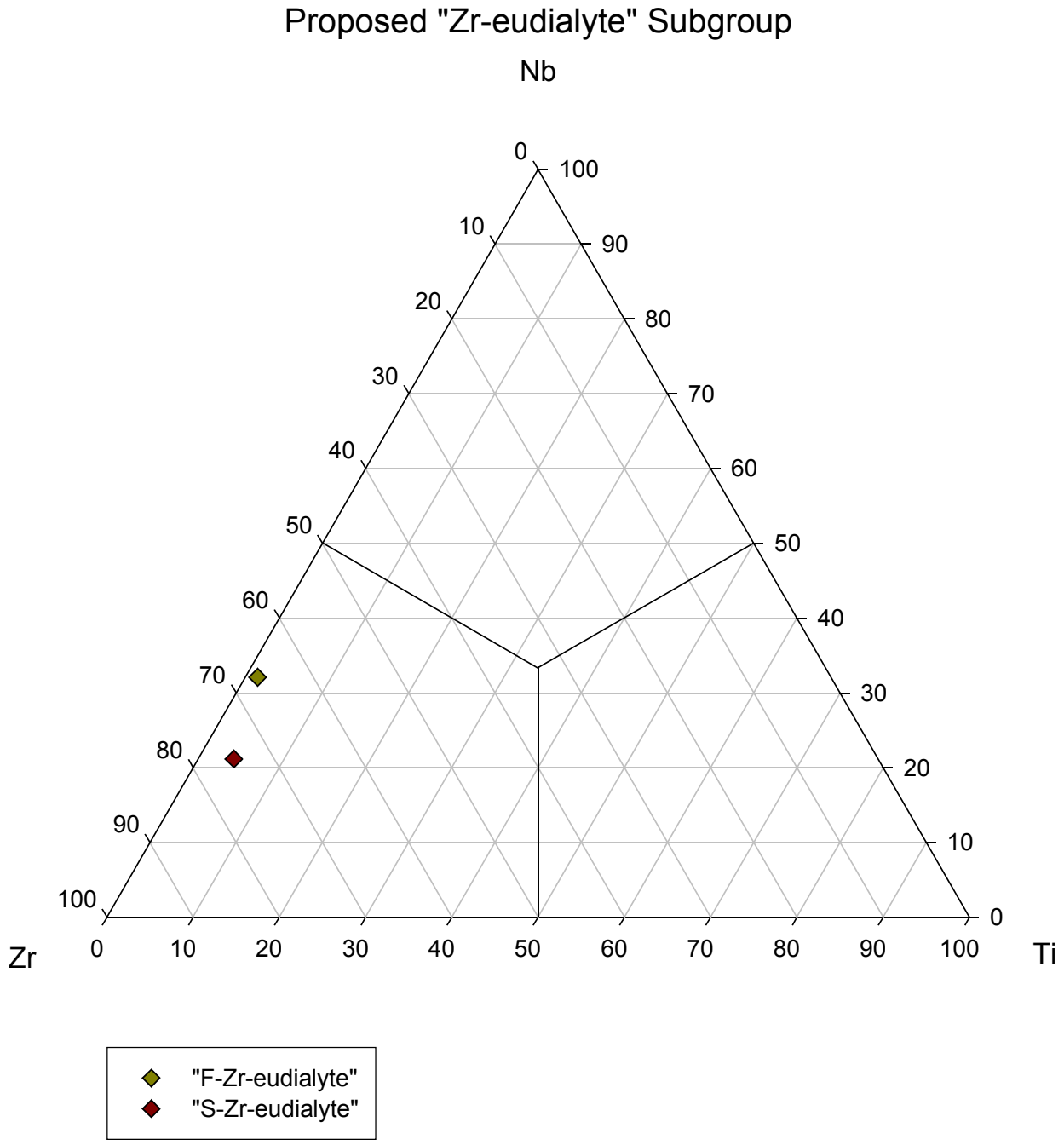

FIGURE 34 – [M(3)](Ti-Nb-Zr)-dominant proposed "Zr-eudialyte" subgroup analyses.

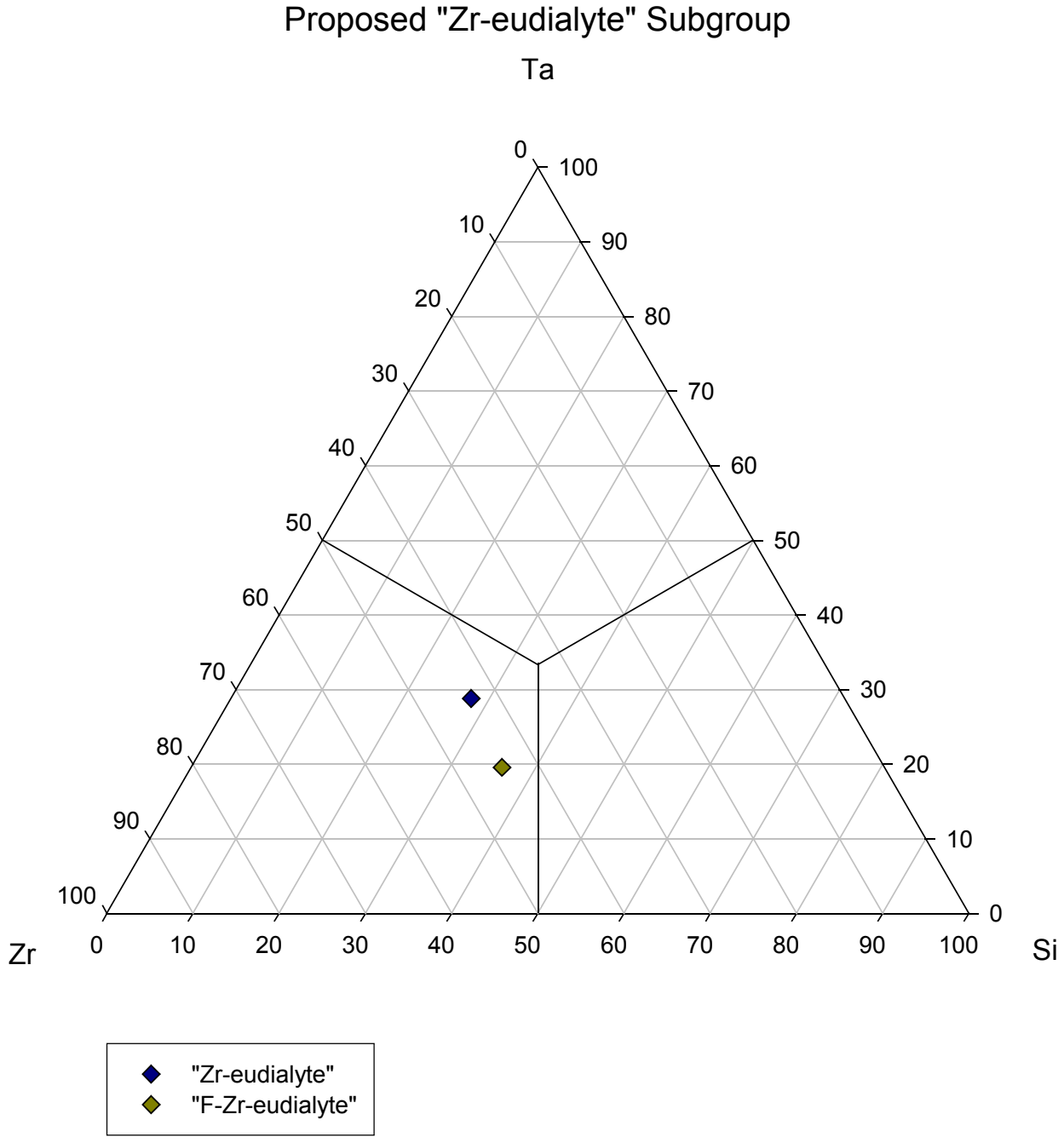

FIGURE 35 – [M(3)](Si-Ta-Zr)-dominant proposed "Zr-eudialyte" subgroup analyses.

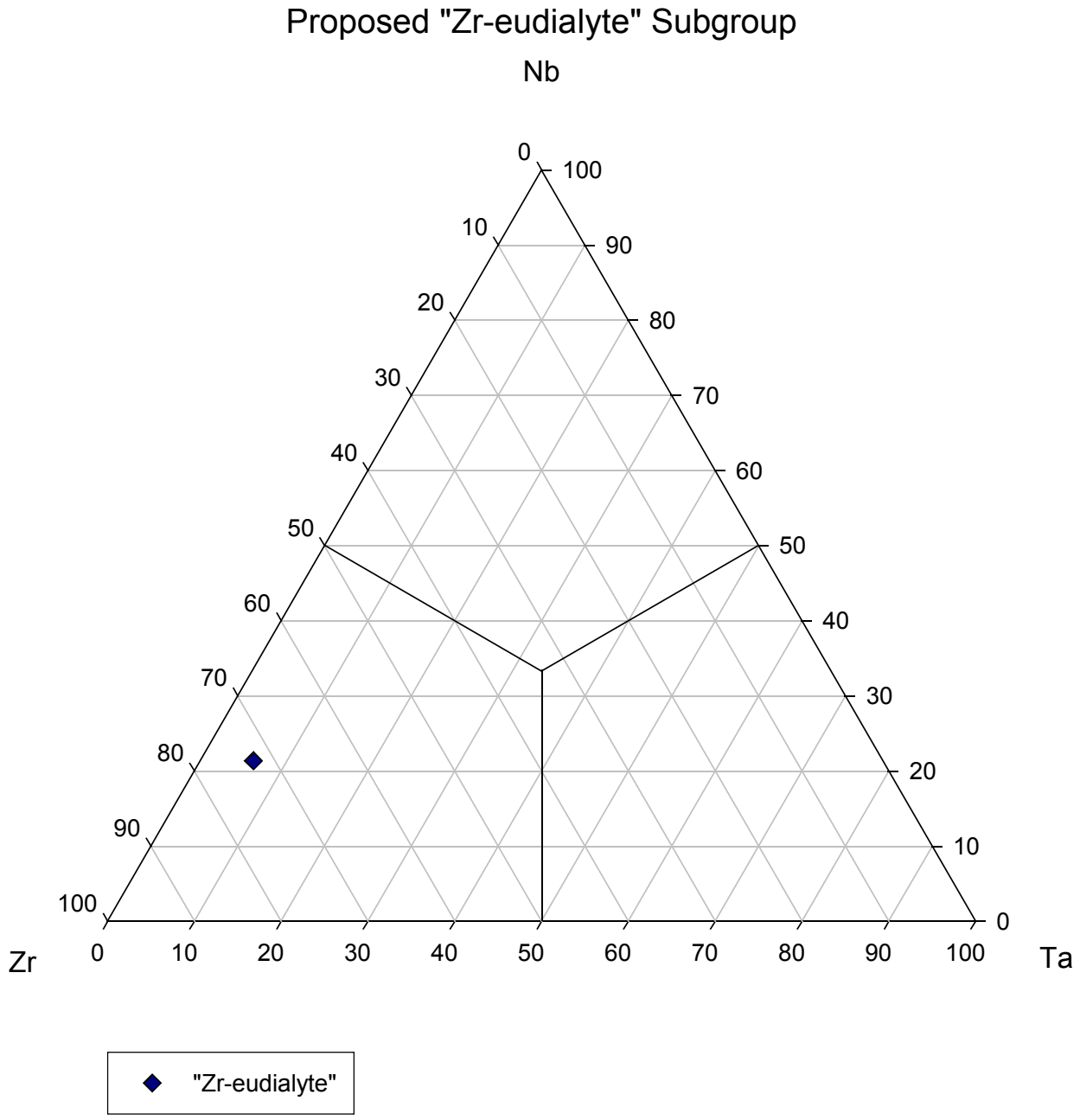

FIGURE 36 – [M(3)](Ta-Nb-Zr)-dominant proposed "Zr-eudialyte" subgroup analysis.

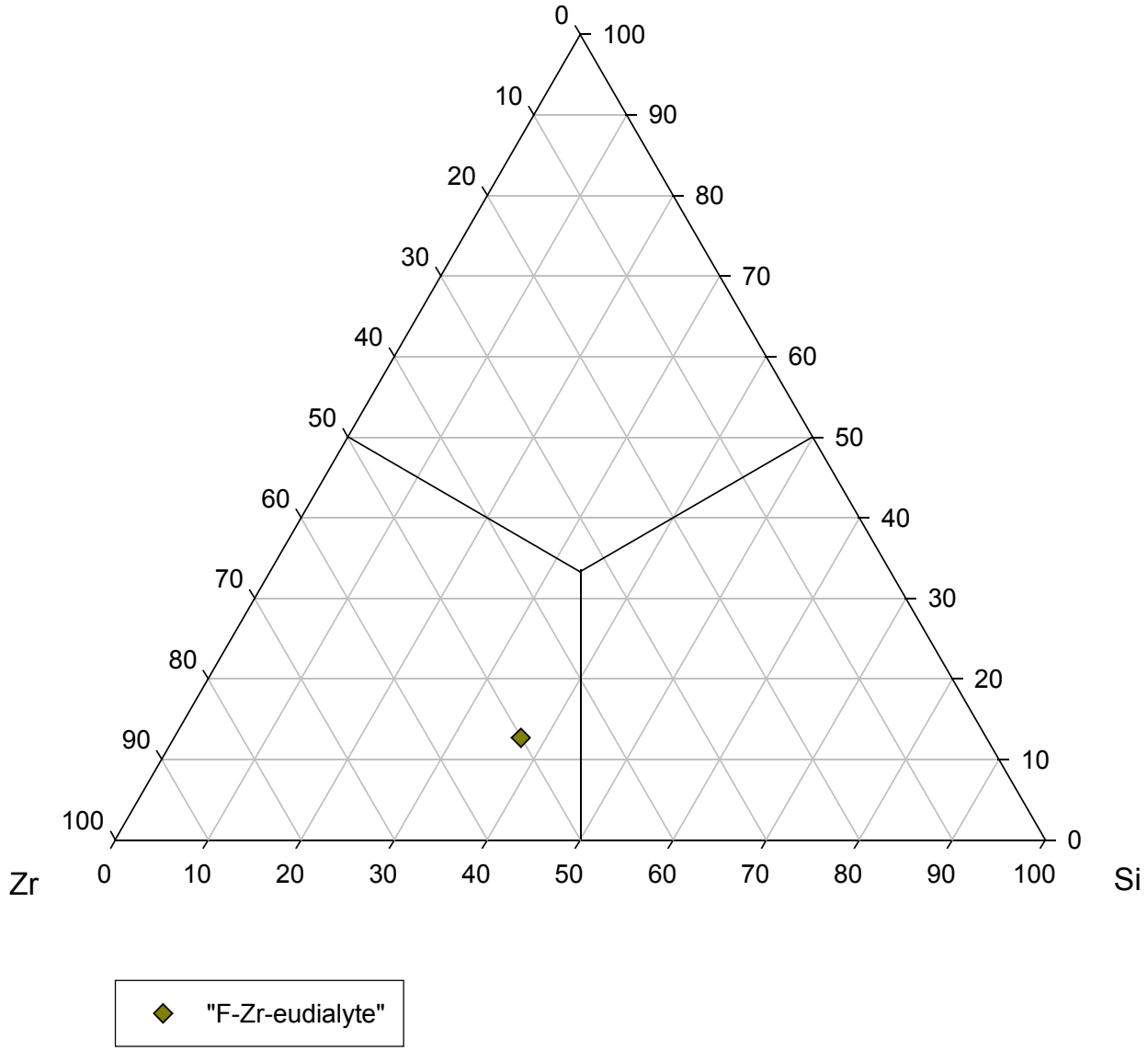

FIGURE 37 – [M(3)](Si-Hf-Zr)-dominant proposed “Zr-eudialyte” subgroup analysis.

PROPOSED "HF-EUDIALYTE" SUBGROUP

The representative analysis of the proposed "Hf-eudialyte" subgroup is shown in TABLE 14. Site-occupancies for the same analysis, recalculated using the alternative algorithm, are shown in TABLE 15.

Composition plots for the proposed "Hf-eudialyte" subgroup, based on the three most-abundant occupants of *M*(3), resulted in one ternary plot (Figure 36). Apart from the essential inclusion of Hf, the plot includes Nb and W.

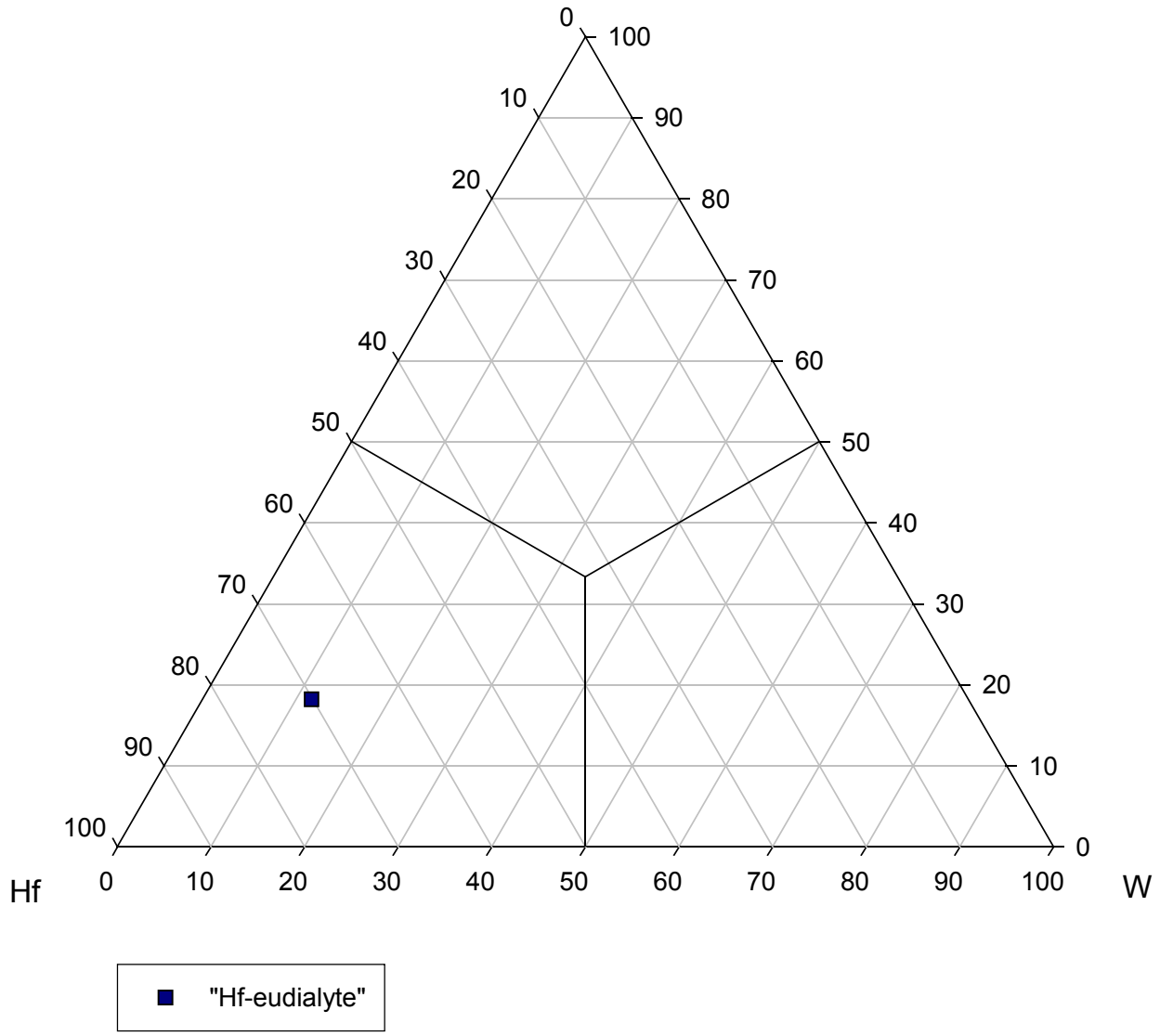

FIGURE 38 – [M(3)](W-Nb-Hf)-dominant proposed “Hf-eudialyte” subgroup analysis.

MAJOR ELEMENT CRYSTAL CHEMISTRY

Introduction

Contents of major and trace elements were plotted against the mole fraction of manganese with respect to iron (X_{Mn}) in the *M*(2) site. This relationship was selected for the same reasons that SiO_2 is used in Harker diagrams: manganese and iron are abundant and ubiquitous in eudialyte group minerals, and like SiO_2 in igneous suites, their ratio is a proxy for magmatic and chemical evolution of the system.

Main Group Elements

Silicon compositions ranged from 39.11 to 50.61 (average 46.02) wt.% SiO_2 (Figure 37). This corresponds to a range of 24.453 to 25.975 *apfu* Si. Silicon is primarily found in the *Si* site, which is full to capacity at 24.000 *apfu* Si in all but five analyses. Silicon is also present in the *M*(3) site, in which it is the most abundant cation in 35 analyses, with 25 having Si in an absolute majority; overflow is partitioned to *M*(4). No linear correlation was observed between SiO_2 content and X_{Mn}.

High Field Strength Elements (HFSE)

Zirconium content of analyzed eudialyte group minerals ranged from 8.32 to 15.54 wt.% ZrO_2 with an average of 11.53 (Figure 38). This translated to a range of 2.215 to 3.913 *apfu* Zr. The *Z* site, the primary site for Zr, only has a total capacity of 3.00 *apfu*, so excess Zr was typically partitioned to *M*(3).

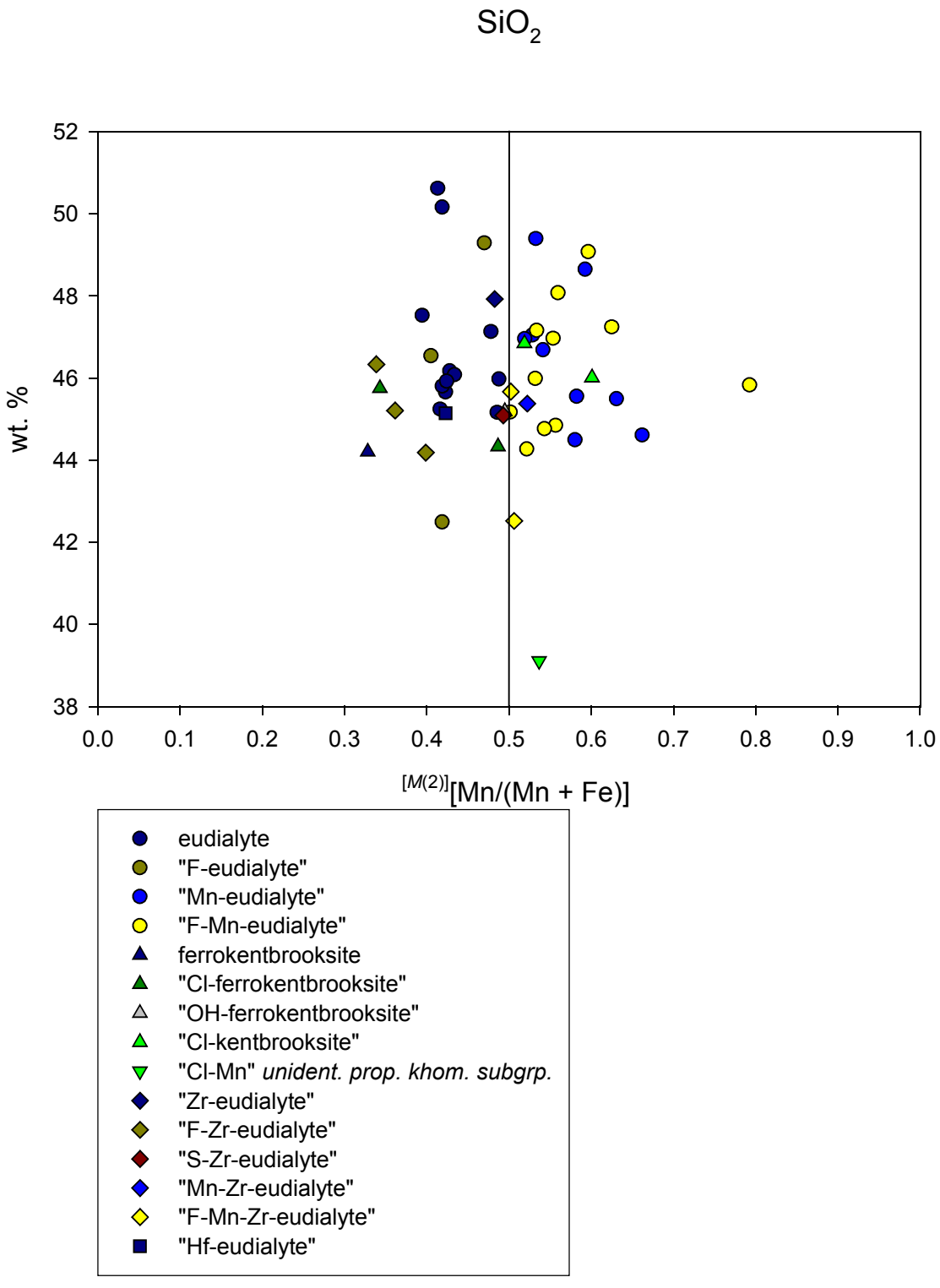

FIGURE 39 – Total SiO_2 *versus* mole fraction $^{[M(2)]}$[Mn/(Mn + Fe)].

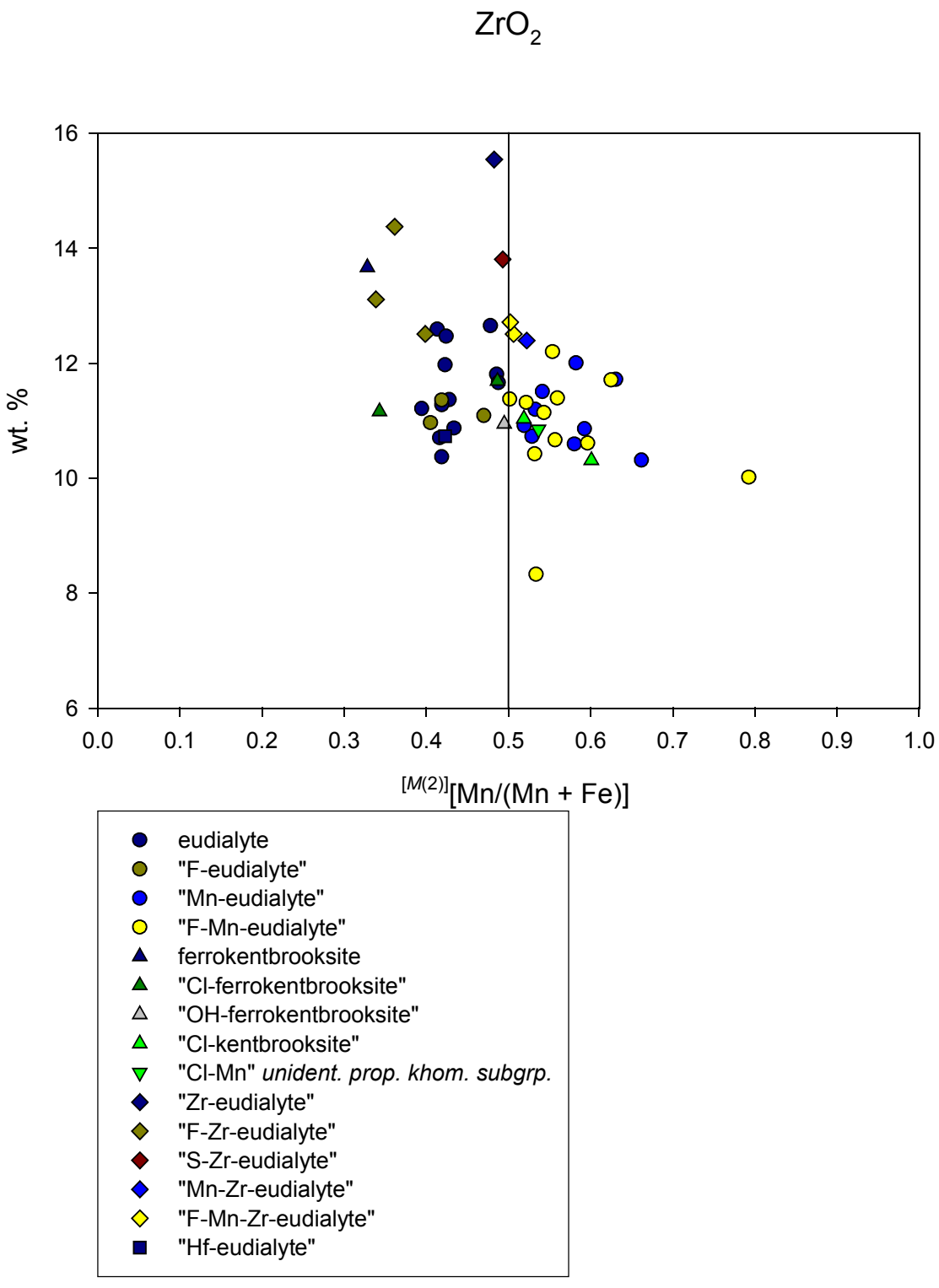

FIGURE 40 – Total ZrO_2 *versus* mole fraction $^{[M(2)]}$[Mn/(Mn + Fe)].

Eight analyses had Zr as the most abundant cation in *M*(3), and in three of them it occupied greater than 50% of the sites. Two analyses had a surplus of Zr and other HFSE so great that some Zr was partitioned to *M*(2). There is a weak trend of decreasing ZrO_2 content with increasing X_{Mn}. This is most prominent amongst analyses from the proposed eudialyte and kentbrooksite subgroups.

Other Transition Elements

Because of their ubiquitous concomitancy and their importance in end-member determination, iron and manganese should be treated together. Manganese dominated iron, with compositional ranges of 3.96 to 11.12 (average 6.71) wt.% MnO (1.737 to 5.228 *apfu* Mn) and 2.45 to 5.62 (average 4.61) wt.% FeO (1.137 to 2.710 *apfu* Fe). Iron is found exclusively in *M*(2) in the eudialyte group analyses from Mont Saint-Hilaire, even though it can occupy sites in *M*(1), as well; in contrast, manganese occupies sites in both *M*(1) and *M*(2). Even though Mn is more abundant (totaling across all sites on an *apfu* basis) than Fe in 80% of the analyses, Mn is the dominant cation in *M*(2) in only about half of the analyses. This is because excess Mn overflows to *M*(1), especially in analyses with low Ca.

Alkali & Alkaline Earth Elements

Calcium content of analyzed eudialyte group minerals ranged from 4.99 to 11.31 wt.% CaO with an average of 7.76 (Figure 39). This translated to a range of 3.368 to 6.070 *apfu* Ca. Calcium is mainly found in *M*(1) in the eudialyte group analyses at Mont Saint-Hilaire, although one analysis with high total Ca showed calcium partitioned to *N*(4). Calcium always holds an absolute majority of sites in *M*(1), although in the analyses from Mont Saint-Hilaire, as few as

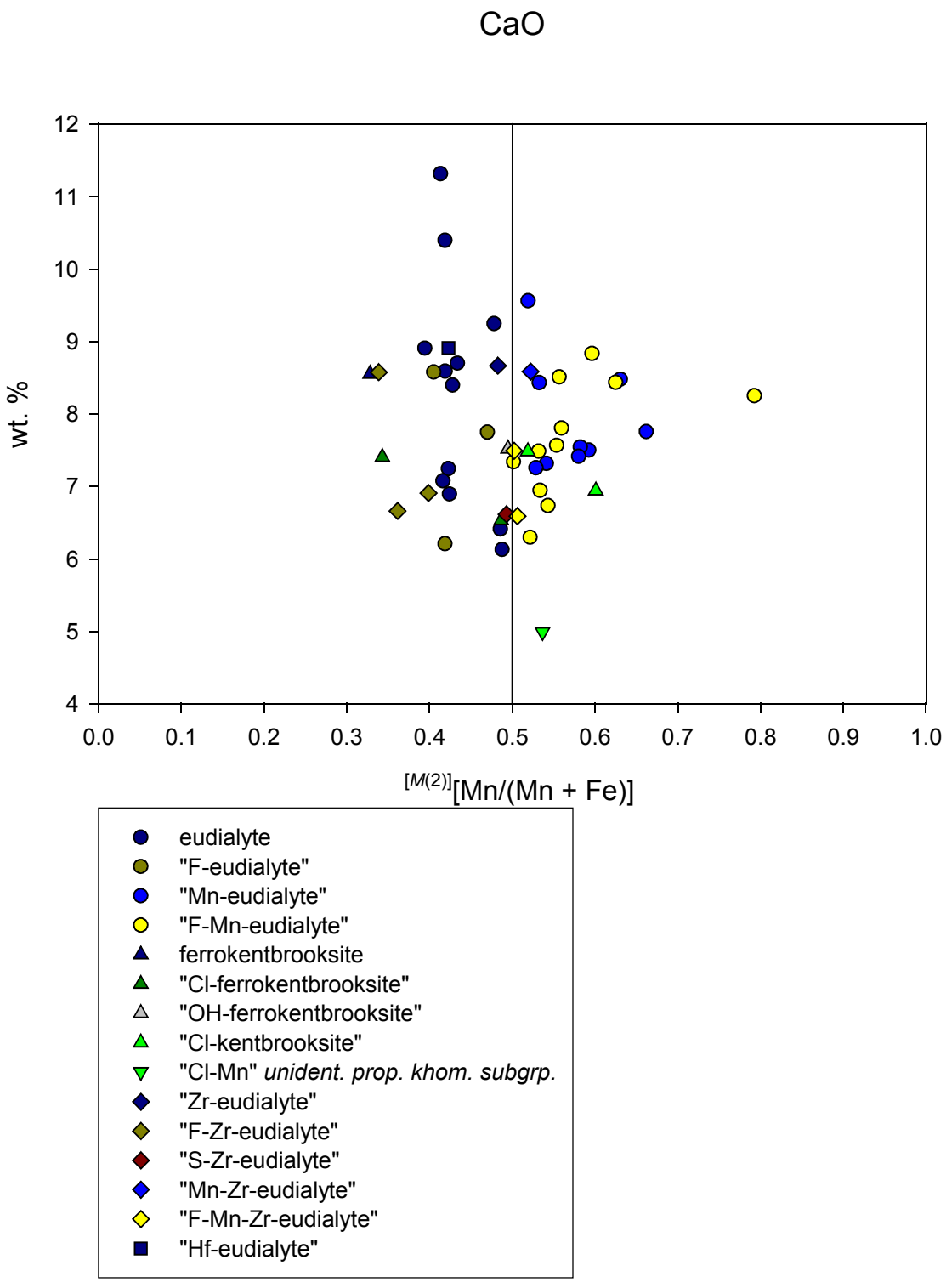

FIGURE 41 – Total CaO *versus* mole fraction $^{[M(2)]}$[Mn/(Mn + Fe)].

56% of the sites in *M*(1) were held by Ca. No linear correlation was observed between CaO content and X_{Mn}.

Sodium content of analyzed eudialyte group minerals ranged from 11.28 to 15.11 (average 13.26) wt.% Na_2O (Figure 40). This corresponds to a range of 10.951 to 17.487 *apfu* total Na. Sodium is partitioned between two sites, *N*(ϕ) and *N*(4). Sodium is the sole occupant of *N*(ϕ), with a range of 6.138 to 9.687 (average 8.060) *apfu* Na. The balance of the sodium is partitioned to *N*(4), with a range of 3.189 to 5.669 (average 4.401) *apfu* Na. Sodium is the dominant cation in *N*(4) in every analysis. No linear correlation was observed between Na_2O content and X_{Mn}.

TRACE ELEMENT CRYSTAL CHEMISTRY

Proposed Eudialyte Subgroup

Iron-dominant members of the proposed eudialyte subgroup exhibit significantly higher average contents of Ta_2O_5, WO_3, Al_2O_3, Sc_2O_3, La_2O_3, Ce_2O_3, and BaO *versus* their manganese-dominant counterparts.

Manganese-dominant members of the proposed eudialyte subgroup exhibit significantly higher average contents of TiO_2, HfO_2, Nb_2O_5, Nd_2O_3, Gd_2O_3, Y_2O_3, MgO, F, and SO_3 *versus* their iron-dominant counterparts.

No significant differences were found for MoO_3, K_2O, and Cl.

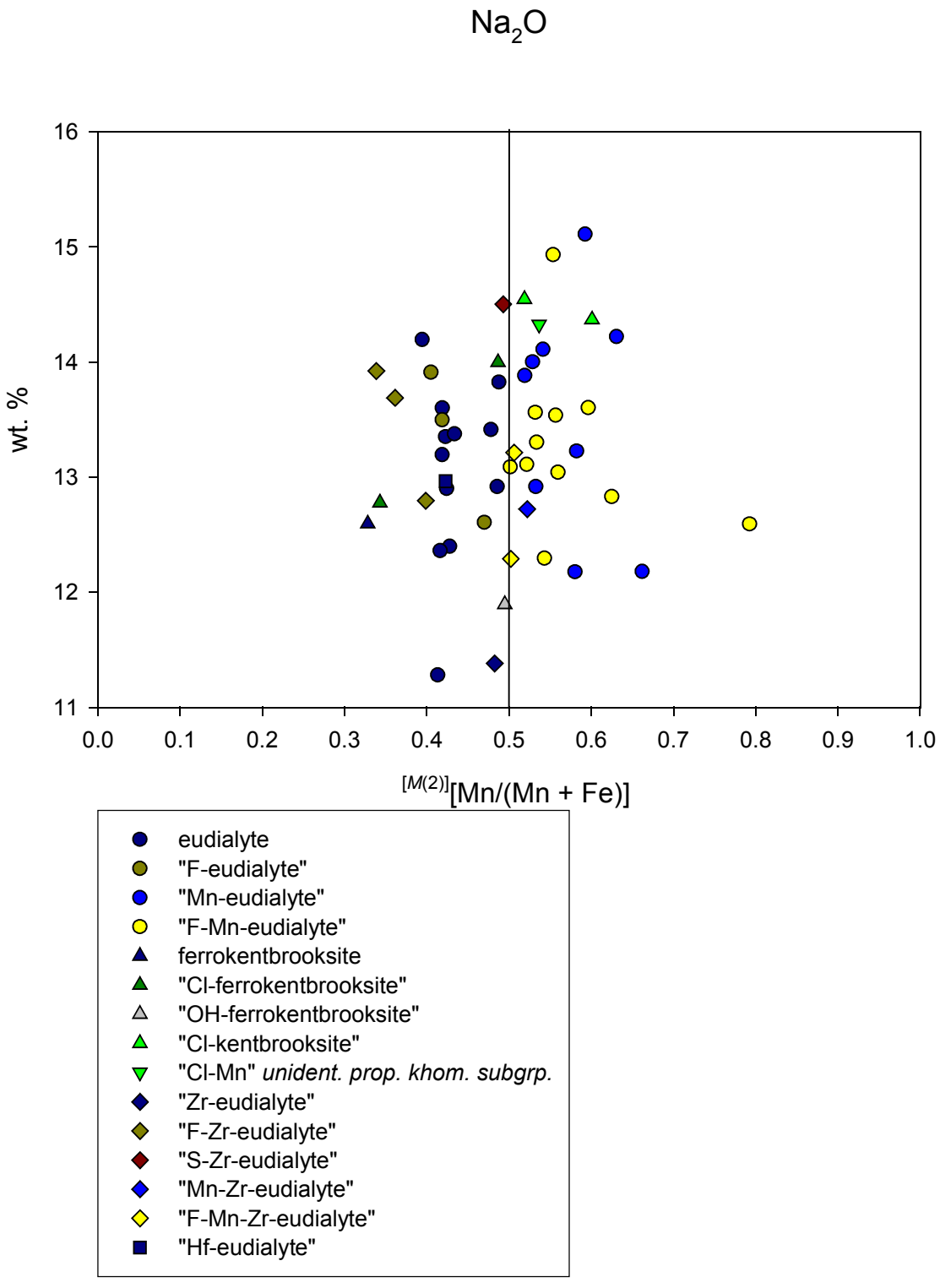

FIGURE 42 – Total Na_2O *versus* mole fraction $^{[M(2)]}$[Mn/(Mn + Fe)].

Proposed Kentbrooksite Subgroup

Iron-dominant members of the proposed kentbrooksite subgroup exhibit significantly higher average contents of Ta_2O_5, Al_2O_3, La_2O_3, Ce_2O_3, Nd_2O_3, Gd_2O_3, Y_2O_3, F, and SO_3 *versus* their manganese-dominant counterparts.

Manganese-dominant members of the proposed kentbrooksite subgroup exhibit significantly higher average contents of TiO_2, HfO_2, Nb_2O_5, BaO, and K_2O *versus* their iron-dominant counterparts.

No significant differences were found for MoO_3, WO_3, Sc_2O_3, MgO, and Cl.

Proposed "Zr-eudialyte" Subgroup

Iron-dominant members of the proposed "Zr-eudialyte" subgroup exhibit significantly higher average contents of HfO_2, Nb_2O_5, Al_2O_3, and BaO *versus* their manganese-dominant counterparts.

Manganese-dominant members of the proposed "Zr-eudialyte" subgroup exhibit significantly higher average contents of TiO_2, Ta_2O_5, MoO_3, La_2O_3, Ce_2O_3, Nd_2O_3, Gd_2O_3, K_2O, Cl, F, and SO_3 *versus* their iron-dominant counterparts.

No significant differences were found for WO_3, Sc_2O_3, Y_2O_3, and MgO.

Proposed Khomyakovite and "Hf-eudialyte" Subgroups

No internal distinctions could be made or trends established for the proposed khomyakovite and "Hf-eudialyte" subgroups since each only contained one analysis.

High Field Strength Elements (HFSE)

Titanium is far less abundant than zirconium in the analyses, typical for the agpaitic environment of Mont Saint-Hilaire, in which $a_{Zr} > a_{Ti}$ is the norm. Contents ranged from 0.01 to 0.47 wt.% TiO_2 with an average of 0.13 (Figure 41). This corresponds to a range of 0.003 to 0.198 *apfu* Ti. Titanium was partitioned primarily to *Z* and *M*(3), with small quantities appearing in *M*(2) in five analyses with high overall HFSE content. Titanium content correlates with increased X_{Mn}, especially in the proposed eudialyte and kentbrooksite subgroups.

Hafnium is a locally abundant trace element in eudialyte group minerals at Mont Saint-Hilaire, with compositions ranging from 0.00 to 4.47 wt.% HfO_2, with an average of 0.37 (Figure 42), and cation content from 0.000 to 0.709 *apfu* Hf. Hafnium appears primarily in *Z* and *M*(3); only one analysis showed Hf in *M*(2), overflowing from *M*(3), which was also overwhelmed with Nb and Ta. In one analysis, Hf possesses an absolute majority of sites in *M*(3). Hafnium content does not correlate linearly to X_{Mn}.

Niobium and tantalum should be treated together, as they are so commonly used as discriminant elements (*e.g.* NYF- *versus* LCT-type pegmatites). Overall, as would be expected in the tectonic environment of Mont Saint-Hilaire, Nb dominates Ta, with compositional ranges of 0.00 to 3.13 (average 0.97) wt.% Nb_2O_5 and 0.00 to 1.95 (average 0.38) wt.% Ta_2O_5, respectively (Figures 43 & 44). This corresponds to maximum cation contents of 0.778 and 0.293 *apfu*, respectively. Nevertheless, Ta is more abundant than Nb in six analyses (counting only non-zero analyses) and equally abundant in one.

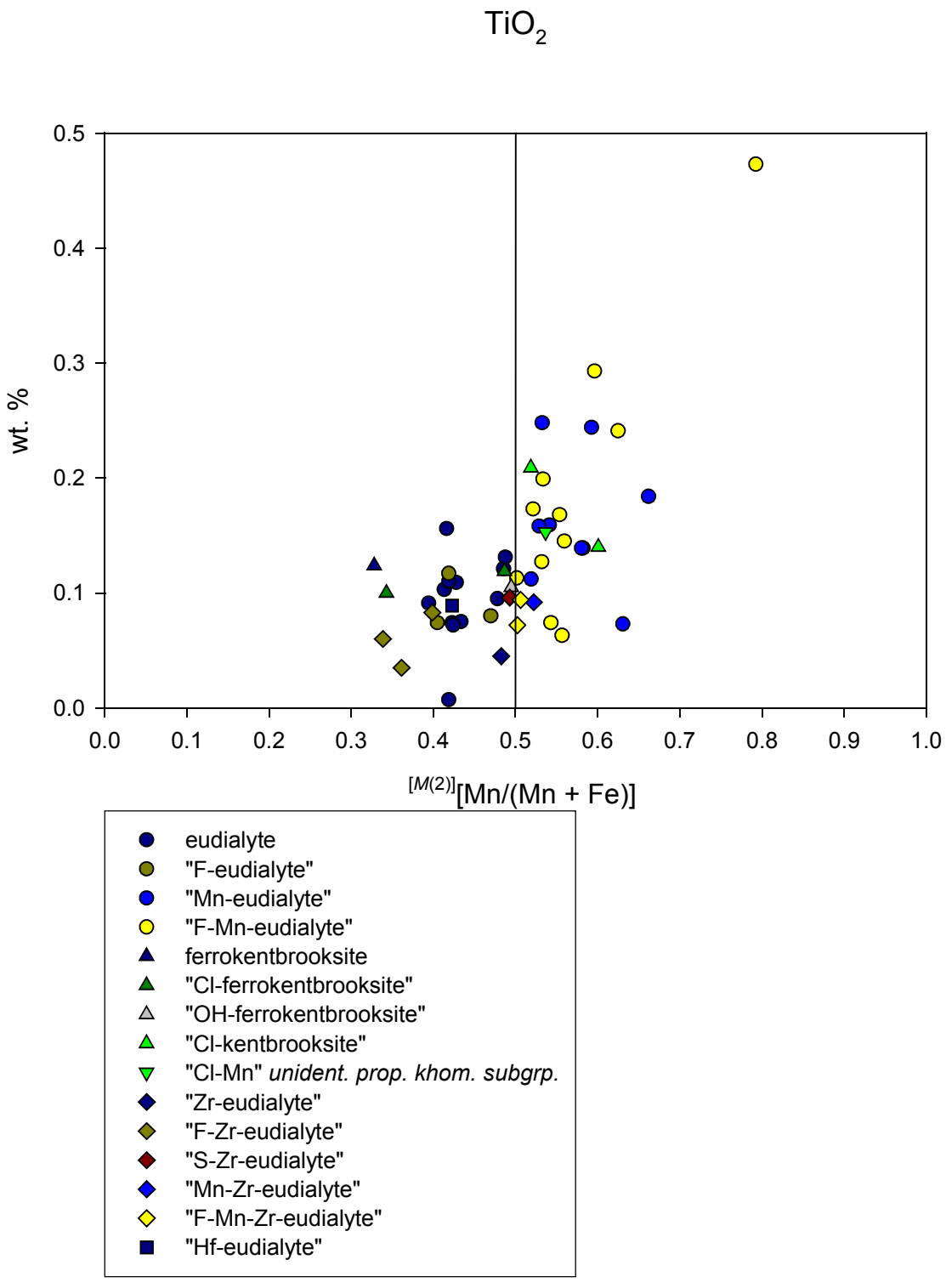

FIGURE 43 – Total TiO_2 *versus* mole fraction $^{[M(2)]}$[Mn/(Mn + Fe)]

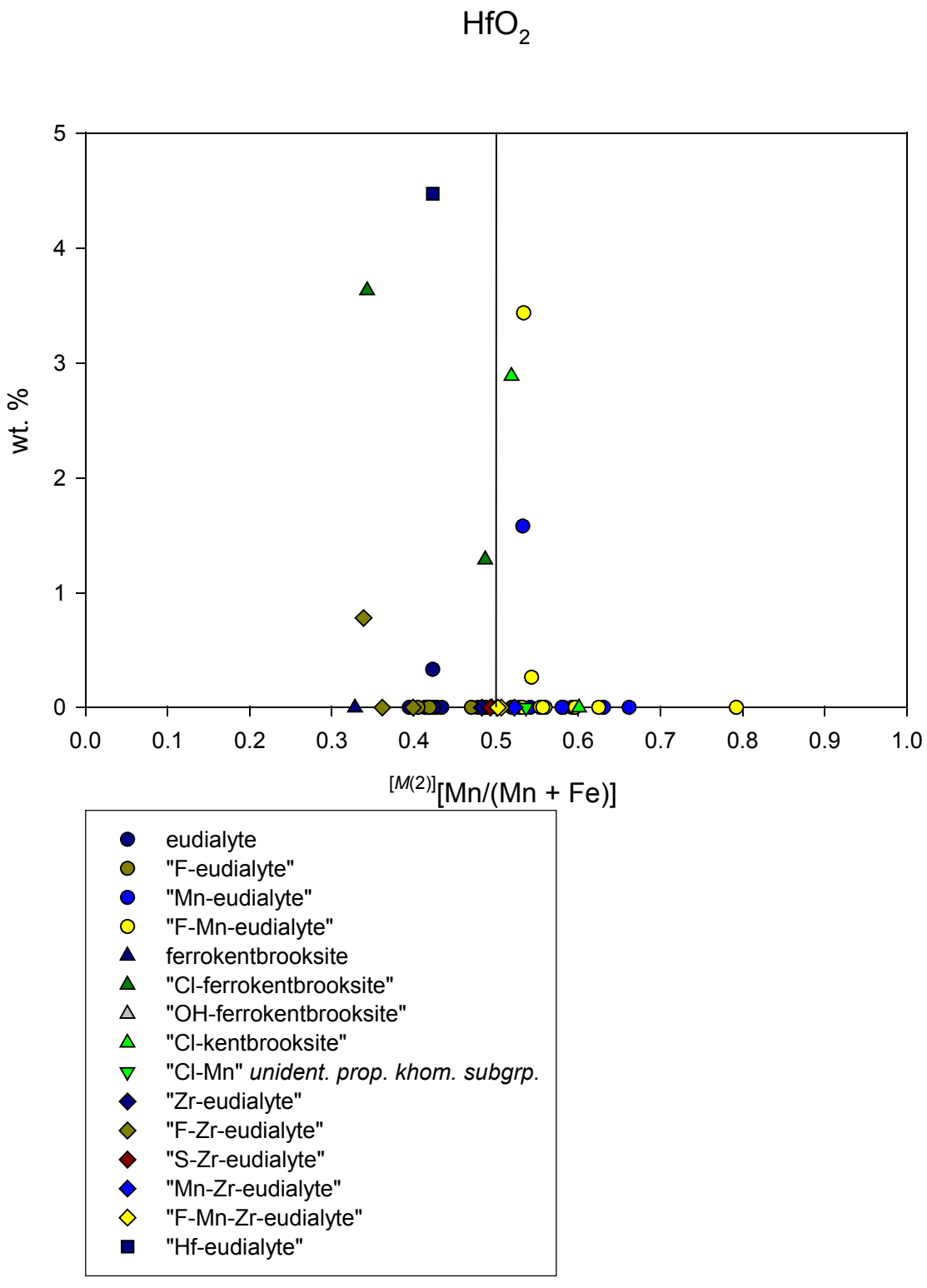

FIGURE 44 – Total HfO_2 *versus* mole fraction $^{[M(2)]}$[Mn/(Mn + Fe)].

Niobium and tantalum primarily occur in *M*(3), but small amounts of Nb occur in *Z* in ten analyses, and Ta in seven. Tantalum is never the most abundant element in *M*(3), but it occupies 20-30% of available sites in three analyses. Niobium, on the other hand, is the most abundant element in *M*(3) in five analyses, and it holds absolute majority in three of them. No linear correlation was found between either Nb_2O_5 or Ta_2O_5 content and X_{Mn}.

Molybdenum is a trace element in eudialyte group minerals at Mont Saint-Hilaire. Compositions ranged from 0.00 to 0.46 wt.% MoO_3, with an average of 0.05 (Figure 45). This corresponds to a range of 0.000 to 0.110 *apfu* Mo. Molybdenum was not considered in the analyses of JOHNSEN & GRICE (1999), and so, was not incorporated into the alternative algorithm. Based on its ionic radius and charge, however, Mo almost certainly occupies *M*(3). In the analyses from the East Hill Suite, Mo is restricted to members of the proposed eudialyte and "Zr-eudialyte" subgroups. Molybdenum content does not correlate linearly with X_{Mn}.

Tungsten is an uncommon trace element in the analyses. This is strongly reflected in the content range, which although it ran from 0.00 to 3.58 wt.% WO_3 (0.000 to 0.584 *apfu* W) only had an average of 0.12 wt.% WO_3 (Figure 46). Tungsten typically occupies sites in *M*(3), although in one analysis with high $^{[M(3)]}$HFSE and low $^{[Z]}$Zr, it is present in *Z*. Tungsten was the most abundant element in *M*(3) in only one analysis, in which it held an absolute majority of sites. No linear correlation exists between WO_3 content and X_{Mn}.

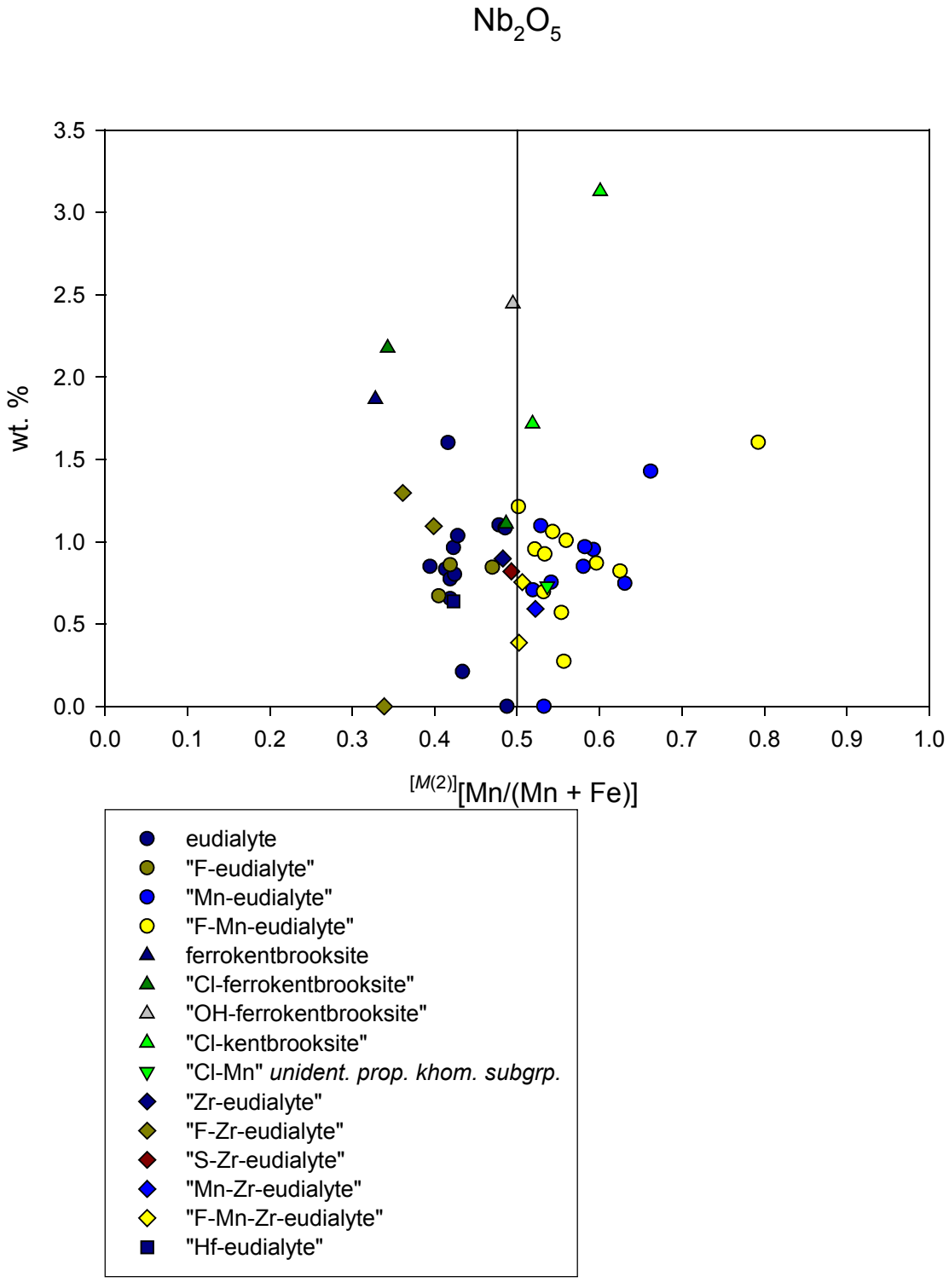

FIGURE 45 – Total Nb_2O_5 *versus* mole fraction $^{[M(2)]}$[Mn/(Mn + Fe)].

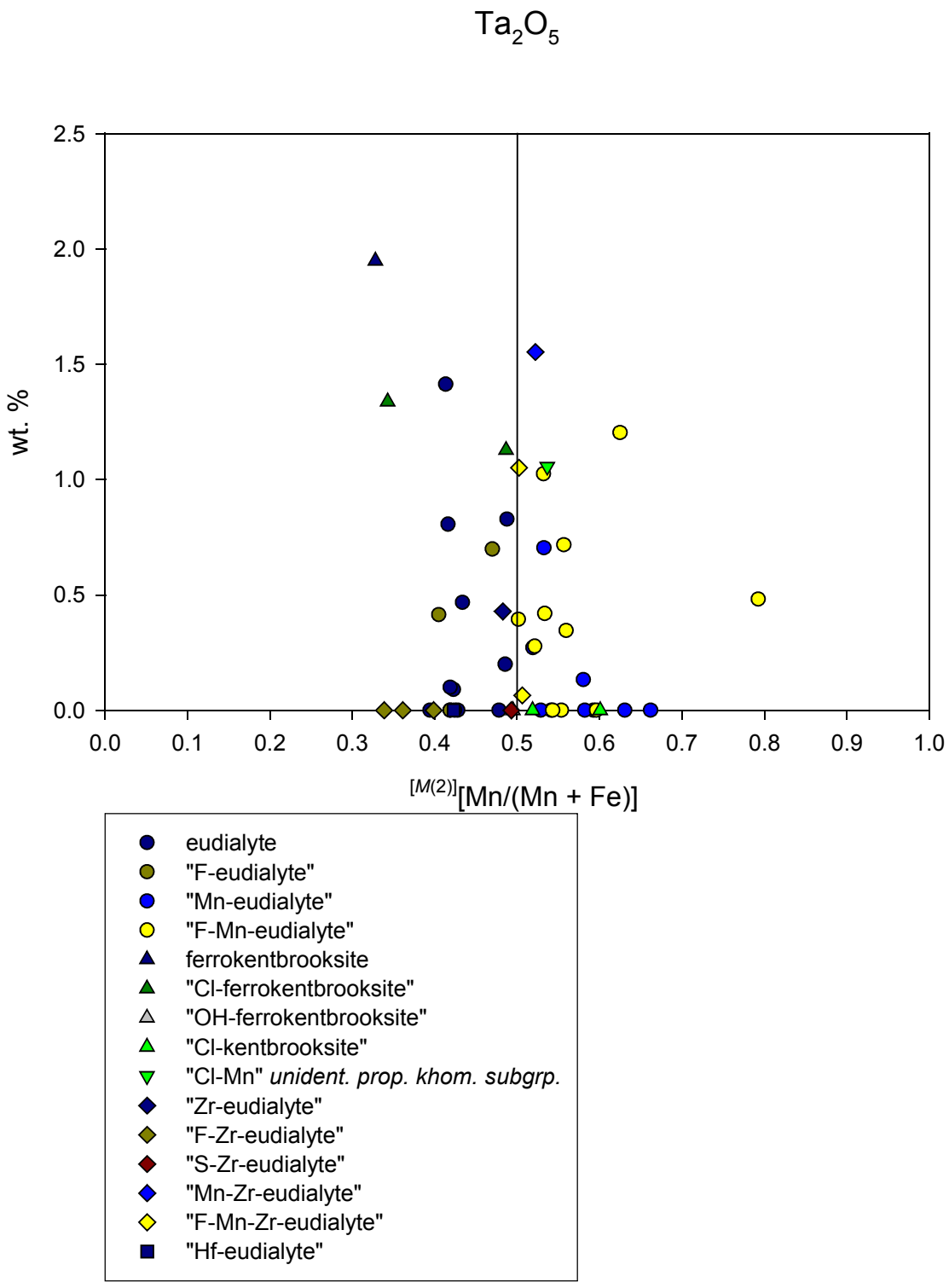

FIGURE 46 – Total Ta_2O_5 *versus* mole fraction $^{[M(2)]}$[Mn/(Mn + Fe)].

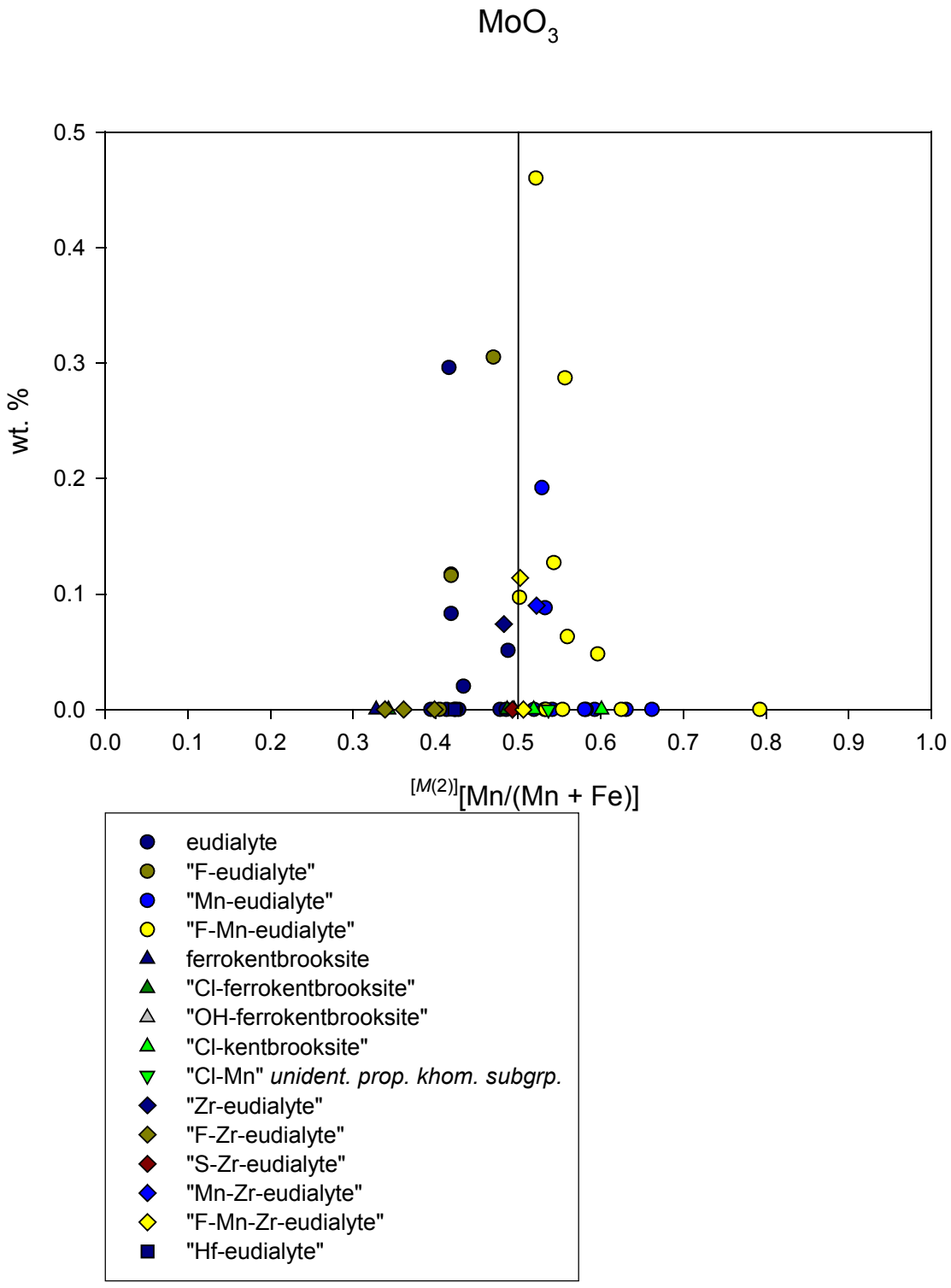

FIGURE 47 – Total MoO_3 *versus* mole fraction $^{[M(2)]}$[Mn/(Mn + Fe)].

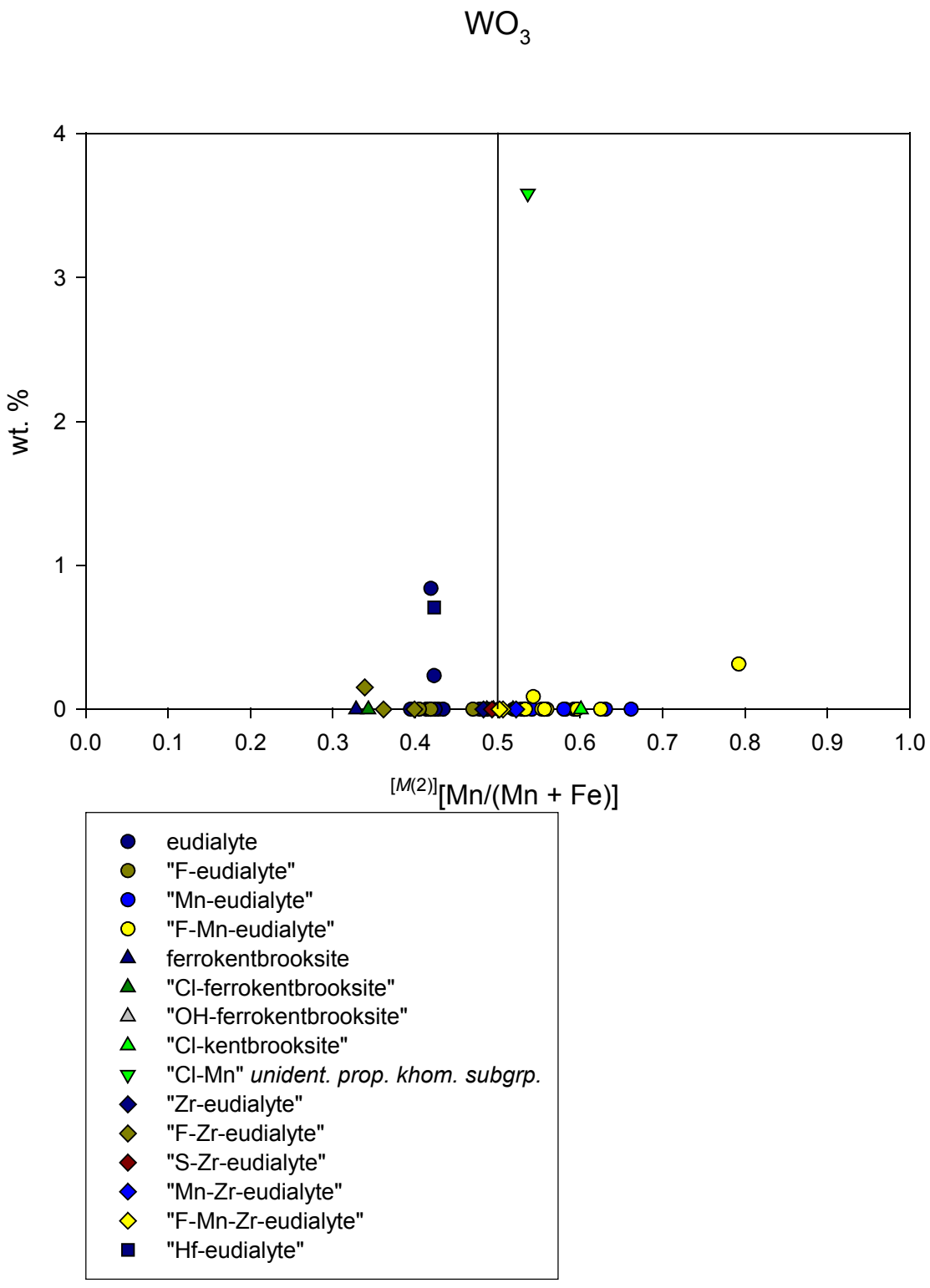

FIGURE 48 – Total WO_3 *versus* mole fraction $^{[M(2)]}$[Mn/(Mn + Fe)].

Main Group Elements

Aluminum content of analyzed eudialyte group minerals ranged from 0.00 to 0.35 wt. % Al_2O_3, with an average of 0.14 (Figure 47). This corresponds to a range of 0.000 to 0.232 *apfu* Al. No linear correlation exists between Al_2O_3 content and X_{Mn}.

Rare-Earth Elements (REE)

Analyses were conducted on nine *REE*: La, Ce, Pr, Nd, Sm, Gd, Dy, Er, and Yb. Total *REE* content of analyzed eudialyte group minerals ranged from 2.01 to 7.50 (average 4.53) wt.% REE_2O_3 (0.392 to 1.604 *apfu* total *REE*). Cerium is the most abundant *REE* with eudialyte group compositions between 0.70 and 4.50 wt.% Ce_2O_3 (Figure 48); it is followed by lanthanum (0.00-2.27 wt.% La_2O_3) (Figure 49), gadolinium (0.00-1.90 wt.% Gd_2O_3) (Figure 50), and neodymium (0.00-1.19 wt.% Nd_2O_3) (Figure 51). No praseodymium, samarium, dysprosium, erbium, or ytterbium was detected in any samples. Chondrite-normalized plots of *REE* content reveal a negative Nd anomaly in all five proposed subgroups (Figures 52-56), a negative Gd anomaly in the proposed kentbrooksite, khomyakovite, and "Hf-eudialyte" subgroups (Figures 53, 54 & 56), and a negative Ce anomaly in the proposed "Hf-eudialyte" subgroup (Figure 56).

Rare earth elements mainly occur in *N*(4), but they may also be present in *M*(1) (true for about 25% of analyses) when primary occupants of *M*(1), such as calcium, are depleted. There was no apparent relationship between the proportional content of specific *REE* and this partitioning behavior; it appears to be strictly linked to site-occupancy of primary *M*(1) cations.

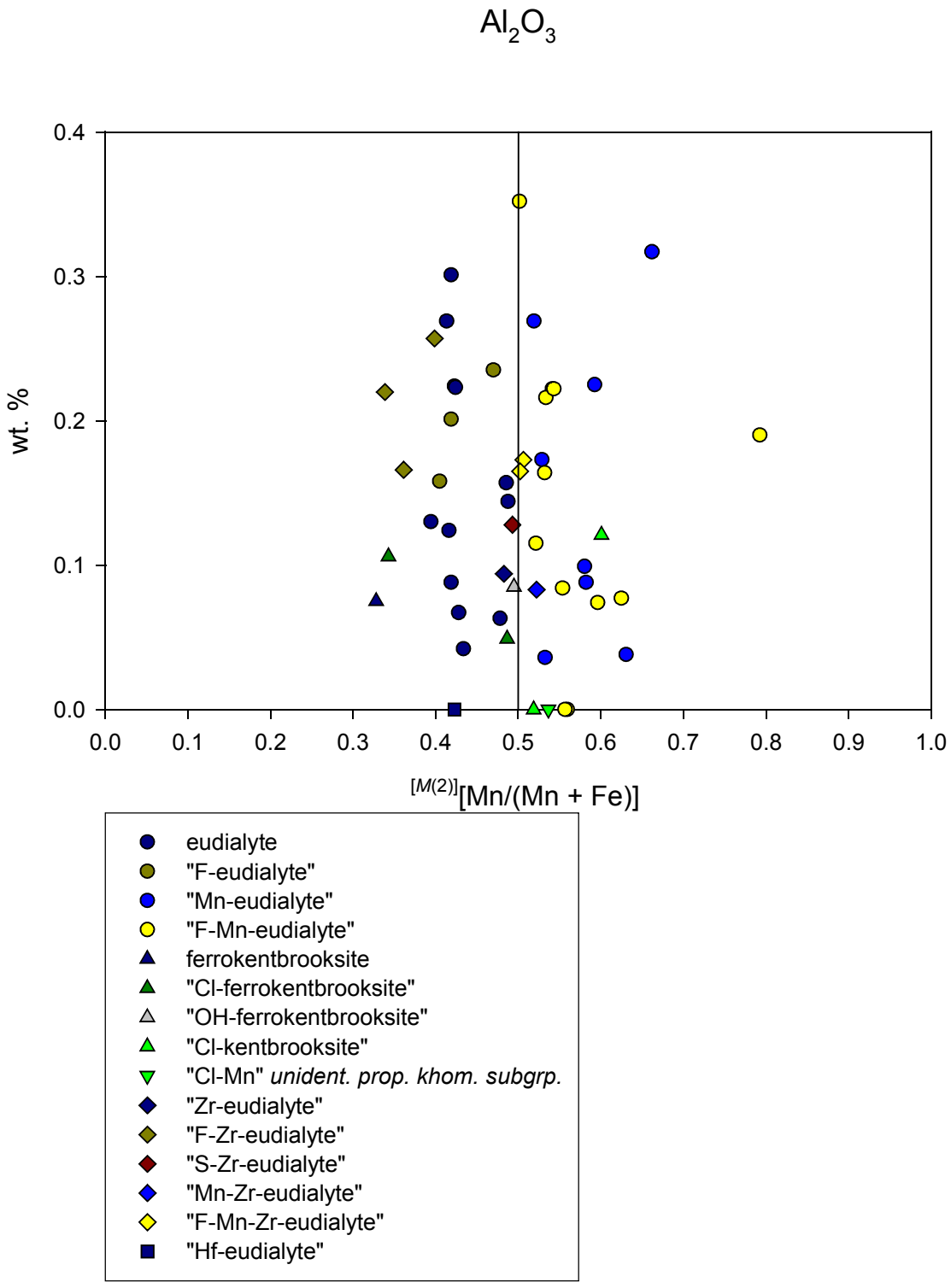

FIGURE 49 – Total Al_2O_3 *versus* mole fraction $^{[M(2)]}$[Mn/(Mn + Fe)].

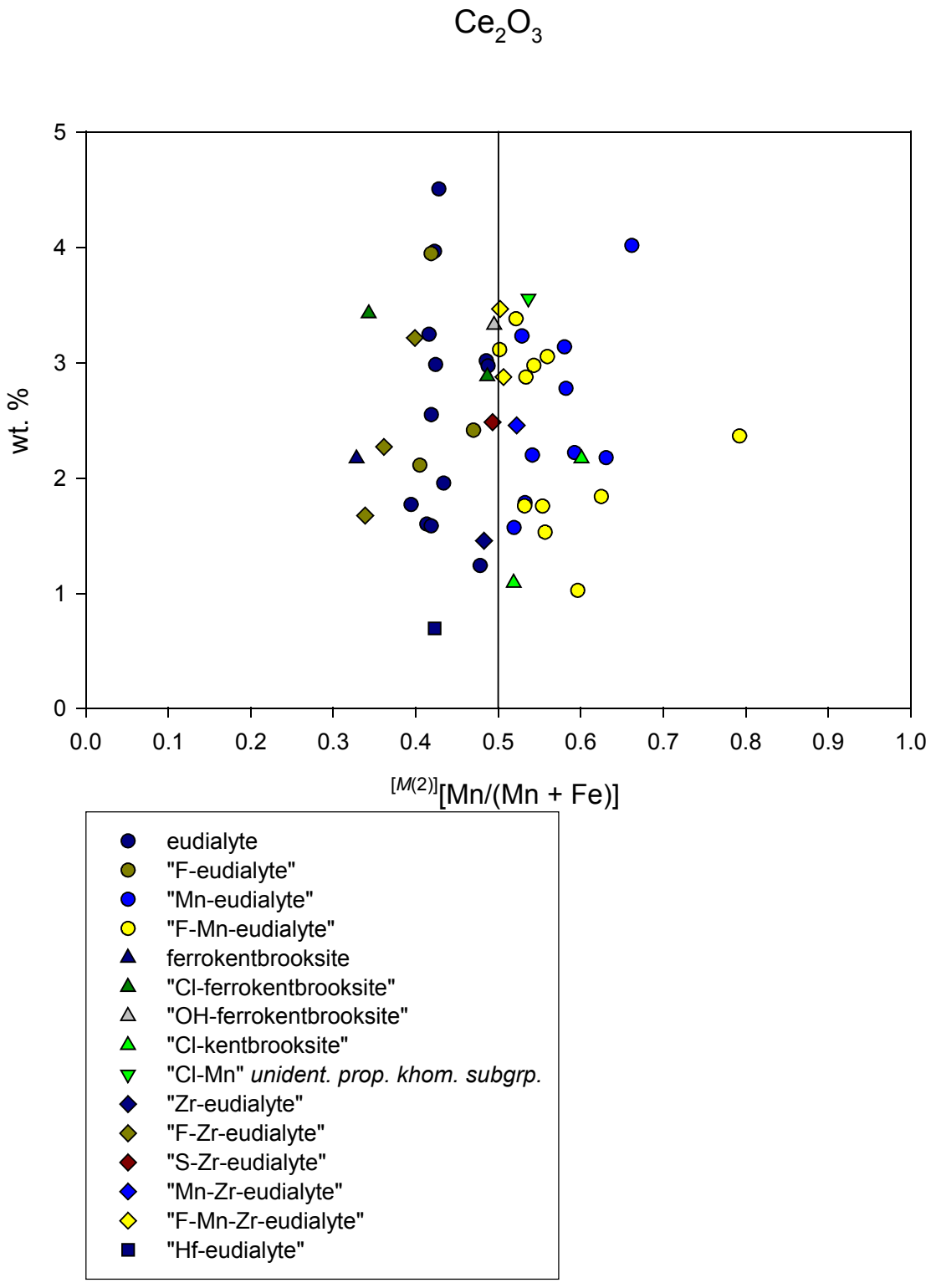

FIGURE 50 – Total Ce_2O_3 *versus* mole fraction $^{[M(2)]}$[Mn/(Mn + Fe)].

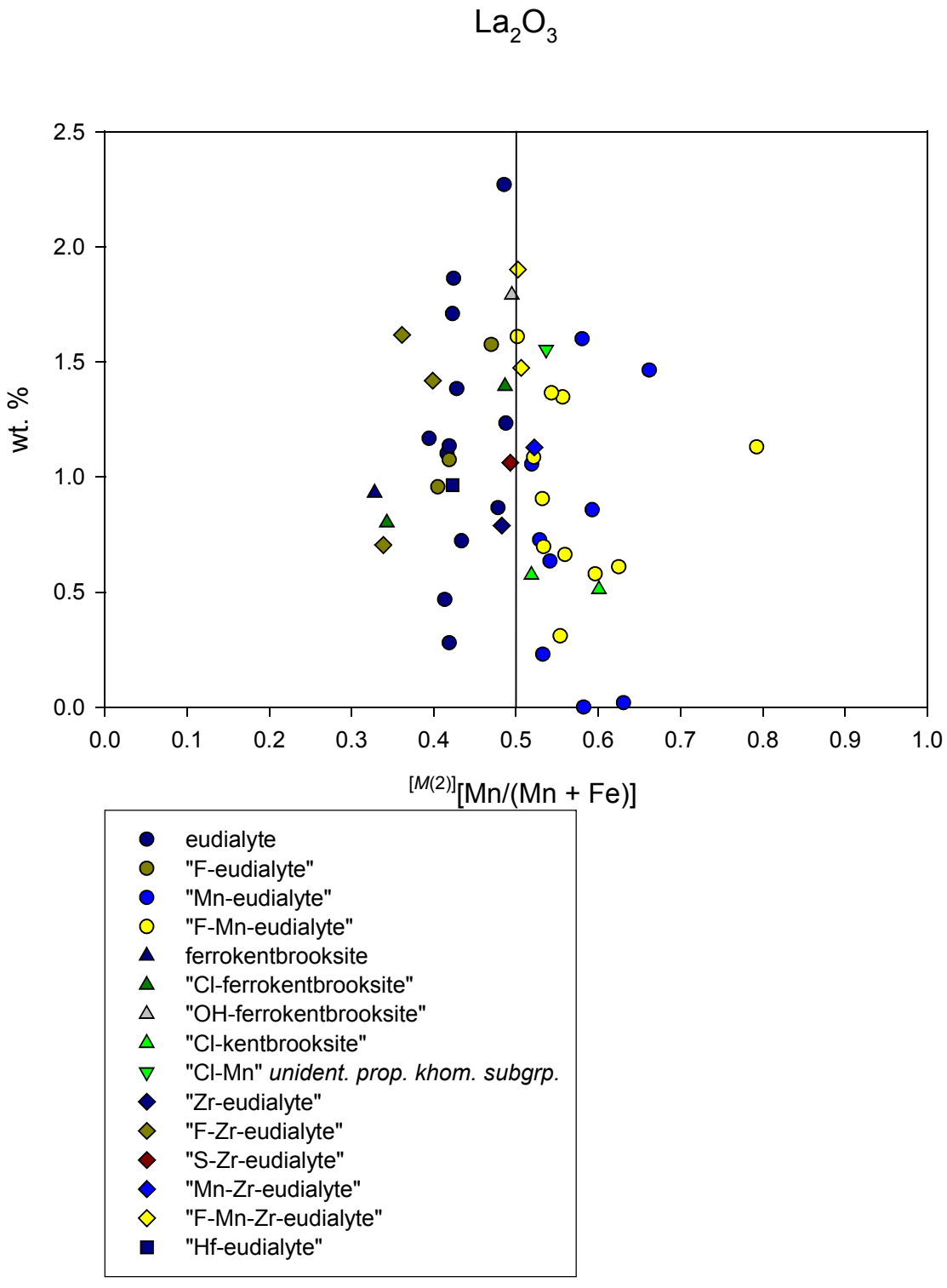

FIGURE 51 – Total La_2O_3 *versus* mole fraction $^{[M(2)]}$[Mn/(Mn + Fe)].

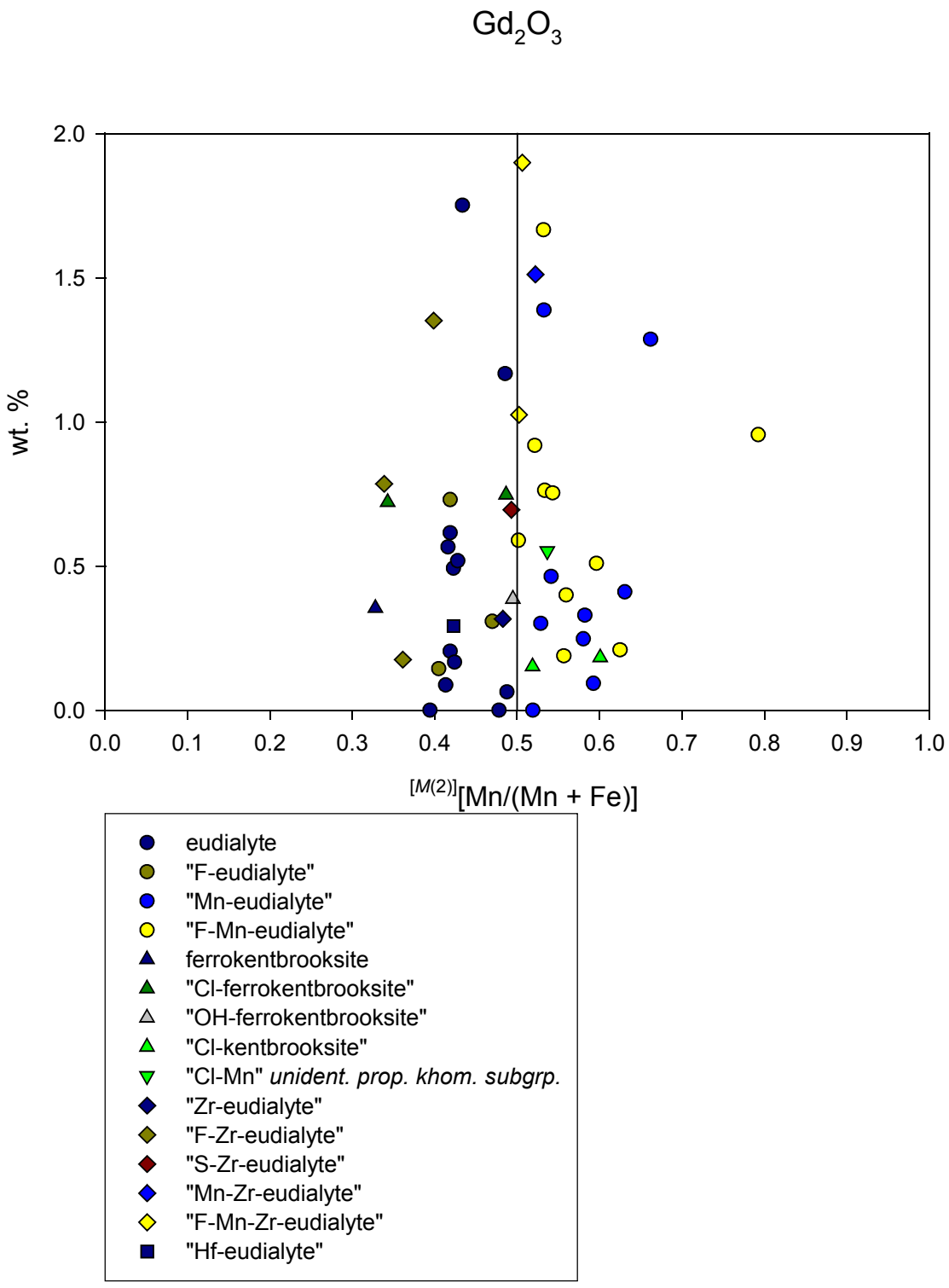

FIGURE 52 – Total Gd_2O_3 *versus* mole fraction $^{[M(2)]}$[Mn/(Mn + Fe)].

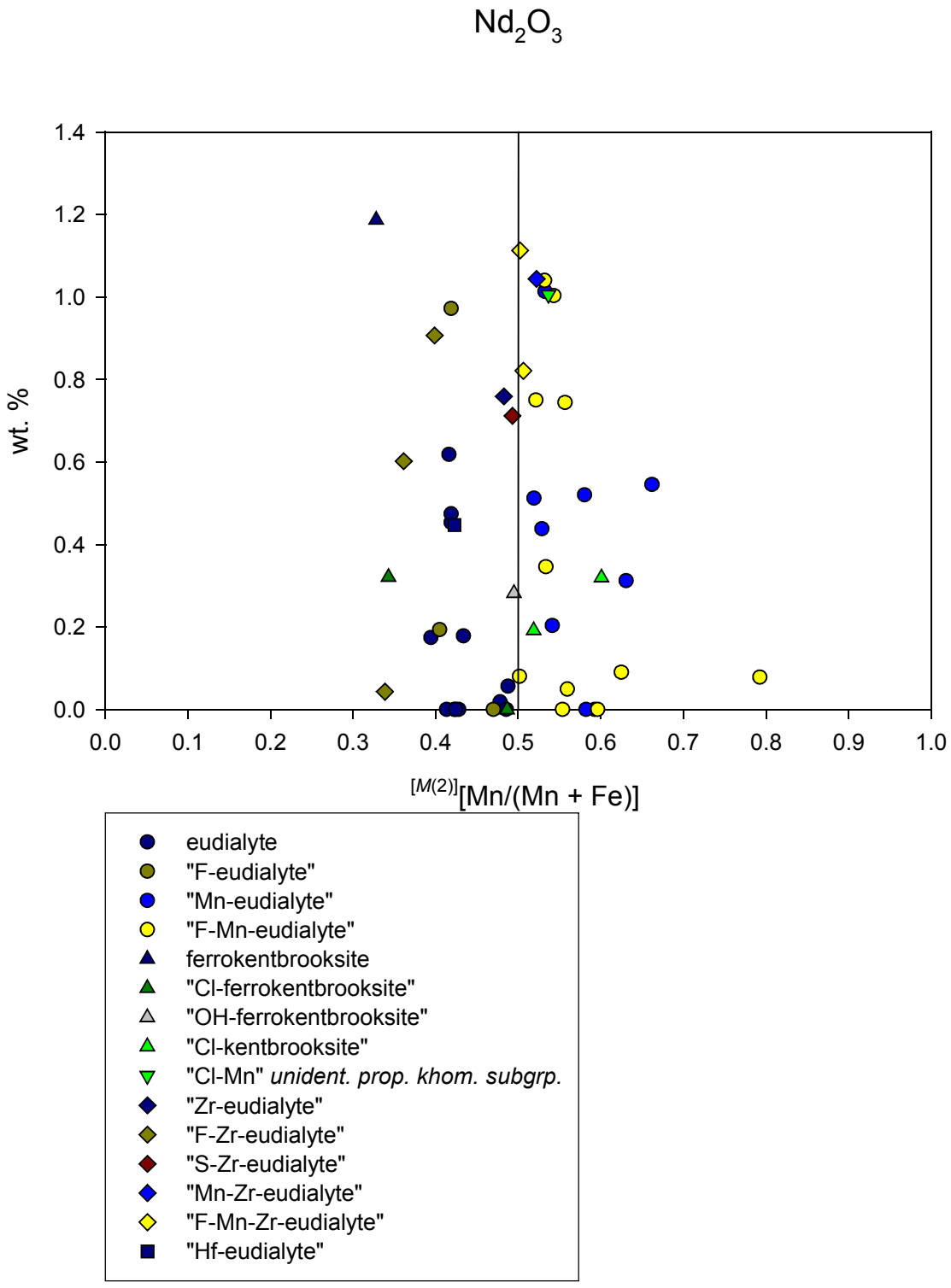

FIGURE 53 – Total Nd_2O_3 *versus* mole fraction $^{[M(2)]}$[Mn/(Mn + Fe)].

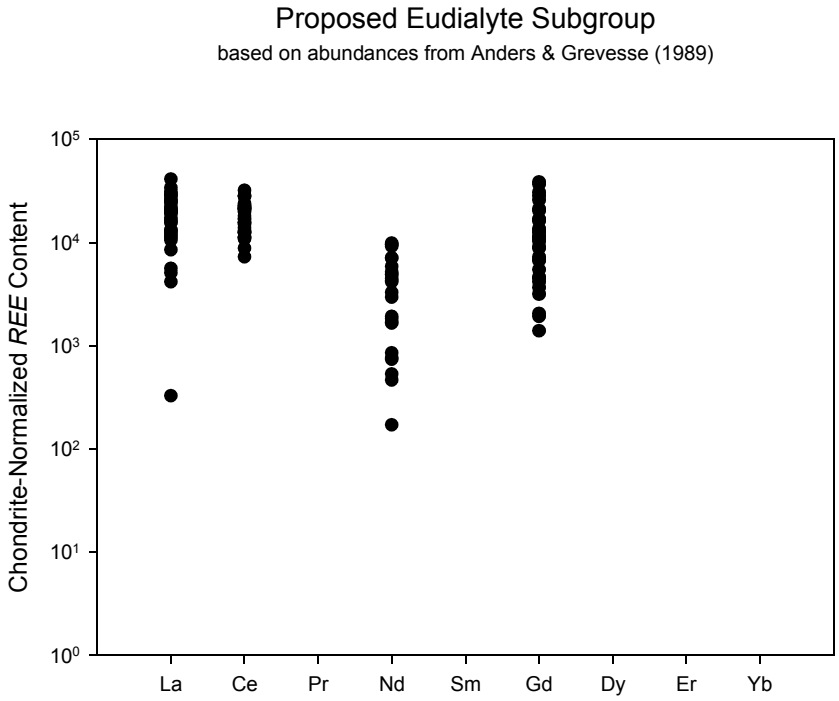

FIGURE 54 – Chondrite-normalized *REE* content in the proposed eudialyte subgroup.

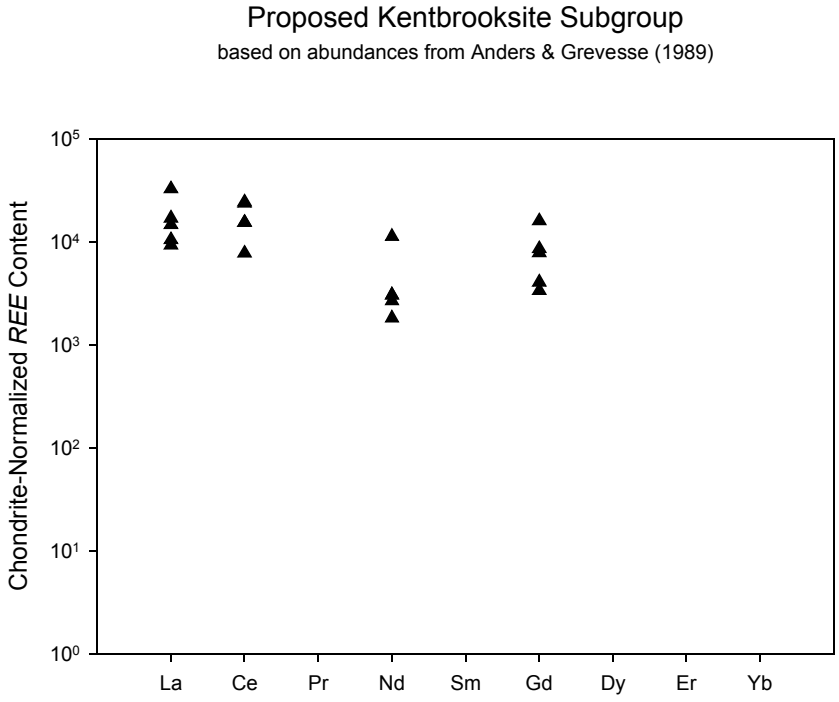

FIGURE 55 – Chondrite-normalized *REE* content in the proposed kentbrooksite subgroup.

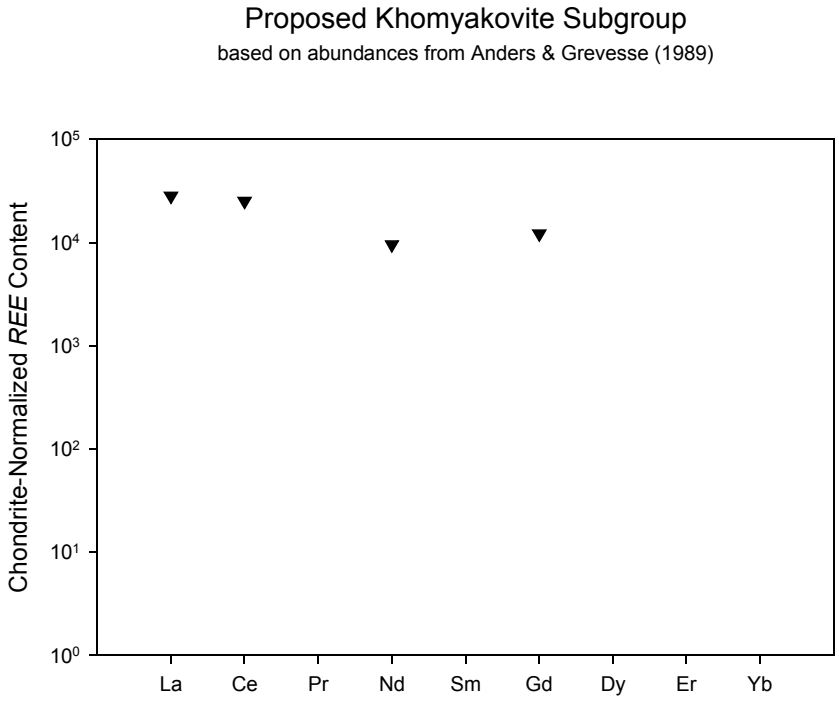

FIGURE 56 – Chondrite-normalized *REE* content in the proposed khomyakovite subgroup.

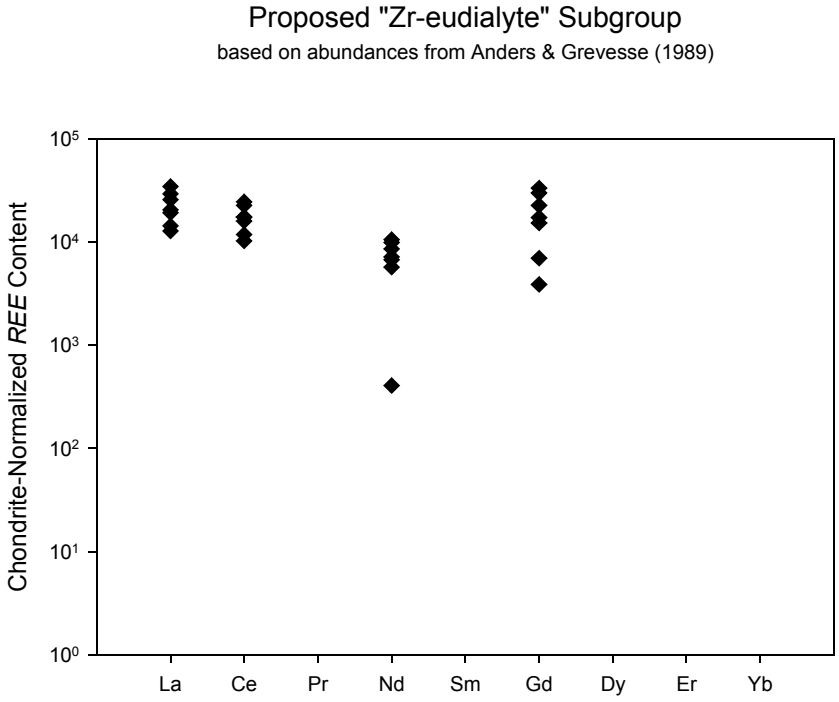

FIGURE 57 – Chondrite-normalized *REE* content in the proposed "Zr-eudialyte" subgroup.

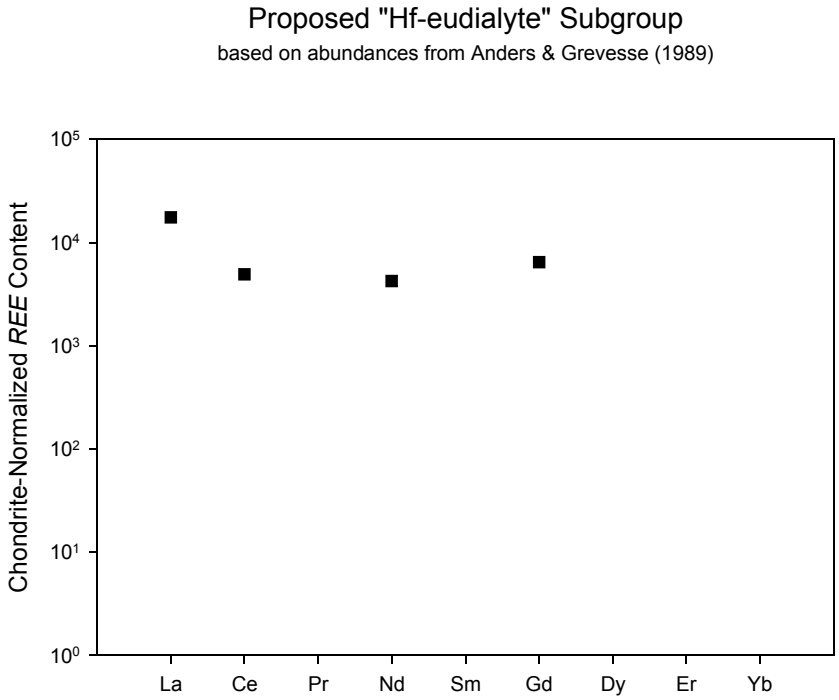

FIGURE 58 – Chondrite-normalized *REE* content in the proposed "Hf-eudialyte" subgroup.

None of the analyses showed single-*REE* content in *N*(4) sufficient to trip speciation to zirsilite-(Ce), johnsenite-(Ce), or any hypothetical member of a series to which zirsilite-(Ce) or johnsenite-(Ce) might belong. The analysis with the highest *REE* content in *N*(4) showed 1.502 *apfu* total *REE*, which for that analysis corresponded to approximately 0.825 *apfu* Ce. Nevertheless, total *REE* content in *N*(4) was equal to or greater than 1.000 *apfu* in one-third of the analyses. No *REE* has a linear correlation to X_{Mn}.

Other Transition Elements

Yttrium is a minor element in eudialyte group minerals at Mont Saint-Hilaire. Compositions ranged from 0.00 to 5.68 wt.% Y_2O_3, with an average of 1.46 (Figure 57). This corresponds to a range of 0.000 to 1.683 *apfu* Y. Yttrium is fixed in *M*(1) by the alternative algorithm. Yttrium content does correlate linearly to X_{Mn}.

Zinc is a trace element in the analyses. Compositions ranged from 0.00 to 0.08 wt.% ZnO, with an average of 0.002. This corresponds to a range of 0.000 to 0.034 *apfu* Zn. Only two analyses, one, a "F-Mn-eudialyte", and the other, a "Zr-eudialyte", showed any zinc content. Zinc was not considered in the analyses of JOHNSEN & GRICE (1999), and so, was not incorporated into the alternative algorithm. Based on its ionic radius and charge, however, Zn almost certainly can occupy sites in both *M*(1) and *M*(2).

Scandium is a trace element in eudialyte group minerals at Mont Saint-Hilaire. Scandium content ranged from 0.00 to 0.18 (average 0.02) wt.% Sc_2O_3 (0.000 to 0.085 *apfu* Sc) (Figure 58). Scandium was not considered in the analyses of JOHNSEN & GRICE (1999), and so, was not incorporated into the alternative algorithm. Based on its ionic radius and charge, however, Sc may occupy sites in *N*(4), *M*(1), or *M*(4). In the analyses from the East Hill Suite, Sc is dominantly present in members of the proposed eudialyte subgroup. No linear correlation exists between Sc_2O_3 and X_{Mn}.

Alkali & Alkaline Earth Elements

Strontium was not analyzed in the eudialyte group minerals from Mont Saint-Hilaire.

Barium is a minor element in eudialyte group minerals at Mont Saint-Hilaire, with content ranging from 0.00 to 1.81 (average 0.28) wt.% BaO (Figure 59). This corresponds to a range of 0.000 to 0.393 *apfu* Ba. Barium is found solely in *N*(4). Barium content does not correlate linearly to X_{Mn}.

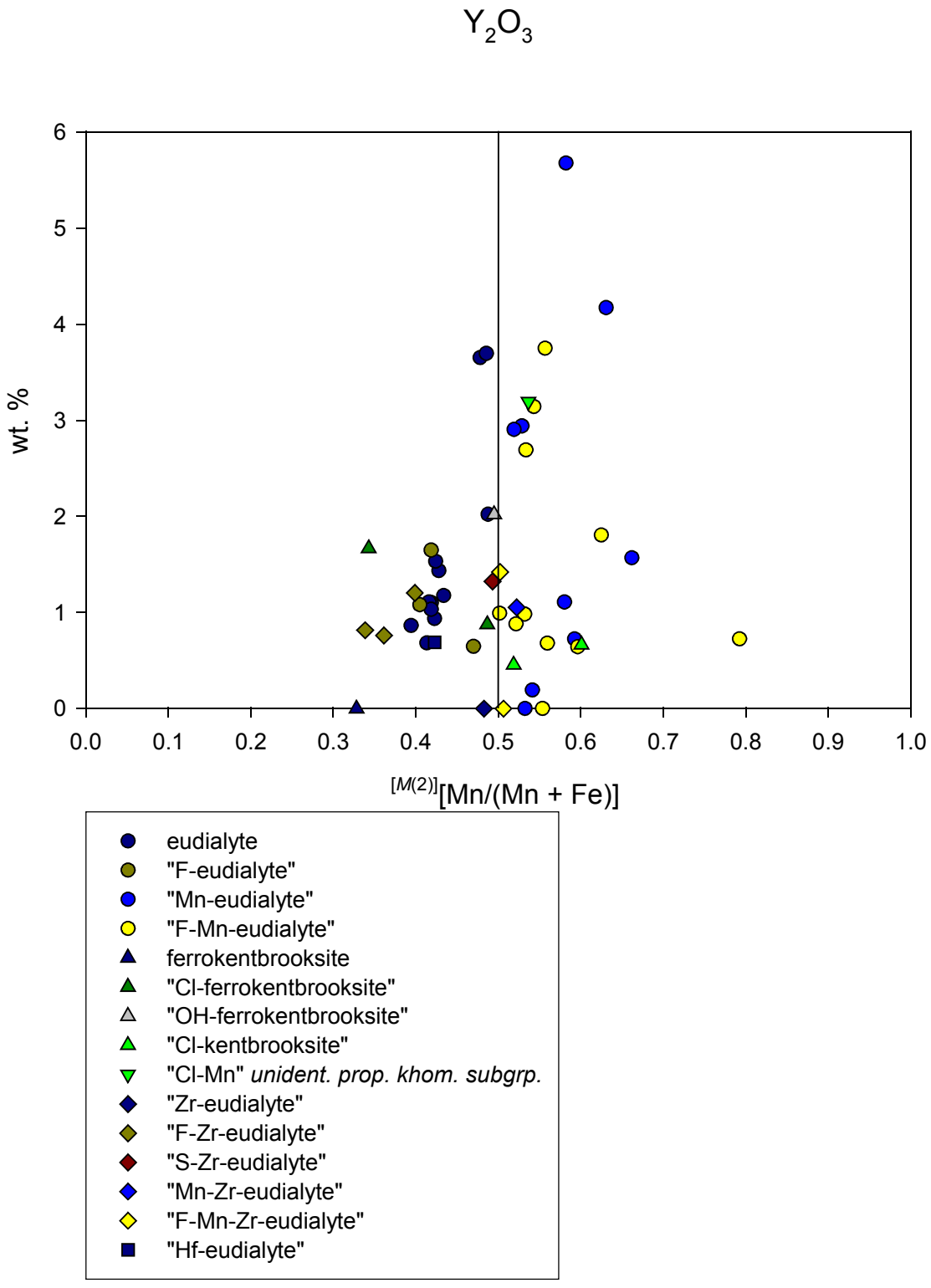

FIGURE 59 – Total Y_2O_3 *versus* mole fraction $^{[M(2)]}$[Mn/(Mn + Fe)].

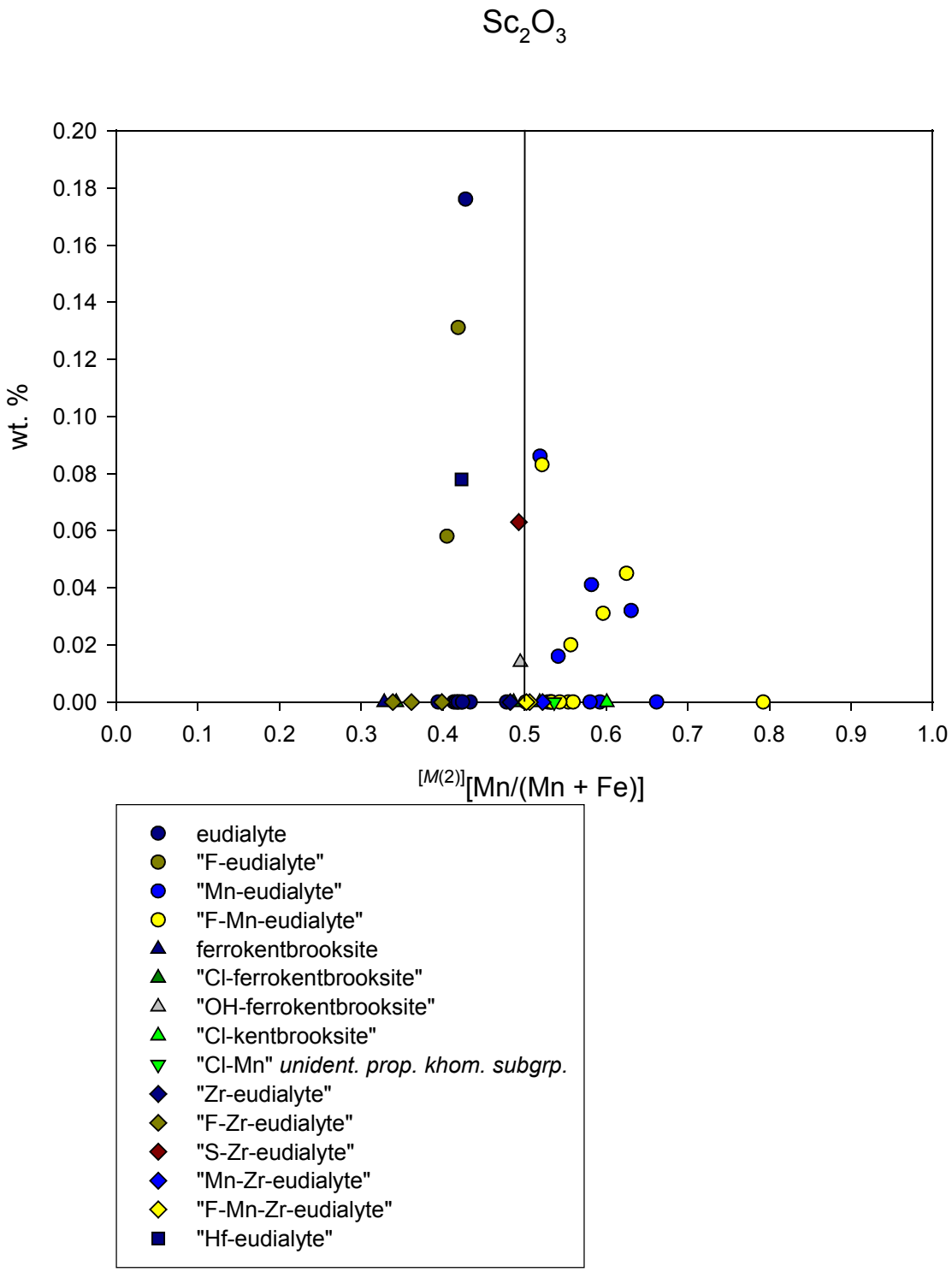

FIGURE 60 – Total Sc_2O_3 *versus* mole fraction $^{[M(2)]}$[Mn/(Mn + Fe)].

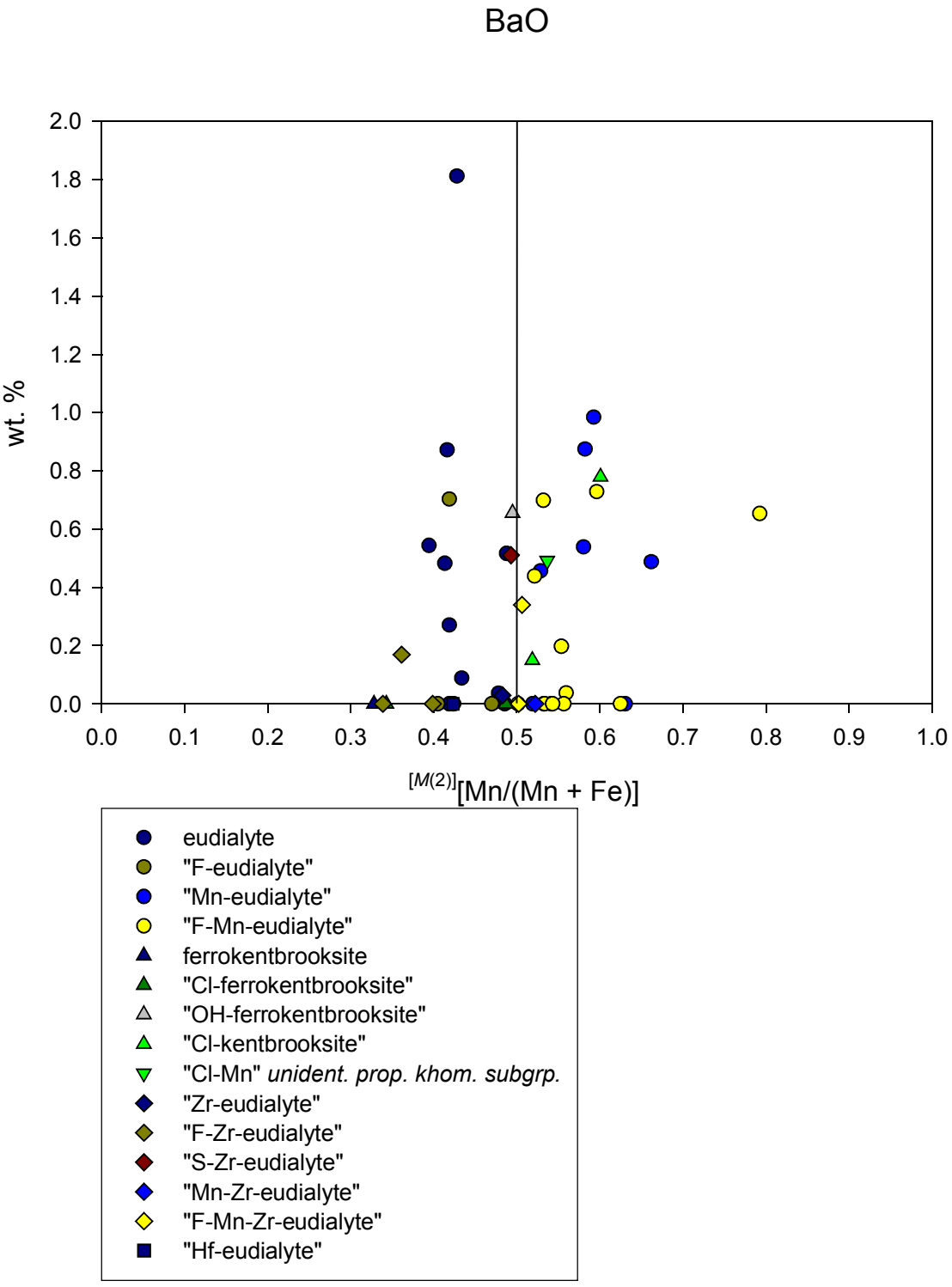

FIGURE 61 – Total BaO *versus* mole fraction $^{[M(2)]}$[Mn/(Mn + Fe)].

Magnesium is a trace element in eudialyte group minerals at Mont Saint-Hilaire. Compositions ranged from 0.00 to 0.12 wt.% MgO, with an average of 0.02 (Figure 60). This corresponds to a range of 0.000 to 0.098 *apfu* Mg. Magnesium is present only in *M*(2). No linear correlation exists between MgO content and X_{Mn}.

Potassium is a trace element in eudialyte group minerals at Mont Saint-Hilaire, with compositions ranging from 0.35 to 0.57 wt.% K_2O, with an average of 0.47 (Figure 61), and cation content from 0.259 to 0.393 *apfu* K. Potassium appears exclusively in *N*(4). No linear correlation exists between K_2O content and X_{Mn}, although potassium content exhibits a remarkably tight range of values.

Volatiles

For similar reasons to the treatment of niobium and tantalum, chlorine and fluorine should be considered together. Although chlorine has a lower maximum to its content range than fluorine (0.00 to 1.31 wt.% Cl versus 0.00 to 1.38 wt.% F) (Figures 62 & 63), Cl has a slight dominance over F in total content (q.v.), with an average content of 0.77 wt.% Cl versus 0.36 wt.% F. The maximum cation contents of Cl and F work out to 1.174 and 2.337 *apfu*, respectively. Chlorine and fluorine are found exclusively in the *X* site, wherein Cl is more abundant than F in about 40% of the analyses; again, only a slight dominance. As was the case with potassium, chlorine content exhibits a fairly narrow range of values, although some outlying analyses keep it from being consistently so. Neither chlorine nor fluorine content correlate linearly to X_{Mn}.

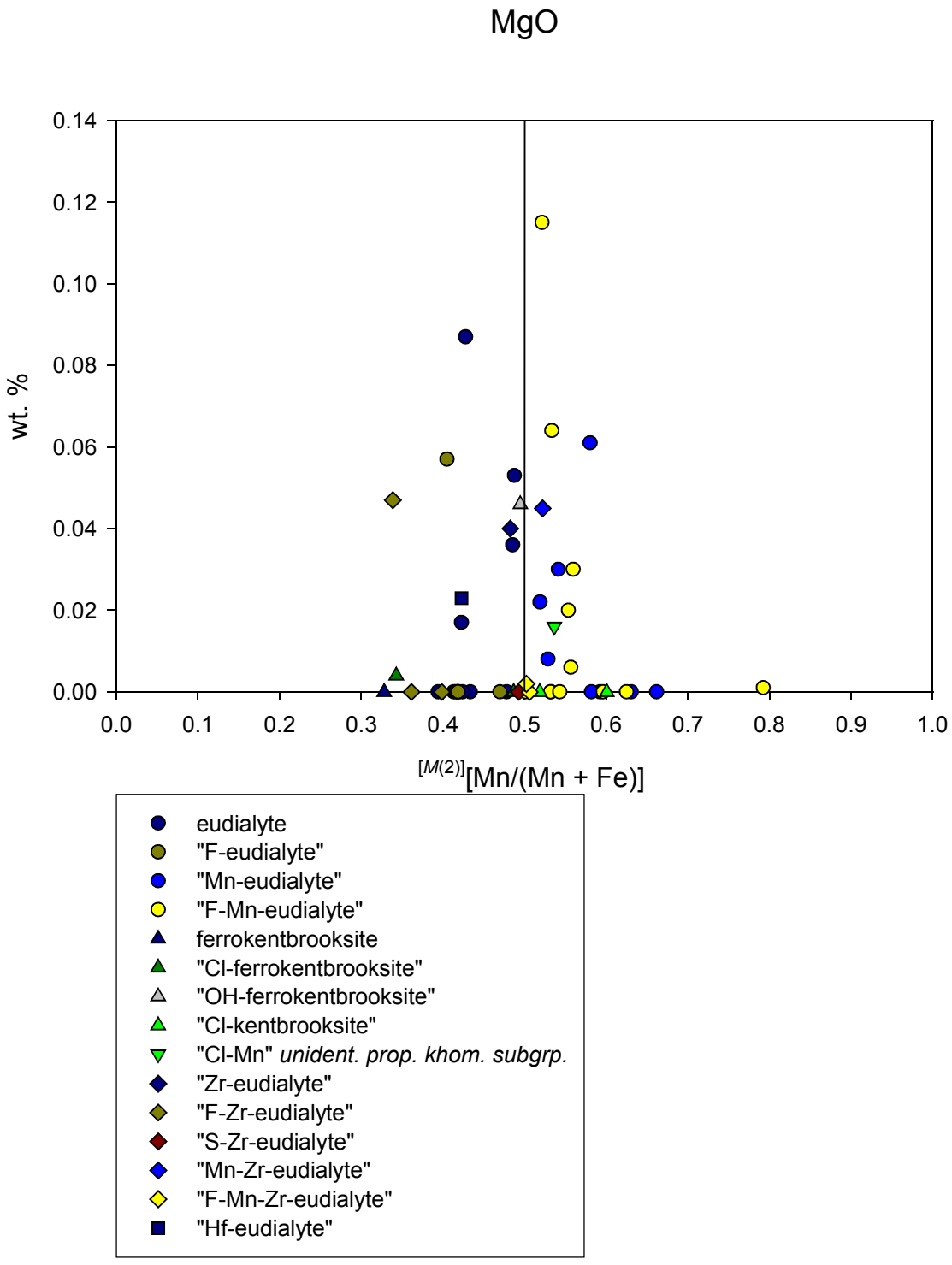

FIGURE 62 – Total MgO *versus* mole fraction $^{[M(2)]}$[Mn/(Mn + Fe)].

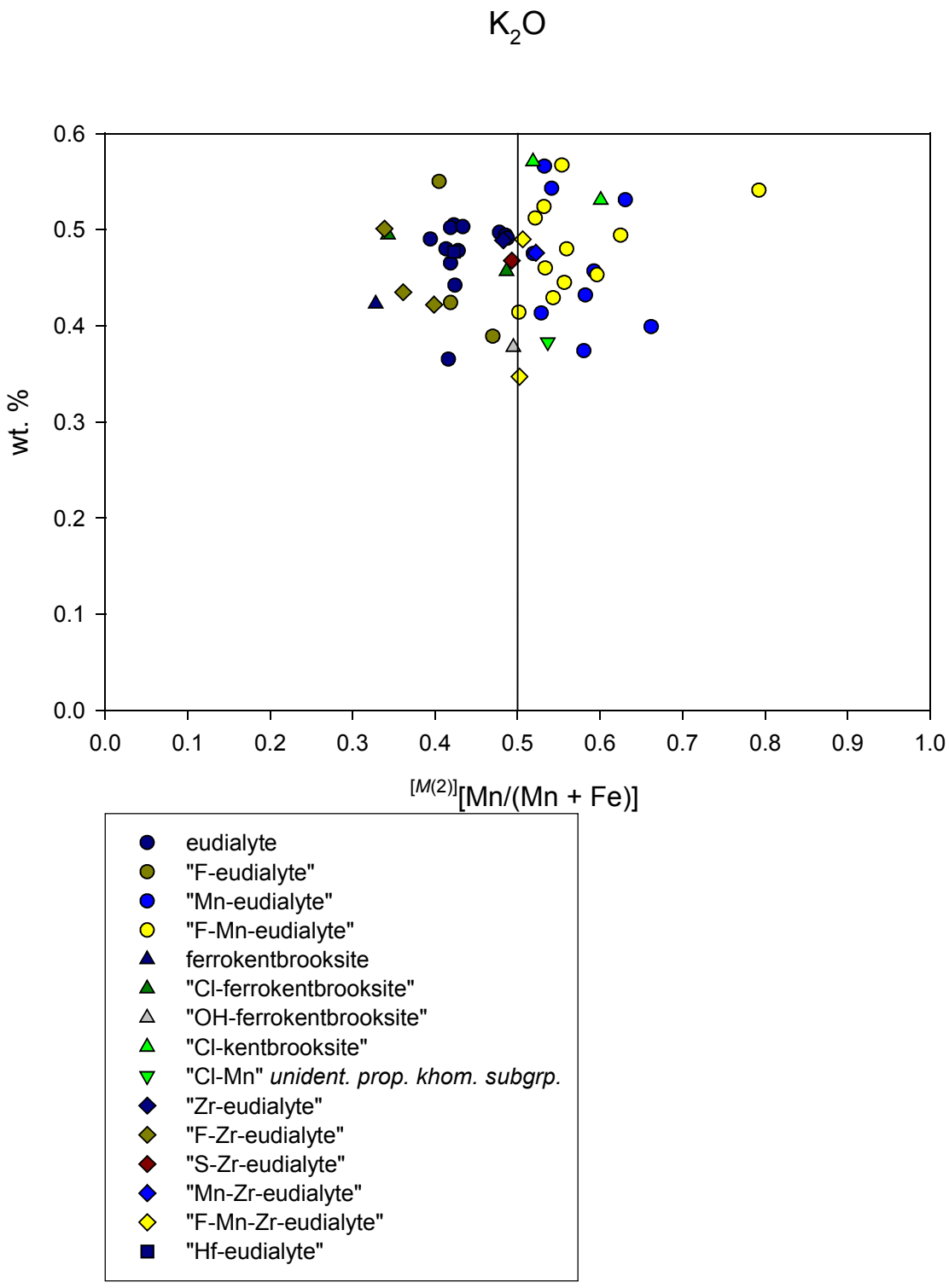

FIGURE 63 – Total K_2O *versus* mole fraction $^{[M(2)]}$[Mn/(Mn + Fe)].

Sulfur content of analyzed eudialyte group minerals ranged from 0.00 to 1.94 wt.% SO_3 with an average of 0.19 (Figure 64). This translated to a range of 0.000 to 0.806 *apfu* S. Sulfur is solely found in *X* in the eudialyte group analyses at Mont Saint-Hilaire. Sulfur occupies a majority of the sites in *X* in one analysis from Mont Saint-Hilaire. No linear correlation exists between SO_3 content and X_{Mn}.

Water was not analyzed directly; rather, it was calculated using the method outlined in JOHNSEN & GRICE (1999). This resulted in a compositional range of 0.02 to 0.74 wt.% H_2O, with an average of 0.28. This corresponds to a range of 0.077 to 2.907 *apfu* H. Hydrogen is found primarily in *X* as OH and, in some specimens, H_2O and in *O* as OH and H_2O; however, using electron microprobe data alone, there is no general basis for assignment or for speciation.

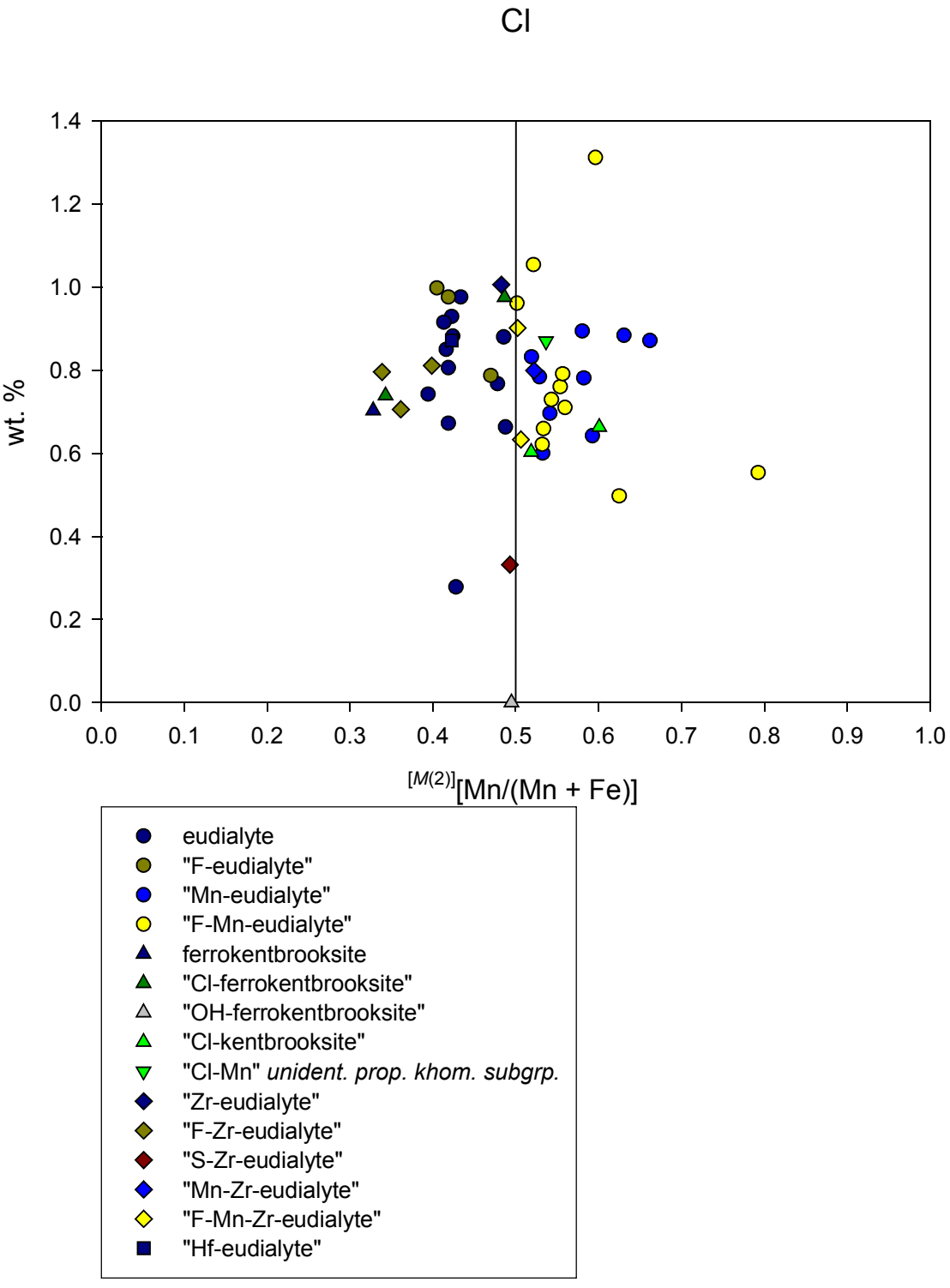

FIGURE 64 – Total Cl *versus* mole fraction $^{[M(2)]}$[Mn/(Mn + Fe)].

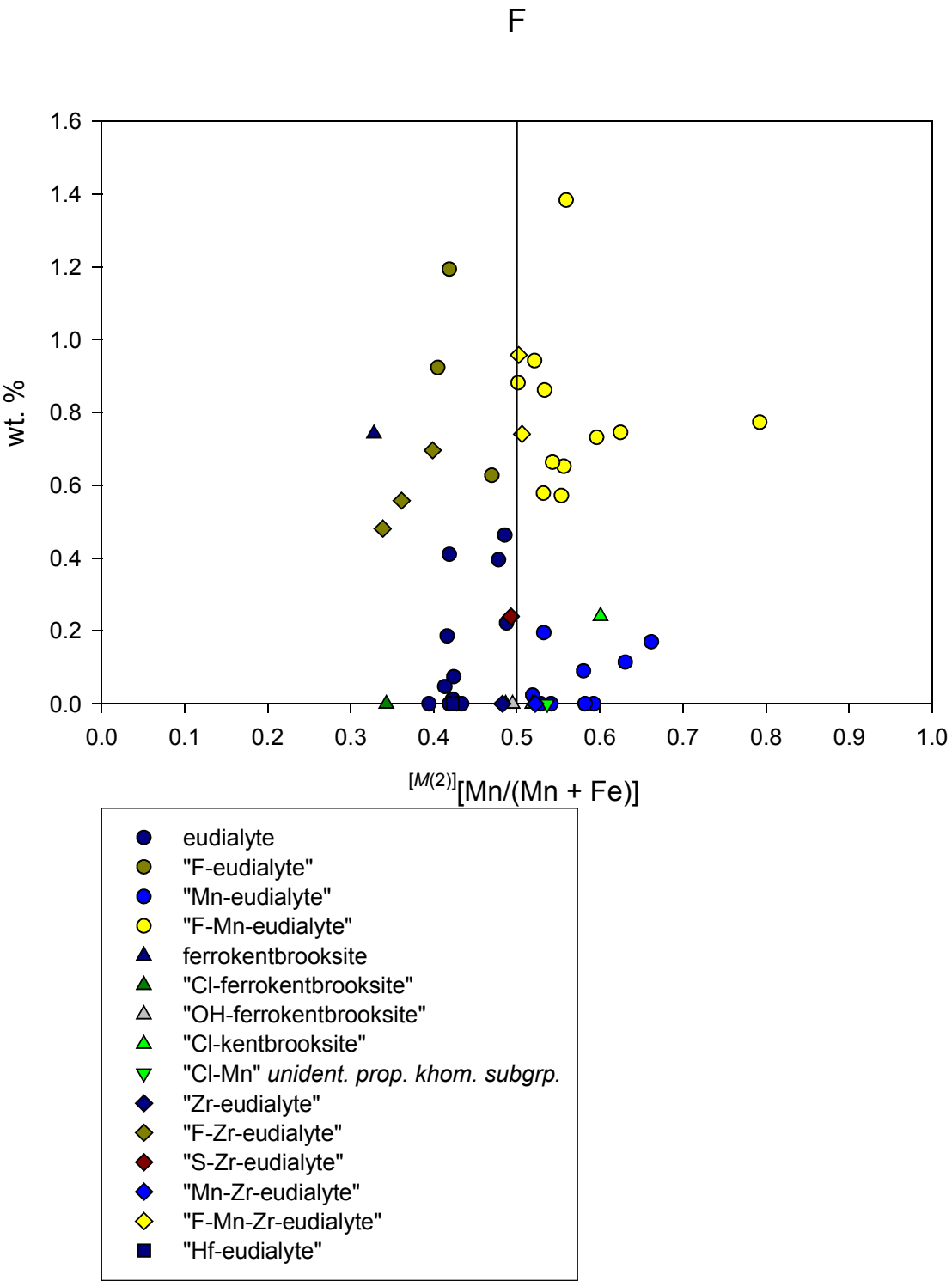

FIGURE 65 – Total F *versus* mole fraction $^{[M(2)]}$[Mn/(Mn + Fe)].

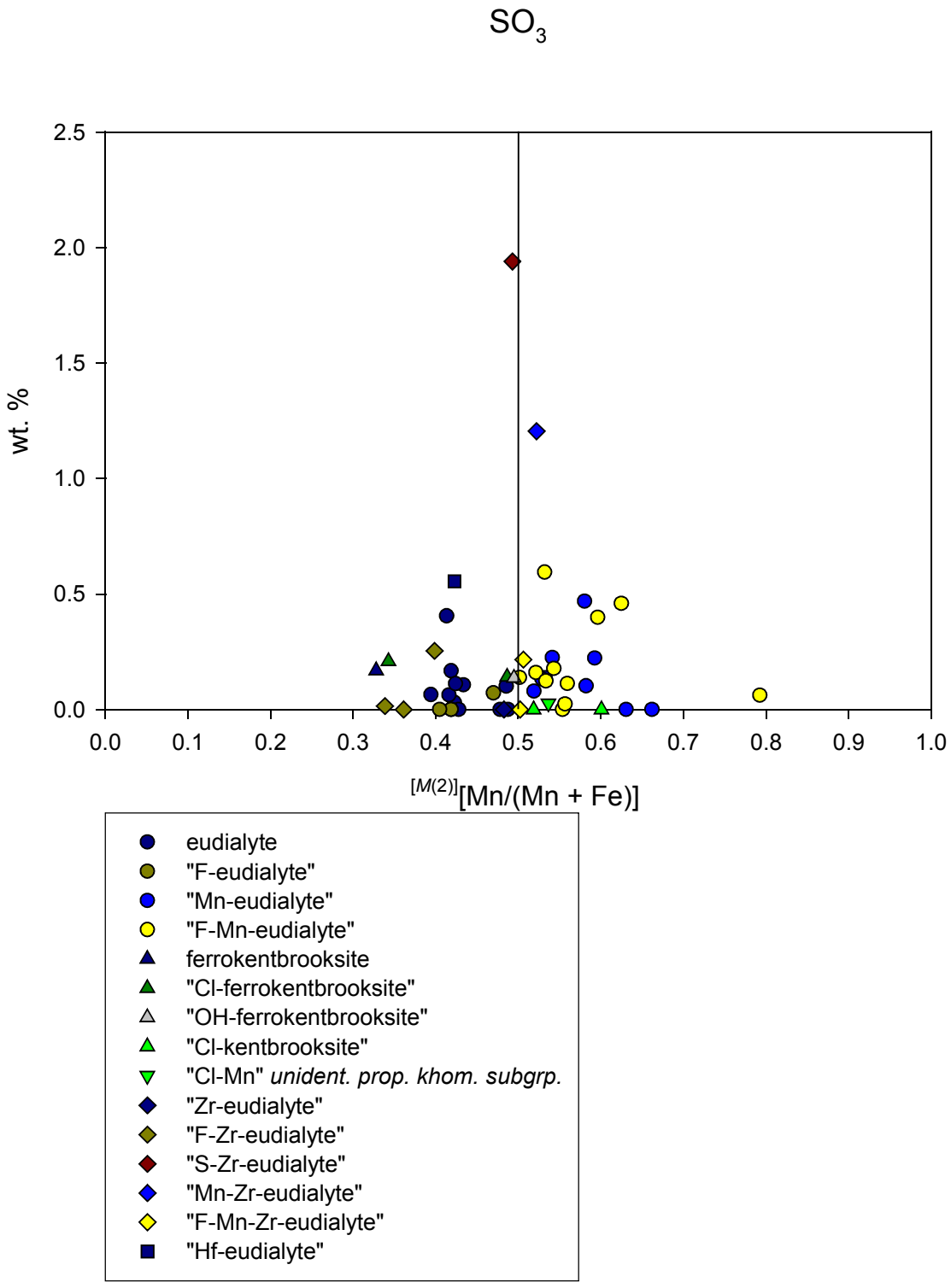

FIGURE 66 – Total SO_3 *versus* mole fraction $^{[M(2)]}$[Mn/(Mn + Fe)].

SITE-OCCUPANCY TOTALS

Site-occupancies varied in terms of the number of vacancies required to total out each site and in terms of surplus occupants (Tables 19 & 20). Ideality of fit (minimum number of vacancies and surpluses) for a given site tended to correlate negatively with its position in the order of site filling in the alternative algorithm. Sites that were filled earlier by the alternative algorithm [*Si*, *M*(4), *M*(3), and *Z*] had the lesser numbers of vacancies and surpluses; those that were filled later [*M*(2), *M*(1), *N*(4), *N*(ϕ), and *X* (the occupancy of which was not determined by the alternative algorithm)] had the greater. Of the latter group, *M*(1) exhibited the most ideal behavior.

TABLE 19 – Vacancies in Mont Saint-Hilaire eudialyte group EMP analyses.

Site	*Min. apfu*	*Avg.*	*Max.*	*Site*	*Min. apfu*	*Avg.*	*Max.*
N(ϕ)	0.000	0.958	2.862	*Z*	0.000	0.003	0.158
N(4)	0.000	0.356	1.369	*M(3)*	0.000	0.000	0.002
M(1)	0.000	0.000	0.000	*M(4) + Si*	0.000	0.029	0.498
M(2)	0.000	0.000	0.000	*X*	0.000	0.343	1.673

TABLE 20 – Surpluses in Mont Saint-Hilaire eudialyte group EMP analyses.

Site	*Min. apfu*	*Avg.*	*Max.*	*Site*	*Min. apfu*	*Avg.*	*Max.*
N(ϕ)	0.000	0.018	0.687	*Z*	0.000	0.000	0.000
N(4)	0.000	0.002	0.104	*M(3)*	0.000	0.003	0.159
M(1)	0.000	0.035	0.443	*M(4) + Si*	0.000	0.000	0.000
M(2)	0.432	1.346	3.240	*X*	0.000	0.112	1.229

DISCUSSION

RATIONALE FOR THE ALTERNATIVE ALGORITHM

Site Assignment of Y

Site assignment of yttrium became an issue because in one analysis from JOHNSEN & GRICE (1999), Y appears in *N*. In the eudialyte group analyses of JOHNSEN & GRICE (1999), *REE* will split their population between sites, but Y will not. This appeared, at first, to be a stable reference point from which to develop an Y site-assignment logic test. It soon became apparent, however, that, since in one analysis $^{[M(1)]}REE > Y$, there was plenty of room for Y in *M*(1) if the *REE* split a corresponding number of its population off to *N*. Therefore, pure algebraic reasoning could not account for the situation. No other characteristics of the analysis (strange site-assignments or site-occupancies of other elements) appear to have an influence on the behavior of Y. Consequently, with microprobe data alone, Y is artificially fixed in *M*(1), and the results (for this sample suite) are inaccurate about 6% of the time.

Sodium Site Splitting

The sodium sites were split, as in structural formulæ from JOHNSEN & GRICE (1999) for a few reasons:

1) doing so eliminated computing errors introduced by circular arguments (previously, Na* depended on *REE*, but *REE* depended on the site-occupancy which depended on Na*, leading to obvious problems)
2) it more realistically addressed the assignment of other elements (Sr, Ba, *etc*.) to *N* sites, as they tend to concentrate in *N*(4)

3) it permitted the creation of more realistic site-occupancies for Na, itself, by accounting for Na-depletion in *N*(4) (due to the incorporation of the aforementioned other elements) and for Na-enrichment (by the same reasoning) in *N*(ϕ)

In a similar vein, the single sites *N*(3) and *N*(4) were melded into the combined site *N*(4), according to the pattern of structural formulæ for disordered structures from JOHNSEN & GRICE (1999), for simplicity in computation and logic. As was the case with Y, there does not exist enough data to distinguish assignment to one site or the other based solely on algebraic logic.

Further Musings on Sodium

The Na correction scheme employed in this study was put into place to address the discrepancy between Na site-occupancies calculated from electron microprobe analyses *versus* those derived from a single-crystal structural refinement. The system is based on accounting for the presence of other atoms substituting into *N* sites; and, while it improves the correspondence between data sets, it does not really explain the origin of the difference between the data collected by the two instruments. Perhaps, in a sense, both data are real. RASTSVETAEVA *ET AL.* (1990) discuss the structural concentration of Na atoms near channels running along [110]. If Na, H_2O, and H_3O^+ can be exchanged along these channels, could not excess Na atoms be stored inside of them, similarly to the situation that is present in the channels of the beryl structure, in which are observed atoms of Cs and molecules of H_2O? The analytical upshot of such a scenario would be that the microprobe would "see" all of the sodium, including that stored within the channels, whereas the XRD would only "see" the sodium occupying a true site. If this were the case, then both instruments would be presenting correct data; furthermore, charge balance could still be maintained *via* the flexible anionic content of the eudialyte structure.

COMPARATIVE PERFORMANCE OF THE SCHEMES

Goals of the Alternative Algorithm Revisited

JOHNSEN & GRICE (1999) recognized two problems with their cationic scheme for recalculation of eudialyte group analyses: 1) it does not account for unusual substitutions of elements (in particular, Al, Ti & Zr) outside of their normal sites and 2) it does not account for vacancies in *M*(3). The alternative algorithm strove to resolve four additional issues:

1) a ubiquitous positive difference in Na *apfu* in recalculated microprobe data relative to structural data
2) frequent, substantial vacancies (*ca.* 0.5-1.0 out of 3.0 *apfu*) in *M*(2)
3) concomitant inaccuracy in the partitioning of Mn between *M*(1) & *M*(2)
4) further variability in site-occupancy by Nb & Hf

Site-Occupancy in N(ϕ) & N(4)

The first issue, the discrepancy between microprobe and structural data for sodium, represented the greatest deviation from reality. Occupancy of *N*(ϕ) is restricted to Na, so disparity in recalculations probably resulted primarily from poor allocations to *N*(4). Occupancy of *N*(4) was, therefore, considered to be the most important factor in addressing this issue.

To fully appreciate the improvements in site-occupancy of *N*(4), the apparently obtuse sodium corrections deserve some further discussion. Considering the 17 analyses examined by JOHNSEN & GRICE (1999), the total-Na site-occupancies for microprobe data recalculated by the cationic scheme are higher than the corresponding values given by structural formulæ in JOHNSEN & GRICE (1999) for 16 out of the 17 analyses (Table 21). Ideally this would have been a systematic difference related to sodium content, allowing for a simple linear correction;

however, it is not. The absolute and relative differences vary with little to no correlation with sodium content. Therefore, it was postulated that the difference might arise due to the presence of other cations in *N* sites. This inspired the creation of sodium corrections based on these other cations.

The first correction, which generates Na*, addresses the discrepancy between microprobe data for Na and structural data for Na (see also below). The first corrected Na value (Na*) was generated by subtracting the total *apfu* of the other substituting elements from the raw recalculated Na (as explained in step #17 of the recalculation scheme). Doing so greatly improved the total Na values (Table 21).

The second correction, which generates $\hat{\text{Na}}$, does not alter the total sodium of the analysis; it is meant to change the way in which Na is distributed between *N* sites. A general scheme for the recalculation puts the average site-occupancy of (Na ÷ 5) *apfu* into each of the five *N* sites. This causes Na excesses in *N*(4), which is taking on other elements, as well. So, the second correction subtracts Na atoms from *N*(4) in proportion to the presence of substituting atoms and puts those subtracted Na atoms into the *N*(ϕ) sites. This slightly diminishes the accuracy of the alternative algorithm with respect to total Na and site-occupancy of *N*(ϕ) but causes a substantial improvement in terms site occupancy of *N*(4) (Table 21).

Although all of the site-occupancy data for sodium are considered here for purposes of gauging the relative performance of the recalculation schemes, only data for site-occupancy in *N*(4) may be rigorously analyzed since data for *N*(ϕ) did not meet the standards for statistical significance. Revisiting the results of *N*(4) recalculation by the alternative algorithm (Figure 5), the alternative algorithm is not only far more precise than the cationic scheme with respect to the

TABLE 21 – Comparative performance of recalculation schemes and corrections *versus* structural data given in JOHNSEN & GRICE (1999) for site-occupancy in $N(\phi)$ & $N(4)$.

	Absolute Difference (apfu)				*Relative Difference*			
	Min.	*Avg.*	*Avg. Abs. Val.*	*Max.*	*Min.*	*Avg.*	*Avg. Abs. Val.*	*Max.*
Total Na Content Cationic Scheme (Johnsen & Grice 1999)	-0.07	+1.73	+1.74	+2.91	-0.54%	13.46%	13.52%	24.81%
Total Na Content Alternative Algorithm After First Na Correction	-2.36	-0.08	+0.54	+0.85	-17.49%	-0.72%	3.80%	5.41%
Total Na Content Alternative Algorithm After Second Na Correction	-2.69	-0.32	+0.80	+0.73	-23.35%	-2.80%	6.39%	5.40%
N(ϕ) Occupancy Alternative Algorithm After Second Na Correction	-2.58	-0.30	+0.66	+0.90	-28.38%	-3.21%	7.67%	11.32%
N(4) Occupancy Cationic Scheme (Johnsen & Grice 1999)	+0.40	+1.49	+1.49	+2.57	7.19%	38.32%	38.32%	105.76%
N(4) Occupancy Alternative Algorithm After Second Na Correction	-1.24	-0.02	+0.31	+0.59	-27.37%	-0.75%	7.16%	13.75%

structural data of JOHNSEN & GRICE (1999), it is also more accurate ($r^2_{J\&G} = 0.41$ *versus* $r^2_{AA} = 0.80$, and $RD_{J\&G} = 24.78\%$ *versus* $RD_{AA} = 5.19\%$).

The sodium corrections may be convenient and coincidental mathematical constructs without any basis in reality; they may also be real. Certainly, for the 17 analyses from JOHNSEN & GRICE (1999), they consistently improve Na site-occupancy accuracy over results from the JOHNSEN & GRICE (1999) cationic scheme by a significant margin, especially in *N*(4).

Vacancies in M(2)

The alternative algorithm most certainly eliminated the issue of vacancies in *M*(2) (Table 19), but the cost was the addition of sometimes-unreasonable surpluses (Table 20). These surpluses in *M*(2) are frequently high, even when there is nothing in it besides Fe and Mn, but if Mn were bumped to *M*(1) to accommodate Mn, then *M*(1) would run high, as it never has any vacancies in the alternative algorithm (Table 19). The solution would be to bump Ca or *REE* to *N*(4) [recall that Y is fixed in *M*(1)], but this would only accommodate part of the needed space. Additionally, 60% of the time, there is not enough room in *N*(ϕ) to push Na from *N*(4) to *N*(ϕ) to accommodate the transferred Ca or *REE*. As far as the 40% of analyses in which the bumping is possible, there are limitations to the algorithm related to circular reasoning faults that hinder this transfer. It is an issue that warrants future refinement.

Partitioning of Mn

The alternative algorithm only slightly improved the partitioning of Mn in *M*(1) and *M*(2) compared to the cationic scheme of JOHNSEN & GRICE (1999). The current limitations of the alternative algorithm in the resolution of surpluses in *M*(2) similarly restrict its ability to address completely partitioning issues of Mn, which is unfortunate, to say the least. The most serious

outcome of which is a degree of uncertainty in discriminating between a manganese-dominant and an iron-dominant species.

Part of the problem in establishing this definition is that a eudialyte group analysis may be overall manganese-dominant, for example, yet be a representative of an iron-dominant species, as dominance with respect to speciation is seated in *M*(2). Comparing total Fe to Mn is insufficient to determine speciation; if enough manganese is partitioned to *M*(1), then iron will dominate *M*(2). In the East Hill Suite samples, only 20% of the analyses were overall iron-dominant, yet 53% recalculated as iron-dominant species.

On the other hand, the alternative algorithm performed well at assigning both Fe and Mn to *M*(2) (Figures 13 & 14) in its test run using the data of JOHNSEN & GRICE (1999), with r^2_{AA} = 0.85 & RD_{AA} = 3.86% for Fe and r^2_{AA} = 0.83 & RD_{AA} = 7.75% for Mn. Consequently, evidence suggests that the level of uncertainty is not unreasonable but that it should be acknowledged.

From a certain viewpoint, site-occupancies of Mn are intimately tied to those of Fe; therefore, fully addressing site assignment of Mn necessitates also resolving site-assignment of Fe. Although the alternative algorithm gave good results in assigning Mn to *M*(1) (Figure 11), with r^2_{AA} = 0.94 & RD_{AA} = 3.37%, it did not assign Fe to *M*(1) in any analyses, which seems unrealistic. Iron is not fixed by the algorithm in *M*(2), rather the algorithm is set up to use *M*(1) as an overflow for iron from *M*(2), and it is simultaneously set up to maximize iron in *M*(2), using this as a reference point to resolve other occupancy logic issues. Reversing the logic of the site assignment of iron, assigning it first to *M*(1) and using *M*(2) as the overflow produces unsatisfactory results of a different kind. In this scenario, *M*(1) carries a surplus and *M*(2) vacancies, the latter of which were specifically meant to be addressed by the alternative algorithm. Somehow, the difference needs to be split without incurring circular logic violations.

Partitioning of Nb & Hf

The alternative algorithm did not improve the assignment of Nb to *M*(3) (Figure 18) over the cationic scheme of JOHNSEN & GRICE (1999). No other site assignments for Nb or Hf satisfied standards for statistical significance.

Summary

TABLE 22 – Summary of the performance of the two recalculation schemes, the cationic scheme of JOHNSEN & GRICE (1999) (subscript J&G) and the alternative algorithm (subscript AA).

Site & Element	$r^2_{J\&G}$	r^2_{AA}	$RD_{J\&G}$	RD_{AA}
$^{[N(4)]}$Na	0.41	**0.80**	24.78%	**5.19%**
$^{[N(4)]}$Sr	**1.00**	**1.00**	**0.32%**	**0.32%**
$^{[N(4)]}$K	**0.95**	**0.95**	**0.15%**	**0.15%**
$^{[N(4)]}$Ca	0.85	**0.95**	3.50%	**1.75%**
$^{[N(4)]}$*REE*	0.32	**0.86**	4.42%	**2.32%**
$^{[M(1)]}$Ca	0.92	**0.98**	3.80%	**1.83%**
$^{[M(1)]}$Mn	**0.92**	**0.94**	**3.69%**	**3.37%**
$^{[M(1)]}$*REE*	0.46	0.23	4.35%	3.37%
$^{[M(2)]}$Fe	**0.85**	**0.85**	**3.96%**	**3.86%**
$^{[M(2)]}$Mn	**0.78**	**0.83**	**7.98%**	**7.75%**
$^{[Z]}$Zr	**0.65**	**0.70**	**1.94%**	**1.69%**
$^{[Z]}$Ti	**0.85**	**0.75**	**1.20%**	**1.76%**
$^{[M(3)]}$Si	0.63	0.73	17.82%	15.94%
$^{[M(3)]}$Nb	**0.96**	**0.93**	**3.47%**	8.00%

The statistic for the superior scheme for each site assignment is indicated in bold type. Both statistics bold or not indicates a tie.

Fourteen site assignments are significant at the 95% confidence level for both site assignment schemes. The coefficient of determination and the relative deviation for each scheme and site assignment are compared in TABLE 22.

The alternative algorithm outperformed the cationic scheme for precision (r^2) in four of the 14 site assignments and performed equally well in the other ten. In particular, it achieved one of the primary goals of substantially improving the site-occupancy of $N(4)$ by resolving occupancy issues with Na and *REE*. The alternative algorithm also surpassed the cationic scheme for accuracy (*RD*) in four of the 14 site assignments, performed equally well in ten, and was beaten in only one site assignment. A larger sample set of single-crystal-based structural recalculations with EMP data is needed to test the performance of the alternative algorithm in the remaining 19 site assignments for which the data did not meet standards of statistical significance. In terms of the 14 site assignments for which the data did meet these standards, the alternative algorithm is an overall success.

Suggestions for Future Work

One of the perhaps-obvious flaws of any recalculation scheme that is based on sequential, subtractive assignment is that the necessity for fixing certain sites' total-occupancy as reference values, combined with the compounding of error from one site-assignment to the next, results in formulæ that have inherently better site-occupancies in the first sites to which elements are assigned. That is to say, in practice, the first site that is dealt with is filled to its ideal occupancy, then, too, is the second, and in minerals with large numbers of sites, perhaps a few more. Eventually, however, surplus *apfu* of elements that could not fit because of assignment limitations or site-occupancy limitations are forced into some "garbage dump" site that can

collect all sorts of elements, which cleans the docket of candidates but which gives variously poor results at the back end of the recalculation.

There is a sort of autocorrelation here. The first sites to which elements are assigned are automatically better, in terms of vacancies and surpluses, than those that receive the last of the elements. The consequence is that by restructuring the assignment scheme, a different set of sites could be the accuracy champions and their once-proud partners could take last place. That is, in part, what took place between the JOHNSEN & GRICE (1999) approach and the alternative algorithm described in this work; one set of problems was traded for another. As was reviewed earlier, whereas JOHNSEN & GRICE (1999) yielded heavy vacancies in *M*(1) and *M*(2), the alternative algorithm yields even heavier surpluses in *M*(2). One the whole, the overall recalculation was substantially improved, but it would be deceptively incomplete not to address possible remedies for this new problem.

It seems that some kind of iterative assignment scheme would be a good place to start. One of the most serious shortcomings of the alternative algorithm was that the need to avoid circular logic in its single-stage, sequential assignment scheme forced certain site-assignments, such as Y in *M*(1), to be fixed in order to serve as reference points for all other elements. "Site-assignment" was stated in the plural because, even though yttrium was the only deliberately fixed element, there were logical consequences to that and to the structure of the site-assignment table.

PROPOSED EUDIALYTE GROUP CLASSIFICATION SYSTEM

Introduction

The eudialyte group is firmly at the complex end of the crystal chemistry continuum. Naturally, as the crystal chemistry of a group grows more complex, so, too, does the task of creating a classification scheme. A system that is comprehensive may become too elaborate to show data meaningfully; and the remedy of repeatedly subdividing such a system into simple, highly chemically related suites of species may detach the data too much from the group as a whole, thus compromising contextual understanding.

Rationale for M(3)

In undertaking to produce a system, the challenges of retaining comprehensiveness and continuity were kept squarely in mind. Ample consideration was also given to the guidelines provided by the IMA Commission on Classification of Minerals (CCM): 1) "…[a mineral group] should comprise at least two species" [and, by extension, so, too, should a mineral subgroup] and 2) "…the species comprising the group should be isostructural, as indicated by similarity of space group and unit-cell parameters". (Nickel 2001) Although these guidelines are not codified, they are the general agreement of the members of the CCM.

Finally, the chemical-structural perspective on mineral classification that has been assiduously developed by Hugo Strunz was used as a parallel set of guidelines for classifying the eudialyte group. PUSHCHAROVSKY (2000) lent his support to Strunz's concept in saying, "…berlinite ($AlPO_4$) and alarsite ($AlAsO_4$) would be assigned to the same group because they are isostructural, and P and As have similar crystallochemical behaviours. However, halite, galena and periclase would not be assigned to the same group because Cl, S and O are

crystallochemically dissimilar." This is particularly important in light of the larger-scale implications of eudialyte group crystal chemistry with regards to chemical environment, magma fractionation, and tectonic associations.

The foundation of the system is the proposition that classification of eudialyte group minerals based on site-occupancy of *M*(3) gives the most meaningful and useful distinctions between chemical and genetic families for four reasons: 1) sorting eudialyte group minerals based on occupancy of *M*(3) yields subgroups that are entire—there are no allied members residing in other subdivisions; 2) this manner of classification leaves no orphaned species—all species can belong to a subgroup[3]; 3) the occupancy of *M*(3) is already defined and accepted in formula form as a single-site, single-element breakpoint between species; and 4) the elements that occupy *M*(3) have the most distinctive genetic and chemical implications.

There are, to be sure, several other distinctions that can be made (such as alkali metal, transition metal, or halogen content), but as these distinctions are common to a number of proposed subgroups, they do not provide as useful of a first step in speciation and classification.

Site-Occupancy of X

Although alkali metals and alkaline earth metals may participate in coupled substitutions in the eudialyte group, the last feature of eudialyte group crystal chemistry that in and of itself appears to be relevant to speciation is the content of halogens and related ions in *X*. Citing potential complications from the multiple possible occupants of the *X* site, JOHNSEN *ET AL.* (2003a) currently advise against employing site-occupancy of *X* as a criterion for speciation.

They make a valid case in terms of graphical representation. Site-occupancy of *X* is not the only variable in speciation, as is the case with halogens and hydroxide in the apatite series, and variable occupancy in *X* may involve any member of the entire group. Consequently, creating a diagram that conveys site-occupancy in *X* on top of all other substitutions would only diminish the readability of the data.

Also, in terms of nomenclature, adding site-occupancy of *X* as a criterion would probably at least double the number of species in the eudialyte group, perhaps without any real gain. At the same time, precedent aside (*e.g.* the amphibole group), such an exclusion may diminish the ability of the speciation of a eudialyte group analysis to convey information about the volatile chemistry of a particular whole-rock sample or sample suite. In light of the importance of volatiles in the petrology and crystallization history of precisely the type of rock in which eudialyte group minerals are likely to be found, this could compromise the greater context of the analyses.

The proposed system advocates overturning the suggestion of JOHNSEN *ET AL.* (2003a) to exclude site-occupancy in *X* from speciation analysis of eudialyte group minerals, but concurs that the potentially high number of new species could limit the effectiveness of graphical interpretation of data. Therefore, it is probably sufficient to limit conveying information about occupancy of *X* to the name of the species (*e.g.* "fluoreudialyte").

---

[3] Only one species, labyrinthite, was left standing alone following sorting, solely due to the minimum two-species guideline regarding subgroups (after Nickel 2001). Nothing about its composition obviates the future discovery of

Graphical Representation of Data

This was certainly the most maddening aspect of conceiving of a classification scheme for the eudialyte group. There appears to be solid solution not only between many members of the group but between different subgroups, as well. Perhaps even worse, from the standpoint of complication, the *M*(3) site can simultaneously be occupied by all seven possible elements; it is absurd to display seven dimensions of compositional data in a single graph.

After considering several possible schemes that included various binary, ternary, and quaternary plots, the system that best reflected the data itself was a ternary plot of *M*(3) based on the three most dominant occupants thereof. This at first glance seems capricious and arbitrary, but it is supported by the nature of the data and of the mineral group, itself.

The data from the eudialyte group analyses from Mont Saint-Hilaire were plotted in terms of the *apfu* of each of the seven possible occupants of *M*(3) (Figure 65). Although there are spikes of other elements in the data, the occupancy of *M*(3) is dominated by three elements: Si, Nb, and Zr. Based on the proposition of plotting a ternary diagram based on the three most abundant occupants of *M*(3), the suite of analyses from Mont Saint-Hilaire would require thirteen different ternary diagrams. This may seem excessive, but consider four aspects of this approach.

Firstly, again taking the Mont Saint-Hilaire analyses as examples, roughly 70% of the analyses plot on only *two* of the thirteen diagrams. Therefore, the dominant chemistry of the system is immediately evident from the populations of the several plots.

Secondly, in the East Hill Suite analyses, the three most abundant occupants of *M*(3) occupy an average of 0.952 out of an available 1.000 *apfu*, meaning that restricting the data to the

---

other related species, thus warranting a hypothetical labyrinthite subgroup.

three most abundant occupants does not artificially skew the transformation or presentation of data on a ternary diagram.

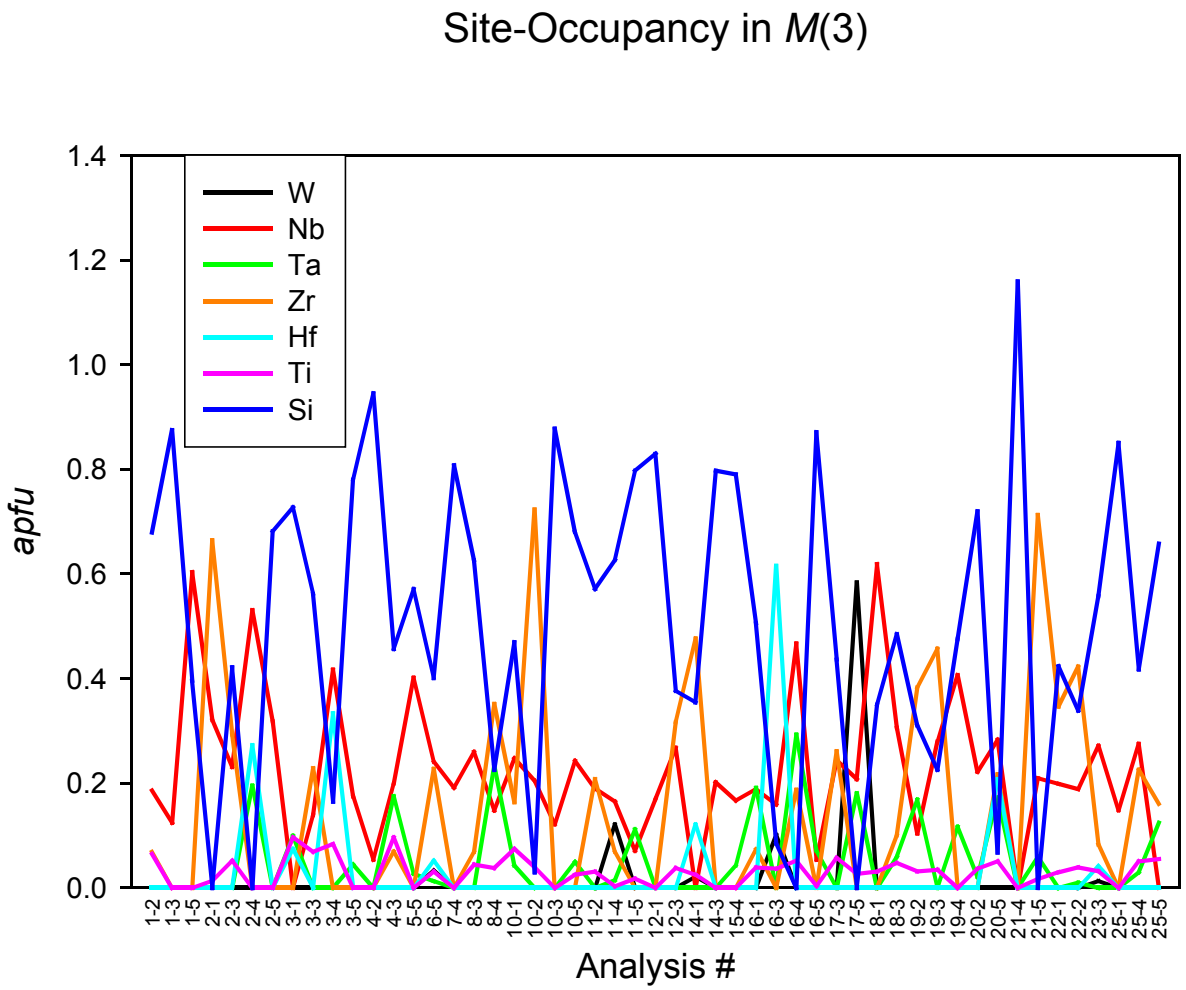

FIGURE 67 – The seven possible occupants of *M*(3) and their abundances in the East Hill Suite analyses.

Thirdly, the multiplicity of diagrams does not promote an overly elaborate classification system; only five proposed subgroups are actually being represented.

Finally, this approach allows the representation of the full range of compositions exhibited in a sample suite, accounting for otherwise-trace elements (such as Hf or W) that, in some analyses, are present in large quantities.

These four aspects relate to the second line of reasoning for the three-highest occupant ternary approach, the relationship of eudialyte group chemistry to host rock. Although the eudialyte group minerals collect several elements in varying quantities in *M*(3), the fact that nearly 70% of the analyses plot on two related ternary diagrams (Si-Nb-Ta & Si-Nb-Zr) is indicative of the overarching chemical theme, that the crystal chemistry of eudialyte group minerals is fundamentally governed by the bulk chemistry of their host system, the mineralogy of which, in this study, is heavily influenced by niobium and zirconium. To further reinforce the point, using a Si-Nb-Zr ternary collects 51% of the analyses from the East Hill Suite.

EUDIALYTE GROUP SPECIATION IN THE EAST HILL SUITE

Out of 115 analyses of eudialyte group minerals in the East Hill Suite, two approved species were detected, eudialyte and ferrokentbrooksite. Additionally, thirteen previously undescribed compositions were found (Table 7). Single specimens from this study contained up to four different species or compositions from up to three proposed subgroups, all within the space of a few millimeters.

Perhaps of equal significance to what was found is what was *not* found. Five of the seven representatives of the eudialyte group that were found at Mont Saint-Hilaire by other investigators (*viz*. johnsenite-(Ce), kentbrooksite, khomyakovite, manganokhomyakovite, and oneillite) were not seen in this study. This is interesting, as the component elements to form all of these species are found in the analyses from this study. One analysis, from the proposed

khomyakovite subgroup, shares crystal chemical characteristics with both manganokhomyakovite and oneillite, as it is tungsten-dominant in *M*(3), but is approaching the 50-50 split-*M*(1) site of oneillite. Similarly, there are several analyses that would recalculate as kentbrooksite, save for their chlorine dominance in *X*. Cerium is a locally abundant trace element, but it is never quite abundant enough to form johnsenite-(Ce) or another *REE*-dominant eudialyte group mineral; this being the most explicable omission in the lot.

This all serves to further underscore the strong relationship between eudialyte group mineral crystal chemistry and their microenvironment. Every necessary element to form most of the members of the eudialyte group is present in the melt, but they are only locally abundant enough to play a role in speciation. Overall, the eudialyte group minerals that are found in a given location are influenced by the bulk chemistry of the system, but the specific species or compositions that are found in a sample are dictated by fine-scale chemistry. The large number of sites and site dimensions in the eudialyte structure is likely responsible for its particular sensitivity to these variations. This suggests a highly dynamic chemical scenario near the concluding phase of crystallization of the East Hill Suite. Furthermore, the extreme variability of chemistry even of single species suggests that heterogeneity is far more strong and widespread in late-stage alkaline systems than previously imagined.

Crystal Chemistry of Eudialyte Group Minerals from Mont Saint-Hilaire

Overview

If it was not already obvious, eudialyte group minerals have certainly proven themselves in this study to be true "garbage can" minerals, taking up a remarkable variety of incompatible (and some compatible) elements near the end of the crystallization sequence of the East Hill

Suite. What is even more certain is that eudialyte group minerals are not only sensitive markers of the subtle differences in chemical microenvironments that pervade Mont Saint-Hilaire, they also apparently indicate that the chemistry of a single microenvironment in the eudialyte syenite is, over time, highly variable at the mm-scale.

One of the most striking features about the chemistry of the eudialyte group minerals from Mont Saint-Hilaire is their almost total lack of correlation to other elements. Before X_{Mn} was chosen as a comparator, the several elements in the eudialyte group analyses were plotted against numerous other abundant and significant elements, such as Zr, Ti, Nb, Ta, and La, to name just a few. Of these, only the mole fraction of manganese in *M*(2) showed any real relationships. Combined with its implications about chemical evolution, especially in an alkaline system, it was an excellent candidate. Even so, X_{Mn} only correlates to *two* out of twenty-three elements, Ti and Zr.

Titanium content increases proportionally with X_{Mn} (Figure 41). This is consistent with the late-stage incompatibility of Ti in alkaline systems that is reflected in the Ti-rich exhalation halos of alkaline complexes such as Magnet Cove, at which brookite (TiO_2) is found in altered novaculite around the perimeter of the complex (Erickson & Blade 1963), and Mont Saint-Hilaire itself, where narsarsukite [$Na_2(Ti,Fe)Si_4(O,F)_{11}$] and neptunite [$KNa_2Li(Fe,Mn)_2Ti_2Si_8O_{24}$] occur in the hornfels aureole surrounding the intrusion (Rajasekaran 1966). As the crystallization of the magma comes to a close and it reaches the end of its chemical evolution, X_{Mn} tends to increase, and in alkaline systems, the bulk magmatic content of TiO_2 tends to rise. This increase is reflected in the chemistry of eudialyte group minerals from the East Hill Suite and indicates their evolutionary proximity to the conclusion of crystallization therein.

In contrast, zirconium content decreases proportionally with X_{Mn} (Figure 38). Zirconium does not exhibit the same late-stage incompatibility as Ti. Although it is a relatively incompatible element over much of the course of crystallization, the overall magmatic content of Zr decreases as crystallization draws to a close, and zirconium becomes largely assimilated at Mont Saint-Hilaire by phases such as eudialyte, hilairite, and elpidite, among others. Zirconium content is not markedly elevated in the periphery of alkaline complexes.

In spite of their general lack of correlation with X_{Mn}, the component elements of the eudialyte group are not without pattern. When present, several elements (Si, Ca, Na, Ce, La, K, and Cl) show a lozenge-shaped distribution of their content against X_{Mn}; others (Hf, Ta, Mo, W, Sc, Ba, Mg, and S) have a central-peak distribution; still others (Nb, Al, Y, Gd, Nd, and F) exhibit a hybrid of the two, a sort of bloated peak. It is not unlikely that these three modes are artifacts of the plots related to the abundance of the element. Elements that are most abundant tend to exhibit the lozenge shape, a bit less abundant, the hybrid, and the least abundant (or those with the fewest occurrences) the peak. In any case, for all of these elements, their content roughly tapers to an average or minimum value at the high and low ends of their X_{Mn} ratio range and to a peak value near $X_{Mn} = 0.5$.

At first, it seemed as though this pattern of distribution might reflect some kind of band of optimal trace-element incorporation that has a maximum near 50-50 occupancy of $M(2)$. However, examination of the analyses from JOHNSEN & GRICE (1999) in large measure refuted this supposition. The 17 analyses from JOHNSEN & GRICE (1999) represent eudialyte group minerals from a wide range of compositions and localities, and more importantly, they represent a broader range of X_{Mn} values than the analyses from Mont Saint-Hilaire, running nearly from end-member to end-member. The examination only largely refuted the supposition because the

analyses from JOHNSEN & GRICE (1999) reflect a similar tapering towards the iron- and manganese-rich ends of *M*(2) occupancy, but their X_{Mn} range is broader and the tapering, if present, is much more gradual. The likely upshot is that since the analyses from Mont Saint-Hilaire represent a much narrower range of X_{Mn} values the interpretation is skewed; the absence of data above or below this band causes a sudden drop-off in values that exaggerates the trend. Nevertheless, in both suites of analyses, trace-element incorporation reaches a maximum at an intermediate value of X_{Mn} rather than exhibiting a linear correlation.

Implications and possibilities aside, two conclusions can be drawn as certain regarding the crystal chemistry of eudialyte group minerals in the East Hill Suite. Firstly, they exhibit a relatively narrow range of manganese to iron ratios. Secondly, the near absence of linear correlation between elements, the sheer scatter of values, further indicates that eudialyte group minerals are more ruled by local chemistry than by the overall chemical evolution of the system.

Paragenesis of Eudialyte Group Minerals

Correlative variation with X_{Mn} of the fundamental chemistry of eudialyte group minerals, in particular in terms of their occupancy in *M*(3), lends some insight into their paragenetic sequence in the East Hill Suite. Recall that with increasing X_{Mn}, Ti content increases and Zr content decreases (Figures 41 & 38). Furthermore, a reëxamination of these and other trace-element diagrams reveals that the three most abundant proposed subgroups—"Zr-eudialyte", kentbrooksite, and eudialyte—exhibit a somewhat systematic grouping associated with X_{Mn}.

Members of the proposed "Zr-eudialyte" subgroup are concentrated at the lower end of X_{Mn} values; those of the proposed kentbrooksite subgroup are concentrated near the 50-50 split; and those of the proposed eudialyte subgroup are concentrated at the higher end of X_{Mn} values.

The early presence of Zr-rich eudialyte group compositions fits well with the higher magmatic Zr content early in the crystallization history of eudialyte group minerals. Similarly, the late-stage occurrence of more Si-rich eudialyte group compositions reflects the spike in silica that occurs near the end of crystallization in alkaline systems and in volatile-rich or pegmatitic calc-alkaline systems, as well—*viz.* hydrothermal quartz in the otherwise silica-undersaturated East Hill Suite and pegmatite quartz cores. (Mandarino & Anderson 1989; London 1992) More particularly, the relationship suggests that members of the proposed "Zr-eudialyte" subgroup crystallized first, followed by those of the proposed kentbrooksite subgroup and the proposed eudialyte subgroup, respectively.

Possible Implications for Parental Magma Chemistry

The negative neodymium anomaly (Figures 52-56) is puzzling and may have implications regarding the parental magma and the magmatic evolution of the Mont Saint-Hilaire complex. Anomalies in ε-^{142}Nd are indicative of association or interaction with an *REE* fractionated mantle reservoir. (Rollinson 2007) Neodymium-142 is a stable isotope of Nd that was formed as a decay product of ^{146}Sm until about 4.0-4.2 Ga. Mantle reservoirs with low Sm/Nd ratios result in magmas that are depleted in ^{142}Nd. (Jagoutz & Jotter 1999) Furthermore, ROLLINSON (2007) points out that the evolution of the isotopic system of Nd correlates with that of Hf, allowing interpretation of mantle mineralogy with respect to a source magma.

Similar interpretations may be derived through an examination of ^{87}Sr/^{86}Sr *versus* Ce/Nd. Tholeiitic volcanic rock from Mount Etna exhibit a positive correlation between ^{87}Sr/^{86}Sr and Ce/Nd. (Carter & Civetta 1977) This is accounted for by fractional melting of source material in

which a Nd-rich residual mineral depletes the melt of its neodymium content. (Chester & Duncan 1985)

EBY (1985) examined Sr and Pb isotopes and Th/U ratios in the Monteregian Hills and concluded that the underlying mantle underwent a depletion event in the Precambrian, which is reminiscent of assertions by CARTER & CIVETTA (1977) and ROLLINSON (2007) with regards to the evolution of comparable isotopic systems. What is not known is the isotopic character of Nd or Hf at Mont Saint-Hilaire, let alone in the eudialyte group minerals. Considering the important and varying implications of the origins and proportions of the several isotopes of neodymium and hafnium, an isotopic analysis is required to pursue the issue further and to attempt to address specifically the negative neodymium anomaly.

Control on Potassium Content

A rather striking feature of the East Hill Suite eudialyte group chemical compositions is the remarkably narrow and evenly distributed range of potassium contents, between 0.35 and 0.57 (average 0.47) wt.% K_2O. Potassium has, by far, the lowest coefficient of variation[4] of any trace element and the fourth-lowest coefficient of variation of any element in the eudialyte group analyses, with a value of 11.64%. This is comparable to the coefficients of the most important essential elements: Na (6.35%), Zr (10.27%), and Si (4.28%). To get an idea of how much tighter the range of potassium contents is compared to that of other trace elements, the trace elements with the next lowest coefficients of variation, titanium and aluminum, have coefficients

[4] The coefficient of variation is defined as the standard deviation of a population divided by its mean (this quotient is sometimes multiplied by 100, to report the coefficient as a percentage). The coefficient of variation gives more meaning to the standard deviation of a population, as it recasts the standard deviation in terms of the magnitude of the data; a given standard deviation represents a larger variance in a population with small values, but it represents a

of 58.65% and 64.01%, respectively; all other trace elements have coefficients between 132.37% (Ba) and 529.79% (Zn).

The potassium content does not correlate with that of any other element, but unlike most trace elements in eudialyte group minerals, it is present in every analysis. Even more striking is that a comparable pattern and levels of potassium content are found in the 17 analyses of JOHNSEN & GRICE (1999), with potassium ranging from 0.28 to 0.61 wt.% K_2O with an average of 0.43 and a coefficient of variation of 20.74%. Recall that the analyses of JOHNSEN & GRICE (1999) also represent a variety of eudialyte group species but, more importantly, they represent a variety of localities. Therefore, this appears to be a common feature of eudialyte group crystal chemistry.

Before comparison with the analyses of JOHNSEN & GRICE (1999), the pattern of potassium content suggested that eudialyte group minerals might serve as some kind of indicator of potassium activity in a given system. Since the same pattern recurs in numerous environments, however, this is unlikely to be true in the original sense of the supposition.

The pattern also suggested that potassium might be buffered in some way in the whole system or in a microenvironment, but the analyses of JOHNSEN & GRICE (1999) discounted this idea, as well.

At this point, the line of thinking turned to the idea that there may be an inherent control or limit on potassium uptake by eudialyte group minerals. At first glance, there appears to be an exception to this assertion. Rastsvetaevite has approximately 20% of its *N* sites substituted by potassium, with an ideal composition that contains 6.12% K_2O (Khomyakov *et al.* 2006a), far

---

smaller variance in a population with large values.

greater than in any analysis from this study or from JOHNSEN & GRICE (1999); however, rastsvetaevite is formed from normal low-K eudialyte group minerals through potassium metasomatism. There are no other eudialyte group minerals that exhibit this level of potassium content or that contain potassium as an essential element. Therefore, the earlier hypothesis is not immediately invalidated and may be restated, with qualification, to say that there may be a control on potassium uptake by *primary* eudialyte group minerals.

What could regulate potassium content in this manner? The first mechanism that comes to mind is simple steric hindrance; for example, in the feldspar group, sodium can participate in complete solid solution with potassium or calcium but not both simultaneously. Rastsvetaevite does contain a relatively large amount of potassium, but it does not have precisely the same crystal structure as most eudialyte group minerals. Its structure is comprised of alluaivite and eudialyte subunits (Khomyakov *et al.* 2006a), which may be more forgiving as far as admitting a larger (with respect to sodium) cation such as potassium. The eudialyte structure may have a limit of K_2O incorporation that hovers around 0.5 wt.% K_2O. Variations in content may be due to concomitant variation in the content of other trace elements. It is indeed true that potassium content did not correlate to that of any *one* other element, but it may correlate to that of several. It would be worthwhile to expand the scope of analyses and to check for more complex correlations or structural shifts, which are already known to occur in eudialyte group minerals from the incorporation of other elements (Johnsen *et al.* 2003a).

One last possible explanation for the consistent potassium content found in eudialyte group minerals from a variety of environments is that, contrary to previous perception, potassium really is an essential element in eudialyte group minerals. Recall that the coefficient of variation of all other trace elements in the eudialyte group analyses is much higher than that of potassium

and of all of the major elements; also, recall that the coefficient of variation for potassium is comparable to that of the major elements, in spite of it being considered a trace element. The upshot is that whereas the other trace elements vary widely in content, presumably based on their chemical environment during crystallization, the potassium content is similarly constant as that of the essential elements, such as sodium and zirconium. This suggests the possibility that potassium is, in fact, an essential element.

Consider the ideal formula of eudialyte:

$$Na_{15}Ca_6Fe_3Zr_3Si(Si_{25}O_{73})(O,OH,H_2O)_3Cl_2$$

An average East Hill Suite analysis contains 0.33 *apfu* of potassium per 15 total *N* sites, so account for their presence:

$$Na_{14.67}K_{0.33}Ca_6Fe_3Zr_3Si(Si_{25}O_{73})(O,OH,H_2O)_3Cl_2$$

Triple the number of formula units in the eudialyte group formula to obtain only whole-number values:

$$Na_{44}KCa_{18}Fe_9Zr_9Si_3(Si_{75}O_{219})(O,OH,H_2O)_9Cl_6$$

This results in an average potassium content of approximately 1.00 *apfu* per 45 total *N* sites.

The argument could be made that the suggestion on this basis of essential potassium content is superficial. For example, the average content of $(OH)^-$ in East Hill Suite eudialyte group analyses is also about 0.33 *apfu*, so the same adjustment of formula units would also result in there being approximately 1.00 *apfu* of $(OH)^-$. Hydroxyl, however—taking water content as a partial proxy—exhibits a coefficient of variation (68.21%) characteristic of a trace element, comparable to that of Nb (58.92%), Ti (58.65%), and Al (64.01%); recall that the coefficient of variation for potassium is only 11.64%, comparable to those of the major, essential elements. Not only are Nb, Ti, and Al clearly not essential, but neither is $(OH)^-$; hydroxyl shares the *X* site

with Cl, F, and S, and is, in fact, absent in 20% of the East Hill Suite analyses. So, where does that leave potassium?

The answer to that question is that the coincidence of arithmetic in the East Hill Suite analyses is not the rationale for the proposition, merely a demonstration of a pattern. The rationale is really based on the consistency of potassium content both in the East Hill Suite and in eudialyte group minerals outside of the East Hill Suite. Recall that the analyses of JOHNSEN & GRICE (1999) revealed potassium contents that are consistent both in terms of content and coefficient of variation. Also, the analyses of JOHNSEN & GRICE (1999) represent numerous localities from a broad range—as broad a range as alkaline rocks can exhibit, at any rate—of geologic and geographic settings: both igneous and metamorphic and from Russia, Greenland, and other Canadian localities. This strongly suggests that the potassium content is a constant feature of eudialyte group minerals. Therefore, potassium may essentially occupy one out of every 45 *N* sites.

In particular, in the analyses of JOHNSEN & GRICE (1999), potassium strongly partitions to the *N*(4) site *sensu stricto*. The *N*(4) site is 9-coördinated with several adjacent *X* sites that allow for local charge balance against high-valence cations and with a flexible site geometry that allows the incorporation of large cations. (Johnsen & Grice 1999) Does the partitioning of K to *N*(4) further indicate that there might be ordering in eudialyte group minerals? And, if there is ordering, can the degree of ordering be correlated to crystallization history in the same sense as feldspar group minerals?

CONCLUSIONS

Simply put, trying to establish eudialyte group mineral site occupancy in the absence of single-crystal X-ray data is a real mess. Nevertheless, within limits, it can be done, and the alternative algorithm provides an overall improvement over the cationic scheme of JOHNSEN & GRICE (1999). Although the alternative algorithm had mixed success in terms of site-assignments in *M*(1) and *M*(2), it was outright effective in terms of resolving site-occupancy issues in *N*(4).

Thirteen potentially-new species of eudialyte group minerals were found in this study, and interestingly, five known species from the East Hill Suite were not. Furthermore, single mm-scale grains were comprised of up to four distinct compositions representing up to three proposed subgroups. Eudialyte group minerals from all proposed subgroups exhibited a near-total lack of correlation between single trace element content and any other element. These data not only suggest that the microenvironment around a growing eudialyte group mineral is highly influential in determining speciation but that melt heterogeneity may be far more pronounced in late-stage crystallization of alkaline systems than previously imagined.

The pattern of trace element incorporation into the several proposed subgroups of the eudialyte group suggests that members of the proposed "Zr-eudialyte" group crystallize at the beginning of the last stages of melt solidification, followed, in order, by members of the proposed kentbrooksite subgroup and the proposed eudialyte subgroup.

All eudialyte group analyses from the East Hill Suite showed a negative neodymium anomaly in chondrite-normalized *REE* data. Comparison of this anomaly to data from other localities from CARTER & CIVETTA (1977) and ROLLINSON (2007) points to a *REE* fractionation event in the mantle underlying Mont Saint-Hilaire, prior to the generation of the East Hill Suite

parental magma, which was supported by strontium isotope work by EBY (1985). Further study of Nd and Hf isotopes is needed to further constrain mantle mineralogy with respect to the parental magma of the East Hill Suite and to more specifically explain the Nd anomaly.

Potassium content of eudialyte group minerals from the East Hill Suite, as well as from a number of other localities (Johnsen & Grice 1999), is remarkably tightly constrained. Steric hindrances in the eudialyte structure are a probable cause, but additional study of this phenomenon will be required to elucidate the mechanism.

The history of the study of the minerals of the eudialyte group is well-documented but poorly-publicized in the geologic community. It is a long history, particularly when viewed in comparison to the level of understanding therefrom derived. Although recognized as distinct species nearly 200 years ago (Stromeyer 1819), it is only in the last decade that mineralogists have truly begun to understand the structure and chemical variation of eudialyte group minerals, as well as their relationship to other minerals and mineral groups. Furthermore, it is clear, considering the large number of species that have appeared under the eudialyte group moniker in the few short years since the publication of the most recent works of authority on the subject, (Johnsen & Grice 1999; Johnsen *et al*. 2003a) that the new understanding of the eudialyte group will result in even more discoveries to come.

REFERENCES

ANDERS, E. & GREVESSE, N. (1989): Abundances of the elements: Meteoritic and solar. *Geochimica et Cosmochimica Acta* **53**, 197-214.

BOISSONAULT, J. (1966): La minéralogie des intrusions alcalines du Mont St-Hilaire, P.Q.. *M. Sc. Thesis*, École polytechnique de Montréal, Canada.

_____ & PERRAULT, G. (1965): Eucolite from St. Hilaire, P.Q.. *Canadian Mineralogist* **8**, 393.

CARTER, S.R. & CIVETTA, L. (1977): Genetic implications of the isotope and trace element variations in the Eastern Sicilian volcanics. *Earth and Planetary Science Letters* **36**, 168-180.

CHAO, G.Y., HARRIS, D.C., HOUNSLOW, A.W., MANDARINO, J.A. & PERRAULT, G. (1967): Minerals from the nepheline syenite, Mont St. Hilaire, Quebec. *Canadian Mineralogist* **9**, 109-123.

CHESTER, D.K. & DUNCAN, A.M. (1985): Mount Etna: The Anatomy of a Volcano. Stanford University Press, Stanford, California. 404 p.

CHUKANOV, N.V., MOISEYEV, M.M., RASTSVETAEVA, R.K., ROZENBERG, K.A., ZADOV, A.E. (2005): Golyshevite, $(Na,Ca)_{10}Ca_9(Fe^{3+},Fe^{2+})_2Zr_3NbSi_{25}O_{72}(CO_3)(OH)_3\cdot H_2O$, and Mogovidite, $Na_9(Ca,Na)_6Ca_6(Fe^{3+},Fe^{2+})_2Zr_3Si_{25}O_{72}(CO_3)(OH,H_2O)_4$, new eudialyte-group minerals from calcium-rich agpaitic pegmatites of the Kovdor massif, Kola Peninsula. *Zapiski Ross. Mineral. Obshch.* **134**(6), 36-47 (in Russian, English abstract).

_____, PEKOV, I.V., ZADOV, A.E., KOROVUSHKIN, V.V., EKIMENKOVA, I.A. & RASTSVETAEVA, R.K. (2003): Ikranite, $(Na,H_3O)_{15}(Ca,Mn,REE)_6Fe_2^{3+}Zr_3$ (□,Zr)(□,Si)$Si_{24}O_{66}$(O,OH)$_6$Cl · *n* H_2O and raslakite, $Na_{15}Ca_3Fe_3(Na,Zr)_3Zr_3(Si,Nb)(Si_{25}O_{73})(OH,H_2O)_3(Cl,OH)$—new eudialyte-group minerals from the Lovozero massif, Kola Peninsula. *Zapiski Vseross. Mineral. Obshch.* **132**(5), 22-33 (in Russian, English abstract).

CLARK, T.H. (1955): St. Jean-Beloeil Area: Iberville, St. Jean, Napierville-Laprairie, Rouville, Chambly, St. Hyacinthe, and Verchères Counties. *Québec Department of Mines, Geological Report* **66**.

COULSON, I.M. & CHAMBERS, A.D. (1996): Patterns of zonation in rare-earth-bearing minerals in nepheline syenites of the North Qôroq Center, South Greenland. *Canadian Mineralogist* **34**, 1163-1178.

CURRIE, K.L. (1970): An hypothesis on the origin of alkaline rocks suggested by the tectonic setting of the Monteregian Hills. *Canadian Mineralogist* **10**, 411-420.

_____ (1983): An interim report on the geology and petrology of the Mont Saint Hilaire pluton, Quebec. In *Current Research, Part B. Geological Survey of Canada, Paper* **83-1B**, 39-46.

_____, EBY, G.N. & GITTINS, J. (1986): The petrology of the Mont Saint Hilaire complex, southern Quebec: An alkaline gabbro-peralkaline syenite association. *Lithos* **19**, 65-81.

DEER, W.A., HOWIE, R.A. & ZUSSMAN, J. (1986): "Eudialyte-Eucolite", *in* Rock-forming minerals, Volume 1B: Disilicates and ring silicates. *2nd edition*. Longman Scientific & Technical, London, 348–363.

DOIG, R. & BARTON, J.M. (1968): Ages of carbonatites and other alkaline rocks in Quebec. *Canadian Journal of Earth Sciences* **5**, 1401-1407.

EBY, G.N. (1985): Sr and Pb isotopes, U and Th chemistry of the alkaline Monteregian and White Mountain igneous provinces, eastern North America. *Geochimica et Cosmochimica Acta* **49**, 1143-1154.

ERICKSON, R.L. & BLADE, L.V. (1963): Geochemistry and petrology of the alkalic igneous complex at Magnet Cove, Arkansas. Professional Paper **425**. *United States Geological Survey*.

GAINES, R.V., SKINNER, H.C.W., FOORD, E.E., MASON, B. & ROSENZWEIG, A. (1997): Dana's New Mineralogy. *8th Edition*. Sections by V.T. King. Illustrated by E. Dowty. John Wiley & Sons, Inc., New York. 1819 p.

GILBERT, L.A. & FOLAND, K.A. (1986): The Mont Saint Hilaire plutonic complex: occurrence of excess ^{40}Ar and short intrusion history. *Canadian Journal of Earth Sciences* **23**, 948-958.

GIUSEPPETTI, G., MAZZI, F. & TADINI, C. (1971): The crystal structure of eudialyte. *Tschermaks Mineral. Petrogr. Mitt.* **16**, 105-127.

GOLD, D.P., EBY, G.N., BELL, K. & VALLEE, M. (1986): Carbonatites, diatremes, and ultra-alkaline rocks in the Oka area, Quebec. *Geological Association of Canada, Mineralogical Association of Canada, Canadian Geophysical Union, Joint Annual Meeting, Ottawa '86*, Field Trip Guidebook **21**, 51 p.

GOLYSHEV, V.M., SIMONOV, V.I. & BELOV, N.V. (1971): Crystal structure of eudialyte. *Sov. Phys. Crystallogr.* **16**(1), 70-74.

GRICE, J.D. & GAULT, R.A. (2006): Johnsenite-(Ce): A new member of the eudialyte group from Mont Saint-Hilaire, Quebec, Canada. *Canadian Mineralogist* **44**, 105-115.

HARRIS, C. & RICKARD, R.S. (1987): Rare-earth-rich eudialyte and dalyite from a peralkaline granite dyke at Straumsvola, Dronning Maud Land, Antarctica. *Canadian Mineralogist* **25**, 755-762.

HORVÁTH, L. & GAULT, R.A. (1990): The mineralogy of Mont Saint-Hilaire Quebec. *Mineralogical Record* **21**, 284-359.

JAGOUTZ, E. & JOTTER, R. (1999): On the search for neodymium-142 in terrestrial rocks. In *Ninth Annual V.M. Goldschmidt Conference*, Abstract #7367. LPI Contribution **971**, Lunar and Planetary Institute, Houston (CD-ROM).

JOHNSEN, O., FERRARIS, G., GAULT, R.A., GRICE, J.D., KAMPF, A.R. & PEKOV, I.V. (2003a): The nomenclature of eudialyte-group minerals. *Canadian Mineralogist* **41**, 785-794.

_____, GAULT, R.A., GRICE, J.D. & ERCIT, T.S. (1999a): Khomyakovite and manganokhomyakovite, two new members of the eudialyte group from Mont Saint-Hilaire, Quebec. *Canadian Mineralogist* **37**, 893-899.

_____ & GRICE, J.D. (1999): The crystal chemistry of the eudialyte group. *Canadian Mineralogist* **37**, 865-891.

_____, _____ & GAULT, R.A. (1999b): Oneillite: a new Ca-deficient and *REE*-rich member of the eudialyte group from Mont Saint-Hilaire, Quebec, Canada. *Canadian Mineralogist* **37**, 1111-1117.

_____, _____ & _____ (2003b): Ferrokentbrooksite, a new member of the eudialyte group from Mont Saint-Hilaire, Quebec, Canada. *Canadian Mineralogist* **41**, 55-60.

_____, PETERSON, O.V. & GAULT, R.A. (1997): Optical data on minerals of the eudialyte group: discussion of the eucolite-mesodialyte-eudialyte terminology. *Neues Jahrbuch für Mineralogie, Monatshefte* **1997**, 371-383.

KHOMYAKOV, A.P. (1995): Mineralogy of Hyperagpaitic Alkaline Rocks. *1st English Edition*. Oxford University Press, Oxford, England. 235 p.

_____, DUSMATOV, V.D., FERRARIS, G., GULA, A., IVALDI, G. & NECHELYUSTOV, G.N. (2003): Zirsilite-(Ce), $(Na,\square)_{12}(Ce,Na)_3Ca_6Mn_3Zr_3Nb(Si_{25}O_{73})(OH)_3(CO_3)\cdot H_2O$, and carbokentbrooksite $(Na,\square)_{12}(Na,Ce)_3Ca_6Mn_3Zr_3Nb(Si_{25}O_{73})(OH)_3(CO_3)\cdot H_2O$—two new eudialyte-group minerals from the Dara-I-Pioz alkaline massif, Tajikistan. *Zapiski Vseross. Mineral. Obshch.* **132**(5), 40-51 (in Russian, English abstract).

_____, NECHELYUSTOV, G.N. & ARAKCHEEVA, A.V. (2006a): Rastsvetaevite, $Na_{27}K_8Ca_{12}Fe_3Zr_6Si_4[Si_3O_9]_4[Si_9O_{27}]_{34}(O,OH,H_2O)_6Cl_2$, a new mineral with a modular

eudialyte-like structure and crystal-chemical systematics of the eudialyte group. *Zapiski Vseross. Mineral. Obshch.* **135**(1), 49-65 (in Russian, English abstract).

_____, _____, EKIMENKOVA,, I.A., RASTSVETAEVA, R.K. (2005): Georgbarsanovite, $Na_{12}(Mn,Sr,REE)_3Ca_6Fe_3^{2+}Zr_3NbSi_{25}O_{76}Cl_2 \cdot H_2O$, a mineral species of the eudialyte group: revalidation of barsanovite and the new name of the mineral. *Zapiski Rossiyskogo Mineralogicheskogo Obshchestva* **134**(6), 47–57 (in Russian, English abstract).

_____, _____ & RASTSVETAEVA, R.K. (2006b): Labyrinthite $(Na,K,Sr)_{35}(Ca_{12}Fe_3Zr_6TiSi_{51}O_{144}(O,OH,H_2O)_9Cl_3$, a new mineral with a modular eudialyte-like structure from Khibiny alkaline massif, Kola Peninsula, Russia. *Zap. Ross. Mineral. Obshch.* **135**(2), 38–49 (in Russian, English abstract).

KUMARAPELI, V.S. & SAULL, V.A. (1966): The St. Lawrence valley system: a North American equivalent of the East African rift valley system. *Canadian Journal of Earth Sciences* **3**, 639-659.

LONDON, D. (1992): The application of experimental petrology to the genesis and crystallization of granitic pegmatites. *Canadian Mineralogist* **30**, 499-540.

MANDARINO, J.A. & ANDERSON, V. (1989): Monteregian Treasures, The Minerals of Mont Saint-Hilaire, Quebec. Cambridge University Press, Cambridge, England. 295 p.

NICKEL, E.H. (2001): Discussion Paper on Mineral Groups. (October 04, 2008) http://www.ima-mineralogy.org/com-wg/CNMNC/2CCMpages/CCM-temp-website/Nickel.pdf

O'NEILL, J.J. (1914): St. Hilaire (Beloeil) and Rougemont Mountains, Quebec. *Canada Department of Mines, Geological Survey Memoir* **43**.

PEKOV, I.V., EKIMENKOVA, I.A., CHUKANOV, N.V., RASTSVETAEVA, R.K., KONONKOVA, N.N., PEKOVA, N.A. & ZADOV, A.E. (2001): Feklichevite, $Na_{11}Ca_9(Fe^{3+},Fe^{2+})_2Zr_3Nb[Si_{25}O_{73}](OH,H_2O,Cl,O)_5$, a new mineral of the eudialyte group from the Kovdor massif, Kola Peninsula. *Zap. Vseross. Mineral. Obshch.* **130**(3), 55–65 (in Russian, English abs.).

PETERSEN, O.V., JOHNSEN, O., GAULT, R.A., NIEDERMAYR, G. & GRICE, J.D. (2004): Taseqite, a new member of the eudialyte group from the Ilímaussaq alkaline complex, South Greenland. *Neues Jahrbuch für Mineralogie, Monatshefte* **2004**, 83-96.

PHILPOTTS, A.R. (1970): Mechanisms of emplacement of the Monteregian intrusions. *Canadian Mineralogist* **10**, 395-410.

_____ (1976): Petrography of Mounts Saint-Bruno and Rougemont. *Québec Ministère des Richesses Naturelles, Rapport* **ES-16**.

PUSHCHAROVSKY, D. (2000): Comments to the *Draft Proposal: Draft Discussion Paper on criteria to establish mineral groups (or families)*. (October 04, 2008) http://www.ima-mineralogy.org/com-wg/CNMNC/2CCMpages/CCM-temp-website/Draft-Push-2.pdf

RAJASEKARAN, K.C. (1966): Narsarsukite from Mont Saint-Hilaire, Quebec, Canada. *Canadian Mineralogist* **8**, 506-514.

RASTSVETAEVA, R.K. & ANDRIANOV, V.I. (1987): New data on the crystal structure of eudialyte. *Dokl. Akad. Nauk SSSR* **293**, 1122-1126 (in Russian).

_____ & BORUTSKII, B.E. (1988): Crystal chemical peculiarities of eudialyte proceeding from new structural data. *Mineral. Zh.* **10**, 48-57 (in Russian).

_____, _____ & GUSEV, A.I. (1988): Crystal structure of eucolite. *Sov. Phys. Crystallogr.* **33**(2), 207-210.

_____ & CHUKANOV, N.V. (2003): Ikranite: composition and structure of a new mineral of the eudialyte group. *Crystallography Reports* **48**(5), 717-720.

_____, IVANOVA, A.G. & KHOMYAKOV, A.P. (2006): Modular structure of hypermanganese eudialyte. *Dokl. Akad. Nauk* **410**, 101-105 (in Russian).

_____, SOKOLOVA, M.N. & BORUTSKII, B.E. (1990): Crystal structure of potassium oxonium eudialyte. *Sov. Phys. Crystallogr.* **35**(6), 814-817.

ROLLINSON, H.R. (2007): Early Earth Systems: A Geochemical Approach. Blackwell Publishing, Oxford, Malden, Carlton. 285 p.

STROMEYER, F. (1819): Summary of meeting 16 December 1819 [Analyse einiger grönlandischen, von Prof. Giesecke erhaltenen Fossilien]. *Göttingische gelehrte Anzeigen* **3**, 1993-2000.

WILSON, A.E. (1964): Geology of the Ottawa-St. Lawrence Lowland, Ontario and Quebec. *Geological Survey of Canada Memoir* **241**.

VITA

Peter Edward Tice was born on September 4, 1972 in Princeton, New Jersey. In July of 1977, his family and he moved to Wyomissing, Pennsylvania, a small semi-agricultural town in Pennsylvania's Amish and German region. The move brought him much closer to the Appalachian Mountains and fed his burgeoning interest in rocks and minerals, which was supported by his maternal grandfather, Ed Stepnowski, an avid collector of minerals from the Franklin, New Jersey mines. Following his high school graduation in 1989, he moved to Montréal, Québec, where he attended McGill University.

At McGill University, Peter's geology curriculum gave him a rigorous exposure to all major fields of geology. While deriving a great deal of pleasure from each of his classes, it did not take long for him to focus in on mineralogy & petrology, especially igneous petrology, as his favorites. During his last year at McGill, he worked with Dr. Robert F. Martin on an Honours Undergraduate Thesis concerning the mineralogy and petrology of a pegmatite dike at Mont Saint-Hilaire. Peter graduated from McGill in 1995 with a B.Sc. in Geology and an American History minor.

Seeking to maintain his course of education in the fundamental principles of mineralogy and igneous petrology, he moved to New Orleans to work with Dr. Wm. B. "Skip" Simmons, Jr. and Mr. Alexander Falster at the University of New Orleans. Following nine consecutive years in university, Peter found himself needing a break and spent a nearly a year between 1998 and 1999 in Greenville, South Carolina. Although he was variously employed as a car salesman, a waiter, a bartender, and a chef, he still found the time to head into the local mountains to collect and study minerals. He returned to the University of New Orleans in September, 1999.

Peter and his wife evacuated from Hurricane Katrina on August 27, 2005. Watching the television news, it soon became apparent that they would not be returning to New Orleans in the near future, and with a baby on the way, they resettled in Austin, Texas.

To make ends meet, Peter worked at the second largest Home Depot in the United States, where, after only six months, he became the assistant supervisor of the Garden department. In the meantime, he took evening and weekend classes in teacher certification, and was hired in July, 2007 by the San Marcos, Texas school district to teach high school science.

Peter is currently the science teacher at PRIDE High School, teaching biology, chemistry, physics, and earth science to at-risk students in 11^{th} and 12^{th} grades. He was recently honored by being selected as a participant in *Project Flowing Waters*, an NSF-funded science-teaching consortium between the San Marcos Consolidated Independent School District and Texas State University that seeks to develop innovative methods of science education that give students more exposure to real-world science investigation and more insight into their local geology and environment. He also serves as the campus technologist, the campus representative to the District Education Improvement Committee, the campus representative of the National Education Association, and is the Vice-President of the San Marcos Education Association.

Peter received his Master's degree in Geology in the summer of 2009, and he is very happy about it.